



**University of  
Leicester**

**Remote sensing of Savannah vegetation structure  
using the Geoscience Laser Altimeter System and  
L-band Synthetic Aperture Radar**

Thesis submitted for the degree of  
Doctor of Philosophy  
at the University of Leicester

by

**Ehsan Fayez Khalefa**

Department of Geography

University of Leicester

March 2012

**I dedicate this thesis to one who left so early... my father...  
GOD bless him**

# **Remote sensing of Savannah vegetation structure using the Geoscience Laser Altimeter System and L-band Synthetic Aperture Radar**

**Ehsan Khalefa**

## **ABSTRACT**

Savannahs are globally important but not well understood systems. They consist of the coexistence of trees and grasses. A major challenge in savannah ecosystems studies is the need of maps of vegetation structure over large areas where the field data collection is impractical and time consuming. Active remote sensing such as spaceborne LiDAR and RADAR has experienced limited use in these complex heterogeneously vegetated systems. This thesis examines the ability of spaceborne ICESat-GLAS data to retrieve vegetation parameters from these more structurally and sparsely complex vegetated ecosystems.

For this main purpose, two methods of retrieving savannah vegetation heights from GLAS data were explored based on Gaussian decomposition. Results showed that the direct method works well over flat areas ( $R=0.63$  and  $RMSE=1.32m$ ;  $R=0.68$  and  $RMSE=2.61m$ ;  $n=12$ ) for GLA01 and GLA14 respectively, while sloped areas need statistical methods to remove the effect of terrain slopes on the waveform extent for better estimation of maximum vegetation height ( $R^2=0.78$  and  $RMSE=14.5m$ ;  $R^2=0.67$  and  $RMSE=17.5m$ ;  $n=6$ ) for using terrain index and waveform width as a terrain correction factor in regression models.

This work has compared the estimation of vegetation parameters derived from airborne LiDAR data and field measured data with results from spaceborne GLAS LiDAR data. GLAS estimated stand density produced  $R=0.98$  with those estimated from airborne LiDAR data. Moreover, GLAS ratio which related to the amount of woody cover in each footprint shows a strong relationship with those extracted from LiDAR airborne data ( $R=0.93$ ) and also presents a good correlation ( $R=0.85$ ) when compared with woody cover field observations.

In addition, ALOS PALSAR RADAR data was used to evaluate the results of estimating woody cover from GLAS LiDAR waveform parameters in another site at the Kruger National Park. This comparison showed a significant correlation between GLAS estimated woody cover and ALOS L-band HH backscatter ( $R=0.59$ ). This work provides an important source of knowledge for the South Africa National Parks (SANParks) Authority with a powerful tool for an adequate spatially-consistent monitoring and assessment of the woody vegetation structure of savannah landscapes.

## **DECLARATION**

This work has not been previously accepted in substance for any degree and is not concurrently being submitted in candidature for any other degree.

Ehsan Khalefa

## ACKNOWLEDGMENTS

First and foremost I would like to thank God. You have given me the power to believe in myself and pursue my dreams. I could never have done this without the faith I have in you, the Almighty.

I take immense pleasure to express my sincere and deep sense of gratitude to my supervising guide and mentor, Prof. Heiko Balzter, for his sustained enthusiasm, creative suggestions, motivation and exemplary guidance throughout the course of my doctoral research. I am sure it would have not been possible without his help. Apart from the subject of my research, I learnt a lot from him, which will be useful in different stages of my life. I solemnly submit my honest and humble thanks to him for bringing my dreams into reality. I would also like to thank Dr. Lex Comber who morally boosted me and provided me with great information resources.

This thesis would not have been possible without the kind support and help of many individuals and organizations. I would like to extend my sincere thanks to all of them.

I am highly indebted to (SANParks), and I would like to thank the staff at Scientific Services: namely Kruger National Park, for their support; in particular, Izak Smit for providing necessary information regarding the project and also for his support in completing the fieldwork for this project; and Sandra MacFadyen for GIS data about the Park. I would like to express also my gratitude to people in South Africa, and Sally Archibald for her kind help and encouragement during the conducting of my fieldwork.

I would also like to thank the German Academic Exchange Service (DAAD), an amazing organization, for offering me the opportunity to conduct part of this project with the institute of Geography at the University of Jena.

I would like to express my special gratitude and thanks to Prof. Chris Schmullius, institute of Geography, University of Jena, for giving me such attention and time and also for her help and encouragement during the period of my research in Jena. Also, I wish to extend my gratitude to thank my colleagues and staff at the institute of Geography, University of Jena, especially, Nicolas Dalla Valle, Caroline Baumgart, Lisa Schwedes, Melanie Fleischer and Claudia Hilbert who have willingly and ably helped me out throughout my stay in Jena. Special thanks must also go to Jackie Rosette, Irfan Iqbal and Gabriella Bucini for their help and support.

I cherish the friendships I had and take this opportunity to thank each one of them. My friends have provided constant encouragement, and their motivation has given me the confidence to reach this stage in my work. Thanks to my special friends, Dr. Anan Younes, Mohammad Kharabsheh, and Sharifa Al-Jabri for their constant support and whole-hearted solidarity.

Extra special thanks must go to my most dear friend Wasim Al-Jerafi and his family for their care and concern; and for nice times shared during my stay with them in their house.

I would like to express also my special gratitude and thanks to my dearest friends in the UK, Germany, France, and Syria for their invaluable friendship and for their support, encouragement, and prayers.

I am speechless! I can barely find words to express all the wisdom, love and support given to me; for that I am eternally grateful to my beloved Mum, for her unconditional love, fidelity, endurance, encouragement and prayers. She has been selfless in giving me the best of everything and I express my deep gratitude for her love without which this work would not have been completed. I would also like to express my gratitude and thanks to brother, Ahmad Khalefa, who helped me in uncountable ways and was a constant source of emotional and spiritual support. His continuous encouragements helped me throughout my life. I am also grateful for the emotional and spiritual support of my sisters and for their concern, prayers and constant enthusiasm.

Words are inadequate in offering my thanks to who taught me that “Nothing is impossible with a strong faith and willing heart”. I pay my deep respect and love for you again.

There are so many others whom I may have inadvertently left out and I sincerely thank all of them for their help.

## CONTENTS

ABSTRACT .....	i
DECLARATION .....	ii
ACKNOWLEDGMENTS .....	iii
ABBREVIATIONS .....	ix
LIST OF TABLES .....	x
LIST OF FIGURES .....	xi

### CHAPTER ONE

#### INTRODUCTION

1.1 Research rationale.....	1
1.2 Vegetation habitat structure and savannah vegetation structure.....	4
1.3 LiDAR remote sensing for vegetation structure.....	8
1.4 LiDAR in vegetation ecosystems and wildlife applications.....	9
1.5 Aim and objectives .....	11
1.6 Summary.....	12

### CHAPTER TWO

#### LITERATURE REVIEW

2.1 Introduction.....	14
2.2 Savannah ecosystems and remote sensing.....	15
2.3 LiDAR and LASER altimetry background.....	22
2.4 The principles of operation of a laser scanning system.....	23
2.5 LiDAR sensor systems and types .....	25
2.6 Types of LiDAR observation systems.....	26
2.6.1 Discrete return LiDAR system .....	26
2.6.2 Full waveform systems.....	29
2.7 ICESat-GLAS spaceborne LiDAR system.....	34
2.7.1 Overview of instrument and mission.....	35
2.7.2 ICESat track coverage .....	38
2.7.3 ICESat-GLAS data products.....	39
2.8 LiDAR applications for vegetation measurements.....	42
2.8.1 Discrete return systems of vegetation applications .....	42
2.8.2 Full waveform systems of vegetation applications.....	44
2.8.3 LiDAR studies of vegetation structure .....	46

2.8.3.1 Vegetation height estimation .....	48
2.8.3.2 Vegetation vertical structure, canopy cover, volume and biomass predictions	50
2.9 Comparison with other remote sensing techniques .....	53
2.10 Summary .....	60

## CHAPTER THREE

### DATASETS AND GENERAL METHODOLOGY

3.1 Introduction.....	63
3.2 Study area and datasets .....	64
3.2.1 Study area .....	64
3.2.2 Field data .....	67
3.2.2.1 Fieldwork and protocol.....	68
3.2.2.2 Fieldwork measurements .....	69
3.2.3 Airborne Laser data .....	75
3.2.4 ICESat-GLAS data .....	75
3.2.4.1 GLAS product summary .....	75
3.2.4.2 Pre-processing of GLAS data .....	77
3.2.5 ALOS PALSAR data.....	79
3.2.5.1 Overview of ALOS satellite .....	79
3.2.5.2 ALOS PALSAR data processing.....	80
3.2.6 Ancillary data.....	82
3.2.6.1 Aerial photography and GIS data .....	82
3.2.6.2 Woody cover map for the KNP .....	82
3.3 Data discussion and accuracy .....	83
3.3.1 Field measurements accuracy assessment .....	83
3.3.2 GLAS footprint geolocation accuracy assessment .....	84
3.4 Methods of analysis .....	85
3.4.1 Broad methodology .....	86
3.4.2 GLAS analysis methodology .....	88
3.4.2.1 GLAS data pre-processing.....	88
3.4.2.1.1 IDLreadGLAS tool .....	88
3.4.2.1.2 NGAT tool .....	89
3.4.2.1.3 Data preparation for waveform analysis.....	89
3.4.2.2 Digital Terrain Models .....	91

3.4.2.3 Waveform processing .....	92
3.4.2.3.1 Gaussian decomposition method/direct method .....	92
3.4.2.3.2 Terrain index/ statistical method .....	94
3.5 Results.....	98
3.5.1 Direct method using parameters of GLAS products.....	98
3.5.2 Statistical method/terrain index/waveform width.....	102
3.6 Discussion.....	105
3.7 Summary.....	109

## CHAPTER FOUR

### COMPARISON OF BIOPHYSICAL PARAMETER RETRIEVAL OF SAVANNAH VEGETATION FROM AIRBORNE AND GLAS SPACEBORNE LIDAR

4.1 Introduction.....	111
4.2 Methodology .....	112
4.2.1 Study site and data .....	113
4.2.1.1 GLAS data .....	114
4.2.1.2 Airborne LiDAR data .....	114
4.2.1.3 Field data .....	115
4.2.2 Data processing.....	115
4.2.2.1 Airborne LiDAR processing .....	116
4.2.2.1.1 Mapping terrain topography .....	118
4.2.2.1.2 Canopy Height Model (CHM).....	118
4.2.2.1.3 Stand density.....	118
4.2.2.1.4 Percentage of crown canopy cover .....	119
4.2.2.2 GLAS data processing .....	119
4.2.2.2.1 Vegetation height.....	120
4.2.2.2.2 Stand density.....	120
4.2.2.2.3 Crown canopy cover .....	120
4.3 Results and discussion .....	121
4.3.1 Mapping terrain topography .....	121
4.3.2 Vegetation structure parameter estimates from airborne LiDAR.....	126
4.3.3 Comparison of vegetation structure parameter estimates from spaceborne LiDAR with airborne LiDAR data .....	130
4.3.4 Evaluation using field measurements .....	137
4.4 Summary.....	143

<b>CHAPTER FIVE</b>	
<b>SAVANNAH WOODY COVER ESTIMATION FROM GLAS: AN EVALUATION USING ALOS-PALSAR RADAR DATA</b>	
5.1 Introduction.....	146
5.2 Methodology.....	151
5.2.1 Study site and data .....	151
5.2.2 Data processing.....	153
5.2.2.1 GLAS data processing .....	153
5.2.2.2 ALOS PALSAR data processing.....	156
5.3 Results and discussion .....	158
5.3.1 Comparison of maximum canopy heights derived from GLA14 and GLA01 products.....	158
5.3.2 Estimation of woody cover from GLAS footprints .....	159
5.4 Summary.....	166
<b>CHAPTER SIX</b>	
<b>SUMMARY OF RESULTS AND GENERAL DISCUSSION</b>	
6.1 Introduction.....	168
6.2 Results of biophysical parameter estimation .....	168
6.2.1 General results of utilizing spaceborne GLAS LiDAR system for estimating savannah vegetation structure .....	169
6.2.2 Discussion of general results of utilizing spaceborne GLAS LiDAR system for estimating savannah vegetation structure .....	176
<b>CHAPTER SEVEN</b>	
<b>CONCLUSION AND FUTURE WORK</b>	
7.1 Conclusions.....	184
7.2 Contribution of this research .....	187
7.3 Research limitations and future work .....	188
REFERENCES ..	191

## ABBREVIATIONS

<b>ALOS</b>	Advanced Land Observing Satellite
<b>CHM</b>	Canopy Height Model
<b>DTM</b>	Digital Terrain Model
<b>DSM</b>	Digital Surface Model
<b>GLAS</b>	Geoscience Laser Altimeter System
<b>LASER</b>	Light Amplification by Stimulated Emission of Radiation
<b>InSAR</b>	Interferometric SAR
<b>JERS-1</b>	Japanese Earth Resources Satellite-1
<b>KNP</b>	Kruger National Park
<b>LiDAR</b>	Light Detection and Ranging
<b>NASA</b>	National Aeronautics and Space Administration
<b>ns</b>	Nanosecond
<b>NSIDC</b>	National Snow and Ice Data Centre
<b>PALSAR</b>	Phased-Array L-band SAR
<b>PolInSAR</b>	Polarimetric Interferometry
<b>RADAR</b>	Radio Detection And Ranging
<b>RMSE</b>	Root Mean Square Error
<b>SANParks</b>	South African National Parks
<b>SAR</b>	Synthetic Aperture Radar
<b>SIR</b>	Shuttle Imaging Radar
<b>SIR-C/X-SAR</b>	Spaceborne Imaging Radar-C, X-Band Synthetic Aperture Radar
<b>SLC</b>	Single-Look-Complex
<b>VCL</b>	Vegetation Canopy LiDAR

## LIST OF TABLES

Table 2.1(a): Main technical specifications for the full waveform recording systems, adopted from (Mallet and Bretar, 2009) .....	33
Table 2.1(b): Illustrates the main technical specifications for the full waveform recording systems (Mallet and Bretar, 2009) .....	34
Table 2.2: Acquisition dates and release numbers for the 13 91-Day ICESat campaigns during ICESat operation (Abdalati <i>et al.</i> ,2010).....	37
Table 2.3: Specifications of ICESat-GLAS (Abdalati <i>et al.</i> ,2010) .....	38
Table 2.4: ICESat-GLAS standard data products (NSID, 2003).....	41
Table 2.5: Characteristics of common commercial discrete LiDAR sensor parameters for natural resource applications (Evans <i>et al.</i> ,2009).....	43
Table 3.1: The field data collected for 29 ICESat-GLAS footprint location in KNP....	73
Table 3.2: The ICESat-GLAS product variables used in this study (NSIDC, 2003) .....	78
Table 3.3: The PALSAR specifications. Source (Shimada <i>et al.</i> , 2004).....	80
Table 3.4: Provided GIS data sets for KNP .....	82
Table 3.5: The shifts, their correlation coefficients and standard deviation for the GLAS footprints.....	84
Table 4.1: Comparison of estimated ground surfaces using airborne and satellite GLAS LiDAR data. ....	125
Table 6.1: Regression model analysis results for height estimations with 6 coincident field measurements, coefficients significance $p$ -value $< 0.001$ , intercepts not statistically significant. ....	173
Table 6.2: Parameters of a single waveform used for estimating savannah vegetation structural characterizations at footprint-level.....	178
Table 6.3: Comparative analysis of the correlation coefficients of GLAS estimated heights with field measured heights and airborne LiDAR predicted heights.....	179
Table 6.4: Comparative analysis of the correlation coefficients of GLAS estimated woody cover with estimates from field, airborne LiDAR data, and ALOS PALSAR data .....	181

## LIST OF FIGURES

Figure 2.1: Global distribution of savannah ecosystems (tree-grass) driven from the Olson Ecoregions of the world (Olson <i>et al.</i> , 2001).....	16
Figure 2.2: Schematic of laser pulse waveform for range measurement of a laser altimeter, copyright line © [Bufton, 1989] IEEE .....	25
Figure 2.3: The basics of airborne mapping LiDAR (Imaging Notes Magazine website, 2011) .....	27
Figure 2.4: Example of LiDAR sensor systems that records first, second and third returns obtained from within a pulse (University of Idaho website, 2006).....	28
Figure 2.5: Conceptual differences between full waveform recording and discrete return LiDAR devices. At the left, Laser signal illuminates area or footprint at different height levels. The return signal as a function of time (LiDAR waveform) that IS collected by waveform recording device. To the right of the waveform, the first and the last return is recorded by discrete return sensor and next to this is the multiple return LiDAR records the height levels in the path of illumination (Lefsky et al., 2002b).....	30
Figure 2.6: Schematic overview of full waveform and discrete laser scanning systems and the resulted illuminated footprints (Dung, 2010) .....	30
Figure 2.7: Illustration of the transmitted and received full waveform signal in a vegetated area. (a) A small-footprint where all targets strongly contribute to the waveform shape LiDAR but the laser beam has a high probability of missing the ground, while in (b) A large footprint LiDAR the last pulse is bound to be the ground but each echo is the integration of several targets at different locations and with different properties (Mallet and Bretar, 2009) .....	31
Figure 2.8: Schematic illustrating the GLAS instrument making measurement from ICESat while orbiting the earth (NASA GLAS, 2009) .....	36
Figure 2.9: GLAS transects on the earth below, adopted from (ICESat-GLAS, 2003)	39
Figure 2.10: GLAS laser world elevations map (NSDIC, 2007).....	39
Figure 2.11: Large-footprint LiDAR waveform records reflections from the nadir-projected vertical distribution of the surface area of canopy components, and the estimated canopy height (Dubayah and Drake, 2000).....	49
Figure 2.12: The electromagnetic spectrum and the microwave bands location (Source: < <a href="http://earth.esa.int">http://earth.esa.int</a> >) .....	54
Figure 2.13: Types of backscattering in a natural surface. a) volume scattering in the tree crown, b) surface scattering, c) tree-soil backscattering (double bounce scattering), d) soil-tree backscattering (double bounce scattering) (Lusch, 1999)..	57
Figure 2.14: The backscattering coefficient $\sigma$ for different surface roughness conditions (González, 2008) .....	57
Figure 3.1: The location of the study area in South Africa and the two study areas in KNP, which shows overlapping between airborne LiDAR tiles and GLAS tracks plus the overlying between GLAS tracks with RADAR (ALOS PALSAR) data...	64

Figure 3.2(a): The simplified geology in KNP .....	65
Figure 3.2(b): The landscapes that characterise KNP.....	66
Figure 3.3(a): Overlaying of GLAS data and both of data sets (airborne LiDAR data and ALOS PALSAR data. b) Representation of the 31 GLAS footprints selected for field data collection in KNP on Google Earth map.....	67
Figure 3.4: Sampling plots within a GLAS footprint: radius of sampling subplots (small circles) is 10 m; the distance between sampling plots is 20 m.....	69
Figure 3.5: The photograph on the left shows an example of dense vegetation within some plots while that on the right shows the open tree savannah in other plots.....	70
Figure 3.6: Use of the clinometer to measure the tree height in flat and sloping ground when the base of the tree is below eye level, while c) measuring the height of the tree when the base of the tree is above eye level. Adapted from (NSW Government website, 2007) .....	71
Figure 3.7: Illustrates measuring tree height using a woodland stick method. Source: (USAD website, 2008) .....	72
Figure 3.8: Examples of percentage crown canopy cover (Law <i>et al.</i> , 2008) .....	74
Figure 3.9: Woody cover map (%) of KNP, adopted from (Bucini <i>et al.</i> , 2010) .....	83
Figure 3.10: Comparing GLAS footprints elevation profiles with the Google Earth elevation profiles for the selected GLAS footprints over the study area. ....	85
Figure 3.11: Flow chart summarizing the procedure employed in this research to characterize savannah vegetation structure. ....	87
Figure 3.12: Examples of two different waveforms on different terrain relief. These waveforms were modelled using the steps described in section 3.2.1 .....	90
Figure 3.13: Comparison of GLAS elevation with digital terrain models from airborne LiDAR with spatial resolution of 3 metres.....	91
Figure 3.14: Different raw waveforms with a dominant peak acquired over forest areas, the solid black line is the ICESat waveforms, the grey dots is the terrain surface and the green dots is the vegetation. It is clear that the peak location along the vertical axis is presenting the ground peak well. The width of this peak contains information on surface slope and terrain roughness. In (a) The surface is rougher while in (b) The surface is partly sloped. As a result, the ground peaks have widened in (b) While in flat and smooth surfaces in (a) Correspond to narrow last peaks (Duong, 2010) .....	93
Figure 3.15: Structure of the returned waveform over flat areas (a, b) and sloped areas (c, d) (Duong, 2010) .....	95
Figure 3.16: Structure of the returned waveform as a Gaussian function used to describe the transmitted pulse with peak position $t_x$ , amplitude $A_x$ , and width $\sigma_x$ (Duong, 2010).....	96
Figure 3.17: Scatterplots of the Pearson`s correlation relationship between maximum canopy height estimates using GLAS parameters of Gaussian decomposition and the field measurements of maximum canopy height .The result gives a weak correlation when the comparison is done for the footprints without considering terrain classification (left graph), but the correlation improves when the comparison is done on just flat and moderate footprints (right graph). ....	99

Figure 3.18: A processed GLAS waveform; the noise mean and standard deviation was estimated separately for tails at the two ends (Signal beginning and Signal end), from which thresholds were set (the dotted red line), and used to locate the signal beginning and end. The ground peak was determined where greatest sufficient energy is reflected from the ground. Hmax is the distance between signal beginning and ground peak. ....	100
Figure 3.19: Scatterplots of the Pearson's correlation relationship between maximum canopy height estimates using GLA01 parameters and field measurements of maximum canopy height. The result gives a weak correlation when the comparison is done for the footprints without considering terrain classification (left graph), but the correlation improves when the comparison is done on only flat and simple footprints (right graph).. ....	101
Figure 3.20: Scatterplots of the Pearson's correlation relationship between MCH estimates using GLA01 waveform and MCH estimates using GLA14 parameters, most points which represent flat terrain of GLAS footprint for both estimated MCH of GLAS products fall close to the 1:1 line.....	101
Figure 3.21: Relationship between measured field of maximum canopy heights and predicted values of maximum canopy height. The left graph shows the fitted values of equation (3.10) compared to field measurements of maximum canopy heights for n=10; while the right graph shows the fitted values of applying equation (3.11) after removing the two very steep GLAS footprints. The line shows the 1:1 relationship.. ....	103
Figure 3.22: Relationship between measured field of maximum canopy heights and predicted values of maximum canopy height. The left graph shows the fitted values of equation (3.12) which applied waveform width as an indicator of the effect of terrain on the GLAS waveform compared to field measurements of maximum canopy heights for n=10; while the right graph shows the fitted values of applying the same equation after removing the two very steep GLAS footprints. The line shows the 1:1 relationship.. ....	104
Figure 3.23: A comparison of the two methods of using terrain index equation (3.10) and waveform width equation (3.12) for predicting GLAS of MCH. The line shows the 1:1 relationship .....	105
Figure 4.1: The location of GLAS footprints which overlap with airborne LiDAR data tiles and were selected for field data collection. The selected study area is located in the granite landscape in KNP (the grey shading area) .....	113
Figure 4.2: Digital elevation model (DEM) extracted from airborne LiDAR points clouds for the overlapped GLAS footprints with airborne LiDAR data of the test site.....	121
Figure 4.3: The relationship between estimates of surface elevation using airborne LiDAR data (the difference between the maximum and minimum detected elevation) and waveform extents extracted from GLA14 (left graph) and GLA01 (right graph) for the satellite LiDAR data for the 38 GLAS footprints overlapped with airborne LiDAR data.....	122

Figure 4.4: Comparison of ground elevation using GLA14 elevation product and estimations of mean elevation of airborne LiDAR ground for the selected GLAS footprints.....	123
Figure 4.5: Distribution of errors in estimates of the ground surface elevation using ground elevation differences extracted from GLAS waveform structure and airborne LiDAR mean elevation surface extracted for each overlapping GLAS footprint .....	124
Figure 4.6: Digital surface model extracted from airborne LiDAR data for the selected footprint. The darker brown refers to the highest LiDAR returns and the light brown indicates very low returns from the vegetation surface.....	126
Figure 4.7: The canopy height model (CHM) was determined using LiDAR by calculating the difference between the first return elevations (canopy height) from the last return (ground elevation). The red colour indicates the highest trees (more than 10 m) and the green colour refers to the lowest vegetation heights (less than 1m) .....	127
Figure 4.8: Stem density map. The darker green represents high stem density and darker brown.....	128
Figure 4.9: The percentage of woody cover extracted from DSM and height > 2 m. .	129
Figure 4.10: Relationship between estimated maximum canopy height from airborne LiDAR and estimates of maximum canopy heights from GLA01 and GLA14 products .....	131
Figure 4.11: Comparisons of airborne LiDAR estimated MCH with GLAS MCH estimates using direct method of applying equation (4.2) for GLA01 parameters and equation (4.3) for GLA14 parameters. These comparisons were done for the classified GLAS footprints according to their slope classes .....	134
Figure 4.12: The relationship between stand density estimates of airborne and satellite LiDAR data. The Pearson correlation shows a strong relationship between estimates of both of the two systems.....	135
Figure 4.13: The relationship between percent cover estimates of airborne and satellite LiDAR data. It is quite obvious that airborne and GLAS percent cover estimates are highly correlated with ( $r = 0.94$ , $p\text{-value} < 0.001$ ). However, RMSE of 10.04% is slightly high crown canopy cover. ....	136
Figure 4.14: Relationships between classified GLAS footprints according to its terrain slopes and MCH of field measurements. The left and right graphs show that the $r$ started to decrease when the terrain slope increased. ....	139
Figure 4.15: The relationship results of estimating MCH using both LiDAR systems and MCH of field measurements. It appears that steep slope affects this relationship producing low $r$ specifically for GLAS MCH estimates in steep slope plots .....	140
Figure 4.16: Relationships between percent crown canopy cover estimates using canopy return ratio parameter (rCanopy) from GLAS waveform (•) (y- axis) and estimates using airborne LiDAR (⊠) (y axis) and those estimates from fieldwork (x) (x-axis). It shows a significant correlation ( $p\text{-value} < 0.001$ ) for both LiDAR systems with field estimates .....	143

Figure 5.1: The study site of the Kruger National Park in South Africa and the location of the GLAS footprint which overlapped with ALOS PALSAR data. ....	151
Figure 5.2: Relationship between MCH estimates using GLA01 waveform and MCH estimates using GLA14 parameters, most points for both estimated MCH of GLAS products fall close to the 1:1 line.....	158
Figure 5.3: Estimated crown canopy cover from GLAS waveform compared with woody cover percent extracted from woody cover map (Bucini <i>et al.</i> ,2010). A strong correlation is found supporting the ability of using GLAS parameters to estimate woody cover .....	160
Figure 5.4: Comparison between predicted MCH from GLAS waveform plotted against the percent woody cover interpolated from KNP woody cover map (right graph) and the predicted woody cover from GLAS waveform for each footprints (left graph). The results show significant correlation in both plots, which indicates a strong relation between increasing MCH and woody cover in each GLAS footprints .....	161
Figure 5.5: Comparison between ALOS L-band backscatter (acquired for June 2007 and June 2008 respectively) in HH and HV polarization and predicted MCH from GLAS waveforms. L-band in HH has the strongest relationship with GLAS derived MCH.....	162
Figure 5.6: ALOS L-band backscatter in HH and HV polarization (acquired for June 2007 and June 2008 respectively) plotted against predicted woody cover from GLAS footprints. This comparison shows also a good correlation between predicted woody cover from GLAS waveforms and backscatter intensity in L-band HH. This result shows the potential ability to use GLAS waveform parameters for measuring the amount of woody cover for larger scales .....	163
Figure 5.7: ALOS L-band backscatter in HH and HV polarization acquired in 2007. A regression analysis revealed the relationship between GLAS ratio as a good function indicator of woody cover in each GLAS footprint with HH and HV L-band backscatter intensity.....	164
Figure 5.8: A regression analysis revealed the relationship between GLAS ratio as a good function indicator of woody cover in each GLAS footprint with HH and HV L-band backscatter intensity for ALOS PALSAR image acquired 2008.....	165
Figure 6.1: The scatterplot relationship of estimating MCH using both GLAS products (GLA01 and GLA14) .....	172
Figure 6.2: Examples of two GLAS waveforms on different topographical surface. The upper graph shows waveform over steep terrain and the lower graph shows waveform on flat terrain .....	173
Figure 6.3: Relationships between maximum canopy height estimates using statistical regression models and field measurements of maximum canopy height .....	174
Figure 6.4: Estimated crown canopy cover from GLAS waveform compared with woody cover percent extracted from woody cover map from (Bucini <i>et al.</i> , 2009), a significant correlation is found ( $p$ -value < 0.001), supporting the ability of using GLAS parameters to estimate woody cover .....	176

# CHAPTER ONE

## INTRODUCTION

### 1.1 Research rationale

Savannahs cover approximately half of the land surface of Africa and comprise one fifth of the earth surface of the world (Scholes and Walker, 1993). They are one of the most important, but least understood, terrestrial ecosystems. Savannah ecosystems are the basis of the African livestock industry and the wildlife diversity they support is of key importance in bringing in tourists (Scholes and Archer, 1997; Scholes *et al.*, 2004). Therefore, an understanding of the savannah landscape structure and dynamics has great implications for land management efforts.

Savannahs can be defined as heterogeneous systems characterized by the coexistence of grasses and woody trees which support high fauna and flora diversity. The balance between these two life forms influences both plant and livestock production, and has profound impacts on several aspects of ecosystem function, including carbon, nutrient and hydrological cycles (Scholes and Archer, 1997; House *et al.*, 2003; Jackson *et al.*, 2002). Growing recognition of the importance of the structural component of savannah landscape diversity has highlighted the demand to understand the spatial distribution and temporal dynamics of woody plant structural diversity (Levick and Rogers, 2008). Moreover, savannah ecosystems show considerable structural variation in tree density and size. This variation has attracted ecologists for several decades (Scholes and Walker, 1993; Sankaran *et al.*, 2004, Sankaran *et al.*, 2005) and explanations for it have been varied: from competition for resources such as water and nutrients, to the effects of disturbance factors such as fire, aridity and large herbivores (Higgins *et al.*, 2000; Styles and Skinner, 2000; Bond *et al.*, 2003).

Since savannah ecosystems are known to have a wide range of highly specialized plants and animals (Solbrig *et al.*, 1996), and an extremely layered structure, they offer a challenge of an altogether different magnitude for new remote sensing techniques (Nagendra, 2001). Due in part to this challenging complexity, the use of passive and active remote sensing in tropical grasslands has largely been limited to studies of fire in savannah systems (i.e., Alleaume, 2005 and Roy *et al.*, 2005). Additionally, most studies of temporal change in savannah have employed the use of satellite images or black and white aerial photography; and, while these methods are useful for investigating changes in woody cover over time, they are not able to portray the three-dimensional structure of vegetation cover. Active systems, such as Light Detection and Ranging (LiDAR) technology have enabled three-dimensional information of vegetation to be obtained remotely over large areas, which provides useful vegetation information for sustainable ecosystem management. However, the use of LiDAR has gained considerable momentum in forested areas but has rarely been applied to savannah ecosystems (Levick and Rogers, 2008).

The relatively new Ice, Cloud and Elevation Satellite (ICESat) and its sole onboard instrument, the Geosciences Laser Altimeter System (GLAS) has been an active area of research in recent years, specifically in temperate and boreal forests (i.e., Ranson *et al.*, 2004a; 2004b; Lefsky *et al.*, 2005; Lefsky *et al.*, 2007; Duong *et al.*, 2008; Neuenschwander *et al.*, 2008; Rosette *et al.*, 2008; Sun *et al.*, 2008; Pang *et al.*, 2008; Chen, 2010; Duncanson *et al.*, 2010), but has been insufficiently explored for ecological research in savannah ecosystems (Levick and Rogers, 2008). Canopy height is one of the leading dimensions of ecological variations among tree species (Westoby *et al.*, 2002) and is central to ecosystem function (Moles *et al.*, 2009).

The main purpose of this research project is to assess firstly the ability of ICESat-GLAS LiDAR full waveforms to retrieve the vertical canopy structure for characterizing canopy structure over savannah vegetation landscapes in Kruger National Park in South Africa. This helps to derive structural indices for savannah landscapes in order to understand the landscape dynamics, which has great implications for land management. Furthermore, the anticipation of ICESat-1 follow-on mission ICESat-2, which is currently being studied by NASA, provides an important prospect for exploring changes in woody vegetation cover over time with the measuring of the three-dimensional structure of ground and vegetation surfaces. For the ICESat-2, the planned mission is a footprint size of approximately 50 m and a sampling rate of 50 Hz with 140 m long track spacing. This will improve mapping of forest heights and biomass as the areas between tracks are filled in and the spatial density of observations increases (Abdalati *et al.*, 2010). However, the vegetation science community desires smaller footprint size and higher sampling rate (i.e. 25 m and 240 Hz) in order to enhance monitoring of the structural changes in woody vegetation over large spatial areas and hence establish the role of disturbance factors in altering the heterogeneity of savannah systems. This would improve understanding of where structural changes occur spatially and how this could help clarify the differential effects of disturbance factors such as fire, aridity, and large herbivores on vegetation structure (Levick and Rogers, 2008).

The outcome of this research will provide an important source of knowledge for the South Africa National Parks (SANParks) Authority and also provide the land managers with a powerful tool for mapping and monitoring the woody vegetation structure of savannah landscapes, which can contribute towards the biodiversity management goals of SANParks and the better management of the national parks.

## **1.2 Vegetation habitat structure and savannah vegetation structure**

Quantifying savannah structure is an important component of understanding savannah ecosystems. Horizontal and vertical diversity are two important components of vegetation habitat structure. Horizontal diversity refers to the complexity of the arrangement of vegetative communities and other habitats. In other words, the greater the range of size classes present, the greater the potential that more plant and animal species will be present. Vertical diversity refers to the extent to which plants are layered within a stand. The level of layering is determined by three elements. The first one is by the arrangement of growth forms of trees, vines, herbs, shrubs, mosses and lichens. The second one is by the distribution of different tree species having different heights and crown characteristics; and the third is by trees of different ages of the same species. The degree to which vertical structure varies within the stand determines the level of vertical diversity. Hence, the number of species (species richness) that occupy a given forest habitat is the mixture of its horizontal and vertical diversities (DeGraaf *et al.*, 2006).

Structural diversity may be applied to a wide array of spatial scales, ranging from the architectural structure of a single tree to community vegetation patterns in the horizontal and vertical plane or mosaic patches on a landscape scale (Tews *et al.*, 2004). Species diversity and structural diversity are closely inter-linked. Indeed, a study by Huang *et al.* (2003) has revealed that species richness was significantly associated with forest structure, which is comprised of stand density, diameter size, and size distribution attributes, and species composition of tropical forest habitats. In arid and semi-arid savannah, structural diversity is largely determined by woody vegetation. Both solitary trees and shrub individuals or patches are key components in savannah landscapes (Tews *et al.*, 2004).

Savannah ecosystems can be defined as heterogeneous environments driven by a wide range of interacting factors (Scholes and Archer, 1997); therefore, the structure of savannah vegetation is influenced by the interactions of several drivers including climate, resource availability, competition, fire, and grazing, which occur at various spatial and temporal scales (Scholes and Archer, 1997). In other words, savannah structure is determined by the availability of the resources, such as water and nutrients; disturbance regimes such as fire and herbivory (Scholes and Archer, 1997; Pickett *et al.*, 2003).

The proportion between trees and grasses in savannah ecosystems has shifted over time, governed by natural and anthropogenic disturbance (Fahrig and Merriam, 1985). Human activity causes the major environmental changes in most parts of African savannah ecosystems either directly as wood cutters and farmers, or indirectly through their ability to operate fire and to influence herbivore numbers and distribution, both by managing domestic animals and by hunting (Frost *et al.*, 1986). However, a study by Sankaran *et al.* (2005) revealed that water is the primary driver of the vegetation structure and ecological stability in Southern African savannahs. Rainfall amount determines grass biomass productivity, fuel load and hence fire frequency, which affects mortality and establishment of trees and grasses (Tews *et al.*, 2004). These findings provide insights into the nature of savannah in Africa and suggest that changes in precipitation in the future may significantly affect savannah dynamics and distribution (Sankaran *et al.*, 2005).

The variability in these ecosystems presents challenges to their management and conservation (Levick and Rogers, 2008). The mechanisms that permit trees and grasses

to coexist without displacing each other, and the driving factors that determine the relative proportions of woody and herbaceous components across different savannah ecosystems are still unclear and have been a vital field of research in biogeography and ecology for decades (Scholes and Archer, 1997; House *et al.*, 2003). The majority of these studies explain the persistence of tree-grass mixtures in savannah ecosystems thus far, but perceptions vary on whether the number of interactions that characterize savannah ecosystems result in a tree-grass coexistence that is ‘stable’ or ‘unstable’ (Scholes and Archer, 1997).

Generally, the suggested explanations for the coexistence of both trees and grasses in savannah systems fall into two categories (Sankaran *et al.*, 2005). The first one is the explanation of the competition-based models, which emphasizes the fundamental role of competitive interactions in promoting the coexistence of both tree and grasses. Competition-based models are predicated on classic niche-separation mechanisms of the persistence of both trees and grasses, and invoke variances in the potential of resource acquisition of trees and grasses as the main process characterizing savannah communities (Walter, 1971; Walker *et al.*, 1981; Eagleson and Segarra 1985; Eagleson, 1989; Langevelde *et al.*, 2003; Fernandez-Illescas and Rodriguez-Iturbe, 2003). In these models, coexistence is due to spatial and/or temporal niche variations between trees and grasses that serve to concentrate the competition of intra-relative to inter-life form (Chesson and Huntley, 1997; Chesson, 2000; Amarasekare, 2003).

The second explanation is focused on the limiting roles of demographic bottlenecks to tree establishment and existence in savannah ecosystems. Demographic bottleneck model explanations argue that the fundamental existence of trees in savannah is

demographic and not competitive in nature (Higgins *et al.*, 2000). Therefore, the coexistence of both trees and grasses in savannah is because of climatic variability and/or disturbance factors such as grazing and fire, which determine successful tree seedling germination, establishment, and/or evolution to mature size classes (Menaut *et al.*, 1990; Hochberg *et al.*, 1994; Jeltsch *et al.*, 2000; Higgins *et al.*, 2000; Van Wijk and Iturbe, 2002).

Indeed, ecologists continue to debate the validity of these two patterns in an attempt to resolve the ‘savannah question’ (Scholes and Archer, 1997; Higgins *et al.*, 2000; Jeltsch *et al.*, 2000). In the recent years, demographic bottleneck models of tree-grass coexistence in savannahs have gained favour over competition-based models (Scholes and Archer, 1997; Higgins *et al.*, 2000; Jeltsch *et al.*, 2000; van Wijk and Iturbe, 2002). However, ecologists still seek additional explanations of savannah mechanisms (Jeltsch *et al.*, 2000). Therefore, understanding the drivers that have the potential to severely alter the vegetation structure in savannah ecosystems is essential to successful management and conservation of those ecosystems (Levick and Rogers, 2008).

Broadly, vegetation canopies have three-dimensional elements, which are length, width, and depth. Therefore, in order to understand the relationship between structural and compositional diversity, vegetation canopies should be described as three-dimensional surfaces (Rotenberry and Wines, 1980). Recently, it has been evident that measuring the horizontal structure alone is insufficient to characterize the impacts of land cover change on structural diversity (Trzcinski *et al.*, 1999). Sufficient consideration of both dimensions simultaneously is lacking (Rotenberry and Wines, 1980). Vegetation structure can be estimated by using three types of measurements: canopy height, crown

canopy cover and biomass distribution (Rotenberry and Wines, 1980). Crown canopy cover is an important predictor of biodiversity (Trzcinski *et al.*, 1999).

### **1.3 LiDAR remote sensing for vegetation structure**

Generally, measurements of vegetation canopy structure are made by developing empirical relationships between field-derived measurements of the biophysical variables and the intensity of the return signal from remote sensing sensors. However, many remote sensing techniques are not ideally suitable for measuring forest canopy structure in the vertical dimension (Harding *et al.*, 2001). This is particularly true in forests that are older or structurally complex or have closed canopies when using passive remote sensing techniques (Steininger, 1996; Treuhaft and Siqueira, 2000; Bebi *et al.*, 2001).

The signal from passive sensors is dominated by the upper layers of vegetation canopies, and very little solar radiation reaches the surface under the canopies and is returned to the sensor. This makes it difficult for these techniques to provide a vertical dimension for the vegetation canopy structure. Unlike passive sensors, active sensors offer a promise of measuring vegetation canopy structure in all vegetation types and uniquely have the ability to provide measurements of vertical structure (Lefsky *et al.*, 1999a; Lefsky *et al.*, 2002; Drake *et al.*, 2003).

Light detection and ranging (LiDAR) technology is an active remote sensing technique which uses precise spatial location and the two way travel time of laser light pulses to produce a highly accurate representation of the targeted ground area, with a capability of simultaneously mapping the Earth surface and overlying features (Means *et al.*, 2000).

Today, LiDAR technology, which until recently has been limited to airborne systems, is the most promising sensor for remote sensing estimation of forest attributes (Lefsky *et al.*, 1999a,b; Lefsky *et al.*, 2002; Drake *et al.*, 2003; Patenaude *et al.*, 2004). Studies have proved that aircraft LiDAR has the capability to measure forest height with high accuracy and that vegetation structure, biomass and other vegetation canopy attributes can be estimated (Lefsky *et al.*, 1999 a, b; Nelson *et al.*, 1997; Means *et al.*, 2000). The success of airborne LiDAR in vegetation environments such as VCL (Vegetation Canopy LiDAR) and LVIS (Laser Vegetation Imaging Sensor) has ultimately led to the implementation of a spaceborne LiDAR mission for vegetation studies (Blair *et al.*, 1999; Hese *et al.*, 2005). These advanced systems record a full vertical profile of data in the vegetation within small sized, medium sized and large sized footprints (Duong *et al.*, 2008).

In January 2003, the Ice, Cloud and land Elevation Satellite spaceborne laser altimeter system (ICESat) was launched with the main objectives to measure polar ice sheet elevation change, aerosol properties and atmospheric profiles, land topography profiles, and height of vegetation canopies (Zwally *et al.*, 2002). These aims are accomplished through the use of the Geosciences Laser Altimeter System (GLAS) which acquires elevation waveform profiles of the entire earth (Zwally *et al.*, 2002). Waveform LiDAR has been used successfully in defining many forest attributes such as canopy height and structure (Harding *et al.*, 2001; Goetz *et al.*, 2007).

#### **1.4 LiDAR in vegetation ecosystems and wildlife applications**

LiDAR technologies in vegetation applications have been successfully used to estimate many vegetation parameters such as canopy height, biomass, canopy density and basal

area (Nilsson, 1996; Nelson, 1997; Lefsky *et al.*, 2002a). Airborne small footprint LiDAR systems have been effectively used in forest inventory and topographic mapping; while spaceborne large footprint LiDAR systems, which cover large areas, have explicated very promising results in forest parameters estimation (Yong and Zengyuan, 2004). Furthermore, despite the complexity of tropical forests, the potential of full waveform LiDAR to estimate the tropical forest attributes is evident (Lim *et al.*, 2003).

LiDAR data have also been used to classify species communities. The work of Douglas (2004) has shown that discriminate analysis can successfully separate pines and mature hardwood in the south-eastern United States, based on the density and intensity of LiDAR returns, with an overall accuracy rate of 72 %. Another study using LiDAR as a predictive tool that helps in creating distribution models that are based on what is known about species preferences was conducted by Nelson *et al.* (2005); they realised that the Delmarva fox squirrel was endemic to older forested stands with closed canopies and open understories. Using this knowledge with LiDAR analysis has successfully improved identification of potential habitat based on height of canopies derived from LiDAR data.

There have been comparatively few studies regarding the airborne LiDAR data in the field of savannah mapping (Levick and Rogers, 2008). However, most conducted research regarding ICESat-GLAS has been in temperate and boreal forests (i.e., Ranson *et al.*, 2004; Lefsky *et al.*, 2005a; Lefsky *et al.*, 2007; Duong *et al.*, 2008; Neuenschwander *et al.*, 2008; Rosette *et al.*, 2008a; Sun *et al.*, 2008; Pang *et al.*, 2008; Chen, 2010b; Duncanson *et al.*, 2010). Therefore, the goal of this research is to evaluate

the use of ICESat-GLAS LiDAR data for characterizing savannah vegetation structure in Kruger National Park in South Africa.

### **1.5 Aim and objectives**

In summary, savannahs are globally important but not well understood ecosystems. They are heterogeneous in their floristic and structural composition. The recent development in LiDAR remote sensing technology offers opportunities to better understand the structure of savannah habitats. The main aim of this research is to evaluate the potential of ICESat-GLAS to estimate vertical canopy structure over savannah landscapes for characterizing savannah vegetation landscapes in Kruger National Park in South Africa.

In order to achieve this, the research objectives are:

1. To investigate the accuracy of the level 2 altimetry product in comparison to reference data.
2. To investigate the GLAS footprint in details by conducting a field study to ascertain the potential of GLAS full waveforms for studying savannah structure in Kruger National Park (KNP).
3. To develop and evaluate methods for deriving vegetation structure parameters from large GLAS footprints LiDAR waveforms which account for the discrepancies in canopy height estimation.
4. To evaluate estimated GLAS waveform parameters using field measurements, airborne LiDAR acquired by the University of Witwatersrand (WITS), and from spaceborne Synthetic Aperture Radar ALOS PALSAR (SAR) provided by Japanese Aerospace Exploration Agency (JAXA) via the European Space Agency (ESA).

This research seeks to provide an important source of knowledge for the South Africa National Parks (SANParks) Authority, and also provides the researchers, decision makers, stakeholders and land managers with a powerful tool for an adequate spatially-consistent monitoring and assessment of mapping and monitoring the woody vegetation structure of savannah landscapes, which can contribute towards the biodiversity management goals of SANParks.

## **1.6 Summary**

This thesis is divided into several self-contained chapters, each of which describes a particular aspect of the research study. Taking in account the importance of vegetation height as a significant forest variable that can provide information relating to the vegetation structure, and also the demands to knowing its accurate quantification and understanding, the spaceborne GLAS satellite with its accuracy and global coverage could help in providing an appropriate benchmark for estimating vegetation height and its related vegetated structure. The overall research aim is to evaluate the potential of ICESat-GLAS to estimate vertical canopy structure over a savannah landscape. This can be broken down into more specific research objectives and associated research questions of this research project applicable to each chapter.

Chapter 2 provides a review of relevant literature, including an overview of the state of the art regarding LiDAR remote sensing of vegetation. Chapter 3 gives a description of the study area, datasets and the broad methodology, including the methodology that developed to address specific research questions described within the associated sections, Chapters 4-5. In order to evaluate the accuracy and the precision of height estimates and woody cover estimates that can be obtained using the ICESat full waveform system, the topic of validation and comparison is studied in Chapters 4 and 5.

In Chapter 4 two methods to extract canopy height from GLAS data have been applied over terrain with different ruggedness and hence developed further; and tests methods of estimating canopy height from within large GLAS footprint LiDAR waveforms with airborne LiDAR data have been applied. Chapter 5 compares the performance of spaceborne LiDAR in extracting the woody vegetation and comparing the results with ALOS PALSAR. Chapter 6 summarises and discusses the results of using GLAS data with the comparison with airborne LiDAR and RADAR data to retrieve savannah vegetation structure. Chapter 7 presents the thesis conclusions with the key findings of the research study. It will also discuss whether these successfully achieve the research objectives; and any limitations of this undertaking will be addressed, and the possibilities of further research will be highlighted.

# CHAPTER TWO

## LITERATURE REVIEW

### 2.1 Introduction

Light Amplification by Stimulated Emission of Radiation (LASER) is a device that transmits a pulse of light towards a target and records the elapsed time between the transmitted laser pulse to the target and its return. This provides the range between sensor and target through a technology known as Light Detection and Ranging (LiDAR) (Wehr and Lohr, 1999). LiDAR systems are active laser remote sensors as they emit their own radiation (Wehr and Lohr, 1999). Modern LiDAR systems provide the ability to acquire very accurate third-dimensional surface images of the world, and have a variety of applications such as locating and mapping buildings in urban environments (Lichti *et al.*, 2002), creating highly accurate hydrological maps (Colson, 2006), and characterization of vegetation structure in forestry and ecology (Edwards *et al.*, 2002; Song and Woodcock, 2003; Wang *et al.*, 2004). Moreover, several studies have shown the potential use of airborne and spaceborne data to map vegetation height, estimating above ground biomass and extracting other vegetation structure parameters (Lefsky *et al.*, 1999a; 1999b; 2002a; 2002b; 2005a; Harding *et al.*, 2001; 2005; Drake *et al.*, 2002; 2003a; 2003b; Patenaude *et al.*, 2004; Anderson *et al.*, 2006; 2008; Popescu, 2007; Chen *et al.*, 2007; Rosette *et al.*, 2008a; 2008b; Pang *et al.*, 2008; Popescu and Zhao, 2008; and Chen, 2010b).

This chapter presents an overview of the hypotheses of tree-grass coexistence in savannah ecosystems and their remote sensing studies. The next section involves the historical context of LiDAR remote sensing. A full description of the principles common to LASER airborne and spaceborne sensors used within this research is

introduced. An overview of LiDAR sensors and their types is given. Moreover, types of LiDAR observation systems related to vegetation applications are described. Then, the spaceborne ICESat mission is described in more detail. Last but not least, an overview of LiDAR applications for vegetation applications is presented; and finally, conclusions are stated at the end of this chapter.

## **2.2 Savannah ecosystems and remote sensing**

Savannah ecosystems are heterogeneous systems consisting of the coexistence of woody and herbaceous plant functional types (Scholes and Archer 1997). Their relative proportion defines different savannah types including shrublands; open canopy savannah with a dominating grass layer and few scattered trees; mosaic savannah with tree clumps; savannah with a mixture of grass, shrubs and trees; closed canopy savannah; and woodlands (Scholes and Walker 1993; Solbrig *et al.*, 1996). It presents high variability in terms of biodiversity, climate as well as the degree of tree cover; and depends strongly on the features that are taken into account (Schultz, 2000). Savannah ecosystems occupy about 1/6 of the earth land surfaces (see Figure 2.1) and account for about 30% of the global terrestrial vegetation productivity (Grace *et al.*, 2006). In the African savannah, savannah biome is estimated to occupy 46% of southern Africa and over one third of South Africa, making it the largest biome in southern Africa (Low and Rebelo, 1996; House *et al.*, 2003).

For many years, the coexistence of two very different vegetation types (tree and grass), and what mechanisms determine the proportions of each, has been a central question in savannah ecology (Scholes and Archer, 1997). Walter (1971) suggested the idea that trees and grasses exploit different rooting niches, so the grasses use superficial soil layers and trees use deeper layers.

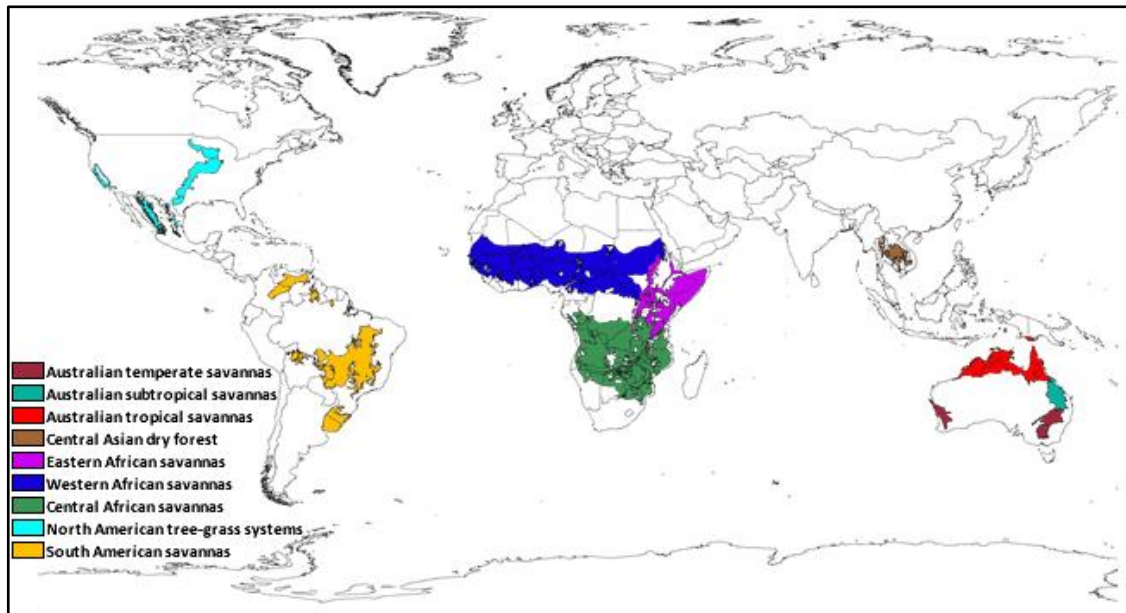


Figure 2.1: Global distribution of savannah ecosystems (tree-grass) derived from the Olson Ecoregions of the world (Olson *et al.*, 2001).

Walter's theory was developed as an analytical model as the root-niche separation hypothesis (NSH) by Walker and Noy-Meir (1982) and has since become widely accepted as the central paradigm for tree-grass interactions in savannah (Polley, 1997). However, Higgins *et al.* (2000) proposed a different hypothesis of the mechanism of the coexistence of trees and grasses. They argued that the critical problem for savannah trees is demographic in nature. Seedlings seldom grow because of frequent droughts and competition with grasses. If they do establish successfully, juvenile plants are burnt by frequent grass fires. Fires kill stems, preventing juvenile plants from escaping to mature size classes. Trees can persist if, firstly, both rainfall and the severity of fires are sufficiently variable to allow occasional opportunity for successful growth to maturity; and secondly, mature trees live long enough to straddle these rare recruitment events. This hypothesis is referred as the demographic bottleneck hypothesis (DBH) of tree-grass coexistence. However, ecologists still seek additional explanations of savannah mechanisms (Jeltsch *et al.*, 2000). Therefore, understanding the drivers that have the potential to severely alter the vegetation structure in savannah ecosystems is essential to

successful management and conservation of those ecosystems (Levick and Rogers, 2008).

The structure of savannah and its dynamics are influenced by many drivers that shaped the vegetation structure and composition. These drivers are divided into primary and secondary determinations. The first one could be available nutrients, available plant moisture, soil types and geographical gradients. These factors influence the vegetation structural composition and vary spatially at both regional and local scales (Tews *et al.*, 2004). A study by Sankaran *et al.* (2005) revealed that water is the primary driver of the vegetation structure and ecological stability in Southern African savannahs. Rainfall amount determines grass biomass productivity, fuel load and hence fire frequency, which affects mortality and establishment of trees and grasses. These findings provide insights into the nature of savannah in Africa and suggest that changes in precipitation in the future may significantly affect savannah dynamics and distribution (Sankaran *et al.*, 2005). The second drivers, secondary determinants, can be fire or herbivores. These drivers have played important historical and evolutionary roles in shaping African savannah by influencing the morphological and physiological traits of savannah vegetation (Stebbins, 1981; Coughenour, 1985).

As can be seen, the structure and dynamics of savannahs are therefore a consequence of various disturbances acting within the constraints of the primary determinants (Mentis and Bailey, 1990). Moreover, anthropogenic process such as global climate change, population growth and its related issues of fuel wood consumption, livestock density, and agricultural over-exploitation could alter the environmental conditions and hence

affect the savannah vegetation structure and dynamic (Biggs *et al.*, 2003; Snyman and Preez, 2005)

As seen from an ecological perspective, the interaction of the abiotic factors as well as the anthropogenic processes influences the structure and dynamic of savannah ecosystems. Furthermore, knowledge about savannah environmental structure and dynamics is still insufficient (Beerling and Osbourne, 2006), particularly knowledge about the spatial distribution of savannah systems (Levick and Rogers, 2008). Therefore, an adequate spatially-consistent monitoring of this key parameter is of particular importance for biodiversity planning and conservation, and decision makers and stakeholders.

Remote sensing technologies have proved to be a key source of data for studying vegetation in savannah. Several studies have utilized passive remote sensing data to quantify woody vegetation structural parameters based on spectral evaluation of remotely sensed vegetation parameters (Baret and Guyot, 1991; Hudak and Wessman, 1998; Gong *et al.*, 2003; Yang and Prince, 2000; Mutanga and Rugege, 2006; Wessels *et al.*, 2006).

Generally, measurements of vegetation canopy structure are made by developing empirical relationships between field-derived measurements of the biophysical variables and the intensity of the return signal from remote sensing sensors. However, many remote sensing techniques are not ideally suited for measuring forest canopy structure in the vertical dimension (Harding *et al.*, 2001). This is particularly true when using passive remote sensing techniques in forests that are older or structurally complex or

have closed canopies (Steininger, 1996; Treuhaft and Siqueira, 2000; Bebi *et al.*, 2001). The signal from passive sensors is dominated by the upper layers of vegetation canopies and very little solar radiation reaches the surface under the canopies to be returned to the sensor. This makes it difficult for these techniques to provide a vertical dimension for the vegetation canopy structure. Unlike passive sensors, active sensors offer a promise of measuring vegetation canopy structure in all vegetation types and uniquely have the ability to provide measurements of vertical structure (Lefsky *et al.*, 1999a; Lefsky *et al.*, 2002; Drake *et al.*, 2003).

Light detection and ranging (LiDAR) technology is an active remote sensing technique that uses precise spatial location and the two way travel time of laser light pulses to produce a highly accurate representation of the targeted ground area with a capability of simultaneously mapping the Earth's surface and overlying features (Means *et al.*, 2000).

Since savannah ecosystems are known to have a wide range of highly specialized woody cover structure (Solbrig *et al.*, 1996) and this has been noted during the field data collection, they offer a challenge of an altogether different magnitude for new remote sensing techniques (Nagendra, 2001). Due in part of this challenging complexity, the use of passive and active remote sensing in tropical grasslands has largely been limited to studies of fire in savannah systems (i.e., Alleaume, 2005 and Roy *et al.*, 2005), additionally, most conducted studies of temporal change in savannahs have employed the use of satellite images or black and white aerial photography, while these methods are useful for investigating changes in woody cover over time, they are not able to portray the three-dimensional structure of vegetation cover.

Today, LiDAR technology, which until recently has been limited to airborne systems, is the most promising sensor for remote sensing estimation of forest attributes (Lefsky *et al.*, 1999a, b; Lefsky *et al.*, 2002b; Drake *et al.*, 2003a; Patenaude *et al.*, 2004). Studies have proved that aircraft LiDAR has the capability to measure forest height with high accuracy and that vegetation structure, biomass and other vegetation canopy attributes can be estimated (Lefsky *et al.*, 1999a, b; Nelson *et al.*, 1997; Means *et al.*, 2000). The success of airborne LiDAR in vegetation environments such as VCL and LVIS, has ultimately led to the implementation of a spaceborne LiDAR mission for vegetation studies (Blair *et al.*, 1999; Hese *et al.*, 2005).

Besides the LiDAR technology, active systems such as RADAR (RADIo Detection And Ranging) systems have shown great potential for monitoring and mapping a wide range of surface and vegetation characteristics in a synoptic, continuous fashion (Kasischke, *et al.*, 1997). The first attempt to address this was made by Harrel *et al.* (1997); this resulted in quantitative vegetation mapping, which referred to the relationship of the intensity channels of a polarimetric SAR to biophysical variables, particularly, the cross-polarized L-Band channel, which proved to be useful. Most of these studies that used advance polarimetric algorithms focused on different cover types of forests (i.e. Thiel *et al.*, 2007) or land-cover classification (i.e. Lee *et al.*, 1994), and few studies used the polarimetric parameters for quantitative assessments of vegetation structural attributes (i.e., Garestier *et al.*, 2009). The study of Garestier *et al.* (2009) revealed a clear linear correlation between the anisotropy parameter in L- and P-bands and the mean tree height. Few studies have used SAR in the savannah environment, for example, the insensitive studies in the Australian savannah woodland and open forest environment of Queensland by Lucas *et al.* (2004, 2006a, 2006b, 2006c and 2009),

which related SAR polarimetric intensity channels to vegetation parameters. These investigations revealed that the C-HV channel was suitable for mapping leaf and small branch biomass, and the L-HV and L-HH channels were sensitive to the trunk and large branch biomass (Lucas *et al.*, 2004).

Moreover, Lucas *et al.* (2006c) showed that the L-HH channel interacted primarily with the trunks and secondarily with volume elements (mainly large branches). Significant contribution of the backscattering signal in the L-HV channel arose from all volume components of the model commensurately (branches, leaves, and understory vegetation). Ground-trunk and the direct ground scattering contributed less compared to L-HH but more than L-HV. A result from the previous studies shows that L-band (especially HH- and HV-polarisation) operates as a complementary component in mapping vegetation structure since it provides information at later growth stages, due to ground-trunk interactions (Lucas *et al.*, 2006c). The above mentioned study dealt with RADAR airborne imagery. A more recent study by Lucas *et al.* (2009) used Advanced Land Observing Satellite (ALOS) Phased-Array L-band SAR (PALSAR) for biomass mapping in open forests. This study achieved  $R^2$  of 0.48 compared to field data for a large scale biomass map of the whole Queensland area, which enabled important insights into the backscattering behaviour of open forests. Moreover, other recent studies by Collins *et al.* (2009) in the Northern Territory of Australia showed possible potential with regard to vegetation structure assessments in open forests. It mapped the Wildman River Reserve with  $R^2$  of 0.92 using the SAR backscatter which was strongly related to the biomass of the vegetation.

The resultant data from both LiDAR and RADAR opened a new door in landscape ecology. The ICESat-GLAS footprints do not cover the whole park but allow an insight for different areas by several square kilometres. Furthermore, airborne LiDAR and ALOS PALSAR data could therefore be used to identify and resolve remaining ICESat processing issues for better estimating of vegetation structure parameters from LiDAR spaceborne. It is therefore very valuable to make comparison of these data to data from spaceborne techniques.

### **2.3 LiDAR and LASER altimetry background**

LiDAR technology has been one of the greatest scientific developments of the twentieth century. It was developed over 40 years ago and still a symbol of high technology. In 1917, Albert Einstein developed the foundation of stimulated emission of radiation which illustrated that atoms can absorb and emit radiation spontaneously and that atoms in certain excited states can be induced to emit radiation. Forty years after Einstein's theory, the concept of his theoretical work on stimulated emission was used only in theoretical discussions and had little relevant empirical work. The American physicist Charles.H.Townes developed the first successful stimulated emission device, called "MASER" – Microwave amplification by the stimulated emission of radiation - which produced a coherent beam of microwaves. In 1960 and following the laser invention race at that time, Theodore. H. Maiman developed the first ruby laser, which is considered a good example of what a laser is expected to be. It emits coherent waves in short pulses in a concentrated beam of light. However, during the 1970s and 1980s, laser altimetry was developed and used in airborne instruments by NASA and the first commercial laser systems started to appear in the mid 1990s (Danson, 1995; Wehr *et al.*, 1999). The development of laser technology for the NASA airborne systems

enabled the use of LiDAR methods and techniques later used by spaceborne altimeter systems. The first global scale laser altimeter dataset was provided in 1996-1997 by the Shuttle Laser Altimeter (SLA; Garvin *et al.*, 1998). In 1997, the Mars Orbiter Laser Altimeter (MOLA), part of the Mars Global Surveyor mission, made its first pass across the surface of Mars and generated measurements of topographic profiles, surface reflectivity, roughness and change (Smith *et al.*, 1998). The next space-based Laser system was the Geoscience Laser Altimeter System (GLAS), an instrument carried on the Ice, Cloud and Land elevation satellite (ICESat), which launched in January 2003.

Even though LiDAR is a new technology, its application to vegetation mapping and topographic mapping issues is already well established. The use of spaceborne LiDAR data and technology has only begun to be significantly utilized in the last seven years to improve our interpretation of the Earth and the global environmental changes that combine and contribute to shape it. Therefore, LiDAR systems and associated technologies will improve our understanding of the 3D distribution of Earth features and offer a great potential for further applications of LiDAR data.

#### **2.4 The principles of operation of a laser scanning system**

The fundamental concept of Light Detecting And Ranging (LiDAR) or Laser altimetry technology involves transmitting pulses of laser light towards the ground and measuring the time of pulse return; hence, distance can be calculated by taking the product of speed of light and the time required for an emitted laser to travel to a target object (see Figure 2.2) (Wehr *et al.*, 1999). There are two techniques to measure the elapsed time from when a laser is emitted from a sensor and intercepts an object: pulsed ranging and continuous wave ranging. The technique of interest in this research utilizes pulsed ranging, which the majority of LiDAR systems used by recording the travel time of a

laser pulse from a sensor to a target object. The travelling time of a pulse of light,  $t$ , is (Boland *et al.*, 2004):

$$t = 2 \frac{z}{c} \quad (2.1)$$

Where:  $z$  is the distance between the instrument and the object and  $c$  the speed of light ( $3 \times 10^8 \text{ m s}^{-1}$ ).

Generally speaking, the LiDAR instrument consists of a system controller, a laser transmitter module, and a receiver telescope. The pulse transmitter generates a short laser pulse of 1064 nm wavelength. The backscattered return signal from the target surface is recorded by the receiver telescope and filtered by a band pass to improve the signal noise ratio, which is spread by the interaction with the intercepted object. The return signal is digitally sampled as a function of time at an interval of at least 1 nanosecond and saved in the data storage module.

This type of return signal is called the full waveform signal and is of interest for this research. Moreover, additional information of the system is obtained, such as platform altitude and position, scanning angle, and time stamps of transmitted laser pulse and returning full waveform signal. The full waveform is then processed and georeferenced to compute multiple elevations together with other parameters like amplitude and pulse width (Duong, 2010).

A laser system acquires data by scanning either along or across the flight direction. In an aircraft system, the long track footprint spacing is determined by the laser pulse repetition rate, the aircraft ground speed, the number of cross track footprints and the pitch information (Duong, 2010). However, airborne and spaceborne systems have

significant differences such as footprint size, altitude operation, spatial coverage, scanning pattern, and scanning angle (Duong, 2010). This will be described in the next section.

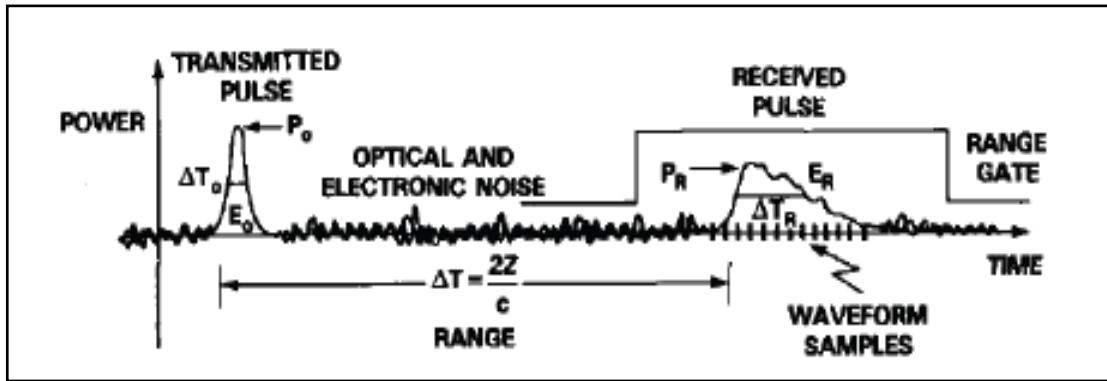


Figure 2.2: Schematic of laser pulse waveform for range measurement of a laser altimeter, copyright line © [Bufton, 1989] IEEE.

## 2.5 LiDAR sensor systems and types

The key differences among LiDAR sensors relate to the laser's power, pulse duration, repetition rate, wavelength, beam size and divergence angle, the specific of the scanning mechanism, and the information recorded for each reflected pulse. Usually, the wavelength of Lasers for terrestrial applications operates in (900–1064) nanometres, which affects the working of these wavelengths during overcast conditions due to absorption by clouds. Bathymetric LiDAR systems, which are used to measure elevation under shallow water bodies, use the wavelengths near 532 nanometres for better penetration of water bodies. However, earlier LiDAR sensors were profiling systems which record observations along a single narrow transect, while most current LiDAR systems work in a scanning mode where the orientation of the laser illumination and receiver field of view is directed from side to side by a rotating mirror, which provides a cross track sampling for the generation of three-dimensional datasets (Wehr *et al.*, 1999 ).

The intensity of the return signal depends on several factors: the fraction of the laser pulse that is intercepted by a surface; the fraction of reflected illumination that travels in the direction of the sensor; the total power of the transmitted pulse; and the reflectance of the intercepted surface at the laser's wavelength. Returned signal that intercepts a morphologically complex surface, such as a vegetation canopy, will be a complex combination of energy returned from surfaces at various distances which are represented later in the reflected signal. The type of information that is collected from the returned signal is divided into two categories of sensor systems: Discrete return LiDAR sensor systems and Waveform recording sensor systems (Wehr *et al.*, 1999).

## **2.6 Types of LiDAR observation systems**

This section focuses on large footprint; full waveform satellite LiDAR system of interest of this project though also incorporates a comparison with small footprint, discrete return airborne LiDAR system. The main characteristics of these different systems are outlined below.

### **2.6.1 Discrete return LiDAR system**

Discrete return LiDAR data are one of the most intuitive forms of LiDAR data available, and have been used in many applications such as generating digital terrain models, forest mapping, archaeology and 3D city modelling (Duong, 2010). In this type of laser scanning system, the laser scanner devices are carried on board helicopter or airplane platforms which produce a dense coverage of small footprints that can be characterized as clouds of points, with each point having a three-dimensional coordinate describing its spatial relation with the sensor (Lewis, 2010).

Most modern LiDAR systems (Figure 2.3) consist of three basic components: the laser scanner, a Global Positioning System (GPS), and the Inertial Measurement Unit (IMU).

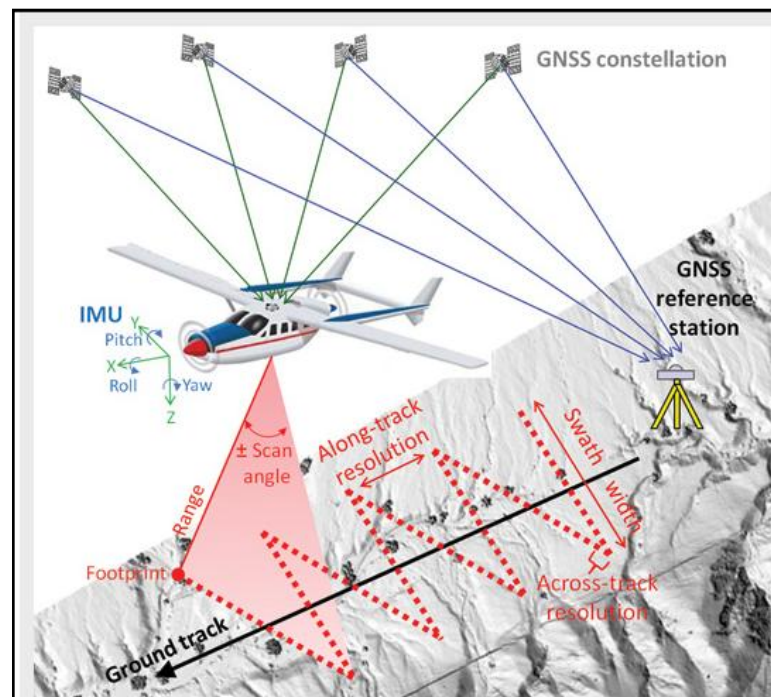


Figure 2.3: The basics of airborne mapping LiDAR. Source: (Imaging Notes Magazine website, 2011).

As already mentioned, discrete return LiDAR systems typically record one to several returns for each pulse in a vertically non-systematic method (Figure 2.4) (Lim *et al.*, 2003). The criterion for collecting multiple returns depends on the intensity of the laser energy returned to the sensor. The footprints of discrete return LiDAR are small and typically vary from 20–80 cm in diameter due to the function of beam divergence, instantaneous scan angle, and flight altitude (Baltavias, 1999); and, in most commercial discrete return LiDAR systems, the range measurements resolution is about 2–3.5m (Ussyshkin and Theriault, 2011).

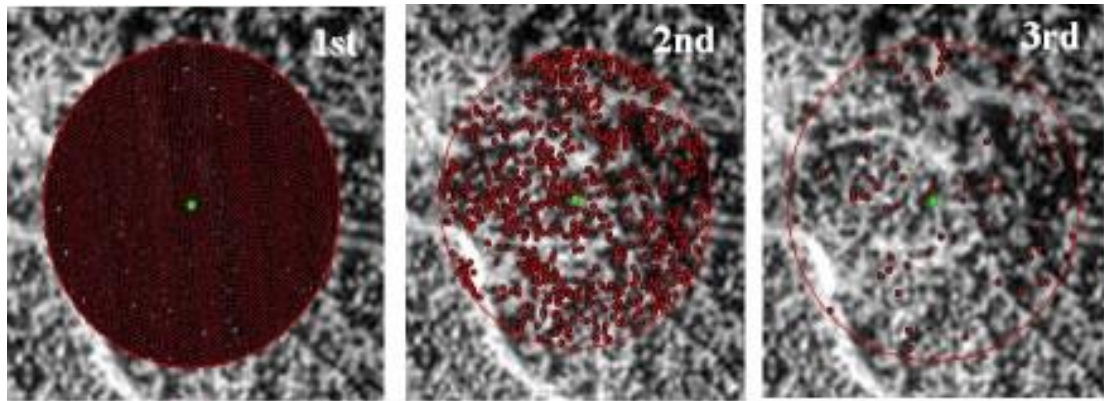


Figure 2.4: Example of LiDAR sensor systems that records first, second and third returns obtained from within a pulse. Source: (University of Idaho website, 2006).

The LiDAR data points that are recorded by discrete LiDAR systems are irregularly spaced with quite large pulse densities (0.3 to 12 pulses/m<sup>2</sup>). The sparse spacing allows for higher flying altitudes, which reduces the acquisition cost. However, the optimum range of pulse densities is pointed by application (i.e., for vegetation application 4 – 6 pulses/m<sup>2</sup> is good for both the acquisition cost and support of application (Evans *et al.*, 2009).

LiDAR point cloud datasets are filtered or classified through special commercial software used by LiDAR vendors to separate ground from non-ground returns in order to generate a ground surface model (Digital Elevation Model) (Baltavias, 1999, Evans *et al.*, 2009). For vegetation application, LiDAR dataset can be classified into ground points and canopy returns above the ground points, and hence interpolate these points to a regular, re-sampled grid that indicates the percentage of LiDAR points in the vegetation in comparison to those that hit the ground (Zhang *et al.*, 2004). However, interpolation can have some uncertainty due to the significant variation between the forms of Digital Terrain Model and Digital Surface Model which is created using different interpolation algorithms on laser scanning data (Smith *et al.*, 2003b).

Most commercial discrete return systems feature high spatial resolution with small diameter of their footprints and high repetition pulse rates (as high as 33,000 points per second), which provides extremely high ground point density that enables detailed mapping of ground and canopy surface topography (Flood and Gutelis, 1997). Moreover, this form of high point density LiDAR has the great advantage of the ability to aggregate the data over areas and scales specified during data analysis; thus it can provide a particular forest inventory plot, or even a single tree crown can be recorded and characterised (Flood and Gutelis, 1997). However, acquisition costs limit the wide use of this form of data (Chen *et al.*, 2011).

### **2.6.2 Full waveform systems**

Laser scanning systems are able to capture the time-varying intensity of the returned signal from each laser pulse, hence, it provides a record of the height distribution of the surfaces illuminated by the laser pulse (Harding *et al.*, 1994 ; Dubayah and Drake *et al.*, 2000 ).As a consequence, the waveform recording systems records the entire signal trace, giving the full shape of the return signal, and structural information on the vertical distribution of objects between the height levels corresponding to the first and last echo (Duong, 2010). Figure 2.5 shows the conceptual differences between the discrete return LiDAR and waveform record devices.

Laser scanning systems of this form of devices are mounted on helicopters, small or large airplanes, and satellites. The illuminated footprints vary in their size according to the difference in scanning height together with the difference in the laser systems itself (Figure 2.6). Therefore, if the footprint assumed to be circled the illuminated footprint diameter on the ground is obtained by multiplying the platform altitude to the beam divergence.

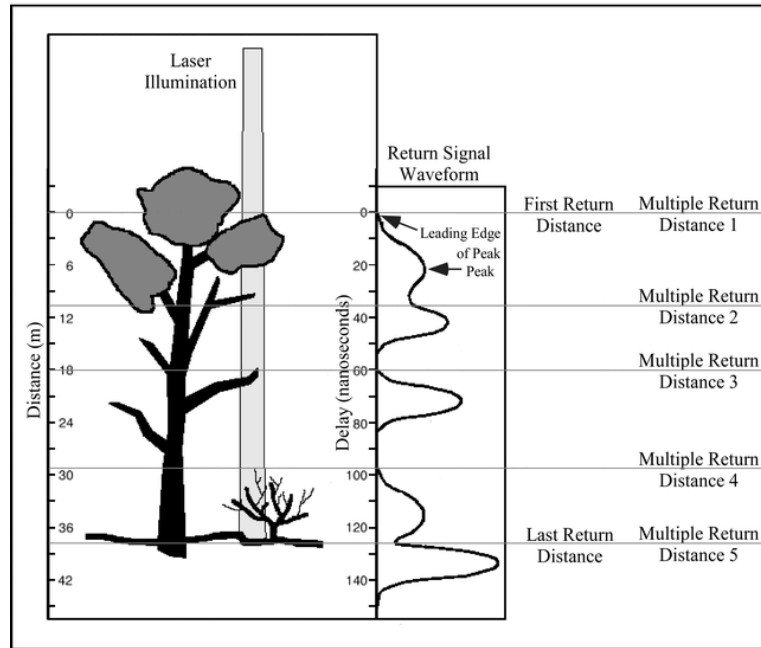


Figure 2.5: Conceptual differences between full waveform recording and discrete return LiDAR devices. On the left, Laser signal illuminates area or footprint at different height levels. The return signal as a function of time (LiDAR waveform) is collected by waveform recording device. To the right of the waveform, the first and the last return are recorded by discrete return sensor and next to this the multiple returns LiDAR records the height levels in the path of illumination (Lefsky *et al.*, 2002b).

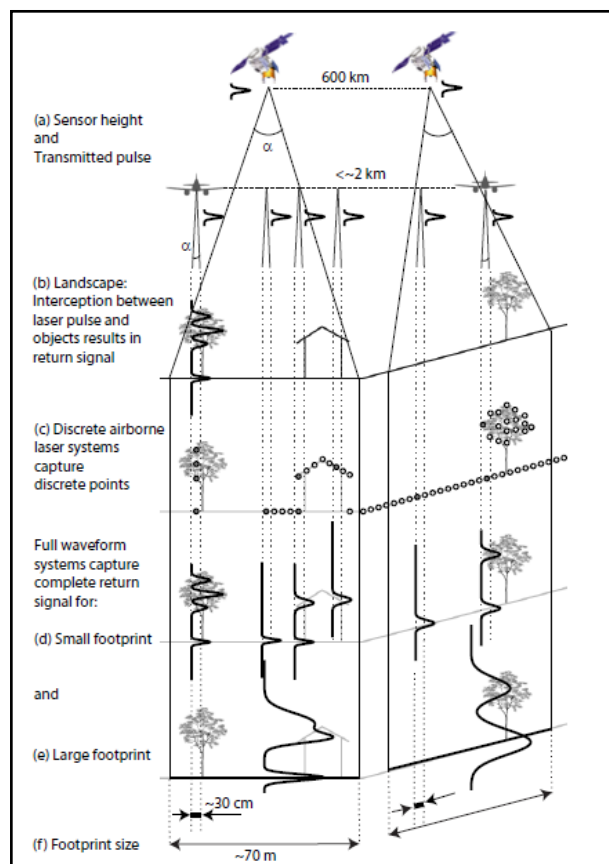


Figure 2.6: Schematic overview of full waveform and discrete laser scanning system and the resultant illuminated footprints (Duong, 2010).

For example, as illustrated in Figure 2.5 above, the footprint diameter for the Riegl airborne LiDAR system operating at altitude of 1–2 km height is between 15–30 cm, while the illuminated footprint is 70 m for the GLAS spaceborne LiDAR system which is operating at an altitude of 600 km (Duong, 2010).

Full waveform LiDAR systems follow the same principles as discrete return systems. The system samples and records the signal returned for equal time interval “bins” and, as stated above, full waveform LiDAR systems have larger footprints. This is due to signal to noise reasons. Fundamentally, the quantity of backscattered signal in a small field of view is low and the energy received per unit time bin is clearly smaller, hence, the sensor needs to be capable of recording very low signal levels faster (see Figure 2.7) (Hug *et al.*, 2004).

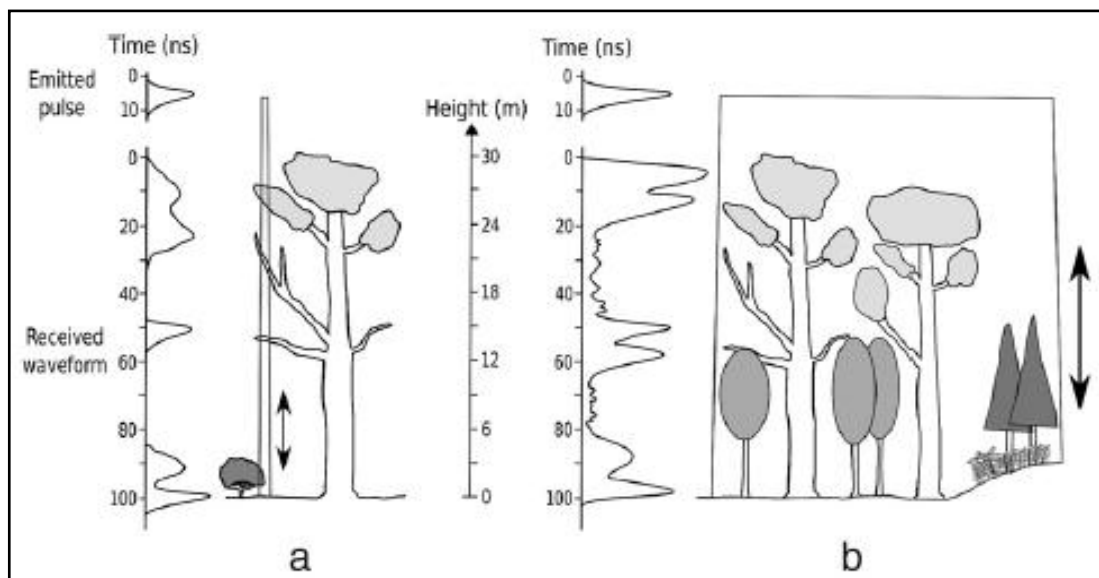


Figure 2.7: Illustration of the transmitted and received full waveform signal in a vegetated area: (a) A small footprint where all targets strongly contribute to the waveform shape LiDAR but the laser beam has a high probability of missing the ground, while in (b) A large footprint LiDAR, the last pulse is bound to be the ground but each echo is the integration of several targets at different locations and with different properties (Mallet and Bretar, 2009).

Most commercial full waveform systems have small footprints (0.2 – 3m) diameter, depending on beam divergence and flying height. They provide a high point density and an accurate altimetry description within the diffraction cone (Figure 2.7(a)). However, mapping large areas needs extensive surveys, and small footprint systems often miss recording tree tops. Therefore, it is difficult to define whether the ground has been hit under dense vegetation. Hence, ground and vegetation heights cannot be estimated properly (Dubayah and Drake, 2000).

Large footprint systems (10 – 70m diameter) enable the measurement of both ground and canopy top. They avoid the biases of small footprint systems, hence the return signal gives a record of vertical distribution of intercepted surface within a larger area (Figure 2.7 (b)) (Mallet and Bretar, 2009).

Despite the fact that the data retrieved from full waveform systems are a more useful tool in vegetation application than the data from discrete return systems, it has some drawbacks. Waveform data need greater data storage and processing capabilities than discrete return data. Moreover, full waveform data require special interpretation: basically, the data are four-dimensional (they have position and intensity), which therefore needs either (or both) imaginative methods of visualising the data or highly tuned computer-based algorithms which compress the data into forms that can be easily analysed, understood and explored operationally by the human mind (Lewis, 2010).

Spaceborne full LiDAR waveform systems have been designed and developed by NASA over the last two decades to assess the characteristics of topography, land cover and woodlands. Fundamentally, they aim to map large areas to provide global data at

resolution of several metres and a swath width up to 1-2 km, producing broad LiDAR footprints such as GLAS, sequentially along the ground track (described in the next section). Table 2.1(a, b) shows the main technical specifications for the full waveform recording systems (Mallet and Bretar, 2009).

Table 2.1(a): Main technical specifications for the full waveform recording systems, adopted from (Mallet and Bretar, 2009).

System	Company manufacturer	Platform	Beam deflection	Beginning -final year	Wavelength (nm)	Flying height (km)	Pulse rate (kHz)
<b>Bathymetric</b>							
<b>LARSEN 500</b>	Terra Surveys Optech	Airborne	Rotating mirror	1983-	1064/532	0.5	0.02
<b>MarkII</b>	LADS TopEye	Airborne	Fibers	1989-	1064/532	0.37-0.5	0.9
<b>Hawk Eye</b>	Saab Optech	Airborne	Oscillating mirror	1990-	1064/532	0.05-0.8	0.2
<b>SHOALS 1000T</b>	US army Optech	Airborne	Oscillating mirror	1994-	1064/532	0.2-0.4	0.4
<b>EAARL</b>	NASA	Airborne	Oscillating mirror	2002-	1064/532	0.3	3
<b>Experimental</b>							
<b>SLICE R</b>	NASA	Airborne	Oscillating mirror	1994-1997	1064	<8	0.075
<b>SLA-02</b>	NASA	Satellite	None	1996-1997	1064	285	0.01
<b>LVIS</b>	NASA	Airborne	Oscillating mirror	1997-	1064	<10	0.1-0.5
<b>GLAS</b>	NASA	Satellite	None	2003-2009	1064/532	600	0.04
<b>MBLA</b>	NASA/University of Maryland	Satellite	Oscillating mirror	None	1064	400	0.01/0.242
<b>Commercial</b>							
<b>LMS Q560</b>	Riegl	Airborne	Polygon	2004-	1550	<1:5	-100
<b>Falcon III</b>	TopoSys	Airborne	Fibers	2005 -	1560	<2:5	50-125
<b>MarkII</b>	TopEye	Airborne	Palmer	2004	1064	<1	-50
<b>ALTM 3100</b>	Optech	Airborne	Oscillating mirror	2004-	1064	-3:5	-70
<b>ALS60</b>	Leica	Airborne	Oscillating mirror	2005 -	1064	0.2-6	-50

Table 2.1(b): Illustration of the main technical specifications for the full waveform recording systems, adopted from (Mallet and Bretar, 2009).

System	Pulse energy (mJ)	Pulse width (ns)	Scan rate (Hz)	Scan angle (°)	Beam divergence (mrad)	Footprint size (m)	Range accuracy (cm)	Digitizer (ns)
<b>LARSEN 500</b>	-	12	20	30	4	2@500 m	30	1
<b>LADS MarkII</b>	7	-	18	27	-	-	15	2
<b>Hawk Eye</b>	2/15	7	0.3_7	0/40	2-15	1_7.5@500 m	30	1
<b>SHOALS 1000T</b>	2/15	6	0.3_7	0/40	2-15	0.8_6@400 m	15	1
<b>EAARL</b>	0.07	1.3	25	22	0.03	0.15@300 m	3	1
<b>SLICER</b>	-	4	80	-	2	10@5 km	11	1.35
<b>SLA-02</b>	40	8	-	-	0.3	85@285 km	150	4
<b>LVIS</b>	5	10	500	14	8	40@5 km	30	2
<b>GLAS</b>	75/35	6	-	0	0.11_0.17	66@600 km	5_20	1
<b>MBLA</b>	10	5	-	-	0.06	24@400 km	100	4
<b>LMS Q560</b>	0.008	4	5_16	45	0.5	0.5@1 km	2	1
<b>Falcon III</b>	-	5	165_415	28	0.7	0.7@1 km	-	-
<b>MarkII</b>	-	4	<50	14/20	1	1@1 km	2_3	1
<b>ALTM 3100</b>	<0:2	8	<70	50	0.3/0.8	0.3/0.8@1 km	1	1
<b>ALS60</b>	<0:2	5	<90	75 usually	0.22	0.22@1 km	2	1

This thesis will mainly focus on the analysis of larger footprint full waveform signals using the Geoscience Laser Altimeter System (GLAS) mounted on the Ice, Cloud and Land Elevation Satellite system (ICESat) and the opportunities and limitations offered by this spaceborne LiDAR. The next section describes this in detail.

## 2.7 ICESat-GLAS spaceborne LiDAR system

Ice, Cloud and Land Elevation Satellite (ICESat) spaceborne laser altimeter system is the first spaceborne that mapping the earth using lasers from a dedicated satellite platform. It is one of NASA series of earth observation spacecraft designed to study environment of our earth and how it may be changing.

### 2.7.1 Overview of instrument and mission

The Ice, Cloud and land Elevation Satellite (ICESat) spaceborne laser altimeter system was launched in January 2003 with the primary objectives being to measure polar ice-sheet elevation change, atmospheric and aerosol and cloud properties, land topography profiles, and height vegetation canopies (Zwally *et al.*, 2002; NSIDC, 2009). These objectives are accomplished through the use of the Geosciences Laser Altimeter System (GLAS) in combination with an onboard GPS receiver and an inertial reference system, used to determine accurate orbit dimension. GLAS uses an Nd:YAG laser altimeter to define the range between the satellite and the surface of the Earth by measuring the round trip travel period of the infrared pulse. GLAS instrument is nadir viewing, at an altitude of 600 km. It acquires elevation profiles of the whole earth along tracks that are revisited in a 183 day repeat elliptically, and the laser footprint on the surface is equivalent to a circular area of 70 m diameter spaced every 175 m (Brenner *et al.*, 2003, Abshire *et al.*, 2005). Figure 2.8 shows how the GLAS instrument makes measurements from ICESat while orbiting the Earth.

GLAS carries three lasers, named L1, L2, and L3, that sequentially send short pulses of visible green light 532 nm and infrared light 1064 nm forty times per second (Zwally *et al.*, 2002). Laser 1 failed in March 2003, after 38 days of its operation; therefore, the two lasers lifetime was reduced. The laser system operated for three 33 day sub-cycles per year acquired in Feb-March, May-June and October-November each year. The sub-cycles are named as a, b, c, and so on... for the 33 day campaign. Laser 2 operated for campaigns in Oct-Nov 2003 (L2a); and Feb-March (L2b) and May-June (L2c) in 2004. The use of Laser 3 started in October 2004 (L3a); and continued in Feb-March (L3b), May-June (L3c) and Oct-Nov (L3d) 2005; Feb-March (L3e), May-June (L3f) and Oct-

Nov (L3g) in 2006; March-April (L3h) and Oct-Nov (L3i) in 2007; and Feb-March (L3j) in 2008. Laser 3 failed to operate during the campaign of (L3k) in October 2008. Laser 2 started again in Nov-Dec (L2d) 2008; and March-April (L2e) and Sep-Oct (L2f) 2009 (NSIDC, 2009).

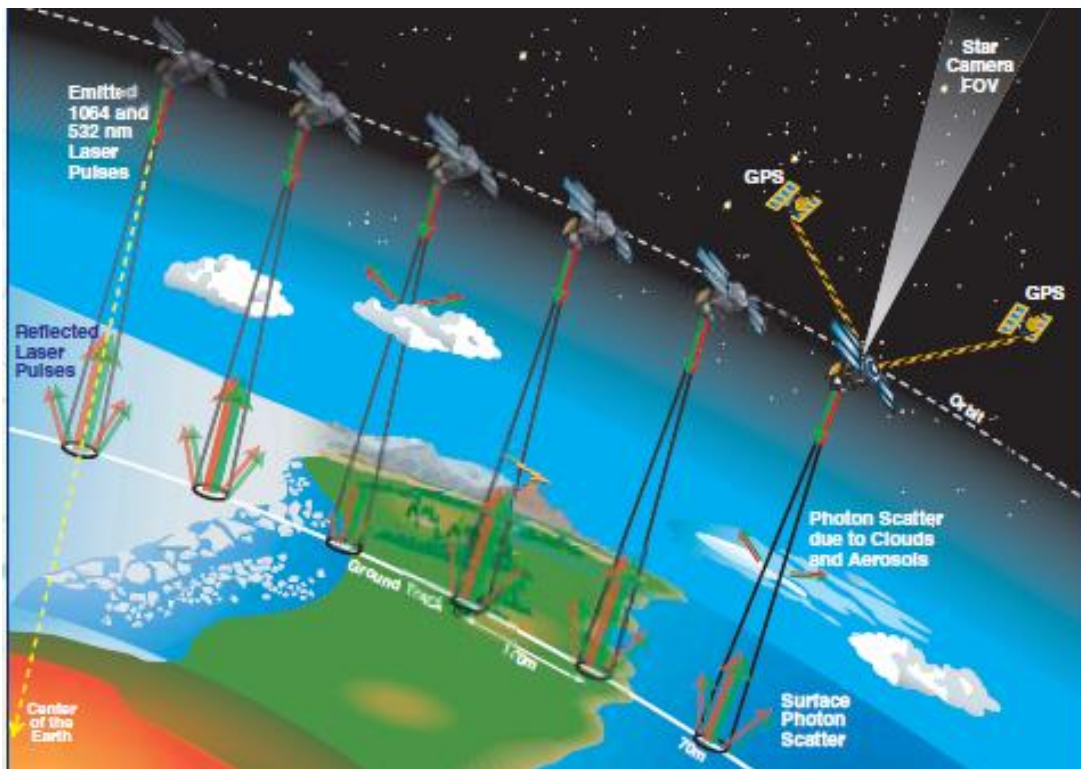


Figure 2.8: Schematic illustrating how the GLAS instrument makes measurements from ICESat while orbiting the earth. Source: (NASA GLAS, 2009)

GLAS records the 1064 nm wavelength energy for each laser echo pulse as a function of time, thus the instrument acquires a vertical profile of the illuminated surfaces within the laser footprint instead of a discrete measurement of elevation. The GLAS instrument digitizer records the whole laser pulse in 1ns over the entire land (Zwally *et al.*, 2002).

Table 2.2: Acquisition dates and release numbers for the 13 91-Day ICESat campaigns during ICESat operation (Abdalati *et al.*, 2010).

Campaign Period	Date	Millions of Shots
Laser 2a	10/04/03-11/19/03	159
Laser 2b	02/17/04-03/21/04	114
Laser 2c	05/18/04-06/21/04	118
Laser 3a	10/03/04-11/08/04	124
Laser 3b	02/17/05-03/24/05	121
Laser 3c	05/20/05-06/23/05	118
Laser 3d	10/21/05-11/24/05	118
Laser 3e	02/22/06-03/28/06	118
Laser 3f	05/24/06-06/26/06	114
Laser 3g	10/25/06-11/27/06	114
Laser 3h	03/12/07-04/14/07	114
Laser 3i	10/02/07-11/05/07	118
Laser3j	02/17/08-03/21/08	114
Laser 3k*	10/04/08-10/19/08	38
Laser 2d*	11/25/08-12/17/08	76
Laser 2e	03/09/09-04/11/09	114
Laser 2f	09/30/09-10/11/09	33
<p><b>*Laser 3 expired 10 days into the October/November 2008 campaign. The campaign was completed using the low-energy laser 2. Diagnosing the Laser 3 failure mode and implementing switch back to Laser 2 took about 1 month. Laser 2 expired on October 11, 2009.</b></p>		

Return waveforms are digitized in 544 bins for ice sheets and land, and 200 bins for oceans and sea ice. The 544 bins of 1 ns intervals equals a range distance of 81.5 m, where 1 ns is the two-way travel time of the pulse which corresponds to a range distance of 15 cm for laser L1 and 150 m for laser L3 (Harding and Carabajal, 2005). Laser 3 has succeeded to operate for a period of 5.5 years of 15 33-day measurement campaigns. However, ICESat mission is no longer operating, as the final GLAS laser ceased firing in October 2009 (Abdalati *et al.*, 2010). Table 2.3 shows the specifications of ICESat-GLAS mission.

Table 2.3: Specifications of ICESat-GLAS (Abdalati *et al.*, 2010).

<b>Description</b>	<b>Surface</b>	<b>Atmosphere</b>
<b>Mass</b>	300 kg	
<b>Altitude</b>	~ 600 km	
<b>Altimeter</b>	Nd:YAG Laser	
<b>Wavelengths</b>	1064 nm	532 nm
<b>Laser Pulse Energy</b>	74 mJ	30 mJ
<b>Shot Frequency</b>	40 Hz	
<b>Laser Beam Diverge</b>	110 $\mu$ rad	
<b>Average Footprint Diameter</b>	70 m	
<b>Laser Pulse Width</b>	5 nsec	
<b>Telescope Diameter</b>	1.0 m	
<b>Receiver FOV</b>	0.5 mrad	0.16 mrad
<b>Receiver Optical Bandwidth</b>	0.8 nm	0.03 nm
<b>Detection Scheme</b>	Analog Photon	Counting
<b>Vertical Sampling Resolution</b>	0.15 m	75 m
<b>Surface Ranging Accuracy (single pulse)</b>	5 cm	
<b>Footprint Location Accuracy</b>	6 m	
<b>Laser Pulse Pointing Knowledge</b>	< 2 arcsec	
<b>Laser Pulse Pointing Control</b>	30 arcsec roll, 30 arcsec pitch, and 1° yaw, up to 5° off-nadir	
<b>Footprint spacing along-track</b>	~ 170 m	

### 2.7.2 ICESat track coverage

NASA ICESat-GLAS captures important scientific data and spectacular three-dimensional views of earth's polar ice sheets, clouds, mountains, and forestlands. ICESat crosses the world below at nearly 17,000 miles per hour and it is covering the earth from space with unprecedented accuracy and detail (see Figure 2.9). ICESat orbit was designed to maximize coverage over the great polar ice sheets, where ground tracks overlap, to produce an intricate grid of data points resulting in three-dimensional high resolution images of ice sheets in Greenland and Antarctica. Therefore, these details of ice and land features enable scientists to view the global earth from space to obtain an unprecedented image of how and where ice sheets are growing and shrinking. Moreover, ICESat data is used to develop digital elevation models which help understanding of how life on earth is affected by climate change (NASA website, 2003).

In addition to acquiring elevation data (see Figure 2.10), ICESat full return waveform shape provides unique information about the highest distribution of the surface features within each laser footprint (NASA website, 2003).

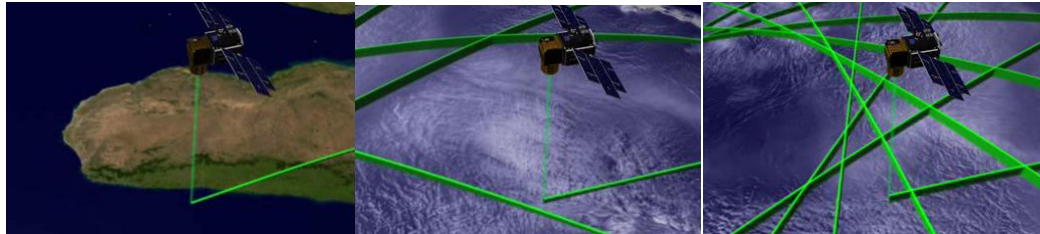


Figure 2.9: GLAS transects on the earth below, adopted from (ICESat-GLAS, 2003)

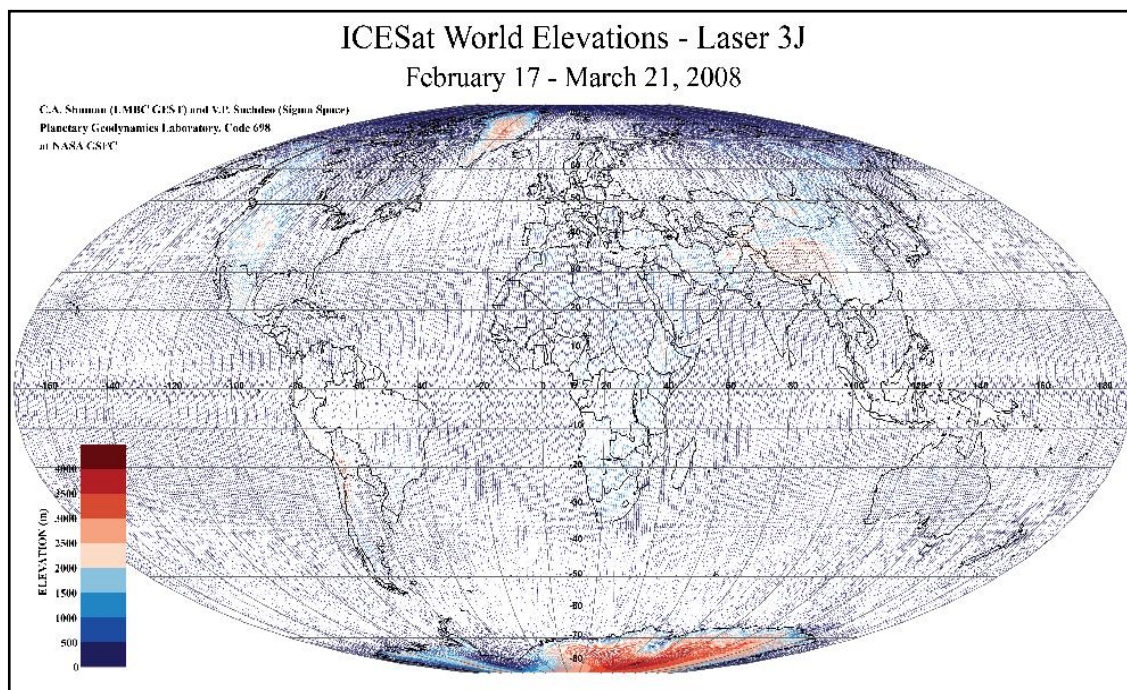


Figure 2.10: GLAS laser world elevations map (NSDIC, 2007)

### 2.7.3 ICESat-GLAS data products

ICESat has acquired a magnitude database of raw and processed data that organises the 15 data products from GLA01 to GLAS15 (Brenner *et al.*, 2003). Each product is developed and processed for particular uses. GLAS data is processed into three different levels from level 0 to level 3. Level 0 contains raw telemetry data; level 1 data includes instrument parameters; level 2 data has geophysical, ice, ocean, atmosphere and land

parameters; and level 3 contains gridded digital elevation model and atmospheric backscattered images.

These data are distributed in granules by the National Snow and Ice Data Centre (NSIDC), which contain different amount of data with different structures, variables and size of data. The data are stored in a binary format in big-endian byte order and are organised in records of 40 footprints. All the data products are time stamped with transmit time of pulse in Coordinated Universal Time (UTC) as collected along track. To relate information from different datasets, a unique record index is assigned to every one second of data. The unique record index is consistent across all products of the same release (NSIDC 2003a; NSIDC 2003b). Table 2.4 show the ICESat-GLAS standards data products.

Two data products of release 29 GLAS were used in this study:

- Level 1A Global Altimetry data (GLA01),
- Level 2 Global Land Surface Altimetry data (GLA14)

GLA01 is level 1A data product which contains granules that have raw LiDAR waveform in digitizer counts, which are afterwards converted to volts (by users). One granule covers  $\frac{1}{4}$  orbit or ~23 minutes of data. This data can be obtained by searching the granule ID or time. GLA01 contains the transmitted and received echo waveforms. This product has variables such as the filter threshold value for signal detection in digitizer counts, laser transmit energy, received energy from all signal above threshold, sampled transmit pulse waveform, 4ns background mean value, and standard deviation (Brenner *et al.*, 2003).

Table 2.4: ICESat-GLAS standard data products. (NSIDC, 2011).

Short Name	Long Name	File Size	Orbits per File
GLA01	L1A Global Altimetry Data	9 MB	1/4
GLA02	L1A Global Atmosphere Data	671MB	2
GLA03	L1A Global Engineering Data	19 MB	2
GLA04	L1A Global Laser Pointing Data	2MB-386MB	2
GLA05	L1B Global Waveform-based Range Corrections Data	25MB	1/4
GLA06	L1B Global Elevation Data	7MB	1/4
GLA07	L1B Global Backscatter Data	827MB	2
GLA08	L2 Global Planetary Boundary Layer and Elevated Aerosol Layer Heights	7MB	14
GLA09	L2 Global Cloud Heights for Multi-Layer Clouds	82MB	14
GLA10	L2 Global Aerosol Vertical Structure Data	289MB	14
GLA11	L2 Global Thin Cloud/Aerosol Optical Depth Data	13MB	14
GLA12	L2 Antarctic and Greenland Ice Sheet Altimetry Data	104MB	14
GLA13	L2 Sea Ice Altimetry Data	107MB	14
GLA14	L2 Global Land Surface Altimetry Data	209MB	14
GLA15	L2 Ocean Altimetry Data	279MB	14

GLA14 is a level 2 data which contains sensor position and pointing information as well as calculated footprint position, size and shape, and land surface elevation. GLA14 granules cover 14 consecutive orbits. Transmitted pulse and recorded waveforms are represented with characteristic shape parameters only. The recorded waveform is decomposed into a series of Gaussian peaks, as described in Hofton *et al.* (2002), Zwally *et al.* (2002) and Brenner *et al.* (2003) (assuming a Gaussian transmit pulse and Gaussian distribution of height surfaces within the footprint):

$$w(t) = \varepsilon + \sum_{m=1}^{N_p} A_m \times e^{\frac{-(t-t_m)^2}{2\sigma^2 m}} \quad (2.2)$$

Where:

$w(t)$  = the amplitude of the waveform at time  $t$ ,  $Np$  = number of peaks in the waveform  
 $A_m$  = amplitude of the  $m$  the peak,  $\varepsilon$  = bias (noise level) of the waveform,  $t_m$  = position  
of  $m$  the peak at time  $t$ ,  $\sigma_m$  = standard deviation of the  $m$  the peak (Brenner *et al.*,  
2003). This equation is solved with non-linear least squares fitting to a maximum  
number of six peaks. The parameters of each fitted peak are given in the datasets  
(Brenner *et al.*, 2003). More details about full waveform processing will be described in  
detail in chapter 3.

## **2.8 LiDAR applications for vegetation measurements**

LiDAR remote sensing is a breakthrough technology for forest applications. It provides  
horizontal and vertical information at height spatial resolutions and vertical accuracies  
(Dubayah and Drake, 2000; Lim *et al.*, 2003a). LiDAR instrument systems have proved  
the capability to accurately estimate important forest structure characteristics such as  
stand volume, basal area, canopy height and aboveground biomass (Magnussen and  
Boudewyn, 1998; Lefsky *et al.*, 1999b; Anderson *et al.*, 2006; Lefsky *et al.*, 2005a;  
Coops *et al.*, 2007; Rosette *et al.*, 2008a; Duncanson *et al.*, 2010b). This section  
provides an overview of current and projected uses of both discrete return and full  
waveform recording LiDAR systems in forest application.

### **2.8.1 Discrete return systems of vegetation applications**

Fundamentally, discrete returns LiDAR are small footprint (approximately 20-80 cm  
diameter) devices that allow for one to several returns to be recorded for each pulse  
during flight. For vegetation applications, it is considered that the ability of small  
footprint discrete return systems to capture multiple returns to penetrate beyond the first  
reflective surface of the canopy is a critical characteristic (Lim *et al.*, 2003b). However,  
the discrete return system is rapidly gaining prominence in natural resource research

applications and management due to its great capability to represent complex vertical structures and ground surfaces elevations with very high precision (Lefsky *et al.*, 2002b; Evans *et al.*, 2009).

Despite the fact that discrete LiDAR sensors are designed to measure the three-dimensional coordinates of a passive target, there is still significant variation in design from one instrument to another; hence, data-processing algorithms and established sensor configurations designed for commercial use may not coincide with scientific objectives because none of these sensors have been specifically designed for vegetation application. Therefore, their data can be processed in a number of ways to create meaningful forest maps information (Lefsky *et al.*, 2002b; Lim *et al.*, 2003b). Table 2.5 describes the general characteristics and specification of common LiDAR sensor parameters used for natural resource application.

Table 2.5: Characteristics of common commercial discrete LiDAR sensors parameters for natural resource applications (Evans *et al.*, 2009).

<b>Parameter</b>	<b>Value</b>
<b>Wavelength</b>	1.064 $\mu\text{m}$
<b>Pulse Repetition Rate (PRF)</b>	~50–150 kHz
<b>Returns per pulse</b>	3 – 4
<b>Pulse width</b>	10 nano-seconds
<b>Beam divergence</b>	10–80 m rad
<b>Scan angle</b>	<15° off-nadir, 30° total look
<b>Scan pattern(s)</b>	Ziz-zag, parallel, elliptical, sinusoidal
<b>GPS frequency</b>	1–2 Hz
<b>INS frequency</b>	50 Hz (200 Hz max)
<b>Operating altitude</b>	100–3,000 m (6,000 m max), average ~2,000 m
<b>Footprint size</b>	0.10–0.30 cm
<b>Pulse Density</b>	> 4 pulse/m <sup>2</sup>
<b>Accuracy (Vertical/Elevation)</b>	< 0.15 m
<b>Delivery format</b>	Binary LiDAR exchange format (LAS)

### **2.8.2 Full waveform systems of vegetation applications**

Unlike discrete return LiDAR systems, full waveform LiDAR samples and records the entire back returned signal intensity at regular time intervals (1ns). The footprint size may vary from (10 - 70 m); hence, the large footprint of full waveform LiDAR will contain information on forest canopy and its structure (Lim *et al.*, 2003b; Mallet and Bretar, 2009; Wulder *et al.*, 2012).

NASA has developed a number of full waveform sensors which have been used for forestry applications:

#### Scanning LiDAR Imager of Canopies by Echo Recovery (SLICER)

The SLICER was developed to characterise the vertical structure of the canopy. The medium size footprint (10 to 25 m) airborne system showed that the full waveform systems could be used to assess the characteristics of woodlands; distinguish tree ages, classes and species; and, in addition, characterize the structure of extensive areas (Lefsky *et al.*, 1999a; Mallet and Bretar, 2009). Several studies have tested the use of SLICER data for canopy height profiling (i.e. Lefsky *et al.*, 1999b; Means *et al.*, 1999; Harding *et al.*, 2001; Parker *et al.*, 2001; Lefsky *et al.*, 2002a, 2005a). However, SLICER no longer exists because parts of it were used to build the Laser Vegetation Imaging Sensor (LVIS) (Harding *et al.*, 2000).

#### Shuttle Laser Altimeter (SLA)

NASA Shuttle Laser Altimeter (SLA) is an improved version of SLICER and was used to develop algorithms, calibrate instruments and evaluate the performance of measurements to assess the future mission of Vegetation Canopy LiDAR (VCL). It was primarily utilized to develop a real-time algorithm for classifying ground points by

analysing the return signal. Moreover, it illustrated the potential of full waveform data to derive canopy structure and measure the surface topography (Blair *et al.*, 1999).

#### Vegetation Canopy LiDAR (VCL)

The VCL is an active space-based LiDAR remote sensing system; it was specifically designed to measure global characteristics of forests and other vegetation canopies (Dubayah *et al.*, 1997; Hofton *et al.*, 2002). However, this sensor has never made it into space (Mallet and Bretar, 2009).

#### Laser Vegetation Imaging Sensor (LVIS)

LVIS is an airborne simulator that was developed by NASA (Blair *et al.*, 1999). This sensor produces 25 m footprints with 25 m contiguous along-track resolution (Mallet and Bretar, 2009). Several studies tested metrics derived from LVIS data obtained over forested area (i.e. Blair *et al.*, 1999; Drake *et al.*, 2002; Anderson *et al.*, 2008). Results showed that LVIS has demonstrated its ability to provide earth scientists with unique dataset allowing studies of surface topography, hydrology, and vegetation height and structure with unmatched accuracy and coverage (Blair *et al.*, 1999).

#### Geoscience Laser Altimeter System (GLAS)

The successful five-year ICESat satellite mission carrying the GLAS sensor was launched in January 2003 mainly to study and measure the roughness and thickness of sea ice, the topography (using a 1064 nm laser), and the vertical structure of clouds and aerosols (532 nm laser) (NSIDC, 2009). Moreover, ICESat classifies the return full waveform in real-time into land/ice and ice sheet/sea by analyzing the return backscattered waveform and recognizing Gaussian distributions, from which the main characteristics are extracted (Brenner *et al.*, 2003). The ICESat mission is no longer

collecting data as the final GLAS laser stopped working in October 2009 (Abdalati *et al.*, 2010). Beside, its potential capability to assess changes in ice sheet elevations (Howat *et al.*, 2008; Slobbe *et al.*, 2008; Pritchard *et al.*, 2009) and measure the ice sea level (Farrell *et al.*; 2009; Kwok *et al.*; 2009), ICESat has also demonstrated its capability to determine vegetation height regionally and globally; and estimate aboveground biomass (Harding and Carabajal, 2005; Lefsky *et al.*, Nelson *et al.*, 2009; 2005a; Lefsky, 2010; Saatchi *et al.*, 2011; Simard *et al.*, 2011).

The success of the ICESat program and its accomplished objectives, coupled with recent observations of dramatic changes in polar ice, has motivated the National Research Council Earth Science Decadal Survey to call for an ICESat-2 follow-on mission (Abdalati *et al.*, 2010). ICESat-2 is intended to follow the original specifications of the first ICESat mission. It is expected to support multidisciplinary applications, mainly targeted at measuring: 1) Ice sheet changes, 2) Sea ice thickness, and 3) Vegetation biomass (Abdalati *et al.*, 2010). ICESat-2 is currently planned for launch in 2015.

### **2.8.3 LiDAR studies of vegetation structure**

Several studies have successfully used discrete small footprint systems in estimating canopy height, percent cover canopy and aboveground biomass (i.e. Nelson *et al.*, 1988; Nilsson, 1996; Naesset, 1997a; Magnussen and Boudewyn, 1998; Means *et al.*, 2000; Reitberger *et al.*, 2008). However, these fine resolution systems typically produced consistent ground returns only in relatively open forest canopies; hence, making vegetation measurements structure estimation difficult in dense forests (Weishampel *et al.*, 2000). Unlike discrete returns systems, large footprint LiDAR systems work effectively in a variety of canopy closure conditions (i.e. Lefsky *et al.*, 1999a; Means *et*

*al.*, 1999b; Drake *et al.*, 2002; Parrish, 2007; Rosette *et al.*, 2008c). This is because these large footprints systems consistently measure sub-canopy topography even under conditions of high canopy closure (Drake *et al.*, 2002).

The LiDAR sensors described above use LiDAR data to make measurements of vegetation structure. The majority of these have been from airborne platforms. Recent years have shown a remarkable advance in using terrestrial and spaceborne LiDAR, due to its ability to rapidly record and measure the three-dimensional structure of canopies (Rosette *et al.*, 2008b). However, up to now, few satellite LiDAR system missions of the earth surface have been realised (Winker *et al.*, 1996; Zwally *et al.*, 2002). Most of their studies have been involved with glaciology (i.e. Smith and Sandwell, 2003; Herzfeld *et al.*, 2008; Zwally *et al.*, 2008; Gudmundsson *et al.*, 2011; Nuth and Kääb, 2011); atmospheric sciences (e.g Spinhirne *et al.*, 2005; Dessler *et al.*, 2006; Yang *et al.*, 2008); and topography (i.e. Garvin *et al.*, 1998; Carabajal and Harding, 2005; Atwood *et al.*, 2007; Yamanokuchi *et al.*, 2007; Alberti and Biscaro, 2010; Chen, 2010a).

ICESat-GLAS has been an active area of research during the last recent years (Yong *et al.*, 2004; Harding and Carabajal, 2005; Lefsky *et al.*, 2006; Sun *et al.*, 2008; Duong *et al.*, 2008; Rosette *et al.*, 2008a; 2008b; 2008c; Chen, 2010a; 2010b). Although it was designed primary to measure ice sheet changes, it has demonstrated its ability to retrieve vegetation biophysical parameters at unprecedented scales (Rosette *et al.*, 2008a; Chen, 2010b); and this field of study is currently without a dedicated GLAS LiDAR campaign for this purpose.

### 2.8.3.1 Vegetation height estimation

Vegetation height is one of the leading dimensions of ecological variation among tree species (Westoby *et al.*, 2002), and a major factor of ecosystem functioning such as species' composition, climate and site quality, and land cover classification (Dubayah and Drake, 2000; Moles *et al.*, 2009). In other words, canopy height is an important attribute as a predictor variable for other forest attributes, such as volume and biomass (Arp *et al.*, 1982; Aldred and Bonner, 1985; Schreier *et al.*, 1985).

LiDAR data recorded from discrete small footprint sensors have been successfully proven efficient in measuring canopy height and vertical distribution of stand (i.e. Nelson *et al.*, 1984; Nelson *et al.*, 1988; Nilsson, 1996; Naesset, 1997; Nelson, 1997; Magnussen and Boudewyn, 1998; Lefsky *et al.*, 1999a; Means *et al.*, 2000; Peterson, 2000; Drake *et al.*, 2003a, Drake *et al.*, 2003b, Hyde *et al.*, 2005). The other experimental full waveform LiDAR systems have been successfully used also to derive forest canopy height and crown canopy cover in a variety of forest types (Lefsky *et al.*, 1999a; Means *et al.*, 1999; Dubayah and Drake, 2000; Peterson, 2000; Drake *et al.*, 2002; Hofton *et al.*, 2002; Hyde *et al.*, 2005; Chen, 2010b). Canopy or vegetation height is calculated by subtracting the elevations of the first and last returns from LiDAR signal (Figure 2.11). However, LiDAR data gathered by either the discrete return or full waveform recording system methods have two main problems in estimating vegetation height. The first one is determining the exact elevation of the ground surface, particularly in complex canopies where the elevations returned from what appears to be the ground level could, in fact, be from the understory which is dense enough to occlude the ground surface (Lefsky *et al.*, 2002b).

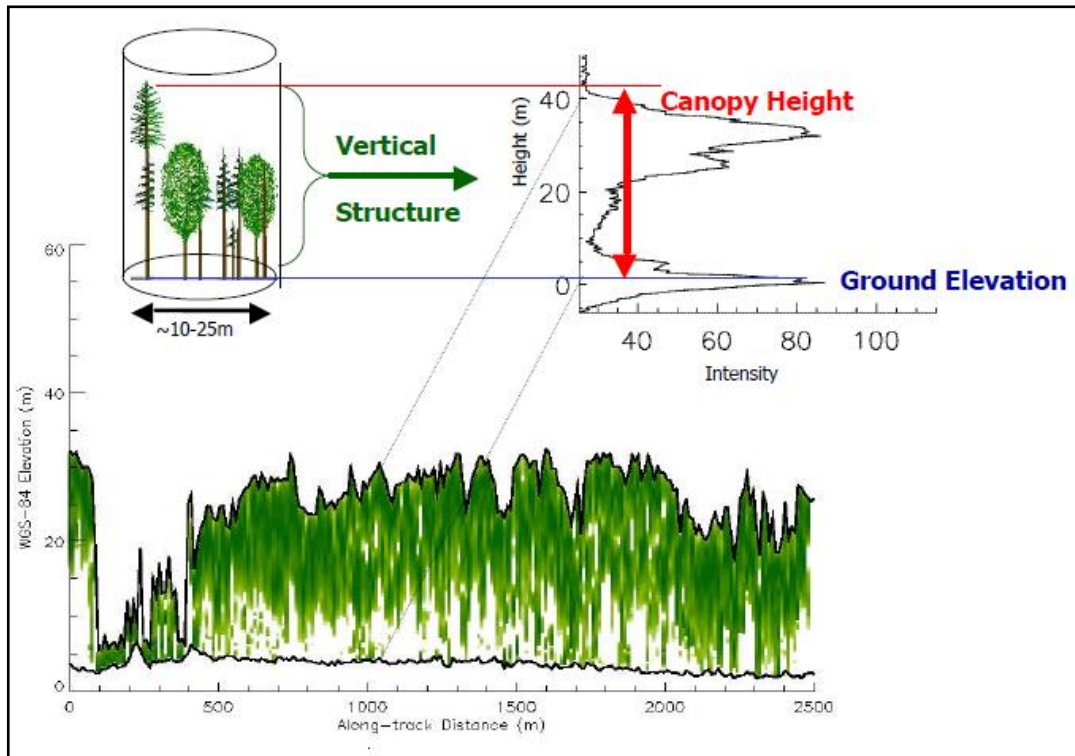


Figure 2.11: Large-footprint LiDAR waveform recording reflections from the nadir-projected vertical distribution of the surface area of canopy components, and the estimated canopy height (Dubayah and Drake, 2000)

The other problem is that each type of LiDAR system has difficulties in detecting the uppermost portion of the tree canopy. In discrete systems, very high footprint densities are required to sample the highest portion of individual tree canopies; while with full waveform sampling sensors, the large footprint is illuminated, which increases the probability that tall tree tops will be illuminated by the laser sensor (Lefsky *et al.*, 2002b). Nevertheless, the top portion of the canopy may not be of sufficient area to be recorded as a significant return signal and therefore may not be detected; or, in both cases, the highest portion of the canopy may be underestimated (Lefsky *et al.*, 2002b). However, only a paucity of studies have explored the use of GLAS for vegetation height retrieval (Lefsky *et al.*, 2005a; Lefsky *et al.*, 2007; Duong *et al.*, 2008; Neuenschwander *et al.*, 2008; Rosette *et al.*, 2008c; Sun *et al.*, 2008; Pang *et al.*, 2008; Duncanson *et al.*, 2010a; Chen, 2010b) using the direct or statistical methods, both of which will be described in Chapter 3.

The previous studies have been conducted specifically in temperate and boreal forests (i.e., Ranson *et al.*, 2004a; Rosette *et al.*, 2008a) and mangrove forests (i.e., Simard *et al.*, 2008); but there has been insufficient exploration for ecological research in savannah ecosystems (Levick and Rogers, 2008). Therefore, the main objective of this study is to assess the ability of ICESat-GLAS LiDAR full waveforms to retrieve canopy height over savannah vegetation landscapes.

### **2.8.3.2 Vegetation vertical structure, canopy cover, volume and biomass predictions**

Various attempts have been made to derive estimates of canopy vertical structure, particularly in forests (Dubayah and Drake 2000; García *et al.*, 2010). It started using discrete return LiDAR data in the work of Maclean and Krabill (1986), who used a photogrammetric technique (the canopy profile cross-sectional area is the total area between the ground and the upper canopy surface along transect) to interpret the LiDAR data. This work was able to explain 92% of the variation in gross merchantable timber volume (Lefsky *et al.*, 2002a).

Moreover, Nelson *et al.* (1988) predicted the volume and biomass of southern pine forests using several estimates of crown canopy cover and height from discrete-return LiDAR data, explaining between 53% and 65% of variance in field measurements of these variables. Later work by Nelson *et al.* (1997) in tropical wet forests produced similar results for prediction of basal area, volume, and biomass, using also the discrete return LiDAR data.

Full waveform recording LiDAR systems have successfully shown the capability of this type of data in predicting forest vertical structure. Nilsson (1996) adapted a bathymetric

LiDAR system for use in forest inventory, and successfully predicted timber volume for stands of even-aged Scots pine. He used the height and the total power of each waveform as independent variables, and explained 78% of variance. Lefsky *et al.* (1999a) used data from SLICER to predict aboveground biomass and basal area in eastern deciduous forests using indices derived from the canopy height profile; they discovered that relationships between height indices and forest structure attributes (basal area and aboveground biomass) could be generated using field estimates of the canopy height profiles, and applied directly to the LiDAR estimated profiles, resulting in unbiased estimates of forest structure. Means *et al.* (2000) applied similar methods to evaluate 26 plots in forests of Douglas-fir and western hemlock of the Experimental Forest. They demonstrated that very accurate estimates of basal area, aboveground biomass, and foliage biomass could be made using LiDAR height and cover estimates.

Moreover, Lefsky *et al.* (1999a) used statistics derived from the canopy volume method to predict numerous forest structural attributes by applying statistical method to predict ground-based measures of stand structure from canopy structure indices and the canopy volume method indices. Drake *et al.* (2002) used LVIS data indices to describe the vertical distribution of the raw waveforms and the fraction of total power associated with the ground returns; which resulted in them predicting field measured quadratic mean stem diameter, basal area, and aboveground biomass, explaining up to 93%, 72%, and 93% of variance, respectively.

The increasing interest in laser data for forest applications has led to the utilization of the spaceborne LiDAR ICESat-GLAS in retrieving vegetation parameters in recent years. Nevertheless, only a paucity of studies have employed the satellite LiDAR GLAS

waveform data to estimate vegetation profiles (Chen, 2010b); and the results revealed variations of other important vegetation parameters such as maximum canopy height, canopy cover, stand volume, and above-ground biomass (i.e. Harding *et al.*, 2001; Harding and Carabajal, 2005; Lefsky *et al.*, 2005a; Lefsky *et al.*, 2007; Duong *et al.*, 2008; Neuenschwander *et al.*, 2008; Rosette *et al.*, 2008a; Pang *et al.*, 2008; Duncanson *et al.*, 2010).

Moreover, few studies show that GLAS waveform parameters have good correlation with the forest aboveground biomass and can be used to obtain biomass data for larger scale forest biomass mapping from other imagery data. One such study by Guo *et al.* (2010) which combined charge-coupled device (CCD) data from the Small Satellite for Disaster and Environment Monitoring and Forecast (HJ-1) and GLAS waveform data for predicting and developing aboveground biomass models for different forest types. The results show that the statistical regression models have an  $R^2$  of 0.68 for conifer forest and  $R^2$  of 0.71 for broadleaf forest. It was found that HJ-1 data and GLAS waveform data can be combined to estimate forest biomass; and, hence the predicted biomass data can be used as input data for future carbon budget studies (Guo *et al.*, 2010). Another study, by Saatchi *et al.* (2011), used estimates of global forest height from GLAS waveform in combination with satellite remote sensing data from multiple sensors (moderate resolution imaging spectra radiometer (MODIS), shuttle radar topography mission (SRTM), and quick scatter-ometer (QSCAT) to extrapolate above and belowground biomass from inventory sample plots. The results presented a “benchmark” map of estimated biomass over 2.5 billion hectares of forests on three continents (Saatchi *et al.*, 2011).

However, new spaceborne remote sensing techniques such as the use of light detection and ranging (LiDAR) and radio detection and ranging (RADAR) are needed to estimate the distribution of biomass plus estimating other important vegetation parameters for large-scale mapping of vegetated areas (Saatchi *et al.*, 2011). From this viewpoint, this approach of using the two spaceborne sensors - LiDAR and RADAR - will be tested and discussed in Chapter 5.

## **2.9 Comparison with other remote sensing techniques**

Most passive remote sensing systems (aerial photography and remote sensing) can map the horizontal organization of canopies but cannot provide direct information on the vertical distribution of canopy elements. Moreover, traditional remote sensing methods cannot measure or account for ground topography in densely vegetated areas (Ni-Meister *et al.*, 2001). LiDAR has the advantage of being able to penetrate the forest canopy structure (Weishampel *et al.*, 2000), and this enables LiDAR to provide a richer picture of forest structure in creating highly accurate three-dimensional representations over wide areas, and hence allows it to be effective for forestry and wildlife applications (Harding *et al.*, 2001; Goetz *et al.*, 2007).

Goetz *et al.* (2007) found that LiDAR metrics have better capability to predict habitat variables such as crown canopy cover than do traditional remote sensing data. However, LiDAR cannot provide the spectral response of passive sensor imagery; therefore, although LiDAR technology may replace other remote sensing technologies in some cases, the relationship on the whole is complementary (Baltsavias, 1999). The work of Hill and Thompson (2005) is a good example of integrating LiDAR and spectral data for estimating canopy parameters. They used data from a hyperspectral optical sensor,

which is useful for determining dominant species, and combined this with canopy height models derived from LiDAR data. This resulted in creating an ecological meaningful thematic map using unsupervised classification with the integrated data (Hill and Thompson, 2005). The full integration of passive optical sensors and LiDAR technology has a lot of potential (Ackermann, 1999).

## RADAR

Radio Detection and Ranging sensors (RADAR) are another remote sensing technique that can penetrate forest canopies and hence be used to characterize vegetation structure such as estimating canopy height and biomass. RADAR sensors transmit and receive radiation in a certain kinds of electromagnetic spectrum region called radio waves and microwaves (Figure 2.12).

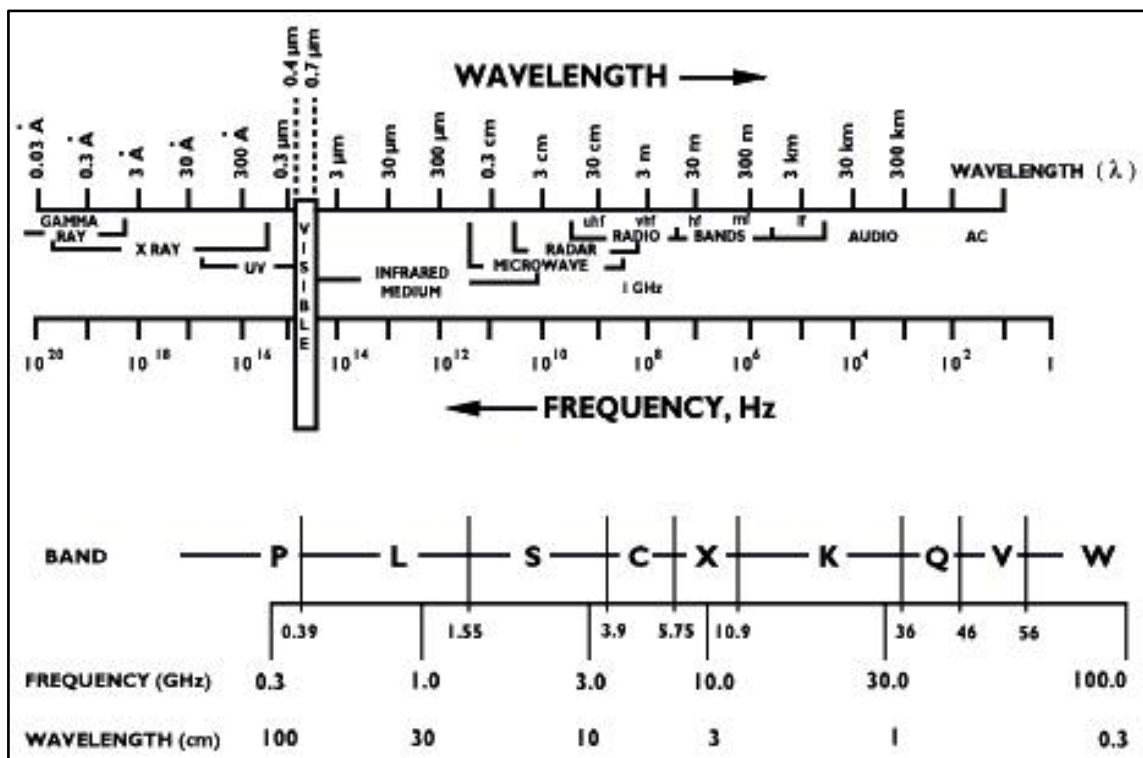


Figure 2.12: The electromagnetic spectrum and the microwave bands location (Source: <http://earth.esa.int>).

The RADAR principle involves transmitting a powered pulse ( $P_T$ ) towards a target and measuring the power received ( $P_R$ ) that is backscattered to the instrument characterised with a gain  $G$ . The RADAR equation (2.3) has been used to explain the RADAR ground return, the differential scattering cross section, or scattering coefficient ( $\sigma$ ). If the same antenna is used for transmission and reception the radar equation is:

$$P_R = \frac{P_t G^2 \lambda^2 \sigma_c}{(4\pi)^3 R^4} \quad (2.3)$$

Where,  $\lambda$  is the wavelength of the signal,  $R$  is the distance from the sensor to the target;  $\sigma_c$  is the backscattering cross-section of a target. The above equation is considered for a single target when an isotropic scatter would return the same amount of power as the target. For multiple or extended targets, the above equation can be generalised as follows:

$$dP_R = \frac{P_t G^2 \lambda^2}{(4\pi)^3} d\sigma_i \quad (2.4)$$

The backscatter coefficient  $\sigma$  is defined as the average backscattering cross section per unit area and it is expressed in dB. The backscattering cross section is the measure of a target's ability to reflect RADAR signals in the direction of the RADAR receiver. Thus, the concept of vegetation study using RADAR remote sensing is based in the relationships between the backscattering coefficient  $\sigma$  and biophysical properties of vegetation.

The backscatter coefficient for a target is visualised as the product of three factors: the projected cross section; reflectivity; and directivity. The projected cross section refers to the amount of power reradiates toward the RADAR from a RADAR target. Reflectivity is the percent of intercepted power reflected or scattered by the target while the

directivity is the ratio of the power scattered back in the radar's direction to the power that would have been backscattered in all directions. When sufficient uncorrelated scatters are available from an illuminated area by the RADAR, the signal received has a Gaussian distribution (De Loor *et al.*, 1974). The backscattering coefficient at polarisation  $pq$  can be obtained from the  $S_{pq}$  elements of the scattering matrix (González, 2008):

$$\sigma_{pq} = \langle S_{pq} S_{pq}^* \rangle \quad (2.5)$$

Where the brackets indicates a spatial average and \* indicates complex conjugate.

Polarimetric parameters can be derived from the covariance matrix and different matrices can be obtained from scattering matrix. The polarimetric parameters can be classified into coherent parameters which require the phase relationships and non-coherent parameters which do not involve phase parameters. The most common non coherence parameters are the backscattering coefficients which are used in this study. They are spatially averaged  $\sigma_{HH}$ ,  $\sigma_{VV}$ , etc. For coherent parameters, the most common are entropy (H), the correlation coefficient ( $\rho_{hh-vv}$ ) or angle alpha ( $\alpha$ ).

In the context of RADAR vegetation applications, the scattering phenomenon occurs when radiation interacts with a particle that has size similar or larger than the radiation wavelength. In general, in a natural surface, there are two main types of scattering, surface and volume scattering (Figure 2.13). Surface scattering arises on natural surfaces such as soil and water, while volume scattering occurs on snow and vegetation. Moreover, the third type of scattering is the interaction between volume and surface, including double bounce scattering. This type of scattering occurs in corner reflectors with perpendicular surfaces (Lusch, 1999). These scattering mechanisms can be distinguished by means of polarimetric approaches.

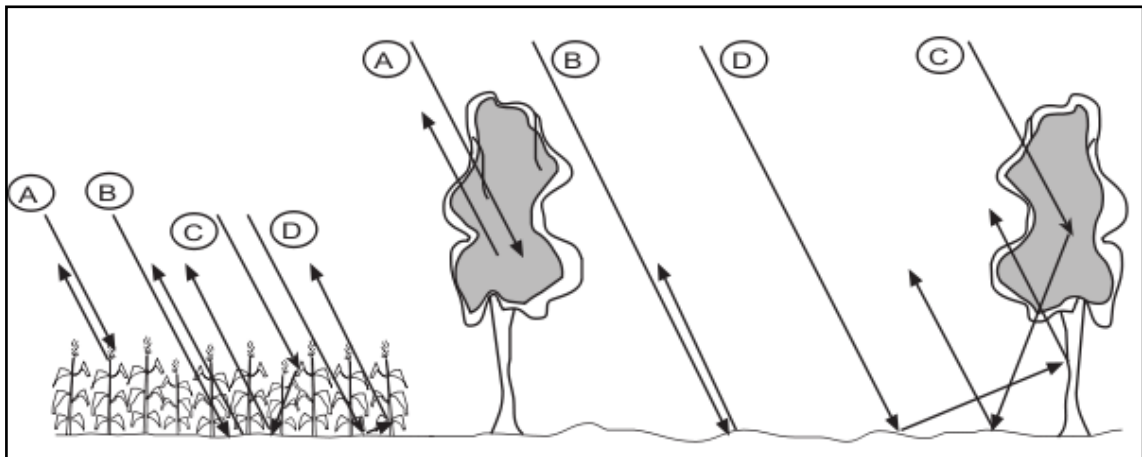


Figure 2.13: Types of backscattering in a natural surface. a) volume scattering in the tree crown, b) surface scattering, c) tree-soil backscattering (double bounce scattering), d) soil-tree backscattering (double bounce scattering) (Lusch, 1999).

The roughness of the surface plays an important role in determining the types of surface scattering. A specular reflection is produced when radiation intercepts with a very smooth surface while if the surface is perfectly smooth, the radiation is reflected forwards with a reflection angle  $\theta_s$  that equals to the incidence angle  $\theta_i$ . In the case of the surface is not perfectly smooth, diffuse reflection occurs and the scattered radiation has two components: a specular component and a diffuse component. The specular component decreases and almost all the scatter radiation is diffuse when the surface becomes rougher (Ulaby *et al.*, 1986). As a result, the backscattering coefficient  $\sigma$  will be close to zero in the case of very smooth surface and  $\sigma$  will be low if the surface is slightly rough while  $\sigma$  will be slightly high and rough if the surface is very rough, see Figure 2.14 (González, 2008).

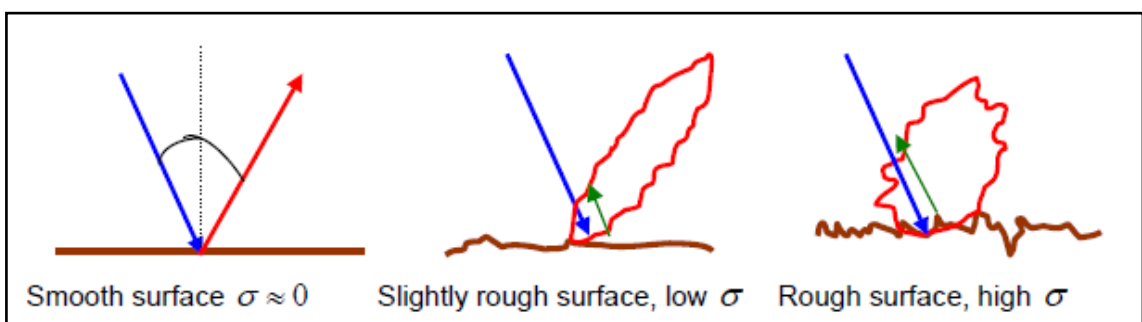


Figure 2.14: the backscattering coefficient  $\sigma$  for different surface roughness conditions (González, 2008).

In this study there is an interest in the behaviour of Savannah woody vegetation surface observed by ALOS PALSAR system at L-band.

In general, the backscattering from vegetation surface is high. However, the orientation, form and size of the plant affect the backscatter behaviour (Henderson and Lewis, 1998). Many studies revealed the relationship of the backscatter intensity channels of a polarimetric SAR to biophysical variables of vegetation, especially the cross-polarised L-band channel which proved to be useful (Harrel *et al.*, 1997). Moreover, Interferometric Synthetic Aperture Radar (InSAR) technology has been studied for use with vegetation. A study by Balzter *et al.* (2007) used airborne dual-wavelength SAR interferometry (InSAR) at X- and L-band to estimate canopy height using a method based on the scattering phase centre separation at different wavelengths, over Monks Wood National Nature Reserve in UK. Results of extracted canopy height model were validated using airborne imaging LiDAR data. The RMSE of estimates of CHM derived from InSAR is 3.49 m compared to LiDAR data. Biomass was then estimated using canopy height estimates with allometric equations.

Compared with LiDAR and passive optical sensors, InSAR has the ability to penetrate cloud cover (Wulder and Franklin, 2003). However, InSAR has proven in many studies to be less accurate for vegetation characterization purposes when compared to LiDAR (Hyde *et al.*, 2006; Goetz *et al.*, 2007). Improved results for forest parameters estimation could be achieved when combining InSAR data with LiDAR data (Slatton *et al.*, 2001; Nelson *et al.*, 2005).

Synthetic aperture radar (SAR) is an all-weather sensor suitable for repetitive monitoring and reliable estimation of forest structure information over large areas due to its long wavelength. Many studies have already been carried out using airborne SAR systems, as well as space systems such as SIR-C/X SAR, ERS and JERS-1; C-Band ENVISAT-ASAR (i.e., Harrel *et al.* 1997; Kasischke *et al.* 1997; Ulaby *et al.* 1990; Chauhan *et al.*, 1991; Lin and Sarabandi, 1999; Garestier *et al.*, 2009; Santoro *et al.*, 2010). In particular, it has been observed that the backscattering coefficient at L-band had some correlation with forest structure such as volume and biomass, with L-VH or HV better than HH or VV (Ranson and Sun, 1994).

However, LiDAR and Synthetic-Aperture RADAR measurements offer promising means to obtain comprehensive measurements of vegetation structure at a regional to global scale (Drake *et al.*, 2002; Popescu *et al.*, 2003, Saatchi *et al.*, 2007; Antonarakis *et al.*, 2008; Sun *et al.*, 2008). LiDAR has been used mainly to extract canopy heights, due to its ability to measure the distance from the sensor to the surfaces in its path. Beside LiDAR, RADAR has the ability to penetrate canopies of different densities depending on the wavelength of the pulse emitted, and thus has been used to estimate basal area, volume, and aboveground biomass from radar backscatter measurements (Cloude ,1998; Sarabandi, 2000; Fransson *et al.*, 2000, Saatchi *et al.*, 2007). The most recent RADAR Interferometry techniques have extended the application of the Radar remote sensing in estimating forest heights (Santoro *et al.*, 2007). However, the past and current studies show that the use of spaceborne LiDAR and Synthetic-Aperture Radar in the savannah environment is rare. In this study, two comparative analyses have been done to validate the ability of spaceborne LiDAR remote-sensing measurements to provide information on savannah vegetation structure. The first one is to compare

GLAS waveforms estimations of vegetation height with those from airborne LiDAR data. The second one is to compare and combine GLAS data and ALOS PALSAR data to predict estimation of woody cover of savannah vegetation.

## **2.10 Summary**

Savannah landscapes offer a challenge of an altogether greater magnitude because they contain greater numbers of species and landscapes than other landscapes (Tews *et al.*, 2004a). Due to this challenging complication, the use of remote sensing in the savannah ecosystems has largely been limited to studies of fire (i.e., Alleaume, 2005 and Roy *et al.*, 2005b) and has been insufficiently explored for ecological research in these areas (Levick and Rogers, 2008).

LiDAR recording systems have the ability to capture information relating to vegetation structure. This provides direct and indirect measurements of vegetation structure (Dubayah and Drake, 2000). Full-waveform LiDAR systems are a promising technique for various forestry applications (Pirotti, 2011). The recently launched Geoscience Laser Altimeter System (GLAS) provides global LiDAR data with a variable diameter of 70 m footprint spaced at approximately 170 m. Some early research has shown that it offers potential in estimating forest structure which could be extended to biomass measurements of savannah systems, but some questions remain over the reliability of the structural measures it generates. This research explores the use of GLAS data in more open sparsely vegetated areas such as savannah ecosystems.

Beside the spaceborne and airborne LiDAR, RADAR offers promising methods to obtain information on the dynamics of vegetation structure, at both the scale of

individual trees and the canopy (Santos *et al.* 2000; Lucas *et al.*, 2006c and 2009). LiDAR, due to its ability to measure the distance from the sensor to the surfaces in its path, has been used mainly to extract canopy heights. Radar pulses have the ability to penetrate canopies of different densities depending on the wavelength of the pulse emitted, and thus have been used to estimate basal area, volume, and aboveground biomass from radar backscatter measurements (Fransson *et al.*, 2001; Saatchi *et al.*, 2007).

This chapter has introduced the hypotheses on the processes of savannah vegetation dynamics and tree-grass coexistence; presented a background of LiDAR and laser systems; and summarized its principles, including a full description of the two types of LiDAR recording data systems - the discrete return and the full waveform recording systems. It also identified the previous applied studies using both types of LiDAR data with comprehensive description of vegetation structural applications using satellite LiDAR sensors. Moreover, this chapter has presented other sources of dataset that will be used for comparative analysis, mainly the airborne LiDAR and the ALOS RADAR, which will be discussed in more detail in the next chapter.

Recently, vegetation LiDAR data have become more widely available to study the link between vegetation LiDAR signals and vegetation structure characteristics. Many studies have demonstrated the potential use of spaceborne and airborne vegetation LiDAR data to map vegetation height, aboveground biomass characteristics, and other vegetation structure parameters (Lefsky *et al.*, 1999a; 2002a; 2002b; 2005b; Harding *et al.*, 2001; Drake *et al.*, 2002; 2003a; 2003b; Patenaude *et al.*, 2004; Anderson *et al.*, 2006; 2008; Popescu, 2007; Popescu and Zhao, 2008; Chen *et al.*, 2007; and Chen,

2010b). Therefore, characterising savannah canopy structure using spaceborne remote sensing sensors would help the advancement of knowledge in the savannah domain.

The spaceborne Geoscience Laser Altimeter System (GLAS), part of the ICESat mission, provides global LiDAR data with a variable diameter of 70 m footprint spaced at approximately 170 m (Zwally *et al.*, 2002). It has successfully shown promising approaches for estimating forest structure (Drake *et al.*, 2002; Lefsky *et al.*, 2002a; Duong *et al.*, 2008; Rosette *et al.*, 2008a; 2008b; 2008c; Chen, 2010b). Whilst GLAS data have demonstrated its ability to retrieve vegetation structure in temperate and boreal forests (i.e., Ranson *et al.*, 2004 a, 2004b; Rosette *et al.*, 2008c), it is important to study its ability in more open sparsely vegetated areas such as savannah ecosystems. The following chapter introduces the sources of satellite and airborne LiDAR data used within this research, with distribution of field measurements data and its techniques. Finally, the methodologies of analysing this data are described.

# CHAPTER THREE

## DATASETS AND GENERAL METHODOLOGY

### 3.1 Introduction

Kruger National Park (KNP) presents a highly suitable site for savannah ecosystem. Ecosystem managers in South Africa, particularly in the Kruger National Park (KNP) have designed the Threshold of Potential Concerns (TPCs) for specific variables to monitor changes in the savannah landscape (Rogers, 2003). Canopy height, canopy cover, and the biomass of the herbaceous vegetation are of special interest to assess woody vegetation structures in KNP (Biggs and Rogers, 2003).

The aim of this research is to evaluate the potential of ICESat/GLAS to estimate vertical canopy structure over savannah landscape for characterizing canopy structure over savannah vegetation landscapes in Kruger National Park. This will involve mainly the methodology of analysing spaceborne LiDAR data plus some fieldwork, and compare it with airborne LiDAR and RADAR data to validate the remote sensing analysis.

This chapter describes the source of the satellite and airborne LiDAR data and other data sets that are used within this study, and also provides a broad methodology to show how the different objectives fit together to achieve the aim of the research. This chapter also presents and discusses the initial results obtained from applying methods of retrieving vegetation heights using full GLAS waveform. Results are presented that show the technique that will be used in the two following chapters 4 and 5.

### 3.2 Study area and datasets

#### 3.2.1 Study area

The two study areas are in Kruger National Park (KNP), which is located in the north-eastern part of South Africa (22.3-25.5° S, 30.8-32° E; Figure 3.1). KNP covers an area of approximately two million hectares, and is adjacent to Mozambique to the east and Zimbabwe to the north. Its boundaries are demarcated by the Limpopo Hills in the east, the Luvuvhu and Limpopo rivers in the north, and the Crocodile River in the south; with three permanent rivers, which are the Olifants, Letaba and the Sabie, flowing from west to east across the Park. In addition to these rivers, there is a multitude of seasonal rivers (Gillson and Duffin, 2007).

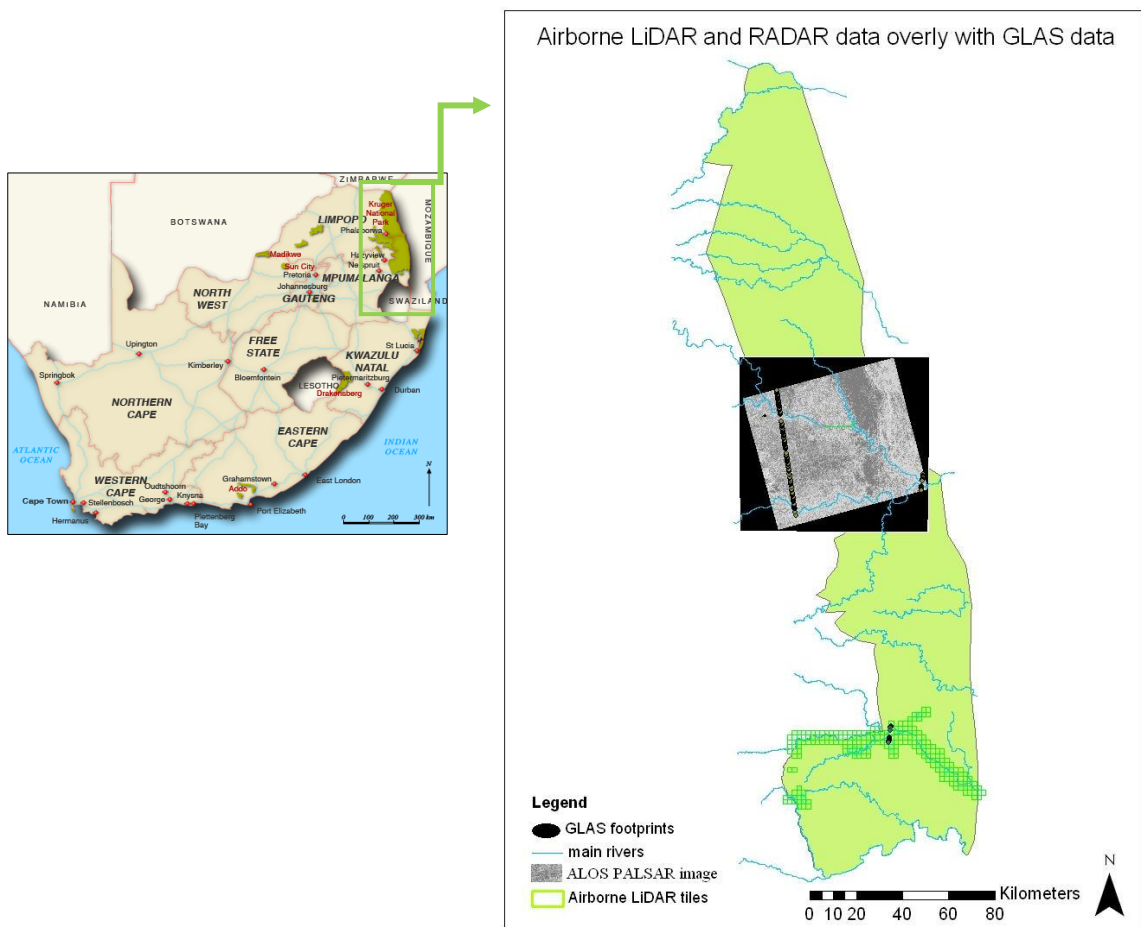


Figure 3.1: The location of the study area in South Africa and the two study areas in KNP, which shows overlapping between airborne LiDAR tiles and GLAS tracks plus the overlying between GLAS tracks and RADAR (ALOS PALSAR) data.

Climatically, KNP is temperate in the south and tropical to subtropical in the north. The average annual rainfall is 400mm per year in the far north and 730 mm in the southwest, with great annual variability. Elevations range from 260m a.s.l. to 839m a.s.l. Geologically, KNP is divided along a central north-south axis, with basalt plains to the east and undulating granite to the west (Gillson and Duffin, 2007). The flora of the park is sub-arid to semi-arid wooded savannah, with a heterogeneous structure varying from open grassy plains with low shrubs to dense woodlands and riparian forests (Gillson and Duffin, 2007). There are 1903 plant species in the KNP, including over 400 tree and shrub species, of which the genera *Acacia*, *Combretum*, *Sclerocarya* and *Colophospermum* are common; and over 220 grasses (Eckhardt *et al.*, 2000). Vegetation in the park is divided into four major types, which are influenced by the underlying geology (Figure 3.2(a)), soil patterns, topography, fire and grazing (Eckhardt *et al.*, 2000).

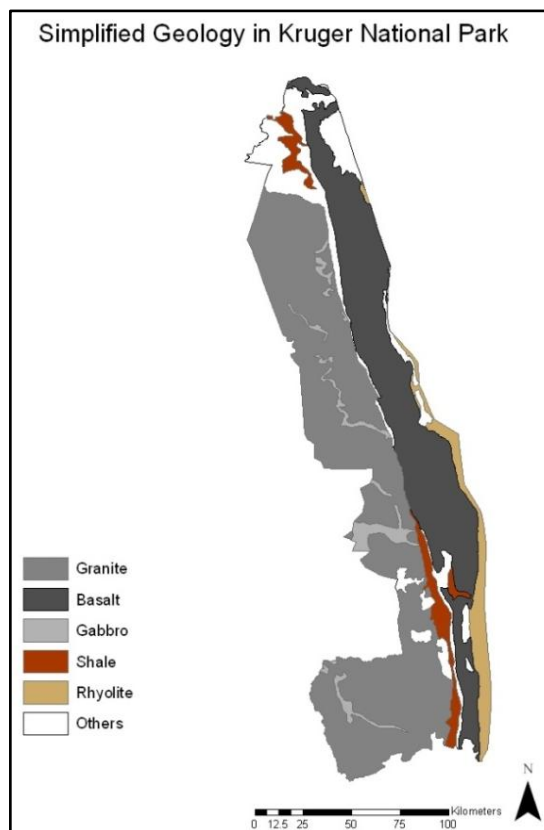


Figure 3.2(a): The simplified geology in KNP.

According to Gertenbach (1983), the Park is divided into 35 landscapes (Figure 3.2(b)): a landscape is defined as an area with a specific climate, geomorphology, soil and vegetation pattern, together with the associated fauna (Gillson and Duffin, 2007). The Park has diverse fauna, including 147 species of mammals, which include important herbivores such as elephant and buffalo; and 492 bird species (Eckhardt *et al.*, 2000).

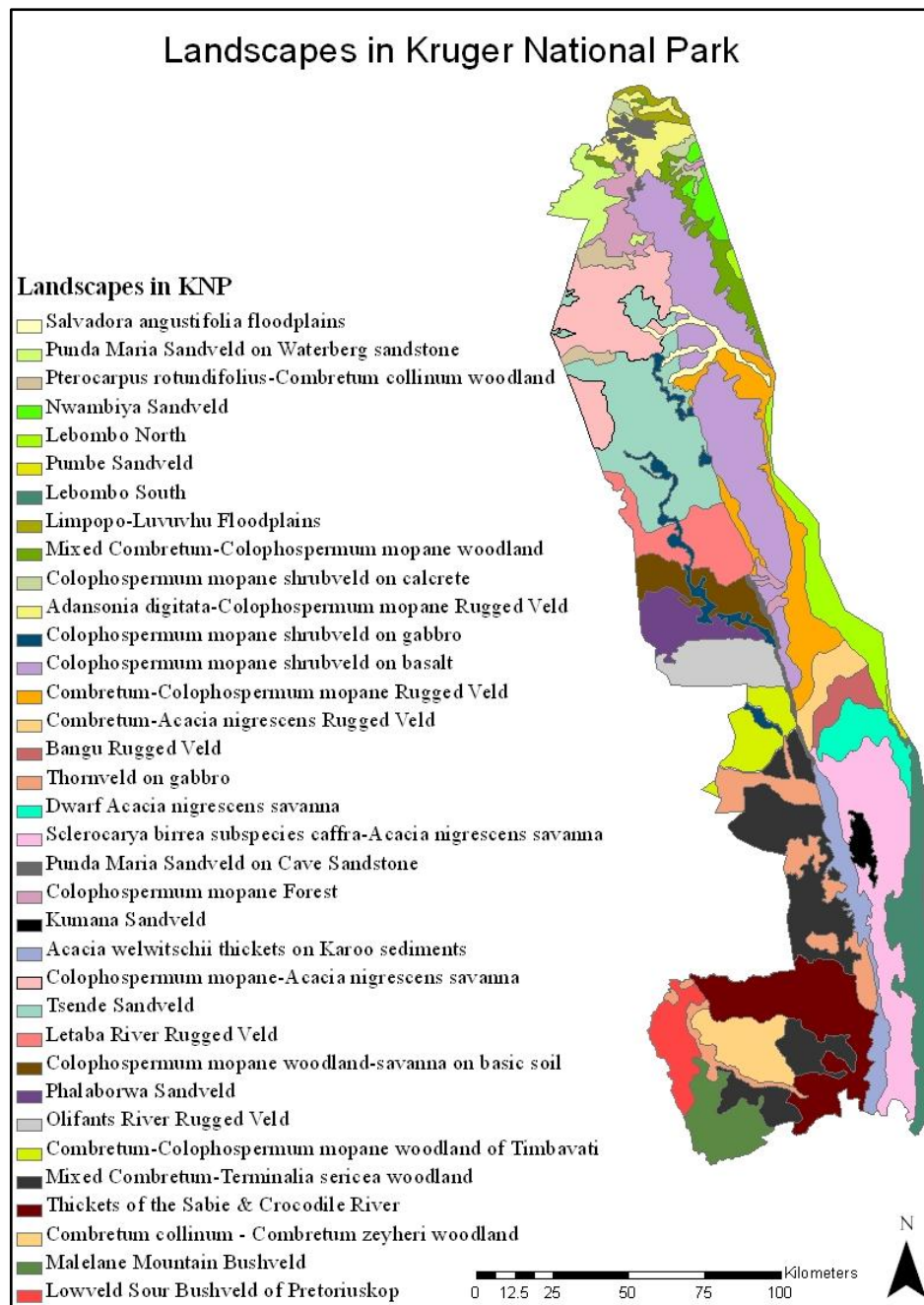


Figure 3.2(b): The landscapes that characterise KNP.

### 3.2.2 Field data

Field data were collected within the GLAS and airborne LiDAR sampling range during the winter of 2010. Field data collection consisted of thirty-one 35 m radius plots for each (footprints); and each plot was divided into four subplots (10 m radius). The heights of the trees were measured and their average was used to compare with airborne LiDAR and GLAS retrieved canopy height. A two year difference between GLAS footprints and field data plus a six year difference between airborne LiDAR and field data were neglected in the data analysis. No field data is available within the overlapping data between ALOS PALSAR data and GLAS footprints. Figure 3.3(a) shows the spatial coverage of GLAS over KNP and the overlaying with airborne LiDAR and ALOS PALSAR data; and Figure 3.3(b) shows the Selected GLAS footprints for field data collection, which are just overlaid with airborne LiDAR data.

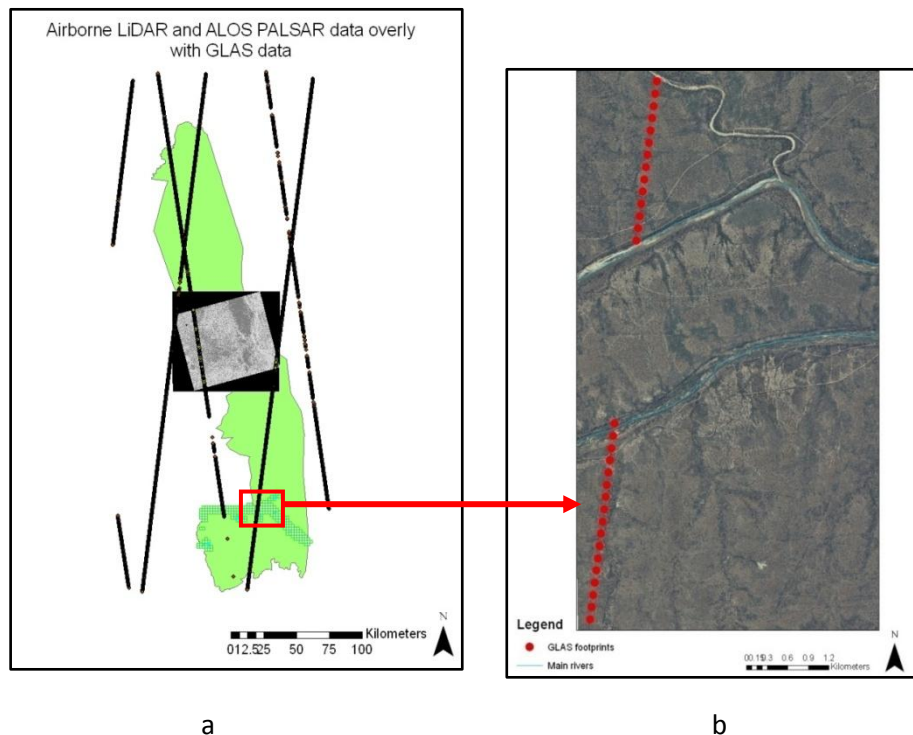


Figure 3.3(a): Overlaying of GLAS data and both of data sets airborne LiDAR data and ALOS PALSAR data. b) Representation of the 31 GLAS footprints selected for field data collection in KNP on Google Earth map.

### 3.2.2.1 Fieldwork and protocol

Before the fieldwork, it was important to identify the footprints to be sampled for vegetation height estimation. Thirty-one samples were selected for the fieldwork. With any fieldwork comes the issue of inaccessibility: two samples fell on the riverine lands. Fieldwork was conducted in August 2010. The aims of the fieldwork were to make measurements of canopy height within the selected sampled footprints to provide comparisons with estimates from the satellite LiDAR estimates.

A handheld Global Positioning System Garmin eTrex (GPS) receiver was used to locate the identified GLAS footprint centres. Further, data was collected in four annular subplots: one in the footprint centre and three on the footprint located 20 m at approximate azimuths of 0°, 120° and 240° from the subplot centre. Radius of subplots were 10 metres each in order to account for the reflected LiDAR energy, which has a central maximum and fades away radial outwards (Duong *et al.*, 2008).

A peg was placed at the footprint centre as the field site reference point. The first subplot, which had the centre reference point, was delineated by placing pegs along a 10 metre radius bearing from the footprint centre. Within the delineated subplot, tree heights 1 metre above the ground surface was systematically measured. Then, after the centre of the GLAS footprint was located, three sampling subplots with a radius of 10 metres to north, south-east and south-west at approximate azimuths of 0°, 120° and 240° respectively from footprint centre were located within the GLAS footprint. Figure 3.4 gives the conceptual sampling design for the GLAS footprint.

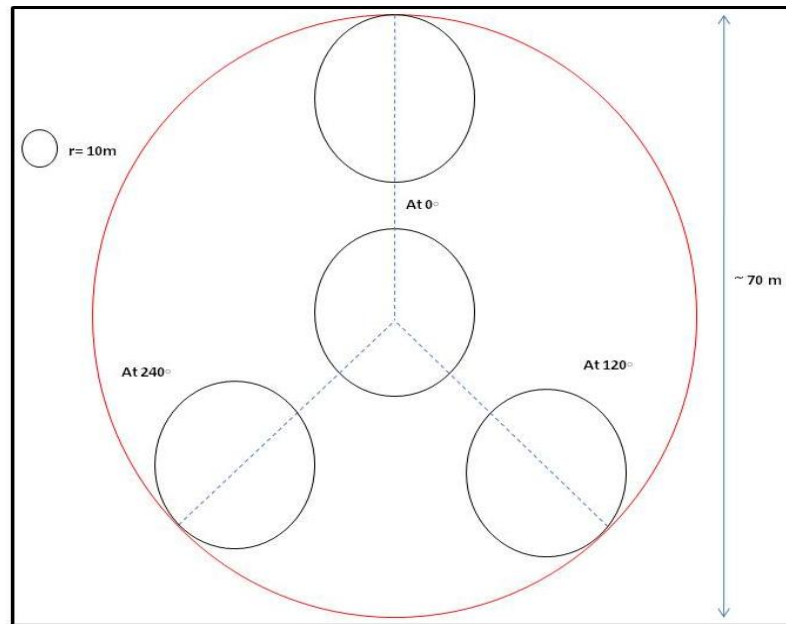


Figure 3.4: Sampling plots within a GLAS footprint: radius of sampling subplots (small circles) is 10 m; the distance between sampling plots is 20 m.

### 3.2.2.2 Fieldwork measurements

The priority for the fieldwork measurements was given to height tree measurement taken at 31 footprints location along the pass to be compared with full waveform derived canopy height estimations.

#### Tree height

Tree height was measured using two methods: the clinometer and woodland stick methods. For the taller trees (more than 10 m), clinometer together with measuring tapes were used to obtain direct height estimates; while routine height measurement using the woodland stick were used to obtain direct height measurements for trees taller than 10 m. The selected footprints for tree height measurements are located in the Sabie/Crocodile Thorn Thickets ecozone, which is characterized by a very dense growth of thorny shrubs. Therefore, for some plots it was easier to use the second height measurement method and much time has been saved by using this woodland stick method.

The vegetation in these sampling plots varies from dense, short bushveld to open tree savannah (Figure 3.5). The dominant species is *Combretum apiculatum*, which is medium sized (4-10 m height), with associated species - mainly *Acacia nigrescens*, which varies in size from 8-20 m height, and other woody species.



Figure 3.5: The photograph on the left shows an example of dense vegetation within some plots while that on the right shows the open tree savannah in other plots.

### 1- Clinometer method

Tree height was measured using the clinometer and tape measure. This is illustrated in Figure 3.6. The clinometer used allowed accurate direct height readings for the tree top and tree base from eye level at horizontal distances (10 or 15 m) from the tree (D).

Equation (3.1) was used to calculate the tree height for the flat footprints and sloping ground when the base of the tree is below eye level (Figure 3.6 (a and b)):

$$\text{Tree Height} = H1 + H2 \quad (3.1)$$

Where  $H1$ : is the distance from eye level to the top tree:  $H1 = \text{Tan } ^\circ a \times D$ ;

$H2$ : is the distance from eye level to the base of the tree:  $H2 = \text{Tan } ^\circ b \times D$

Equation (3.2) was used to calculate the tree height when the base of the tree is above the eye level of the observer (Figure 3.6(c)).

$$\text{Tree Height} = H1 - H2 \quad (3.2)$$

Where  $H1$ : is the distance from eye level to the top tree:  $H1 = \tan \alpha \times D$ ; and  $H2$ : is the distance from eye level to the base of the tree:  $H2 = \tan \beta \times D$

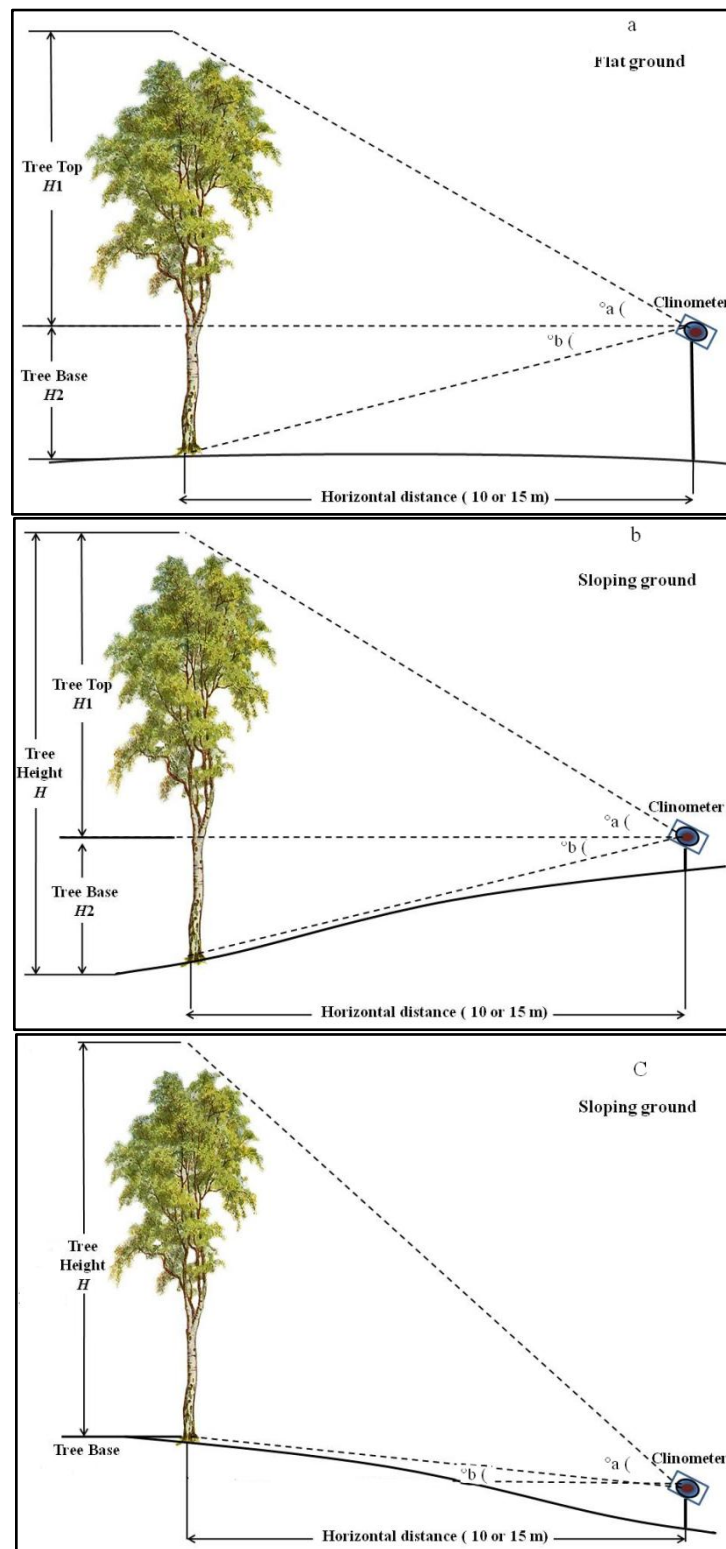


Figure 3.6: Use of the clinometer to measure the tree height in flat and sloping ground when the base of the tree is below eye level, while c) measuring the height of the tree when the base of the tree is above eye level, adapted from (NSW Government website, 2007).

## 2- A woodland stick method

A straight stick was used to measure tree height by holding its base vertically at arm length, making sure that the length of the stick above the observer hand equals the distance from the observer hand to their eye. Then, the observer walked backwards away from the tree and stopped when the length of the stick above the observer hand is the same length as the tree. Measuring the distance from the tree to where the observer is standing gives the tree height (Figure 3.7).

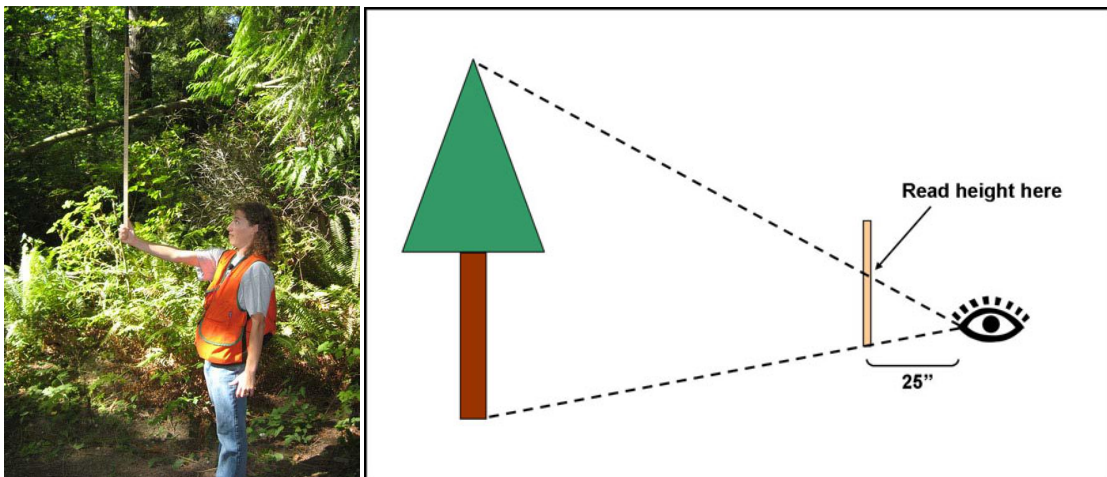


Figure 3.7: Illustrates measuring tree height using a woodland stick method. Source: (USAD website, 2008).

Species also have been recorded for the sampling footprints and an approximation of percentage coverage of species (trees, shrubs and non-woody vegetation) was also recorded. These measurements were repeated for each selected GLAS footprint for the field site. Table 3.1 shows the field data collected for the 29 GLAS footprints using both methods described above.

Table 3.1: The field data collected for 29 ICESat-GLAS footprints location in KNP.

<b>Footprint ID</b>	<b>Longitude</b>	<b>Latitude</b>	<b>Maximum Height (m)</b>	<b>canopy cover (%)</b>
<b>1627010654-20</b>	24.93138	31.660736	56	70
<b>1627010654-21</b>	24.932933	31.660497	46	70
<b>1627010654-22</b>	24.934485	31.660258	16	70
<b>1627010654-23</b>	24.936037	31.660018	22	70
<b>1627010654-24</b>	24.937589	31.659776	11.5	70
<b>1627010654-25</b>	24.939141	31.659532	14	70
<b>1627010654-26</b>	24.940692	31.659287	22	70
<b>1627010654-27</b>	24.942243	31.659042	10	70
<b>1627010654-28</b>	24.943794	31.658797	14.5	70
<b>1627010654-29</b>	24.945348	31.658554	12	70
<b>1627010654-30</b>	24.946901	31.658312	24	70
<b>1627010654-31</b>	24.948455	31.658072	25	50
<b>1627010654-32</b>	24.950008	31.657832	18	50
<b>1627010654-33</b>	24.95156	31.657594	16	60
<b>1627010664-10</b>	24.97793	31.65368	11	12
<b>1627010664-11</b>	24.97948	31.653448	20	15
<b>1627010664-12</b>	24.981031	31.653214	9.5	10
<b>1627010664-13</b>	24.982584	31.652979	10.5	10
<b>1627010664-14</b>	24.984138	31.652742	16.5	10
<b>1627010664-15</b>	24.985692	31.652505	17.5	10
<b>1627010664-16</b>	24.987246	31.652266	16.5	10
<b>1627010664-17</b>	24.988799	31.652027	10	30
<b>1627010664-18</b>	24.990351	31.651788	14.8	5
<b>1627010664-19</b>	24.991903	31.651547	14	15
<b>1627010664-20</b>	24.993454	31.651306	11	5
<b>1627010664-21</b>	24.995006	31.651064	12	70
<b>1627010664-22</b>	24.996557	31.650822	8	30
<b>1627010664-23</b>	24.998109	31.650579	12	30
<b>1627010664-24</b>	24.99966	31.650337	12	40

### **Crown canopy cover**

Crown canopy cover is a good ecologically significant parameter to estimate how much a plant dominates an ecosystem; it is highly related to biomass and reflects the amount of CO<sub>2</sub> and light that the plant captures and turns into phytomass (aboveground plant biomass). Cover also reflects the amount of soil water and nutrients that the plant can harvest. Crown canopy cover is expressed as % of area. Therefore, the meaning of cover is the same for grasses, shrubs, wood, etc (Daubenmire, 1959). In this study, an ocular estimation of percentage ground cover has been recorded for each subplot, and an

average total of crown canopy cover has been calculated for the whole GLAS footprint. This was done using the guidance explained in the work of Law *et al.* (2008) for the 29 GLAS footprints (Table 3.1). Figure 3.8 shows examples of cover percentage and Table 3.1 contains a summary for the recorded field data.

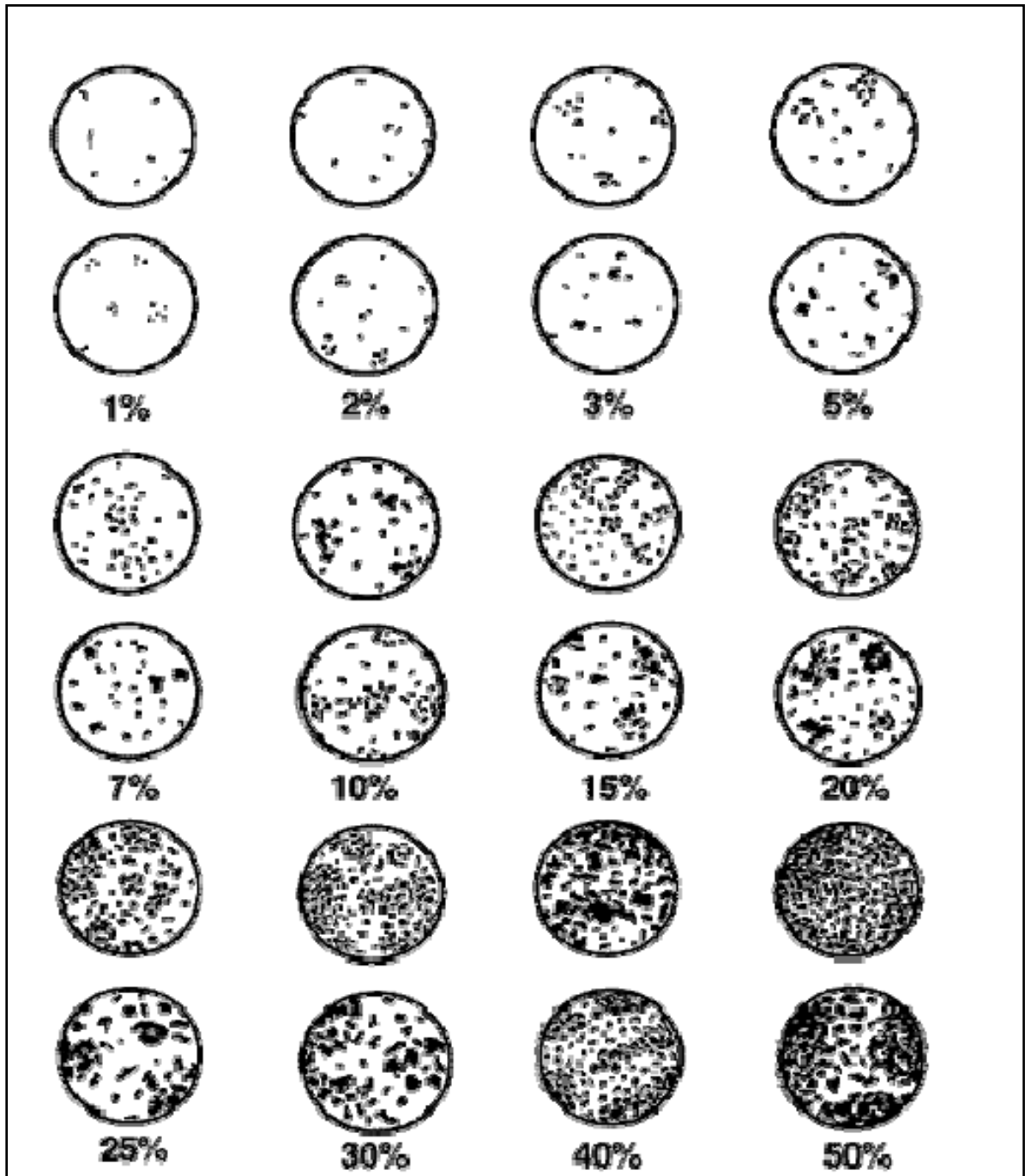


Figure 3.8: Examples of percent crown canopy cover (Law *et al.*, 2008).

### **3.2.3 Airborne Laser data**

The airborne LiDAR data that were used in this study were acquired by the University of Witwatersrand (WITS) on 24 August and 9 September 2004. Data are supplied in WGS84 UTM South Zone36 orthometric height in comma delimited (.las) format as follows: East, North, Height, and Intensity. Laser points were converted from WGS84 ellipsoidal to WGS84 orthometric height using the South African Quasi geoid in Xform ver.4.3 by the data provider.

Before any analysis is performed with LiDAR data, the data received has to be checked for any inconsistencies using the point file information tool in ArcGIS 3D Analyst™ tool. This tool is designed to read the headers of LAS files for further analysis. The average point spacing tends to be approximately 1 metre, which gives a good sampling for further analysis for GLAS footprint data. LAS files captured since 2004 conform to the LAS 1.0 specification. This specification allows the separation of LiDAR data into ground returns and non-ground returns by the classification field associated with LAS files. A full explanation of the specification can be found in LAS specification (Version 1.0, 2002). The LAS data files were read by the LAS to Multipoint tool in ArcGIS 3D Analyst™, and accommodated classifications and separations for the LiDAR points into unique feature classes at 1 metre resolution were done to extract Digital Surface Model and Digital Elevation Model for further analysis.

### **3.2.4 ICESat-GLAS data**

#### **3.2.4.1 GLAS product summary**

As described in the previous chapter, ICESat has acquired a magnitude database of raw and processed data, which is organised into the 15 data products from GLA01 to

GLA15 (Brenner *et al.*, 2003). Each product is developed and processed for particular uses. GLAS data is pre- processed into different levels from level 0 to level 3. Level 0 contains waveform raw data; level 1 data includes instrument parameters; level 2 data contains geophysical, ice, ocean, atmosphere and land parameters; and level 3 contains gridded digital elevation model and atmospheric backscattered images. These data are distributed by the National Snow and Ice Data Centre (NSIDC) in granules, which contain different amounts of data with different structure, variables and size of data. The data are stored in a binary format in big-endian byte order and are organised in records of 40 footprints. All the data products are time-stamped with transmit time of pulse in Coordinated Universal Time (UTC) as collected along-track. To relate information from different datasets, a unique record index is assigned to every one second of data. The unique record index is consistent across all products of the same release (NSIDC, 2003).

Two data products of release 29 GLAS were used in this study: Level 1A Global Altimetry data (GLA01) and Level 2 Global Land Surface Altimetry data (GLA14).

‘GLA01’ is a level 1A data product, which contains granules that have raw LiDAR waveform in digitizer counts, which are afterwards converted to volts (by users). One granule covers  $\frac{1}{4}$  orbit or ~23 minutes of data. This data can be obtained by searching the granule ID or time. GLA01 contains the transmitted and received echo waveforms. This product has variables such as the filter threshold value for signal detection in digitizer counts, laser transmit energy, received energy from all signals above threshold, sampled transmit pulse waveform, 4ns background mean value, and standard deviation (Brenner *et al.*, 2003). ‘GLA14’ is a level 2 data, which contains sensor position and pointing information as well as calculated footprint position, size and shape, and land

surface elevation. GLA14 granules cover 14 consecutive orbits. Transmitted pulse and recorded waveforms are represented with characteristic shape parameters only. The recorded waveform is decomposed into a series of Gaussian peaks, as described in Hofton *et al.* (2002), Zwally *et al.* (2002) and Brenner *et al.* (2003).

These products are of interest for this study because GLA01 carries the signal strength, while GLA14 contains geolocation of the incident LiDAR beam. The record number, shot time and shot number are common fields across GLAS products.

#### **3.2.4.2 Pre-processing of GLAS data**

GLAS data were acquired in the period from 19 February 2008 to 15 March 2008. GLA14 altimetry product data are distributed in binary (\*.DAT) format, which were converted to ASCII format using the NSIDC GLAS Altimetry elevation extractor tool (NGAT) version 11 to derive each shot unique number, date and time and acquisition, latitude and longitude (in decimal degrees), elevation (metres), and geoid (which is defined as the height at which half the return energy is above and half is below (Ranson *et al.*, 2004b)). GLA01 data are in counts and were converted to voltages using IDLreadGLAS software codes provided by the National Snow and Ice Data Centre. These codes were used to process and explore the waveforms and to identify and extract parameters of interest.

Raw data that was ordered from NASA were generated to produce usable data, including unique number, shot number, shot time, number of samples, and uncompressed waveform values in volts (Seidel, 2005); and then GLA01 waveforms were linked to GLA14 on the basis of record and shot numbers. GLAS footprints were

then identified over the study area and waveforms with high level of echo saturation were filtered out.

These datasets were acquired in the period from 19 February 2008 to 15 March 2008, during the temporal coverage of laser L3J, whose operational period was between 17 February and 21 March, and are all from release 29. There are 6 tracks with 8519 waveforms in total, and 2629 waveforms are located within the study area (Figure 3.3).

Table 3.2 describes the GLAS variables used in this study.

Table 3.2: The ICESat-GLAS product variables used in this study (NSIDC, 2003).

<b>Variable</b>	<b>Element of data product of</b>	<b>Description</b>
<b>Record Number</b>	GLA01, GLA14	GLAS digitizes 40 echo signals per second. Each set of forty shots is assigned a unique record number during processing of level 0 data.
<b>Shot Number</b>	GLA01, GLA14	There are forty shots in each record and each is assigned a number called the shot number,
<b>Date</b>	GLA14	Date of transmitted pulse in mm/dd/yyyy
<b>Time</b>	GLA01, GLA14	Time of transmitted pulse in hh:mm:ss.sss
<b>i_lat</b>	GLA014	Geodetic latitude of the laser shot in degrees
<b>i_lon</b>	GLA014	Longitude of the laser shot in degrees
<b>i_elev</b>	GLA014	Surface elevation in meters of the laser shot from the reference ellipsoid
<b>i_gdHt</b>	GLA014	Height of the geoid above the reference ellipsoid in meters
<b>i_UTCTime</b>	GLA01, GLA14	Transmit time in UTC
<b>i_Gamp</b>	GLA014	Amplitude of each Gaussian solved for (up to six) waveform processing in 0.01 volts.
<b>d_4nsBgMean</b>	GLA01	The mean background noise value
<b>d_4nsBgSDEV</b>	GLA01	The standard deviation of the background noise
<b>i_SigBegOff</b>	GLA014	Signal Begin Range Offset
<b>i_SigEndOff</b>	GLA014	Signal End Range Increment
<b>i_nPeaks</b>	GLA014	The initial number of peaks of the received echo determined from the smoothed waveform, using alternative parameters.

### **3.2.5 ALOS PALSAR data**

#### **3.2.5.1 Overview of ALOS satellite**

The Advanced Land Observation Satellite (ALOS), which has been operational since its launch in January 2006, is the largest satellite developed in Japan. It designed for four major application themes of detailed observation of the earth surface which involves generation of 1:25,000 geographical maps, regional and frequent monitoring of global environmental changes, information distribution for disaster mitigation and resource exploration. It operated for five years, although it was designed to only operate for three years. However, ALOS terminated its mission on May 2011. That is, the termination was accomplished by using three high resolution optical and microwave sensors: the Panchromatic Remote-Sensing Instrument for Stereo Mapping (PRISM); the Advanced Visible and Near-Infrared radiometer 2 (AVNIR-2); and the Phased-Array L-band Synthetic Aperture Radar (PALSAR) (Shimada *et al.*, 2009).

#### PALSAR

The Phased Array L-band Synthetic Aperture Radar (PALSAR) is an enhanced version of the Synthetic Aperture Radar on JERS-1 (L-band; HH-polarisation; 35°off-nadir angle); like its predecessor, PALSAR was developed jointly by the Japan Aerospace Exploration Agency JAXA and the Japan Resources Observation Systems Organization (JAROS) (Rosenqvist *et al.*, 2004).

PALSAR is a fully polarimetric instrument, operating in fine-beam mode with single polarisation (HH or VV), dual polarisation (HH+HV or VV+VH), or full polarimetry (HH+HV+VH+VV), where the first note of H (horizontal or V (vertical) is the transmit polarization and the second is the receive polarization. PALSAR is used to image the earth surface under all weathers and day/night conditions. It has two selectable

resolutions: a high-resolution mode with a bandwidth of 28 MHz, allowing the slant range resolution of 5 m; and a low resolution with a bandwidth of 14 MHz, allowing the slant range resolution of 10 m (Shimada *et al.*, 2009). Table 3.3 lists the PALSAR characteristics. The PALSAR acquisition data allowed the establishment of an unprecedented, global Data Observation Strategy in support of climate change research and environmental conventions; and enriches land use classification, interferometry, tree-height estimation, and sea-ice monitoring (Rosenqvist *et al.*, 2004; Shimada *et al.*, 2009).

Table 3.3: The PALSAR specifications. Source (Shimada *et al.*, 2009).

Mode	High resolution		ScanSAR	Polarimetry
Frequency	1,270.00MHz (L-band)			
Bandwidth (MHz)	28.0	14.0	14.0, 28.0	14.0
Polarization	HH or VV	HH+HV or VV+VH	HH or VV	HH+HV+VH+VV
Incidence angle	8 ~ 60°	8 ~ 60°	18 ~ 43°	18 ~ 43°
Resolution (m)	7 ~ 44	14 ~ 88	100(multi look)	24 ~ 89
Swath (Km)	40 ~ 70	40 ~ 70	250 ~ 350	20 ~ 65
Number of bits	5I+5Q	5I+5Q	5I+5Q	5I+5Q
Data rate (Mbps)	240	240	120, 240	240
NESZ (dB)	< -23 (70 km) < -25 (60 km)		< -25	< -29
(S/A :Db)	> 16 (70 km) > 21 (60 km)		>21	>19
Antenna :m	Azimuth : 8.9 x range: 3.1			
<b>Note:</b> NESZ:Noise Equivalent Sigma-zero <b>S/A:</b> Signal-to-ambiguity Ratio <b>I:</b> In phase signal and <b>Q:</b> quardric phase signal <b>ScanSAR:</b> Scanning SAR				

### 3.2.5.2 ALOS PALSAR data processing

L-band SAR data from PALSAR sensor used in this study were acquired over the test site during the period June 2007 to June 2008. The imagery of ALOS PALSAR in Fine Beam Double Mode (FBD) was acquired through ALOS Data European Node (ADEN) provided by the Japanese Aerospace Exploration Agency (JAXA) and the European

Space Agency (ESA). The HH and HV polarized images were received in single look complex (SLC) format and slant range geometry (processing level 1.1), with an off-nadir angle of 34.3 degree and a pixel-spacing of 9.4m in range and 3.2m in azimuth direction, respectively. The swath width approximated 70 km.

The processing of the SAR data took place using GAMMA SAR processing software. The images were undertaken as multi-looking of 1 look in range and 4 looks in azimuth direction resulting in ground range pixel-spacing of approximately 14m and 13m, respectively; and then re-sampled to a resolution of 15 m using bilinear interpolation with the Differential Interferometry and Geocoding package (DIFF and GEO). The images were co-registered using a cross-correlation algorithm and a signal to noise ratio (SNR) of 10, resulting in a discrepancy of less than one pixel.

For geocoding, a 20 m resolution Digital Elevation Model (DEM) of Kruger National Park provided by South African National Space Agency (SANSA) was sampled to 15m using bilinear interpolation. From this DEM a SAR backscatter image was simulated and transferred to slant range geometry and a geocoding look up table was created using orbit parameters. A refinement of this look up table by cross-correlating the simulated with the original images was tried but, due to the faint relief, no accurate matching points were found, and lower SNR values resulted in huge geometric distortions; so that the geocoding is relying on orbit parameters alone, resulting in an unquantified error. This processing did not involve a terrain correction as well, so that SAR inherent features like layover or foreshortening are not corrected but, with regard to the flat topography terrain, correction should not play an important role.

### 3.2.6 Ancillary data

#### 3.2.6.1 Aerial photography and GIS data

Aerial photographs acquired in 2009 for the selected study area in KNP were supplied by the National Geospatial Information in Cape Town, South Africa. They were used for visual interpretation only. The aerial photos are orthorectified and colour balanced using dodging techniques and are supplied as Band 1 = Red, Band 2 = Green, Band 3 = Blue (conventional aerial photography band order). Furthermore, Geographical Information System (GIS)-layers (Table 3.4) have been provided by SANParks were only included into the interpretation of the results.

Table 3.4: Provided GIS data sets for KNP

<b>GIS Layer</b>	<b>Type of data</b>	<b>Reference</b>
<b>Classified simplified geology</b>	Vector	Venter (1990)
<b>Classified Landscapes</b>	Vector	Gertenbach (1983)
<b>Main rivers</b>	Vector	SANParks

#### 3.2.6.2 Woody cover map for the KNP

A woody cover map for the entire park (Figure 3.9), derived from remote sensing data, was produced by Bucini *et al.* (2010). Based on the Akaike information criterion, a combination of *Japanese Earth Resources Satellite-1* (JERS-1) and Landsat imagery has been used and the result ended up in a woody cover map with a spatial resolution of 90m with  $R^2$  of 0.61 and an RMSE of 8.1%.

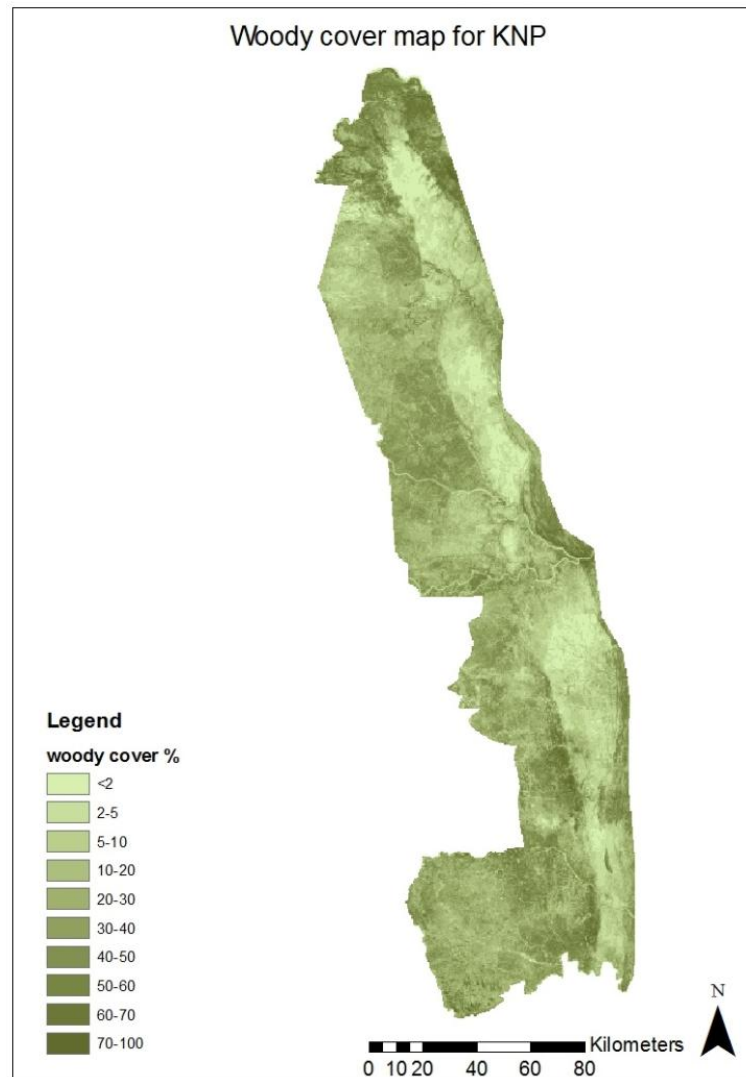


Figure 3.9: Woody cover map (%) of KNP, adapted from (Bucini *et al.*, 2010).

### 3.3 Data discussion and accuracy

#### 3.3.1 Field measurements accuracy assessment

Accuracy is defined as giving a measurement or estimation to the nearest part, of some unit of measurement (West, 2009). The first method used a clinometer, which is the most accurate and recommended method of measuring tree height, to measure tree height. However, the accuracy of height results depends on both instrument error and distance measuring error stated within the instrument documentation. The first method, using the clinometers, was used to measure tall trees (more than 10 metres) in the GLAS footprints; while the second method, which used a woodland stick, was used to

measure the trees up to a height of 10 metres in very dense subplots in GLAS footprints. A comparison was made between both methods in the field and resulted in a mean error of  $\pm 2$  metres.

### 3.3.2 GLAS footprint geolocation accuracy assessment

Footprint geolocation accuracy was assessed for the footprint over the selected study area by comparison with reference DEMs derived from airborne LiDAR data to investigate their accuracy in estimating surface elevation. The centre of the footprint was shifted 1 pixel (2 metres), two pixel (4 metres), and 3 pixel (6 metres) around the original centre of the footprint location towards North, South, East and West. Then, the correlation coefficients between the airborne and GLAS LiDAR DEMs shifted was derived for each shift. The shifts, their correlation coefficients, and standard deviation are given in Table 3.5.

Table 3.5: The shifts, their correlation coefficients and standard deviation for the GLAS footprints.

<b>Shift</b>		<b>North</b>	<b>South</b>	<b>East</b>	<b>West</b>
0 pixel	Correlation coefficient	0.998	0.998	0.998	0.996
	SD	1.89	1.94	1.82	1.99
1 pixel	Correlation coefficient	0.997	0.997	0.998	0.997
	SD	1.89	1.94	1.80	1.99
2 pixel	Correlation coefficient	0.997	0.998	0.998	0.996
	SD	2.05	1.90	1.76	2.07
3 pixel	Correlation coefficient	0.997	0.998	0.998	0.99
	SD	2.04	1.80	1.72	2.00

In general, the standard deviations for the shifted GLAS footprints show that the new locations of the GLAS footprints have little variation with the airborne LiDAR DEMs.

Hence, the differences in footprints geolocation will be neglected, giving that these uncertainties of several metres will not affect the analysis of the GLAS waveforms (Zwally *et al.*, 2002).

For better visualization of ICESat footprints over terrain, the GLAS footprints were georeferenced and converted to KML and then were visualized in Google Earth. This visualization of the ICESat footprints provided better analysis of the footprint shape and size, and illuminated features within each footprint. Moreover, the Surface elevation profiles based on GLA14 data has been compared with the Elevation profile of Google Earth for the selected GLAS footprints (See Figure 3.10).

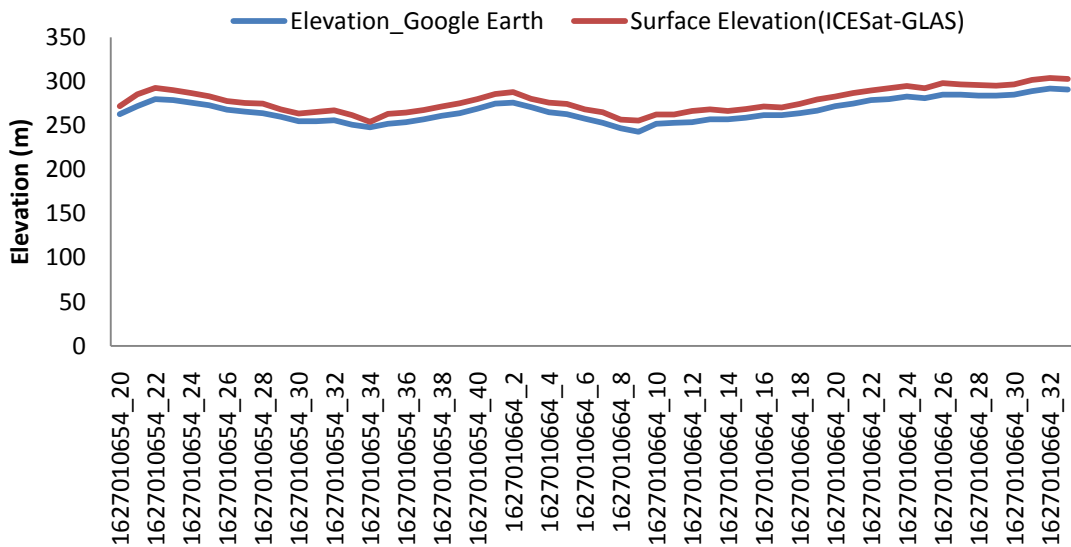


Figure 3.10: Comparison GLAS footprint elevation profiles with the Google Earth elevation profiles for the selected GLAS footprints over the study area.

### 3.4 Methods of analysis

The basic idea of the data analysis and the expected outcomes was presented in section 1.5. This section presents a comprehensive review of the signal processing steps that have been carried out to achieve the final results. It includes the pre-processing as well as the data analysis itself. The outline is structured in accordance to the main data

source, which are GLAS data and their analysis. It also provides a broad methodology to show how the different objectives fit together to achieve the aim of the research.

### **3.4.1 Broad methodology**

The vegetation structure parameters extracted from the full waveform GLAS data over KNP are canopy height and woody cover, based on GLAS waveform parameter analysis and the relationships between the estimations parameters from GLAS full waveforms and airborne LiDAR, Radar, and Field data. The overall aim of incorporating the use of other datasets is to gain an insight into the possibility of using spaceborne LiDAR altimetry for characterizing vegetation structure in the savannah environment.

Using airborne LiDAR data to extract canopy height metrics and generating a digital elevation model was undertaken for GLAS footprints for which there was airborne LiDAR coverage (n=24). The results from the analysis of airborne estimates were used as a reference with field measurements for comparison and validation with canopy height estimates derived from GLAS footprints. Results of woody cover estimations utilizing the L-band ALOS-PALSAR data were used to evaluate the use of ICESat-GLAS LiDAR data for estimating savannah woody cover utilizing an empirical model; and the woody cover map was used as a reference to compare and validate the results from both datasets.

The comparisons between airborne LiDAR data, RADAR data and GLAS data are defined in detail, along with the methods, in Chapters 4 and 5, respectively. The results of the accuracy assessment are evaluated with respect to the field measurements for canopy heights and ancillary data of woody cover map for woody cover estimations. The broad methodology for achieving the five objectives is shown in the flow chart (Figure,3.11).

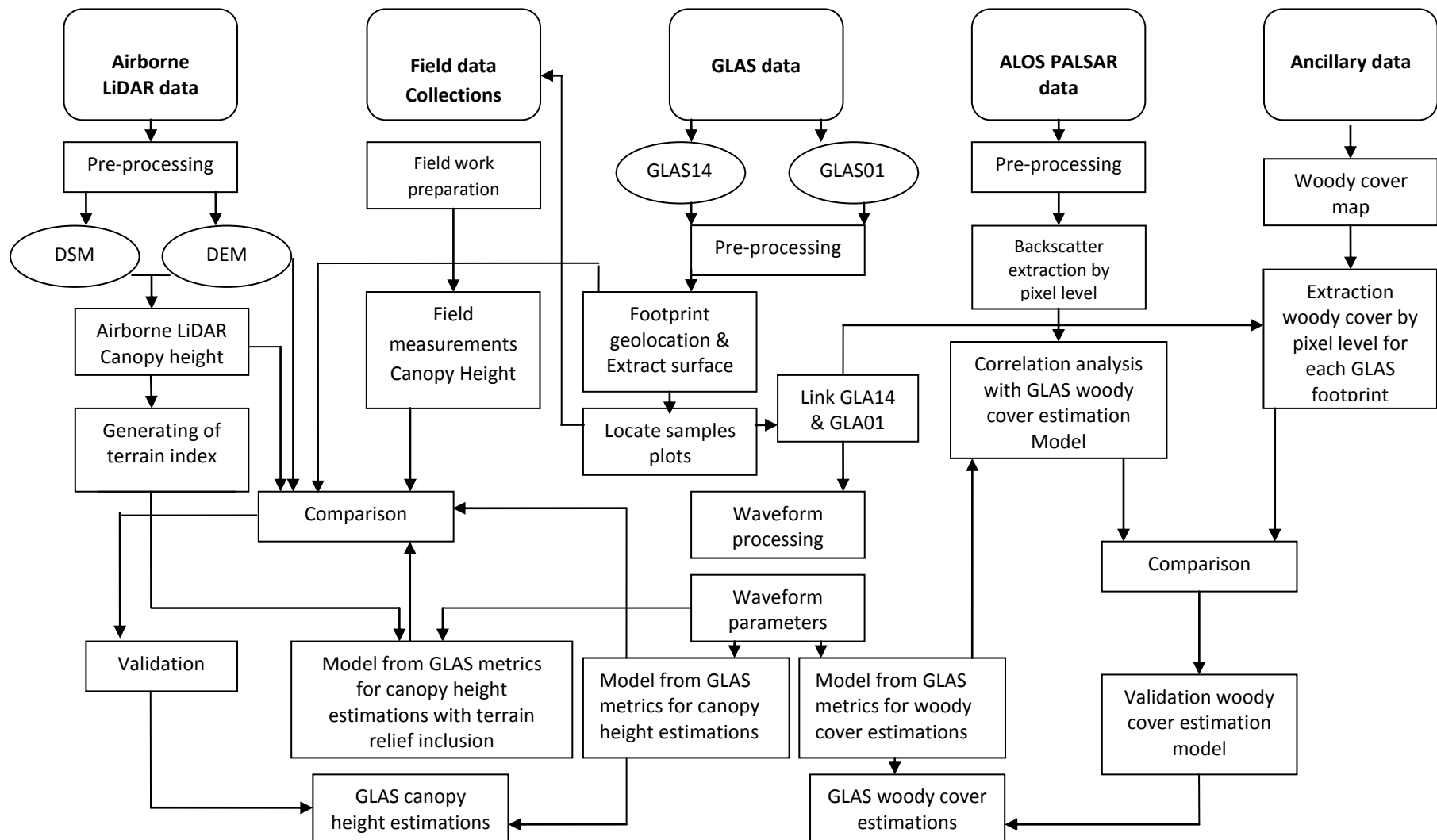


Figure 3.11: Flow chart summarizing the procedure employed in this research to characterize savannah vegetation structure.

### **3.4.2 GLAS analysis methodology**

In this section, the main topic of this study methodology is to describe systematically the full waveform ICESat-GLAS processing analysis. It aims to ascertain whether estimates of vegetation heights and woody cover can be extracted from large GLAS footprints satellite LiDAR data. The results of this methodology are used in comparison with field measured vegetation heights from coincident areas with airborne LiDAR and ALOS PALSAR data.

#### **3.4.2.1 GLAS data pre-processing**

ICESat-GLAS full waveform data obtained from the ICESat Science team (Zwally *et al.*, 2008) for vegetation profiling were used in this study. Products needed are cloud-free profiles acquired during the laser L3j observation period; waveforms from GLA01 Global Altimetry Data Product; and geolocated footprint locations from GLA14 Global Land Surface Altimetry Data Product. The GLAS Visualizer and data conversion tool (NSIDC, 2007) was used with the IDL virtual machine and MATLAB to process and explore the waveforms, as well as to identify and extract parameters of interest. The sections below describe the GLAS data analysis tools, which were used to process the waveforms, and the steps used for preparation of data for waveform analysis.

##### **3.4.2.1.1 IDLreadGLAS tool**

IDLreadGLAS software was downloaded from NASA's ICESat CLAS data tool webpage <<http://nsidc.org/data/icesat/tools.html>>. This tool inputs the raw data that were ordered from NASA to generate and produce usable data, including unique number, shot number, shot time, number of samples, and uncompressed waveform values in volts (Seidel, 2005). These usable data will be used to process and explore the waveforms and to identify and extract parameters of interest.

#### **3.4.2.1.2 NGAT tool**

The NSIDC GLAS Altimetry elevation extractor tool (NGAT) version 11 was also downloaded from <http://nsidc.org/data/icesat/tools.html>. This tool uses the GLA14 altimetry product which is distributed in binary format (\*.DAT) and was converted to ASCII format to derive each shot's unique number, date and time and acquisition, latitude and longitude (in decimal degrees), elevation (meters), and geoid (which is defined as the height at which half the return energy is above and half below) (Ranson *et al.*, 2004b). The latitude and longitude information for GLAS point locations were buffered to footprints using footprints information size for laser 3 (NSIDC, 2009).

#### **3.4.2.1.3 Data preparation for waveform analysis**

As it stated above, the use of the GLAS Visualizer tool was based on one freely available from <http://nsidc.org/data/icesat/tools.html> to process the waveforms.

These main steps were performed:

- 1- The first step is to convert the original GLA01 and GLA14 data files (which come in binary files) from NSIDC into information that presented in an easy to use (i.e. Excel files) for further processing.
- 2- The converted data files were then subset and modified; therefore, only data that fell within the study area remained for subsequent analysis.
- 3- Since the elevation from GLA14 is for the footprint centre of the GLA01 waveform, this step involved generating a common field between GLA01 and GLA14 data, so this will give common and corresponding information. Because of this process, each footprint data in the two data files would be linked by a common index number and a short number.

- 4- For every index number, a file with return waveforms in voltage converted from raw waveforms data was created.
- 5- This step involves waveforms decomposition. At this fitting step, the waveform is modelled, defining some constraints such as maximum number of modes (Gaussian curves), minimum height of mode, minimum distance between modes, minimum width of mode, and maximum position of mode.

The goal of pre-processing was to determine those waveforms that are suitable for identifying waveform parameters of interest. Each modelled waveform (Figure 3.12) had at least one mode that corresponded to the ground return; additional modes would therefore correspond to sub-canopy levels or sub-terrain returns at different elevations. The waveform extent is defined through a noise threshold, which will be used to determine the point of signal start and signal end and hence determine the waveform extent (Lefsky *et al.*, 2005c).

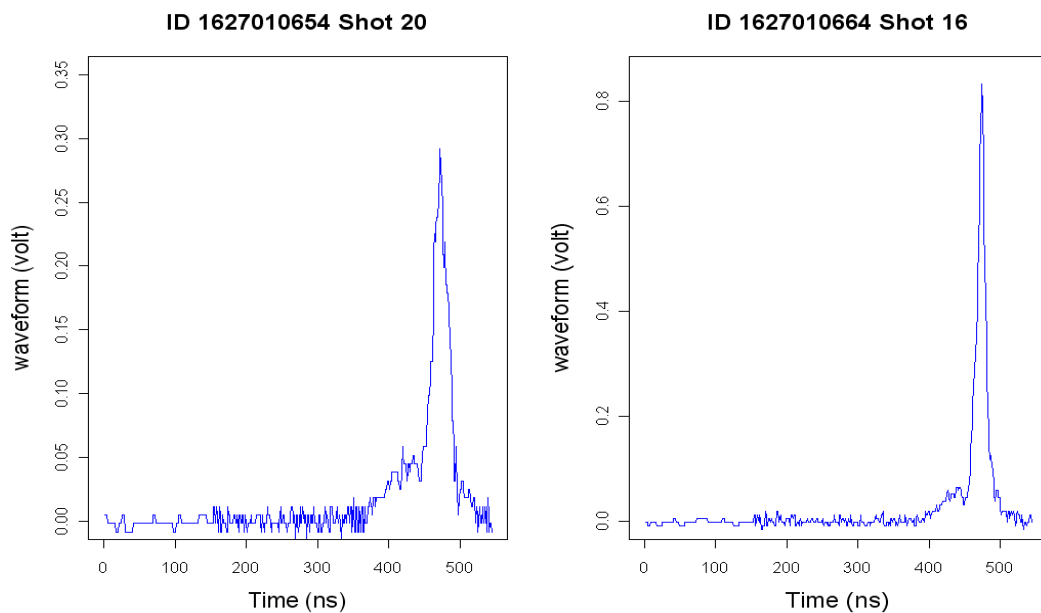


Figure 3.12: Examples of two different waveforms on different terrain relief. These waveforms were modelled using the steps described in 3.2.1

### 3.4.2.2 Digital Terrain Models

For comparing GLAS elevations with elevations from LiDAR airborne, digital terrain models of 3 m resolution were interpolated from GLAS point elevations (DTM\_GLA14). The study sites that were covered with both GLAS and airborne LiDAR data were tested. Since GLAS gives the mean elevation of the footprint, 3 metres resolution for the DTM was selected so that their mean elevations within the incident beam could be easily worked out. Similarly, DTM from airborne LiDAR data were created and interpolated to produce digital terrain models (referred to as DTM\_LiDAR), with the same spatial resolution for these test sites. Figure 3.13 shows the digital terrain models of the test sites. The mean elevations within footprints were calculated from DTM and compared with DTM from the LiDAR airborne. Coefficient of correlation was used as indicator of goodness of fit.

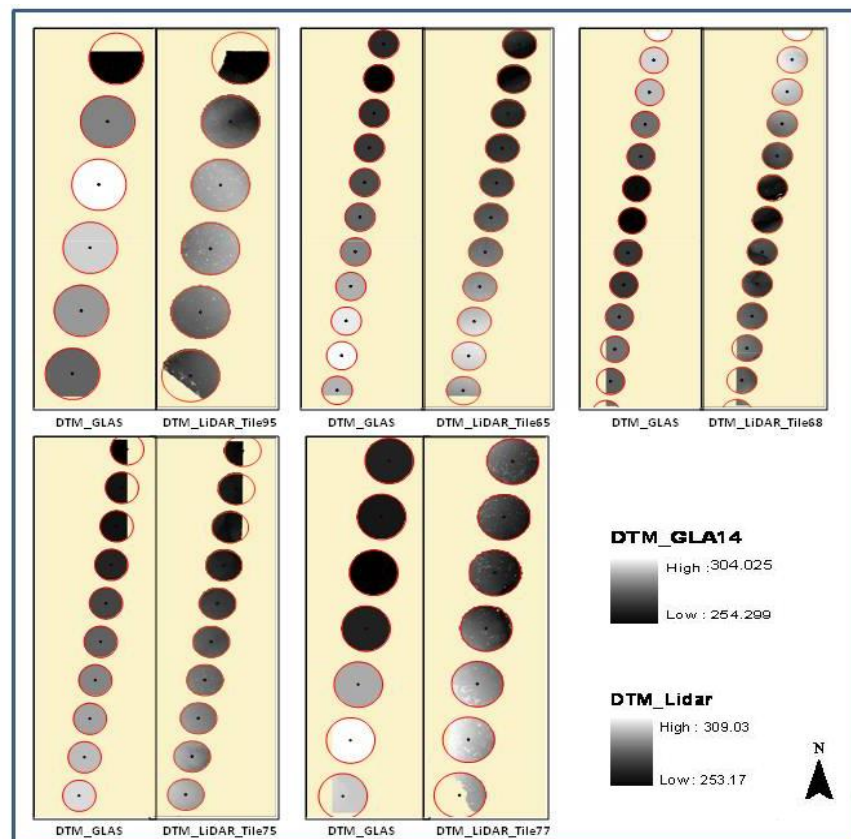


Figure 3.13: Comparison of GLAS elevation with digital terrain models from airborne LIDAR with spatial resolution of 3 metres.

### **3.4.2.3 Waveform processing**

This section forms the core of this study. It ascertains whether savannah vegetation structure parameters can be extracted from satellite LiDAR GLAS full waveforms. Waveform parameters for vegetation structure are compared with field-measured vegetation heights from coincident areas with airborne LiDAR data, and the ALOS PALSAR data in two separate study sites, which were both covered with GLAS spaceborne LiDAR data.

Two methods that extract waveform parameters of interest for vegetation study are developed. The first one utilizes the parameters derived directly from GLAS products, mainly the Global Land Surface Altimetry Data Product (GLA14). The second one uses the parameters extracted from Global Altimetry Data Product (GLA01), using DEM to adjust the waveform extent, particularly in high relief areas. Calculations within this study were carried out using the statistical analysis program package R Version 2.9.0. The results of these methods are further developed within research discussion in the following chapters.

#### **3.4.2.3.1 Gaussian decomposition method/direct method**

The first method uses the parameters, which were extracted entirely from GLA14 product for deriving vegetation height estimates using the parameters that structured the returned signal. The shape of the waveform varies according to the characteristics of intercepted surfaces and their spatial locations, taking into account the fact that the laser energy diminishes towards the footprint margins (Carabajal and Harding, 2001). However, in open and sparsely vegetated areas, the majority of signal returns may be anticipated to come from the ground surface creating the greatest amplitude peak within the returned waveform; while in denser

canopies, the laser energy penetration is reduced resulting in a lower amplitude peak (Harding *et al*, 2001) (see Figure 3.14). GLAS products provide parameters that contain a Gaussian decomposition, particularly in GLA14. The ICESat GLAS Visualizer software iteratively fits six Gaussian curves to the waveform. This was used to compare Gaussian parameters, so it is assumed that the largest amplitude of any fitted six Gaussian parameters corresponds to the ground, and the difference in elevation between the centroid of this Gaussian and the beginning of the waveform signal is the estimated maximum vegetation height (Rosette, 2009). This equation was used to estimate maximum canopy height using the Gaussian decomposition method of GLAS parameters:

$$H_{max} = H_s - GP \quad (3.3)$$

Where  $H_{max}$  is the maximum canopy height estimated from GLAS data (m),  $H_s$  = the signal start (m),  $GP$  = ground peak (m) (the centroid of the greatest amplitude of Gaussian decomposition peak).

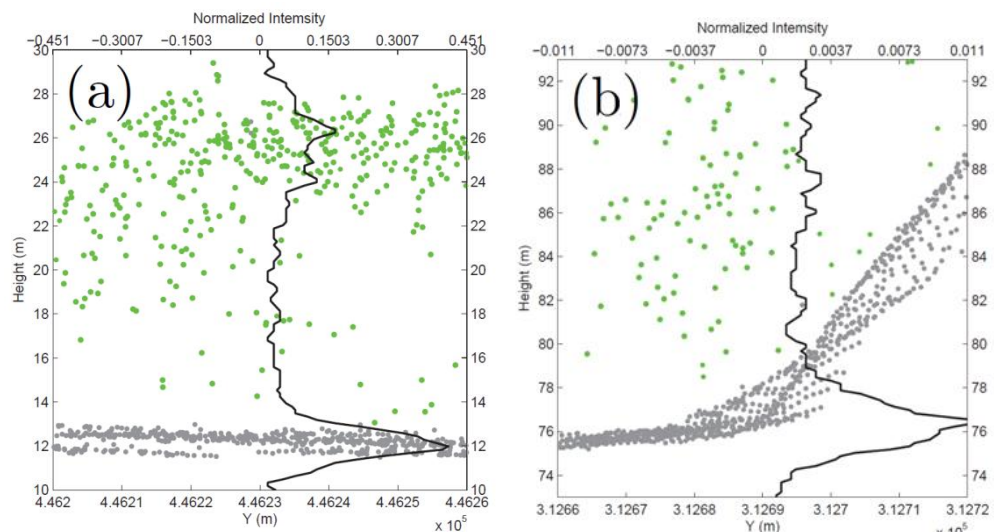


Figure 3.14: Different raw waveforms with a dominant peak that were acquired over forest areas: the solid black line is the ICESat waveforms; the grey dots are the terrain surface; and the green dots are the vegetation. It is clear that the peak location along the vertical axis is presenting the ground peak well. The width of this peak contains information on surface slope and terrain roughness. In (a) The surface is rougher while in (b) The surface is partly sloped. As a result, the ground peaks have widened in (b) While the flat and smooth surfaces in (a) correspond to narrow last peaks (Duong, 2010).

The waveform extent was estimated manually using the signal beginning ( $d\_sigbegoff$ ) and signal ending ( $d\_sigendoff$ ) from GLA14 product parameters to estimate maximum canopy heights:

$$WE = d\_sigbegoff - d\_sigendoff \quad (3.4)$$

Where: WE = the waveform extent,  $d\_sigbegoff$  = signal beginning defined from GLA14,  $d\_sigendoff$  = signal ending defined from GLA14.

#### **3.4.2.3.2 Terrain index/ statistical method**

The return GLAS waveform is typically characterised by multiple energy peaks caused by the reflection from ground surface and the objects (i.e. trees) above it. Theoretically, over flat and simple surfaces (Figure 3.15(a)), the return waveform can be modelled as a single Gaussian bell shape, which usually corresponds to the ground if enough energy penetrates through the surface objects. Hence, canopy height can be estimated directly and simply (Figure 3.15(b)) based on the vertical differences between the signal start, which is assumed to be the top of the canopy, and the lowest peak, which is the ground peak (Chen, 2010b; Duong *et al.*, 2008). However, over vegetated sloped areas with large reliefs and more complex terrain, the return waveform depends on the location of the tree. Therefore, if the tree is located at the top of the slope, with respect to the footprint location, the ground peak has a larger width and less energy, compared to the ground peak for return waveform over flat areas (Figure 3.15(c)). In this case, the widening of the ground peak is mainly caused by the effect of the surface slope on the peak width. On the other hand, if the tree is located at the bottom of this slope (Figure 3.15 (d)), the separation between the surface slope and tree is somehow not clear. Methods for

extracting canopy heights should therefore carefully consider the effect of the slope and relief (Chen, 2010b; Duong, 2010).

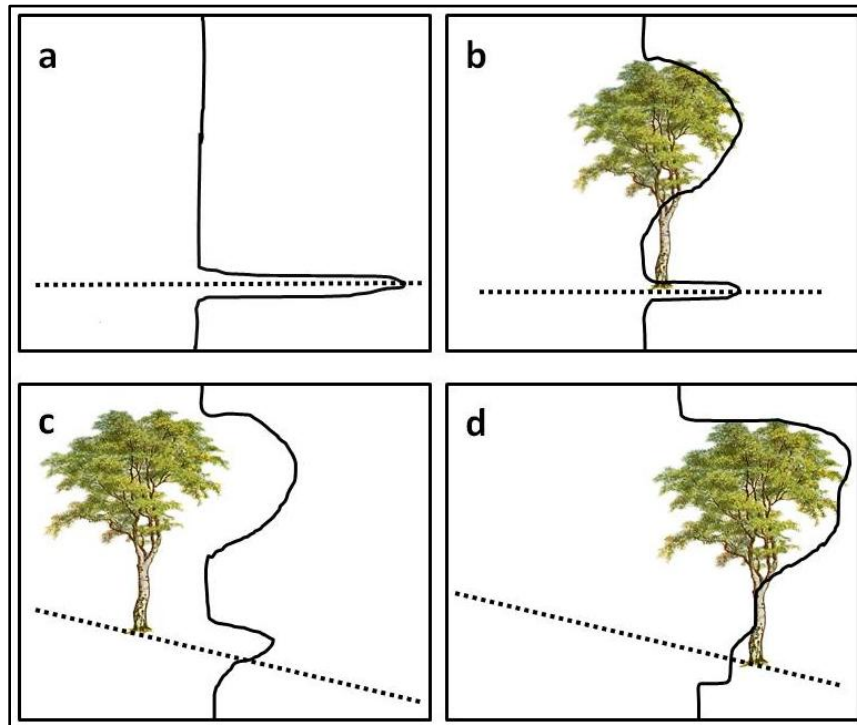


Figure 3.15: Structure of the returned waveform over flat areas (a, b) and sloped areas (c, d) (Duong, 2010).

This method was adapted from the work of Lefsky *et al.* (2005) and Rosette *et al.* (2009), which account for the effect of slope on the waveform structure.

#### Calculating Terrain Index using airborne LiDAR data

To consider the contribution of topographic relief on waveform shape, a terrain index was calculated for each footprint location (Lefsky *et al.*, 2005a). Terrain index was defined as the difference between maximum and minimum elevation of airborne LiDAR within GLAS footprint (Chen, 2010b). This was applied in this study by calculating the terrain index ( $g$ ) for each GLAS footprint as the difference in metres between the highest and lowest elevations contained within a  $7 \times 7$  subset of the DEM generated from airborne LiDAR data, and applying equation modified

after Lefsky *et al.* (2005a) :

$$H = b_0 * w - b_1 * g \quad (3.5)$$

Where  $H$  = GLAS Height (m),  $w$  = waveform Extent (m),  $g$  = Terrain Index (m),  $b_1$  = the coefficient applied to the waveform extent,  $b_0$  = the coefficient applied to the terrain index. This method offers a means of removing the effect of topographic relief from the waveform extent and hence estimating the vegetation height from the returned signal:

$$H = w - g \quad (3.6)$$

Where  $H$  = GLAS Height (m),  $w$  = waveform Extent (m),  $g$  = Terrain Index (m)

#### Calculating Terrain Index using GLAS parameters

Generally speaking, a laser full waveform altimetry system transmits a signal having either a bell shape or a slightly skewed shape with a sharp rise and a slow fall (Duong, 2010). The laser pulse of the ICESat system resembles a Gaussian function with a certain width, amplitude and mean value of peak location (see Figure 3.16 (Duong, 2010)).

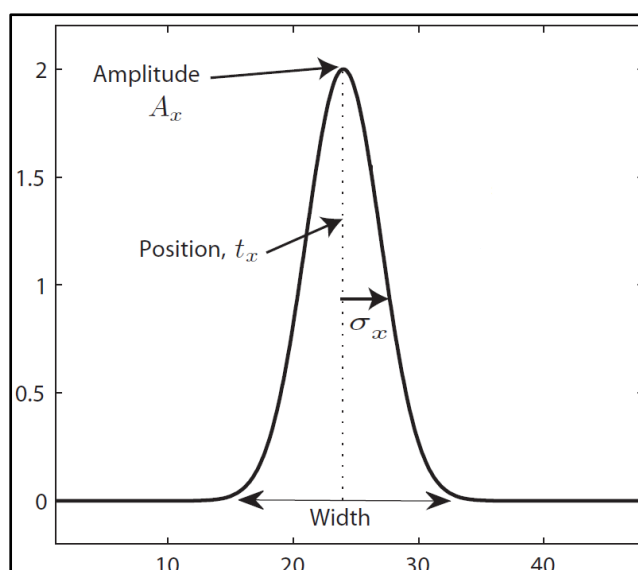


Figure 3.16: Structure of the returned waveform as a Gaussian function used to describe the transmitted pulse with peak position  $t_x$ , amplitude  $A_x$ , and width  $\sigma_x$  (Duong, 2010).

The ICESat processing software iteratively fits six Gaussian curves to the returned waveform. This Gaussian decomposition is provided within product GLA14. The six Gaussian peaks are parameterized by values reporting the shape of the peaks, which are the amplitude  $A_x$ , width  $\sigma_x$  and area under the Gaussian peaks (Duong, 2010). As is described in Figure 15(c), a greater slope will broaden the ground peak; hence it will have a larger width compared to the ground peak in a flat area (Figures 15(a) and (b)). Additionally, the energy of the ground peak on sloped areas is less than the ground peak on flat areas (see Figure 3.16).

To consider the effect of terrain on the waveform shape over sloped areas, it is assumed that the return waveform has a Gaussian shape with a larger width ( $\sigma$ ) and less amplitude ( $A$ ); hence, terrain index is considered to have the same effect as the waveform width ( $\sigma$ ) on sloped areas. If it is assumed that the terrain index equals waveform width ( $\sigma$ ), so it holds:

$$g = 2\sigma \quad (3.7)$$

Where  $g$  = Terrain Index (m),  $\sigma$  = waveform width (m)

The GLAS estimates heights can be calculated using the equation (3.5) after combining with equation (3.7) which results in equation (3.8):

$$H = b_0 * w - b_1 * (2 * \sigma) \quad (3.8)$$

Where  $H$  = GLAS Height (m),  $w$  = waveform Extent (m),  $\sigma$  = waveform width (m),  $b_1$  = the coefficient applied to the waveform extent,  $b_0$  = the coefficient applied to the waveform width.

This method is also adopted from Lefsky *et al.*, (2005a), and offers a means of extracting GLAS height estimates from the Gaussian decomposition provided parameters with GLAS products.

### **3.5 Results**

#### **3.5.1 Direct method using parameters of GLAS products**

This method used the parameters provided within GLAS products (GLA14 and GLA01) to estimate vegetation heights. These parameters involve the use of Gaussian peak positions 1 and 2 and their amplitudes to identify the ground return peak within the return signal, with the respect to the narrow width and large amount of returned energy within the returned signal. This method aims to employ the parameters of GLAS products to develop an algorithm to help to derive vegetation heights.

GLA14 product has Gaussian decomposition parameters. Hence, estimates of vegetation height using these parameters in equation (3.3) and compared with field measurements of maximum vegetation height produce correlation with  $r$  of 0.39 and RMSE 8.47 m and (p-value > 0.05) not statistically significant for the entire selected GLAS footprints for the field collected data  $n=23$ . However, after classifying the GLAS footprints according to the terrain slope for flat and steep footprints and excluding the steep footprints that have  $> 45^\circ$  from this relationship analysis, the results gave height correlation with  $r$  of 0.68 and RMSE 2.1m for  $n=12$  and this improve the correlation coefficient and was statistically significant (p-value < 0.01). These results indicate the potential for estimating maximum vegetation height directly from returned satellite LiDAR signals using the parameters of GLA14 waveforms product. Figure 3.17 shows height estimates from GLA14 product parameters compared with field measurements of maximum canopy height for all GLAS footprints  $n=23$  and for the flat terrain GLAS footprints  $n=12$ .

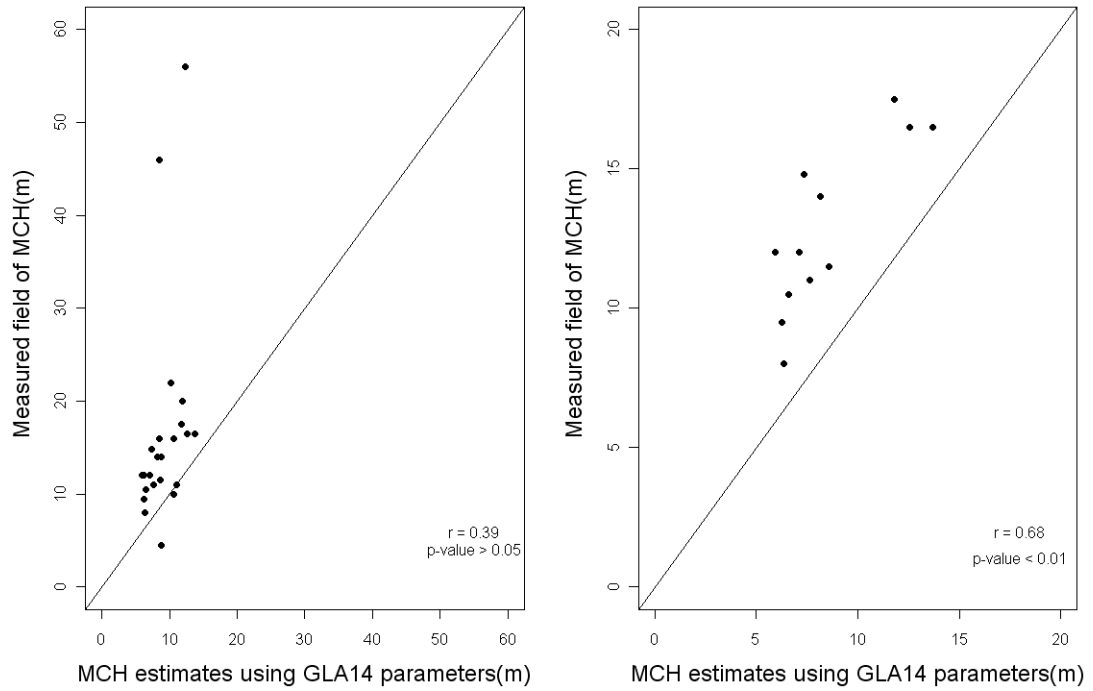


Figure 3.17: Scatterplots of the Pearson's correlation relationship between maximum canopy height estimates using GLAS parameters of Gaussian decomposition and the field measurements of maximum canopy height. The result gives a weak correlation when the comparison is done for the footprints without considering terrain classification (left graph), but the correlation improves when the comparison is done on just flat and moderate footprints (right graph).

On the other hand, height estimates were also calculated from GLA01. As was explained earlier, raw waveforms have ambient system noise at the beginning and the end of the waveform signal. Therefore, the real signal of the waveform was identified by thresholding the raw waveforms. In this study, the threshold value ( $nv$ ) for each raw waveform was individually determined to the mean background noise value estimated in the GLA01 product (GLAS product variable:  $d\_4nsBgMean$ ) plus 4 times the standard deviation of the background noise (GLAS product variable:  $d\_4nsBgSDEV$ ) (Lefsky *et al.*, 2007), as it is described in this equation:

$$nv = (d\_4nsBgMean) + 4 * (d\_4nsBgSDEV) \quad (3.9)$$

Where  $nv$  = Threshold level value,  $(d\_4nsBgMean)$  = mean noise,  $(d\_4nsBgSDEV)$  = noise standard deviation.

By determining that the noise threshold level value ( $nv$ ) for the 544 bins corresponds to a height of 81.6 metres over land for each waveform individually, signal start and signal end locations were identified (Harding and Carabajal, 2005); and, to detect the ground peak location, the maximum amplitude was used as a reference. Hence, the peak with maximum amplitude was designated as the ground return (Figure 3.18).

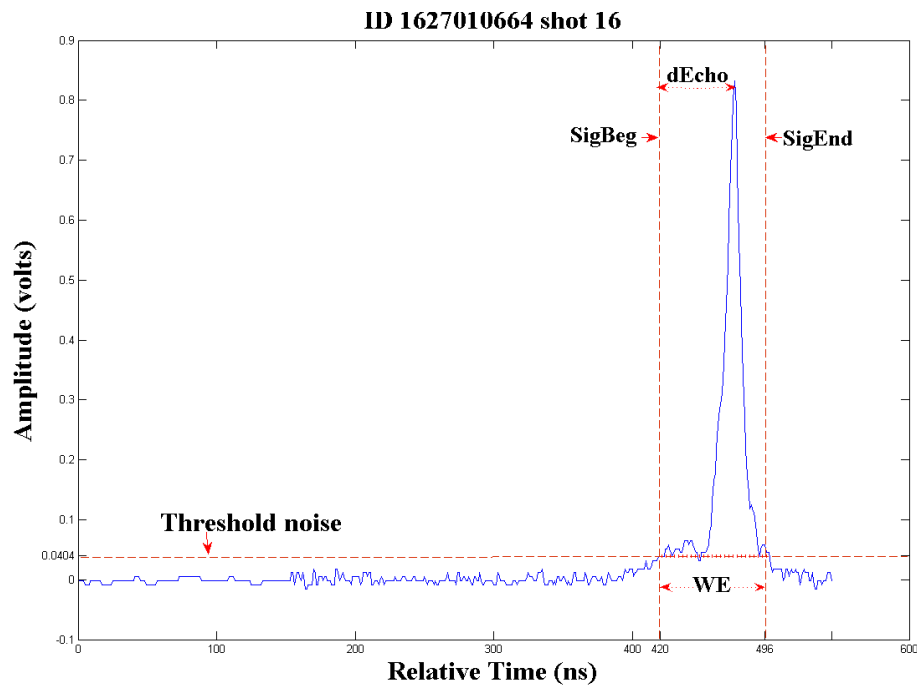


Figure 3.18: A processed GLAS waveform; the noise mean and standard deviation were estimated separately for tails at the two ends (Signal beginning and Signal end), from which thresholds were set (the ditched red line) and used to locate the signal beginning and end. The ground peak was determined where greatest sufficient energy is reflected from the ground. The  $H_{max}$  is the distance between signal beginning and ground peak.

Results of estimating vegetation height using GLA01 parameters in equation (3.3) and compared with field measurements of maximum vegetation height produce the heights correlation with  $r$  of 0.24 and RMSE 12.47m for all footprints with flat and steep terrain, the correlation was not significant (p-value  $>0.05$ ) while the Pearson's correlation improved and was statistically significant (p-value  $<0.01$ ) when using this method with footprints that have flat and simple terrain  $r$  of 0.63 and RMSE 2.47m (Figure 3.19). Comparison of maximum canopy heights derived from

GLA14 and GLA01 products gives  $r$  of 0.95 (Figure 3.20). This result indicates the potential of estimating maximum canopy height directly from GLAS products using characteristics of the waveform structure.

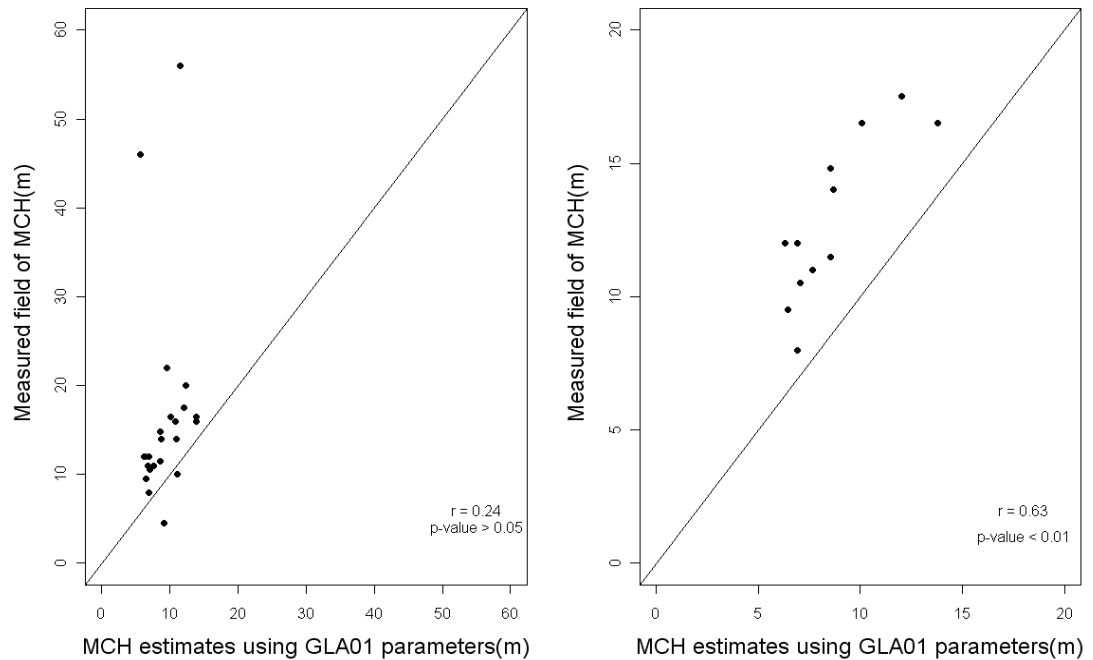


Figure 3.19: Scatterplots of the Pearson's correlation relationship between maximum canopy height estimates using GLA01 parameters and field measurements of maximum canopy height. The result gives a weak correlation when the comparison is done for the footprints without considering terrain classification (left graph), but the correlation improves when the comparison is done on only flat and simple footprints (right graph).

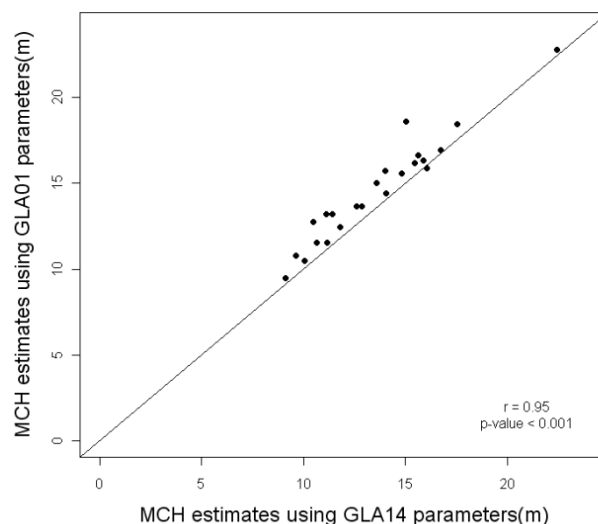


Figure 3.20: Scatterplots of the Pearson's correlation relationship between MCH estimates using GLA01 waveform and MCH estimates using GLA14 parameters, most points which represent flat terrain of GLAS footprint for both estimated MCH of GLAS products fall close to the 1:1 line.

### 3.5.2 Statistical method/terrain index/waveform width

This method aims to consider the effect of the slope on the waveform extent. Two methods of calculating the terrain index were applied. The first method generates terrain index from airborne LiDAR data. It is defined as the highest and lowest elevations contained within a 7x7 subset of the DEM generated from airborne LiDAR data as an indicator of slope effect on the waveform extent. Following the method of Lefsky *et al.* (2005), multiple regression was used with field measurements to assess the relationship between the waveform extent and terrain index. The multiple regression analysis was done twice to the steep footprints. The first one was done on 10 footprints (n=10) and it produces  $R^2$  of 0.80, RMSE 12.49 m. Both coefficients are statistically significant and the intercept was not significant. The resulting equation (3.10):

$$H = -0.7899479 * w + 4.095529 * g \quad (3.10)$$

Where  $H$  = field height (m),  $w$  = waveform extent (m),  $g$  = terrain index (m),  $b_1$  = the coefficient applied to the waveform extent,  $b_0$  = the coefficient applied to the terrain index.

The second one was done on eight footprints (n=8), after removing two footprints due to the location of the trees at the bottom of the sloped areas. The resulting equation (3.11) produces  $R^2$  of 0.87 and RMSE 4.84m for n=8. Both coefficients are statistically significant and the intercept was not significant.

$$H = 1.4725603 * w - 0.5374219 * g \quad (3.11)$$

To assess the improved relationship between the waveform extent and terrain index with field measurements, a plot with the predicted values of both equation (3.10)

and (3.11) was plotted vs. the observed values of the field measurements of maximum canopy heights (Figure 3.21).

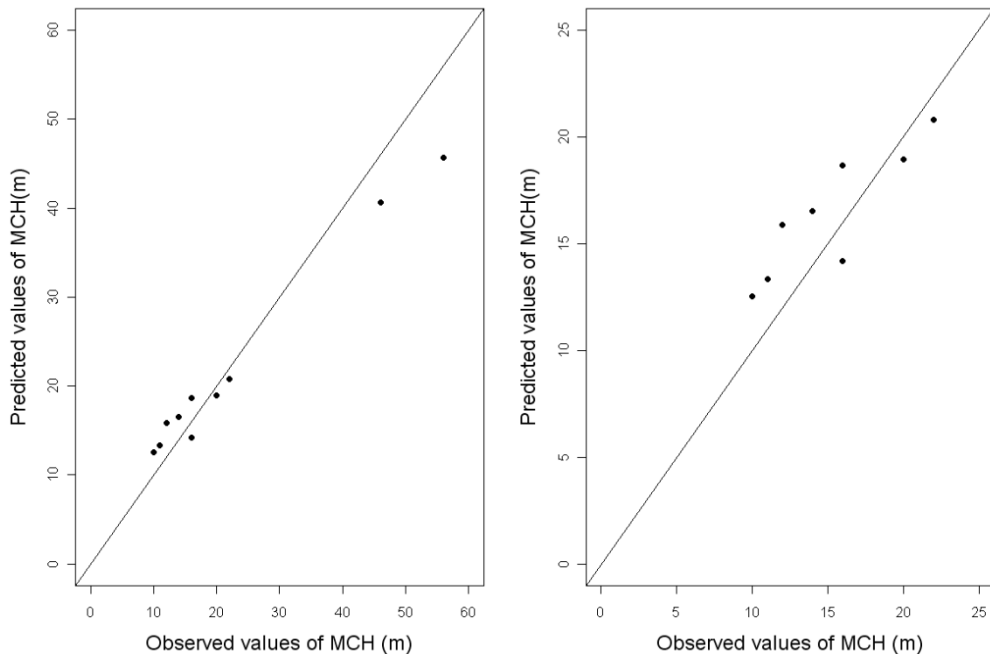


Figure 3:21: Relationship between measured field of maximum canopy heights and predicted values of maximum canopy height. The left graph shows the fitted values of equation (3.10) compared to field measurements of maximum canopy heights for  $n=10$ ; while the right graph shows the fitted values of applying equation (3.11) after removing the two very steep GLAS footprints. The line shows the 1:1 relationship.

The second method for calculating terrain index uses Gaussian decomposition parameters provided in GLA14. Again, following the method of Lefsky *et al.*, (2005), multiple regression was used to assess the relationship between the waveform extent and waveform width ( $\sigma$ ) as indicator of terrain index with field measurements. The resulting equation (3.12) produces  $R^2$  of 0.70 and RMSE 16.34m for the all steep footprints ( $n=10$ ). Both coefficients are statistically significant and the intercept was not significant:

$$H = 1.5948 * w - 0.5172 * \sigma \quad (3.12)$$

The equation (3.12) was applied again after removing the two step footprints, and resulted in improving the coefficient  $R^2$  of 0.95 and RMSE 4.0m for  $n=8$ , Both coefficients are statistically significant, the intercept was not significant :

$$H = 0.8998 * w - 1.4161 * \sigma \quad (3.13)$$

Figure 3.22 shows the relationship between the predicted MCH using equations (3.12) and (3.13) vs. observed field measurements of MCH.

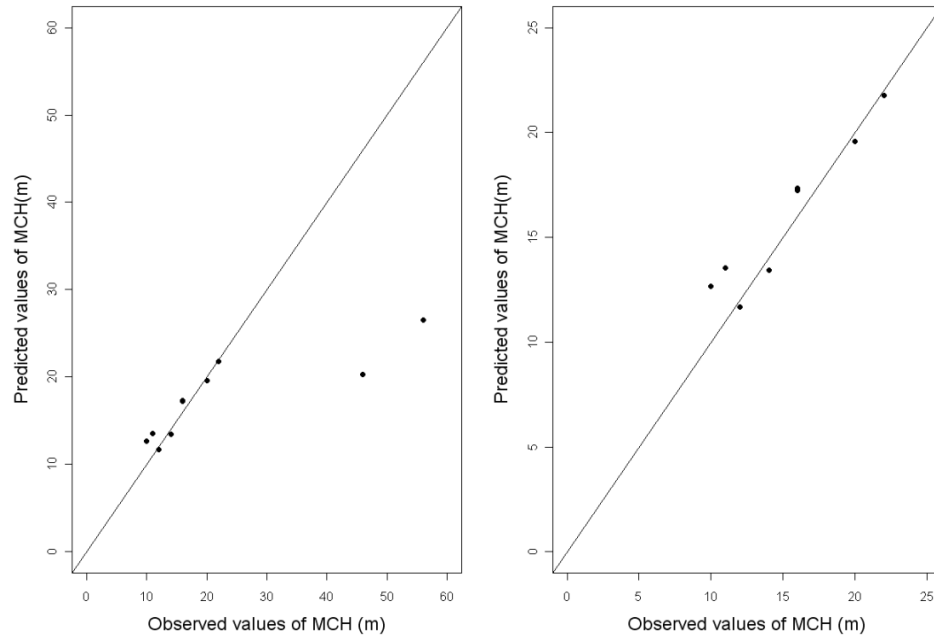


Figure 3:22 Relationship between measured field of maximum canopy heights and predicted values of maximum canopy height. The left graph shows the fitted values of equation (3.12) which applied waveform width as an indicator of the effect of terrain on the GLAS waveform compared to field measurements of maximum canopy heights for  $n=10$ ; while the right graph shows the fitted values of applying the same equation after removing the two very steep GLAS footprints. The line shows the 1:1 relationship.

Figure 3.23 shows that the first method of using terrain index extracted from airborne LiDAR data as an indicator of the effect of slope on the GLAS height estimates is comparatively well correlated (Pearson's correlation  $r = 0.80$ ) with the second method, which used waveform width of Gaussian function from GLA14 product.

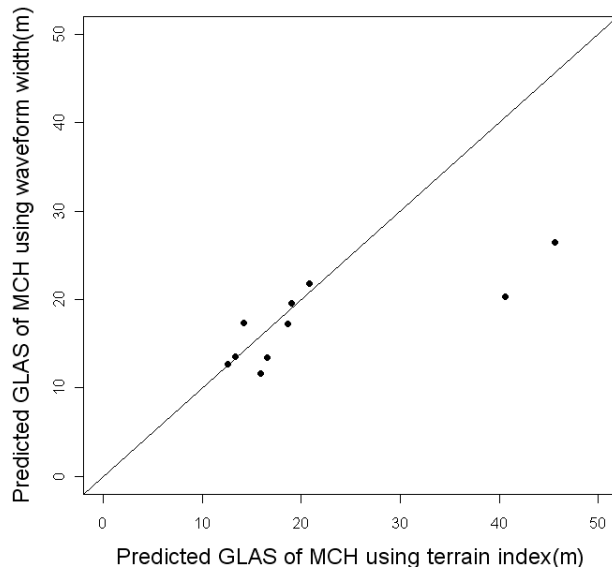


Figure 3.23: A comparison of the two methods of using terrain index equation (3.10) and waveform width equation (3.12) for predicting GLAS of MCH. The line shows the 1:1 relationship.

### 3.6 Discussion

Vegetation height is one of the leading dimensions of ecological variations among tree species and is central to ecosystem functioning (Westoby *et al.*, 2002; Moles *et al.*, 2009). This study investigates the potential of the GLAS (Geoscience Laser Altimeter System) on board ICESat (Ice, Cloud, and land Elevation Satellite), for retrieving savannah vegetation height in Kruger National Park.

GLAS data offer an unprecedented opportunity for canopy height retrieval at a regional to global scale. In addition, the data provide useful information for forest stand level assessment at coincident locations. In this section, height indices from spaceborne LiDAR waveforms were explored as a means of extracting canopy height; these were examined with reference to the field measurements of maximum canopy heights.

Comparing the results of estimating maximum canopy heights using GLA14

parameters and GLA01 parameters have shown significant correlation coefficient (p-value <0.001),  $r$  of 0.95 and RMSE 2.1m. However, it also shows an overestimation of vegetation height from GLAS waveform structure. A likely explanation may involve the nature of Savannah environment, which is considerably sparse and has more open vegetation canopies; therefore, the majority of returns may be anticipated from the ground, and hence there is a misplacement of signal's start (Rossetti *et al.*, 2010).

The two methods of using parameters of GLAS14 and GLA01 products for flat footprints (5°-15°) give correlation coefficient  $r = 0.68$  and  $r = 0.63$  respectively. This result indicates the potential of estimating maximum canopy height directly from GLAS products using characteristics of the waveform structure. The direct method avoids the necessity of using ancillary datasets, and so it is suitable where relief and topographic data are not available for just the flat and simple terrain.

Besides the direct methods, the statistical regression method has been developed to predict canopy height with waveform metrics. The regression models typically include waveform extent and terrain index interpolated from DEMs airborne LiDAR (Lefsky *et al.*, 2005a; Rosette *et al.*, 2008a; 2008b), and waveform width ( $\sigma$ ) extracted from GLA01 product for Gaussian function as an indicator of the effect of slope on the terrain. This method is more appropriate for the sloped footprints > 45°.

Slope within footprint is anticipated to most influence height estimations, which identify the ground surface using the shape of the returned waveform. Where

relatively dense vegetation is located at the top of steep slopes, there is a greater likelihood for the returned signal from ground and canopy surfaces to be combined within the waveform. This may increase the possibility of wrongly estimated results. Moreover, if the vegetation is located at the bottom of these steep slopes, the separation between the surface slope and tree is not clear and leads to possibility of wrongly identifying the Gaussian peak relating to the ground surface. For savannah vegetation in KNP where the within-footprint terrain index ranged from 1.5 m to 15 m, with a mean difference of 6.2 m, this rarely prevented the presence of a distinct ground peak. However, the method of estimating vegetation height using waveform extent and terrain index/waveform width ( $\sigma$ ) could avoid this potential difficulty. Most importantly, the effect of terrain slope can be estimated using waveform width ( $\sigma$ ) as indicator of terrain index, which can be extracted directly from GLAS parameters as an indicator of the effect of slope on the shape of the waveform. This indicates that the potential of using waveform width ( $\sigma$ ) as a good indicator of the effect of topography and slope on vegetation height estimates from GLAS without the need of additional ancillary data such as airborne LiDAR data.

The statistical method does not rely on a clear ground signal being distinguished, as it only requires the waveform limits to be determined (the first and last return LiDAR). However, accuracy of these indices is most sensitive to local conditions, as vegetation structure will influence the ability to assign the beginning of the waveform to the elevation of the highest vegetation, and multiple scattering will extend the waveform tail.

Results of the statistical method compare favourably with those of Lefsky *et al.*, (2005a) in which maximum  $R^2$  value achieved was 0.87 and lowest RMSE was 4.85m. It should be noted that it is not possible to draw direct conclusions by comparing results of savannah vegetation of Kruger National Park and findings in the above paper due to differences in slope and vegetation height. Field measurements undertaken in Lefsky's study are coincident with GLAS footprints; however, the method differs from that undertaken in this research.

Of the 10 footprints considered for sloped areas, the difference between Waveform Extent and Terrain Index resulted in a negative value. This ranged from -0.3 to -39.25m, the latter of which occurred at a site used for field measurements and represents a hilly steep slope with dense vegetation. A number of sources of error are possible: algorithm misidentification of signal beginning and signal end, error in footprint location, discrepancy between the DTM subset used to calculate terrain index and the ellipsoidal footprint dimensions, or the effect of diminishing laser energy distribution towards the edge of the footprint resulting in less effect of extremes of slope in this region of footprints.

The RMSE of ~2.1- 16.34m found for vegetation height during this research suggests that estimates from GLAS waveforms may be insensitive to topography conditions. However, more concern and suggestions are required for estimating vegetation heights for the very steep slope footprints, with respect to the location of vegetation at the bottom of these sloped footprints.

### 3.7 Summary

This chapter has introduced the data sets which describe the study site, data sources, protocol of fieldwork measurements, and the methodology that have been used in this investigation. The chapter also has explored the use of the ICESat-GLAS satellite LiDAR for vegetation height retrieval over savannah vegetation of varied relief. The use of terrain index and waveform width to adjust the waveform extent provided the least dispersed estimates of canopy height for the steep slope footprints when compared with field height measurements at footprint locations.

Moreover, waveform width presents a good indicator of the effect of topography and slope on the waveform extent ( $R^2$  of 0.87 and RMSE 4.84m for the sloped areas  $n=8$ ); hence GLAS height estimates can be directly retrieved through statistical methods using only GLAS Gaussian function parameters without the need to use other ancillary data such as DEMs airborne LiDAR data.

Maximum canopy height estimates using a direct approach to ground identification based on iterative fitting of Gaussian peaks in GLA14 or GLA01 parameters results in a correlation coefficient  $r$  of 0.68 and RMSE 2.1m, and  $r$  of 0.63 and RMSE 2.47m respectively, when compared with field measurements. The results suggest that maximum canopy height estimates from ICESat-GLAS can provide a reliable indicator of actual canopy height for savannah vegetation with flat relief.

Contributions to the error in waveform estimates of vegetation height estimates using large footprint satellite LiDAR are formed by complex interactions including vegetation stature, upper canopy surface roughness, canopy cover, and slope and

species heterogeneity. Greater understanding is needed of the effects of topography and canopy properties on waveform composition.

This chapter aimed to determine whether the signal representing vegetation could be identified within waveforms returned from the broad dimensions of GLAS footprints. The study has presented two straightforward, repeatable methods for reliably extracting maximum vegetation height estimates for savannah vegetation.

The following chapters further apply these methods to develop potential approaches for retrieving vegetation structure of savannah (vegetation height and woody cover) and comparing the results with the described airborne LiDAR data and RADAR (ALOS PALSAR in order to evaluate the accuracy and the precision of estimating vegetation structure obtained from using ICESat-GLAS large footprint waveform.

## CHAPTER FOUR

### COMPARISON OF BIOPHYSICAL PARAMETER RETRIEVAL OF SAVANNAH VEGETATION FROM AIRBORNE AND GLAS SPACEBORNE LIDAR

#### 4.1 Introduction

LiDAR remote sensing provides an accurate and efficient means of estimating and monitoring vegetation structural properties. It has the potential to measure direct three-dimensional structure of vegetation surface including tree height, volume and biomass, and also ground surface (Lefsky *et al.*, 2002a; 2002b; Popescu *et al.*, 2011).

While LiDAR from the two platforms (airborne and spaceborne) has been intensely researched in forestry applications and has been shown to be a promising tool for providing reliable information about return ground elevation and forest estimation parameters (i.e. Næsset and Bjercknes, 2001, Hyypä *et al.*, 2001; Coops *et al.*, 2004; Holmgren *et al.*, 2003; Holmgren and Persson, 2004; Lim *et al.*, 2003; Popescu *et al.*, 2002; 2003; Hall *et al.*, 2005; Lefsky *et al.*, 2005; Chen *et al.*, 2006; Lefsky *et al.*, 2007; Duong *et al.*, 2008; Pang *et al.*, 2008; Popescu and Zhao, 2008; Roberts *et al.*, 2005; Nelson *et al.*, 2009; Neuenschwander *et al.*, 2008; Rosette *et al.*, 2008a; 2008b; Sun *et al.*, 2008; Zhao and Popescu, 2009; Duncanson *et al.*, 2010; Chen, 2010b ; Popescu *et al.*, 2011), it has experienced limited use in savannah environment systems; however, there are few studies using airborne LiDAR data to show its reliability in these complex and sparsely vegetated systems (i.e., Chen *et al.*, 2006; Levick and Rogers, 2008; Wu *et al.*, 2009). Moreover, the full waveform spaceborne satellite LiDAR data, namely, the Geoscience Laser

Altimeter System (GLAS) aboard the Ice Cloud and land Elevation Satellite (ICESat), has not been explored yet in savannah systems, although it has successfully demonstrated its capabilities for estimating forest canopy heights and biomass in several studies (i.e., Harding and Carabajal, 2005; Lefsky *et al.*, 2007; Rosette *et al.*, 2008; Boudreau *et al.*, 2008; Lefsky *et al.*, 2005a; Nelson *et al.*, 2009).

This chapter will evaluate the capability of satellite LiDAR data to be used in savannah environments by comparing it with airborne LiDAR data measurements for estimating vegetation heights and other vegetation structure parameters. Furthermore, the facilities offered by the discrete return airborne LiDAR data for vegetation structural properties have been explored and evaluated against field data, and also for evaluating the surface elevation.

## **4.2 Methodology**

Exploring satellite LiDAR large full waveform data for savannah vegetation structural parameters retrieval is justified based on previous work using airborne LiDAR data. An overview of the two systems is provided in Chapter 3, where the method of processing satellite GLAS LiDAR data is also presented.

The aim of this chapter's methodology is to process and analyse airborne LiDAR data for retrieving savannah vegetation structural parameters, and compare the results with a developed methods of estimating savannah vegetation structural parameters from satellite LiDAR and field measurements.

#### 4.2.1 Study site and data

As explained in section 3.2, the study area is Kruger National Park, located in South Africa (Figure 4.1). It is one of the largest protected areas in Africa (19,485 km<sup>2</sup>). Various habitats and ecological regions exist within the boundary of the Kruger, with at least 16 recognized ‘ecozones’, each one characterized by specific vegetation, geology, soils, rainfall rate, and temperature (Gillson and Duffin, 2007).

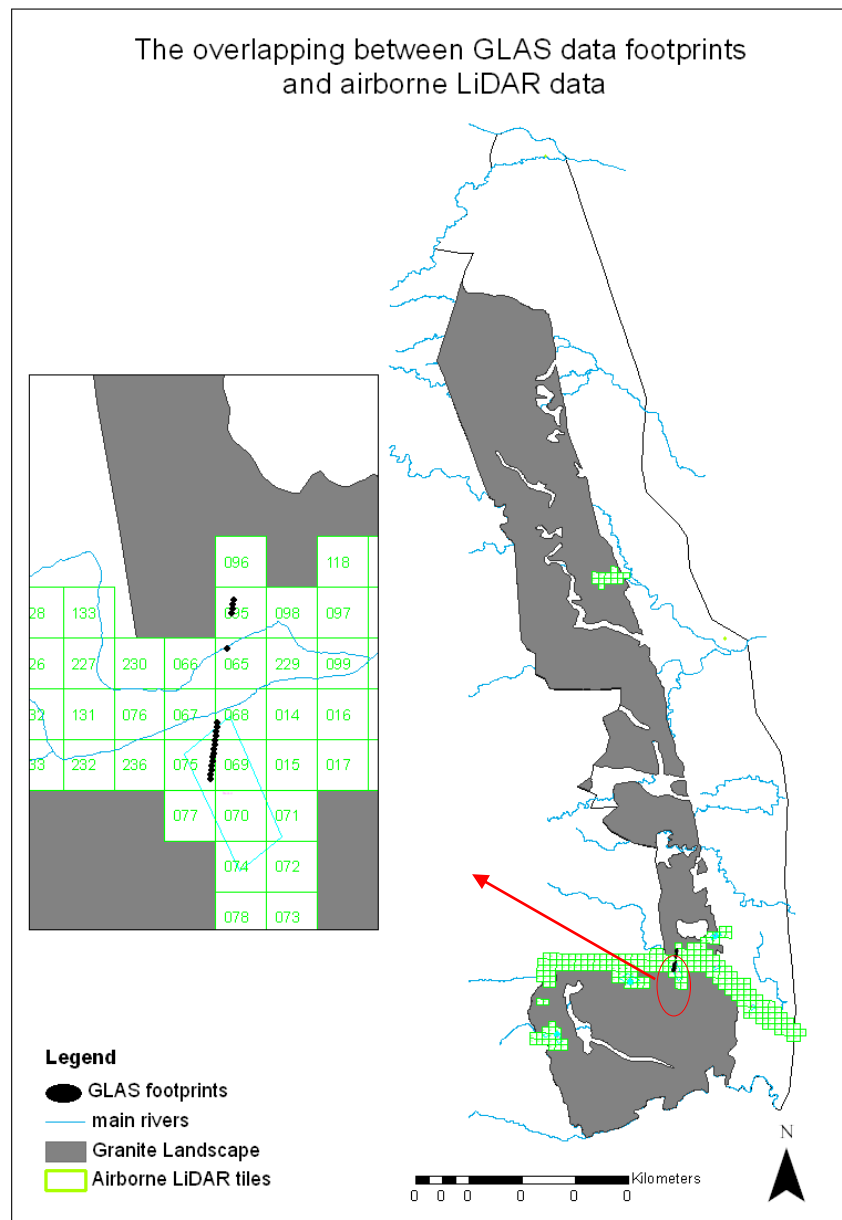


Figure 4.1: The location of GLAS footprints which overlap with airborne LiDAR data tiles and were selected for field data collection. The selected study area is located in the granite landscape in KNP (the gray shading area).

#### **4.2.1.1 GLAS data**

Two data products of release 29 GLAS were used in this study: Level 1A Global Altimetry data (GLA01), and Level 2 Global Land Surface Altimetry data (GLA14). As described in section 3.2.4, GLA01 is a level 1A data product which contains granules that have raw LiDAR waveform in digitizer counts which are afterwards converted to volts (by users). GLA01 contains the transmitted and received echo waveforms. This product has variables such as the filter threshold value for signal detection in digitizer counts, laser transmitter energy, received energy from all signals above threshold, sampled transmit pulse waveform, 4ns background mean value, and standard deviation (Brenner *et al.*, 2003).

GLA14 is a level 2 data which contains sensor position and pointing information as well as calculated footprint position, size and shape, and land surface elevation. Transmit pulse and recorded waveforms are represented with characteristic shape parameters only. The recorded waveform is decomposed into a series of Gaussian peaks, as described in Zwally *et al.* (2002) and Brenner *et al.* (2003).

#### **4.2.1.2 Airborne LiDAR data**

The discrete return airborne LiDAR dataset was acquired during the period 24 August- 9 September 2004 for the University of Witwatersrand (WITS) by Airborne Laser Solutions, South Africa. An ALTM 1225 (Optech, Canada) sensor with an operational frequency of 25 kHz was used. Average height of the fixed-wing aircraft housing the sensor was 500 m above ground level, and 15 cm vertical accuracy was achieved. Raw processing was conducted by ALS in Microstation SE/JTM (Bentley Systems) with the TerraModeler<sup>TM</sup>, TerraScan<sup>TM</sup> and TerraPhoto<sup>TM</sup> add-ons (Terrasolid).

Subsets of airborne LiDAR data were created using a radius of 35 m for each geolocated ICESat/GLAS footprint position. The analysis of airborne LiDAR indicates that the topography over the GLAS footprints for the selected overlapped footprints is classified to flat terrain with low and moderate slope ( $0^{\circ}$ - $30^{\circ}$ ) and steep slope ( $> 30^{\circ}$ ).

#### **4.2.1.3 Field data**

The entire selected GLAS footprints for field data collection are located in the granitic areas. The criteria for selecting the field data were based on the overlap between spaceborne LiDAR data and airborne LiDAR data. Thirty-one GLAS footprints were sampled for canopy height estimation. Further, out of these 31 identified plots, 22 fell in the airborne LiDAR tiles. Along with any fieldwork comes the issue of inaccessibility. Two footprints fell on the riverbank area; however, in the remaining 29 footprints, canopy heights were recorded. Fieldwork was conducted in August 2010. The aim of the fieldwork was to make measurements of canopy height within the selected sampled footprints to provide comparisons with estimates from both platforms: airborne and satellite LiDAR estimates.

#### **4.2.2 Data processing**

The basic idea of the data analysis and the expected outcomes was presented in section 3.4.1. This chapter presents a comprehensive description of the airborne LiDAR processing steps that have been carried out, and compares the outcomes with results obtained from developed methods for estimating vegetation structural parameters from satellite LiDAR, in order to achieve the final results. It includes

the processing of airborne LiDAR data as well as the data analysis of methods applied for estimating vegetation structural metrics from satellite LiDAR data.

The outline is structured in accordance with the two main data sources as well as their comparative analysis with field measurements. Firstly, the processing of discrete airborne LiDAR data for extracting digital surface model, digital elevation model, and vegetation height estimations is presented. In the last section, the comparative analysis between both datasets and field measurements is described. Secondly, the developed methods of processing the GLAS full waveform, which were explained in section 3.4.2.3, will be shown.

#### **4.2.2.1 Airborne LiDAR processing**

Discrete return LiDAR data were acquired for the study area on 24 August and 9 September 2004 with an average high density of 2 points/m<sup>2</sup> and with average point spacing of approximately 1 metre. Analysis was carried out for GLAS footprints which have overlapping footprints with airborne LiDAR data (n=22). As mentioned above, this excluded footprints which fell in the river area. The raw airborne LiDAR data were provided in LAS format. It is necessary to filter the LiDAR returns to provide accurate digital representations of terrain and canopy height. eCognition Developer 8 software was used to separate airborne LiDAR data to first and last returns in LAS format, which used ArcMap™ 9.3.1 to create the DSM and DEM.

The literature review on airborne scanning LiDAR in Chapter 3 shows that discrete small footprint airborne LiDAR provides the best measurement accuracy of terrain elevation and vegetation heights. In this study, airborne LiDAR hits were classified

as vegetation and ground hits; and hence, a digital surface model (DSM) and a digital elevation model were generated. These data were also used to calculate terrain slope for each GLAS footprint. The canopy height model was calculated as the difference between DSM and DEM. Observations with height values less than 1 metre were excluded from the dataset in order to eliminate the effect of grasses and understory vegetation.

The airborne LiDAR data were processed using eCognition Developer 8 and ESRI ArcMAP™ 9.3.1 to generate DSMs and DEMs; and hence extract vegetation height stand density, and percent cover or canopy closure estimates.

#### **4.2.2.1.1 Mapping terrain topography (Digital elevation model (DEM) and Digital surface model (DSM))**

Characterizing the terrain elevation and creation DEM is a crucial step that needs to be accomplished before attempting to estimate vegetation parameters. One of the major advantages that LiDAR offers is the capability to measure ground elevation in vegetated areas (Means *et al.*, 2000). Some LiDAR hits penetrate gaps in the canopy and hit lower layers of vegetation or ground. These returned hits are assumed to correspond to the ground surface and are used with appropriate interpolation methods to derive a high accuracy digital elevation model (Popescu *et al.*, 2002). The work of Lam (1983) presents a comprehensive review of spatial interpolation methods, which are categorised as a real and point interpolation methods. For point interpolation techniques, exact and approximate methods are used, depending on whether original sample point values are able to be reserved. Approximate methods include Fourier models, power-series, trend models, least-squares fitted with splines, and distance-weighted least squares. Exact methods

include Distance-Weighting, Spline interpolation, Kriging, Finite-difference, and Interpolating Polynomials methods. However, previous studies that attempted to generate DEM with airborne LiDAR data preferred to use exact interpolation techniques in order to preserve the original raw LiDAR data values (Liu, 2008).

In order to create a DEM from raw LiDAR data; firstly, LiDAR point clouds are loaded and pre-classified into non-ground (first return) and ground (last return) points using eCognition Developer 8 software. The DEM was generated by selecting the minimum elevation points from the first LiDAR returns dataset within a 1x1 metre cell representing the size of one pixel. Similarly, the same processing steps were applied to produce DSM by selecting the maximum elevation values within a 1x1 metre cell. Secondly, to perform the terrain analysis on the created ground surface and ground points, the first and last returns were converted to shape files format in ArcMAP™ 9.3.1, and then LiDAR analysis tools were used to create ground surface and canopy surface, and the ArcMap 3D analyst extension tool was used to produce a DEM and DSM rasterized and raster slopes for the selected GLAS footprints.

#### **4.2.2.1.2 Canopy Height Model (CHM)**

The tree canopy height model was created by subtracting the DSM from the DEM values. Tree height values then could be extracted from the canopy height model generated for each GLAS footprint.

#### **4.2.2.1.3 Stand density**

The number of trees with maxima points in each 1 m pixel is counted and a value for the stand density is assigned to the pixel. The total maxima within one GLAS footprint is an indicator of the number of stems per GLAS plot. In this study, the

stand density is presented in a raster with a range value between 0.0 and 1.0. in this case, dense vegetation is represented by a value of 1 and no vegetation is represented by 0 value. Thus, stand density is represented by vegetation returns at height >5m divided by the total returns.

#### **4.2.2.1.4 Percentage of crown canopy cover**

McGaughey (2007) defines the value for this metric as “the number of returns over a specified height threshold divided by the total number of returns within each cell”. To compute this metric, the raw LiDAR point cloud and DSM are used to estimate the crown canopy cover in each cell size. The cell size and the surface height are specified by the user. In this analysis, 2 metres is used as the height surface parameter to estimate percent cover of the tree canopy.

#### **4.2.2.2 GLAS data processing**

The methods described in the previous chapter were used to estimate vegetation structural metrics, vegetation heights, stand density, and crown canopy overestimates.

The estimation of GLAS waveform parameters in this study is based on the work of Duong (2010), which describes how to extract parameters of signal GLAS full waveform, and its physical explanation regarding vegetation environment. The waveform parameters used in this study to estimate the above savannah vegetation structural metrics from GLAS waveform are the waveform extent ( $w$ ), which is defined as the distance between the start and end of the waveform; ground return energy ( $e_{Ground}$ ), which is the total intensity of the last peak; canopy return energy ( $e_{Canopy}$ ), which is the difference between return waveform energy and ground

return energy; and return waveform energy, which is the received energy below the curve of the start and end waveform (*eEcho*).

#### **4.2.2.2.1 Vegetation height**

Maximum vegetation height estimates are calculated using the direct and statistical methods described in the previous chapter. These methods take into account the effect of topographic on waveform extent (*w*).

#### **4.2.2.2.2 Stand density**

The concept of Gaussian decomposition was used to estimate the stand density, which can be estimated from GLAS waveform parameters by calculating three parameters, canopy return energy (*eCanopy*), return waveform energy (*eEcho*), and the LiDAR height (*LH*) for each GLAS plot (Nilsson, 1996; Drake *et al.*, 2002) using the equation below which represents the stand density as a value between 0 and 1 where value of 0 indicates no return energy from the vegetation and value of 1 indicates high vegetation returns and thus dense vegetation :

$$\text{Stand density (D)} = \frac{eCanopy - LH}{eEcho} \quad (4.1)$$

#### **4.2.2.2.3 Crown canopy cover**

Again, depending on the Gaussian fitting concept applied to GLAS waveform, the measure of crown canopy cover utilizes canopy return ratio parameter (*rCanopy*), which is calculated by dividing the canopy return energy (*eCanopy*) by return waveform energy (*eEcho*) (Harding and Carabajal, 2005).

## 4.3 Results and discussion

### 4.3.1 Mapping terrain topography

#### - Digital Elevation Model (DEM)

The DEMs created using airborne LiDAR data for the selected GLAS footprints are shown below in Figure (4.2).

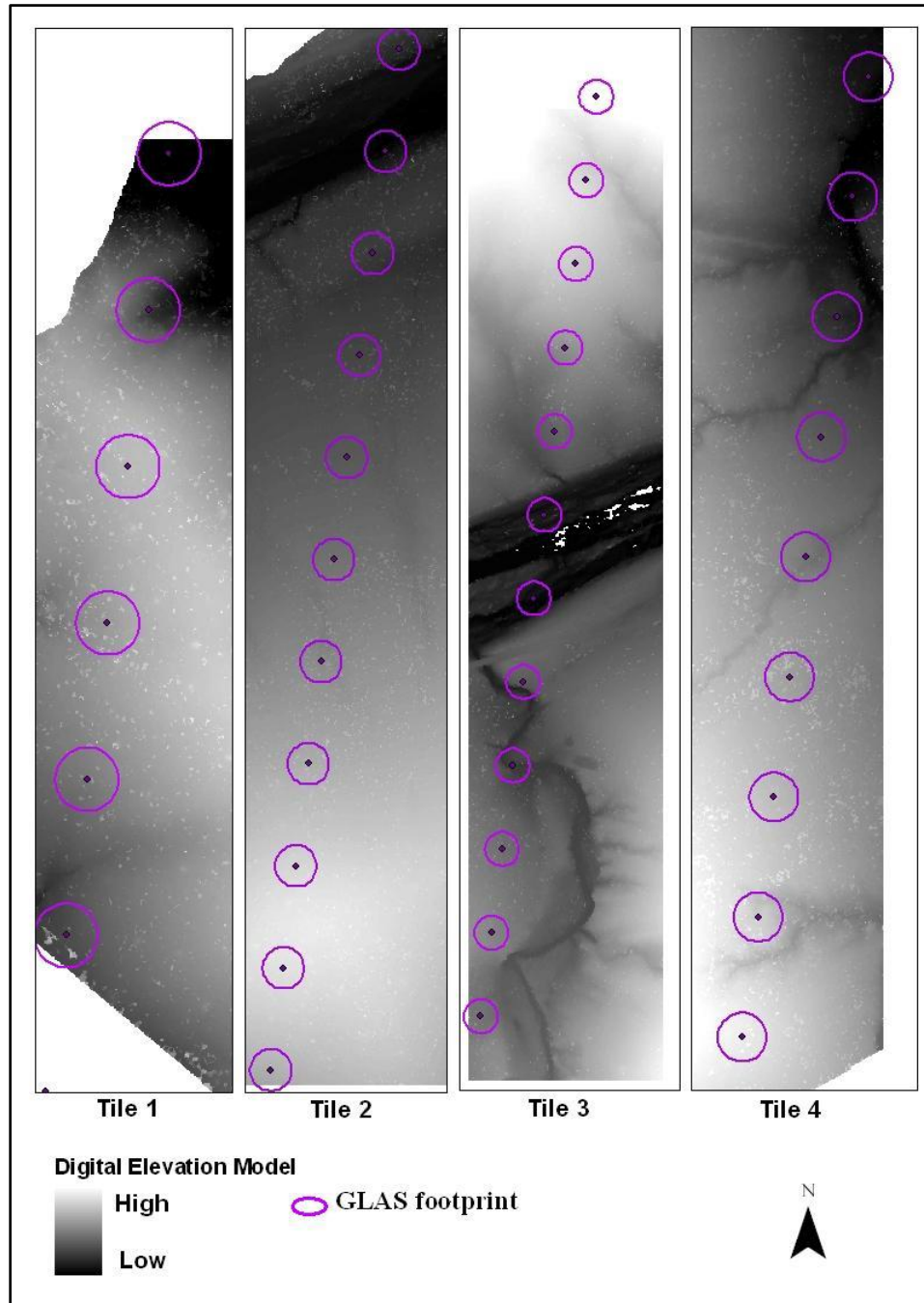


Figure 4.2: Digital Elevation Model (DEM) extracted from airborne LiDAR points clouds for the overlapped GLAS footprints with airborne LiDAR data of the test site.

Results of correlation between the waveform extents detected from GLAS satellite LiDAR (GLA14 and GLA01) on the ground surface and the coincident airborne LiDAR mean elevation for each GLAS footprint demonstrated a close correlation, producing  $r$  of 0.86 and 0.80 with RMSE of 2.16m and 2.50m respectively, and  $p$ -value  $< 0.001$  statistically significant for both correlations (Figure 4.3).

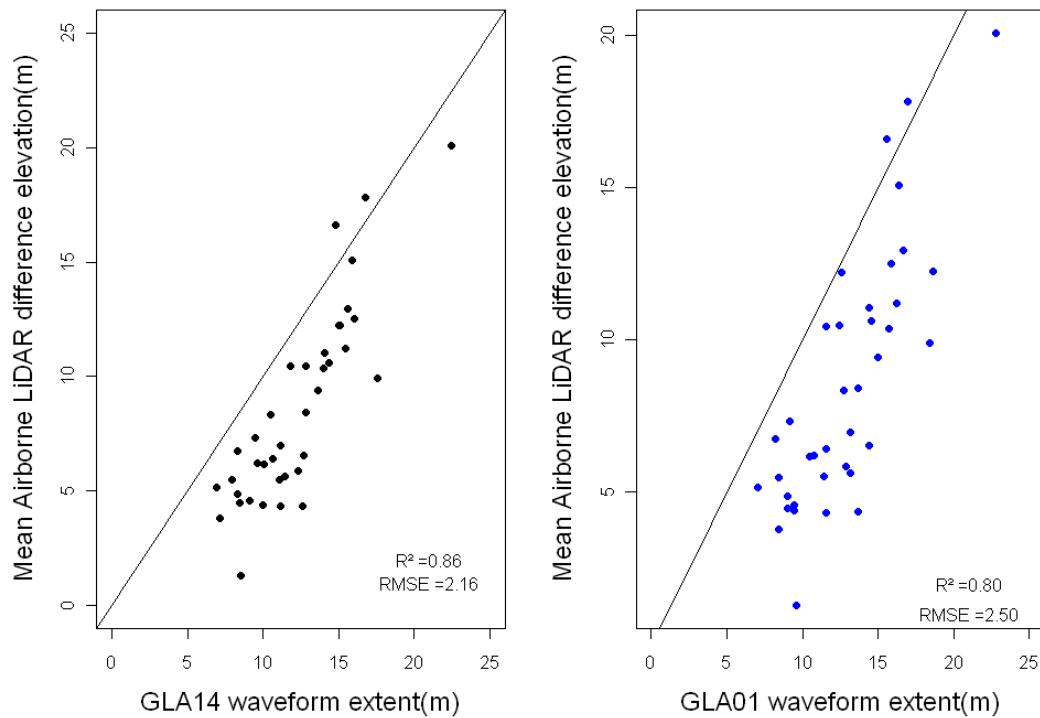


Figure 4.3: The relationship between estimates of surface elevation using airborne LiDAR data (the difference between the maximum and minimum detected elevation) and waveform extents extracted from GLA14(left graph) and GLA01(right graph) for the satellite LiDAR data for the 38 GLAS footprints overlapped with airborne LiDAR data.

Figure 4.4 shows estimation of within footprint mean ground elevation using LiDAR airborne data, and ICESat-GLAS estimated ground surface using GLA14 and GLA01 product. Estimates can be seen to correspond closely throughout the pass with maximum difference of 2.5 m and minimum difference of 0.3 m.

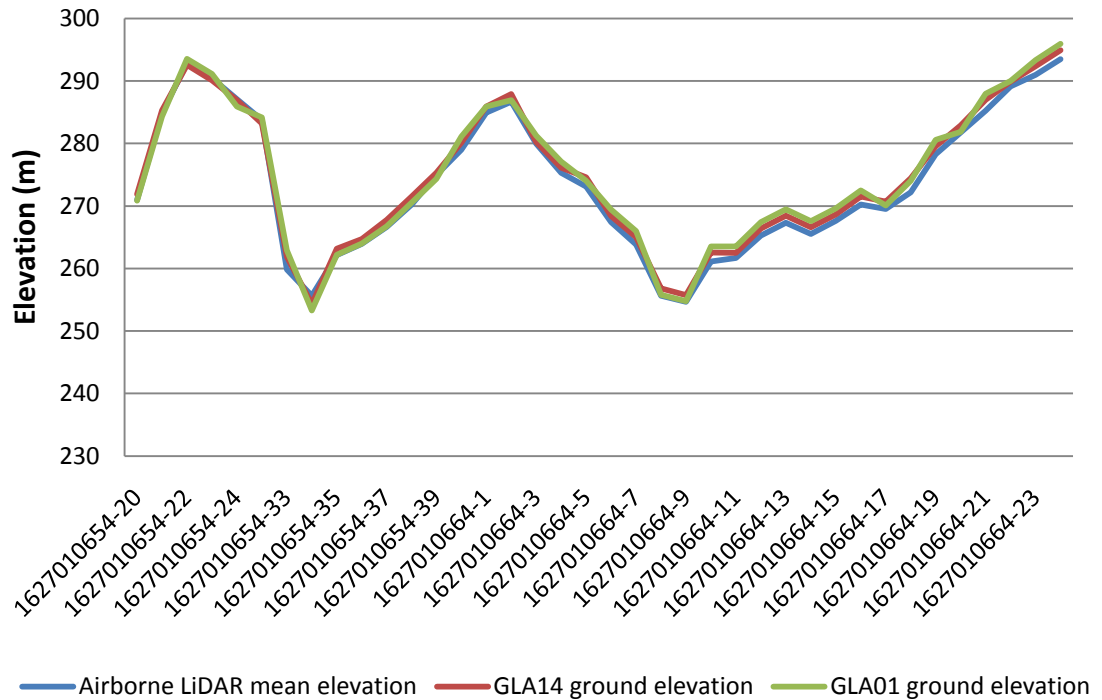


Figure 4.4: Comparison of ground elevation using GLA14 elevation product and estimations of mean elevation of airborne LiDAR ground for the selected GLAS footprints.

It is important to identify the elevation of the ground surface in order to obtain accurate estimates of vegetation height. Therefore, it is important to assess the methods used in this research to identify ground elevation in order to ascertain sources of errors within estimates.

The use of direct method of utilizing waveform structure parameters to identify ground surface has resulted in acceptable ground elevation estimates from LiDAR airborne data. The direct method relies on using the waveform structure parameters (width and amplitude) to identify ground surface signal.

The distribution of error found in airborne LiDAR data in relation to surface elevation extracted from waveform structure is illustrated in Figure 4.5, and statistical relationships are presented in Table 4.1.

### Analysis of elevation estimates error

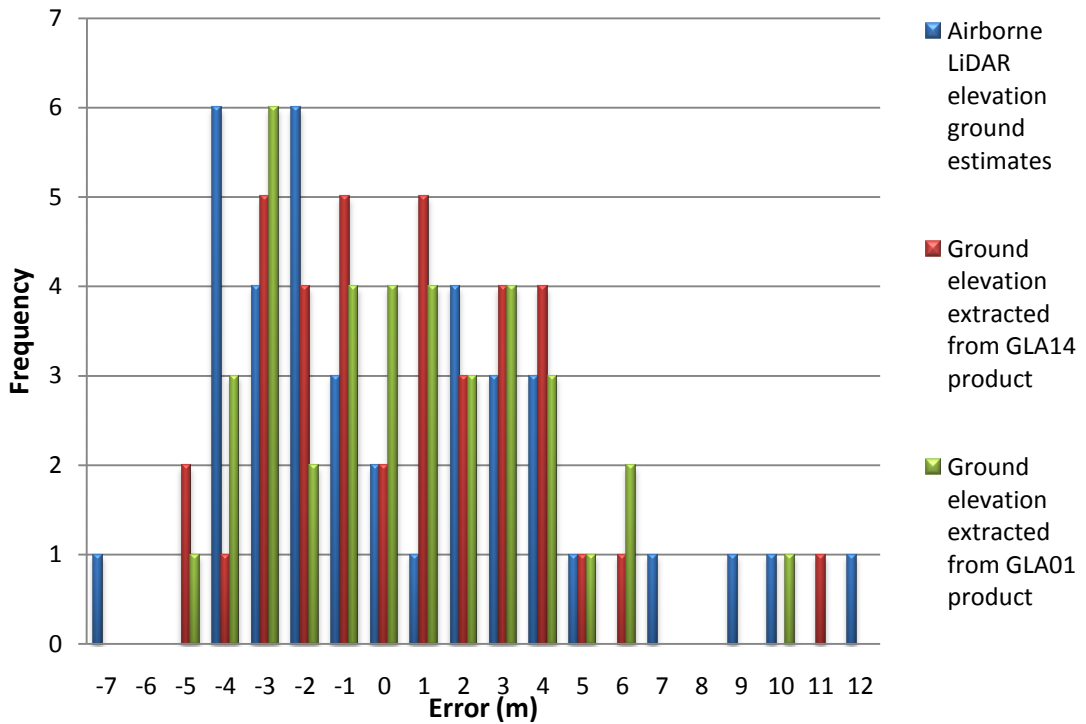


Figure.4.5: Distribution of errors in estimates of the ground surface elevation using ground elevation differences extracted from GLAS waveform structure and airborne LiDAR mean elevation surface extracted for each overlapped GLAS footprint.

Both methods of extracting elevation ground from GLA01 and GLA14 products underestimated mean ground elevations of airborne LiDAR estimates of surface elevation by - 4.34m and - 3.68m respectively. This could be to the differences in the ellipsoid characteristic used by the airborne LiDAR sensor and the ellipsoid used by the ICESat-GLAS elevations product.

When compared with airborne LiDAR ground surface, it is recognised that mean slopes from airborne LiDAR data calculated for each GLAS footprint explained 80% and 69% of the percentage error using GLA01 and GLA14 estimates of ground elevation surface differences. This suggests that using a statistical method

of waveform extent has succeeded in removing the effect of terrain as a source of error in calculating vegetation heights.

Table 4.1: Comparison of estimated ground surfaces using airborne and satellite GLAS LiDAR data.

<b>Comparison</b>	<b>Elevation airborne LiDAR-Elevation GLA14 (m)</b>	<b>Elevation airborne LiDAR-Elevation GLA01 (m)</b>
Mean offset	-3.68	-4.34
Min differences	-8.25	-9.29
Max differences	1.80	1.02
Standard Deviation	2.17	2.53

#### - **Digital Surface Model (DSM)**

The digital surface model was generated from the first pulse data of the airborne LiDAR data (Figure 4.6). Typically, the DSM contains the returns from canopy surface. Hence, canopy height model (CHM) is calculated by subtracting DSM from DEM.

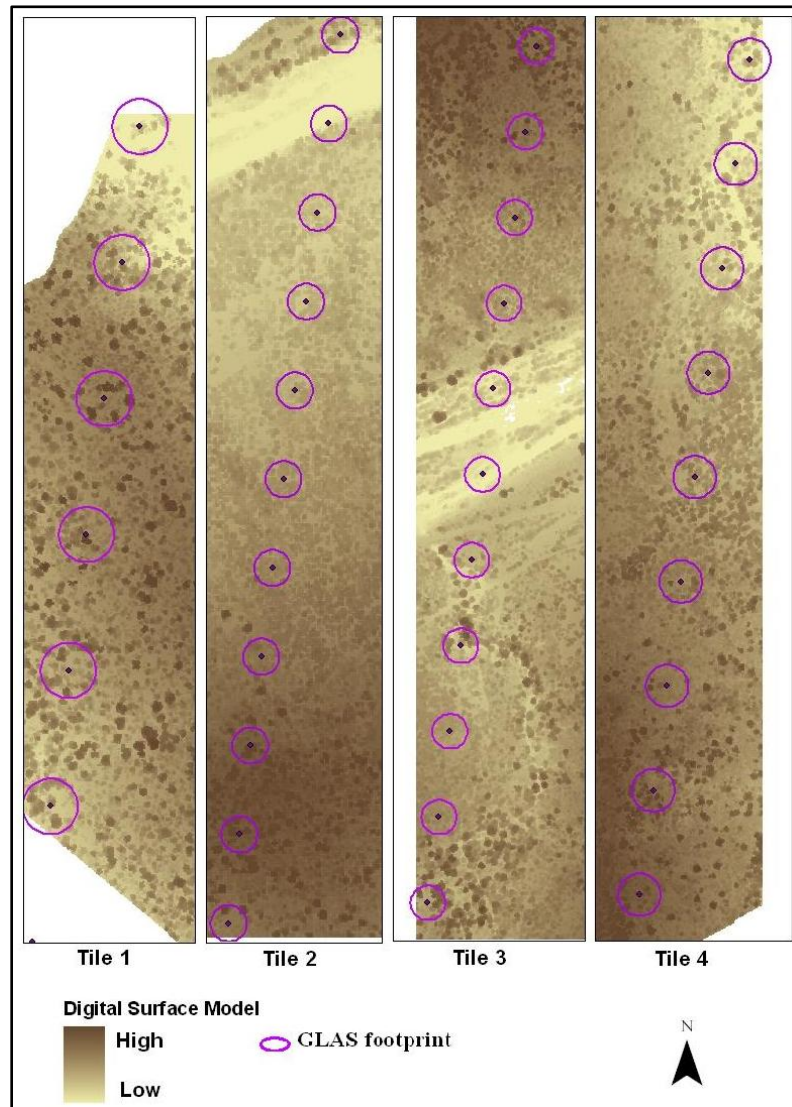


Figure 4.6: Digital surface model extracted from airborne LiDAR data for the selected footprint. The darker brown refers to the highest LiDAR returns, and the light brown indicates very low returns from the vegetation surface.

### 4.3.2 Vegetation structure parameter estimates from airborne LiDAR

#### - Canopy Height Model (CHM)

Ground and surface returns were interpolated as above to form a digital elevation model (DEM) and a digital surface model (DSM) with 1-m raster grid cell size. The vegetation CHM was to obtain by subtracting the DEM from the DSM. The LiDAR CHM represents a canopy height range from 0.0 to 23.5m (Figure 4.7), with an average height of 8.5 m and a standard deviation of 4.2 m over the entire selected GLAS footprints.

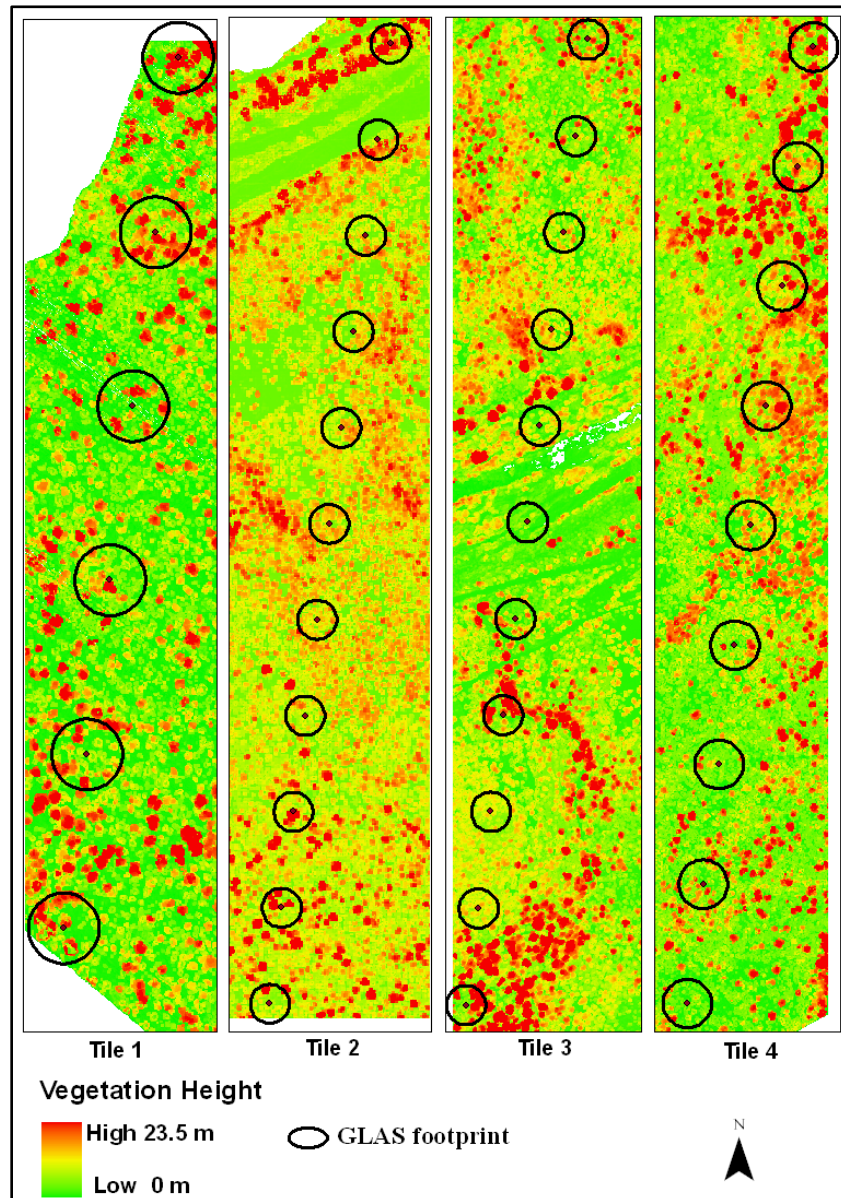


Figure 4.7: The canopy height model CHM was determined using LiDAR by calculating the difference between the first return elevations (canopy height) from the last return (ground elevation). The red colour indicates the highest trees (more than 10 m) and the green colour refers to the lowest vegetation heights (less than 1m)

- **Stand density**

Figure 4.8 shows estimations of stand density for all vegetated footprints across the study site within footprints using airborne LiDAR points. The map below (Figure 4.8) provides a measure of the relative difference in stem densities between savannah species types. Using the created CHM, a stem density is created per pixel that is more than or equal to 5 metres in height.

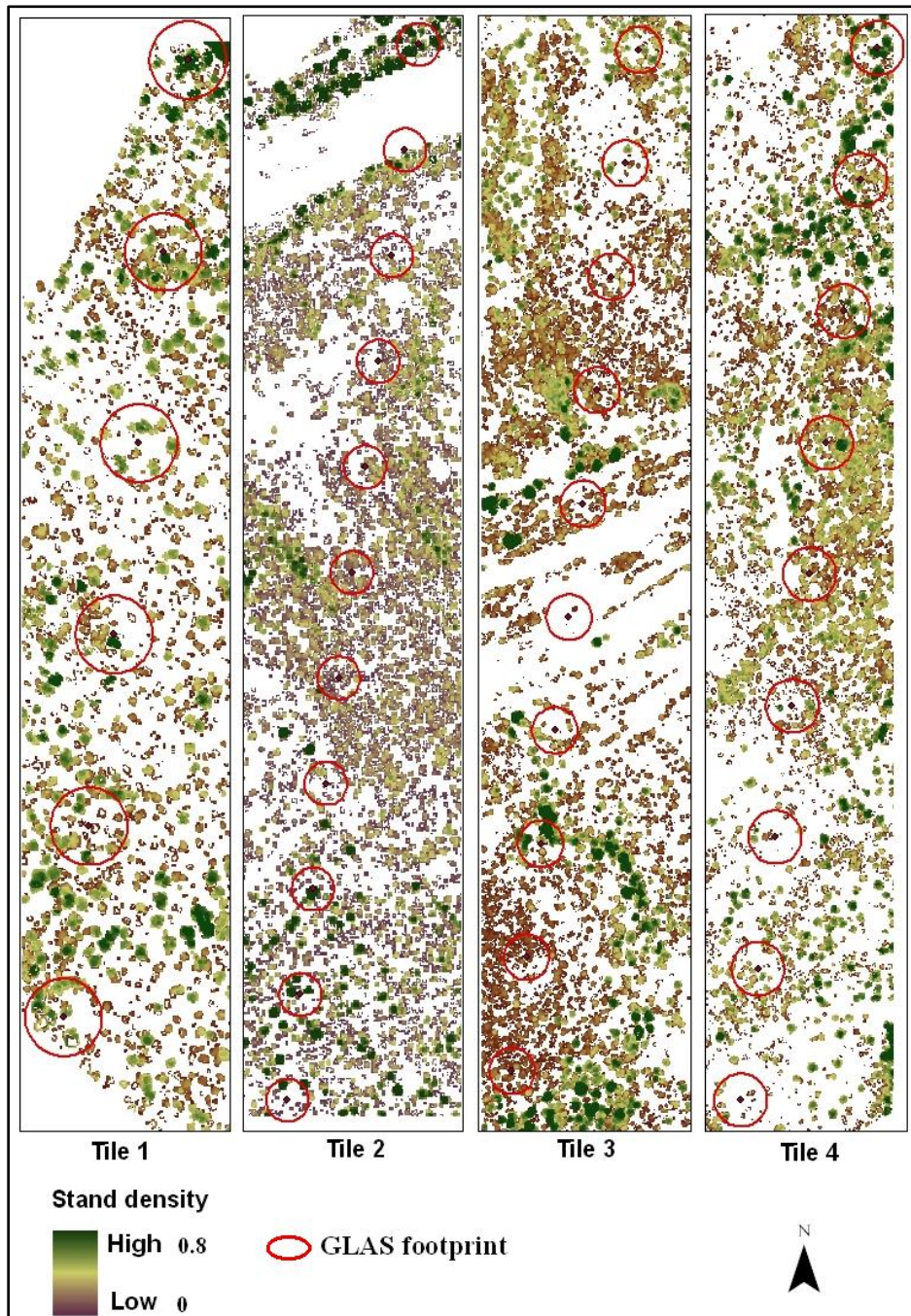


Figure 4.8: Stem density map. The darker green represents high stem density, and darker brown represents lower stem density.

- **Percent cover**

The percent cover estimations shown in Figure 4.9 provide an indication of the amount of crown canopy cover and the distribution of canopy gaps, depending on the amount of returned LiDAR points from the canopy surface. The map represent the woody cover percentages, which ranged from 70% (closed woodlands savannah

canopies) down to less than 1% (open sparse grasslands); significant areas with less than 40% woody cover were consistently present on the map.

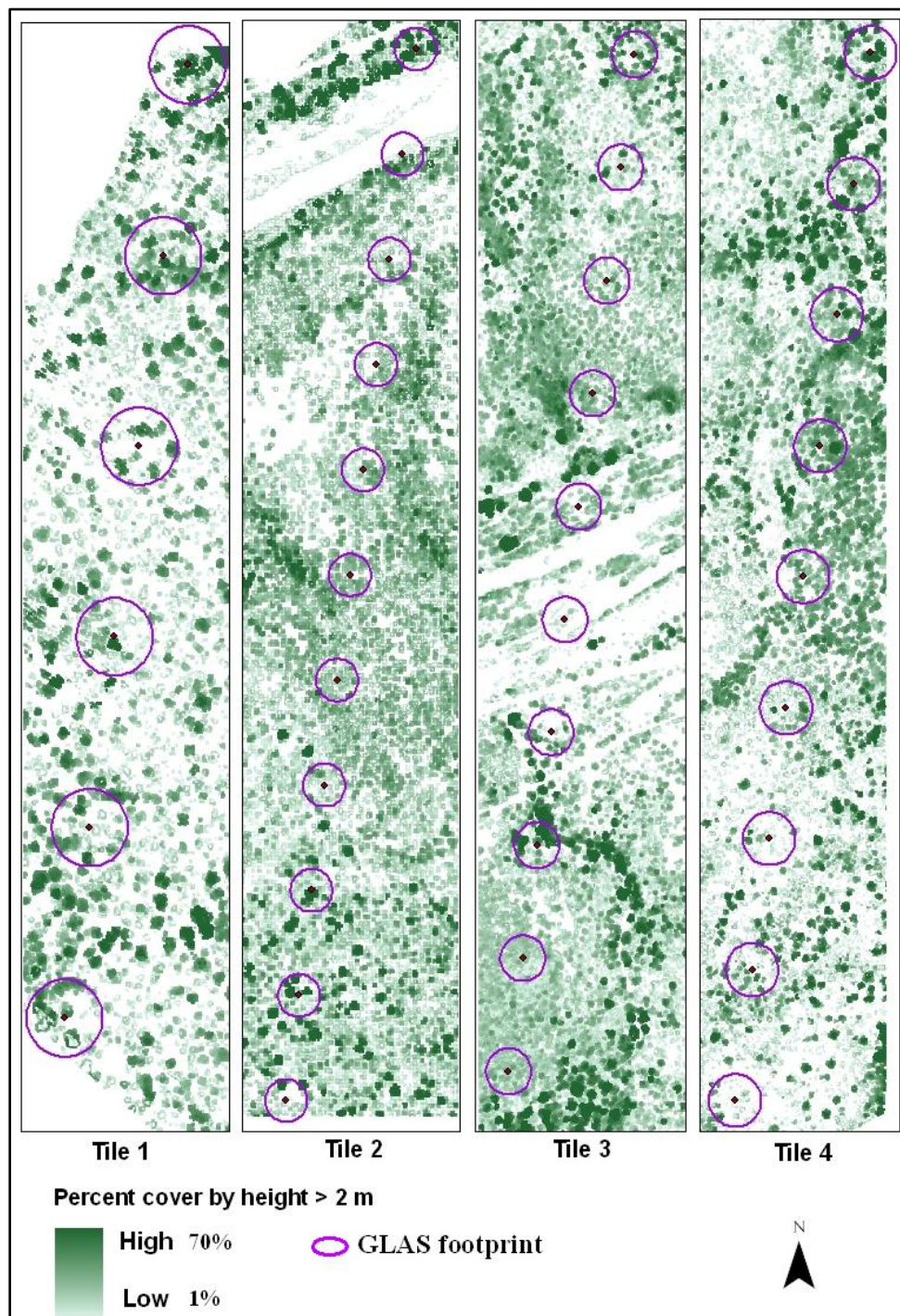


Figure 4.9: The percentage of woody cover extracted from DSM and height >2 m.

### **4.3.3 Comparison of vegetation structure parameter estimates from spaceborne LiDAR with airborne LiDAR data**

The study describes here the outcomes of using methods of estimating vegetation structure from GLAS waveforms presented in the previous chapter and compares them with vegetation structure estimates from airborne LiDAR data.

#### **- Vegetation height**

Vegetation height is an important vegetation parameter for leading dimensions of ecological variations amongst tree species (Westtoby *et al.*, 2002); it can provide information relating to vegetation structure such as stand density and biomass (McInerney *et al.*, 2010).

The objectives of this comparison are to evaluate the use of ICESat-GLAS data to estimate vegetation structure in savannah environment, and to develop reliable methods for estimating vegetation height, stand density, crown canopy cover and biomass that can be applied to regional and national scales.

Figure 4.10 shows canopy height estimates from airborne LiDAR data compared with those estimates from GLAS waveforms using both methods - the direct and statistical methods of GLAS waveform processing.

An analysis of the relationship between airborne LiDAR and GLAS estimations of maximum canopy height using GLA01 and GLA14 parameters produced correlation coefficient  $r$  of 0.68 and 0.71 and RMSE of 2.67m and 2.58m respectively for  $n=38$ . Both correlations are statistically significant ( $p$ -value < 0.001).

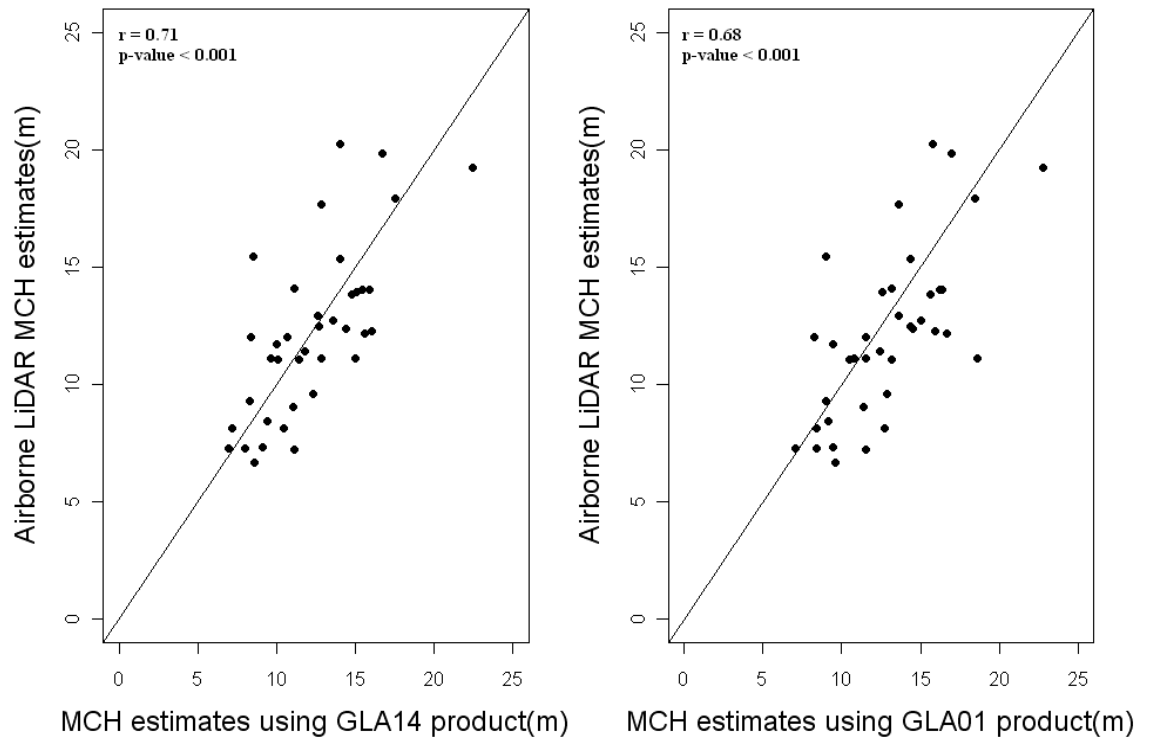


Figure 4.10: Relationship between estimated maximum canopy height from airborne LiDAR and estimates of maximum canopy heights from GLA01 and GLA14 products.

Figure 4.10 shows that MCH estimates ( $n=38$ ) from GLA14 and GLA01 using direct method, which employs parameters extracted from both products based on the Gaussian decomposition analysis method, explained a close correlation relationship with airborne LiDAR estimates with  $r$  of 0.71 and 0.68 for GLA14 and GLA01 respectively. This demonstrates that, despite the effect of terrain topography, satellite LiDAR waveforms and coincident airborne LiDAR data can be seen to give similar estimations of maximum vegetation height. However, it is well known that airborne LiDAR data have been widely used and accepted in forest applications; therefore, the results found between both systems suggest prospects for future practical applications for satellite LiDAR remote sensing in savannah vegetation profiles.

However, the analysis of airborne LiDAR data indicates that the topography over the GLAS footprints for the study area is generally flat to moderated relief with areas of steep slopes. The average mean slope is around of 17 degrees. Slopes have effects on the shape of the waveforms and hence the waveform extent and shape. Increasing surface slope results in larger width of the ground peak with less ground energy (Duong, 2010). Therefore, it is important to incorporate this important effect to obtain accurate estimation of vegetation height from GLAS waveform.

The terrain slopes were classified into 4 categorises of 0-15° (flat), 15-30° (moderate), 30-45° (steep), and > 45 very steep. As a result of this classification, 18 GLAS footprints fall in the flat class, 12 GLAS footprints are located in moderate slope areas, while 8 footprints fall in a steep slope areas.

In order to evaluate the use of the direct method of estimating maximum vegetation height from the classified GLAS waveform according to their terrain slopes, comparisons between height estimates from airborne LiDAR and estimations of maximum vegetation heights using direct methods for the classified GLAS footprints are shown in Figure 4.11. It was recognised that estimations of vegetation height over a flat surface using the direct method of applying equation (4.2) or (4.3) for GLA14 and GLA01 parameters produced improved results on the flat footprints, using GLA01 parameters in equation (4.2) produced  $r = 0.71$  with RMSE of 2.86m and  $p\text{-value} < 0.001$  when compared with MCH estimates from airborne LiDAR data; and using GLA14 parameters in the same equation (4.2) gave  $r$  of 0.68 and RMSE= 2.32m and  $p\text{-value} < 0.001$  when also compared with those estimates from airborne LiDAR data:

$$H_{max} = H_s - GP \quad (4.2)$$

Where  $H_{max}$  is the maximum canopy height estimated from GLAS data (m),  $H_s$  = the signal start (m),  $GP$  = ground peak (m) (the centroid of the greatest amplitude of Gaussian decomposition peak).

Moreover, using the direct method of applying equation (4.3) produced correlation coefficient  $r = 0.86$ ,  $RMSE = 1.50m$  and the correlation was statistically significant (p-value < 0.001) for applying GLA14 parameters and compared with MCH estimates from airborne LiDAR data. Applying the same equation (4.3) also on GLA01 parameters gave  $r = 0.89$  and  $RMSE = 1.32m$  and the correlation was statistically significant (p-value < 0.001 when compared with those predicted from airborne LiDAR data).

$$WE = d_{sigbegoff} - d_{sigendoff} \quad (4.3)$$

Where

$WE$  = the waveform extent,  $d_{sigbegoff}$  = signal beginning,  $d_{sigendoff}$  = signal ending.

For vegetation height over moderate surface with moderate uplands and lowlands, the equations (4.2) and (4.3) of direct method produced  $r$  value of 0.70 and  $r$  of 0.64 with  $RMSE$  of 2.61m and 2.79m respectively and both correlations are statistically significant ( p-value < 0.001), while the lowest  $r$  results were obtained from the steep slope footprints with  $r$  value of 0.55 and  $r$  0.48 with  $RMSE$  of 3.01m and 3.19m respectively, and both correlations are not statistically significant (p-value > 0.05) (Figure 4.11). The results in Figure 4.11 show acceptable estimations of MCH that could be achieved using the direct method of estimating MCH from

GLAS waveform matrices using Gaussian decomposition or direct method. Therefore, there is no need to apply the statistical method here due to the similar results that could be achieved to estimate MCH from both airborne sensors and satellite LiDAR systems.

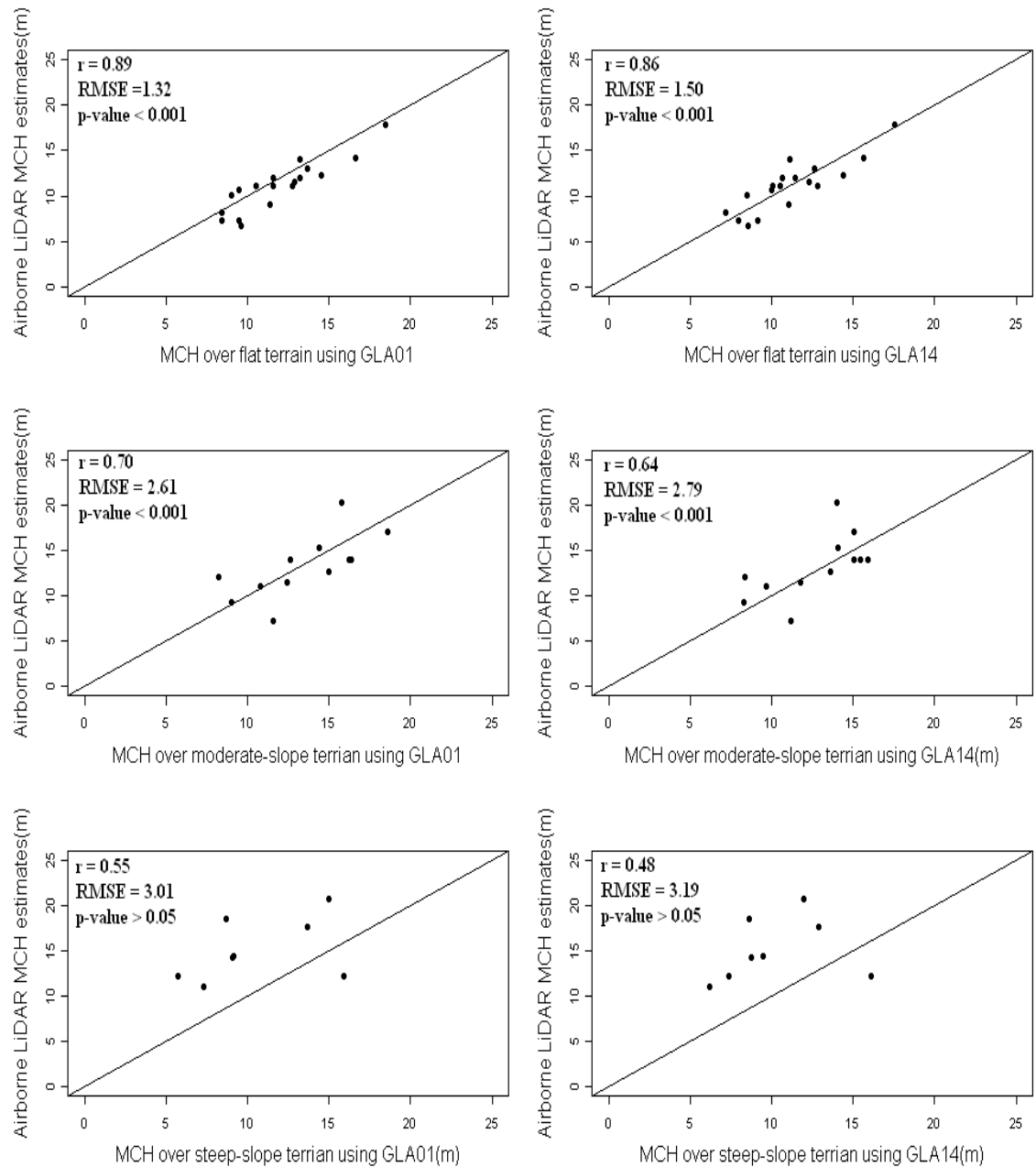


Figure 4.11: Comparisons of airborne LiDAR estimates MCH with GLAS MCH estimates using the direct method of applying equation (4.2) for GLA01 parameters and equation (4.3) for GLA14 parameters. These comparisons were done for the classified GLAS footprints according to their slope classes.

### - Stand density

Three waveform metrics were derived from GLA01 waveforms to estimate stand density for each GLAS footprint: LiDAR height ( $LH$ ), which was calculated using the first and the last Gaussian peak in the GLAS waveform; mean canopy energy ( $eCanopy$ ); and return waveform energy ( $eEcho$ ) (Nilsson, 1996; Drake *et al.*, 2002). Stand density calculated from each GLAS footprint ( $n= 38$ ) using volume-related parameters (illustrated above) was found to have a significant relationship with stand density volume extracted from LiDAR airborne data, which produced  $r$  value of 0.95 and RMSE of 0.98 %, the correlation was statistically significant ( $p$ -value  $< 0.001$ ) (Figure 4.12).

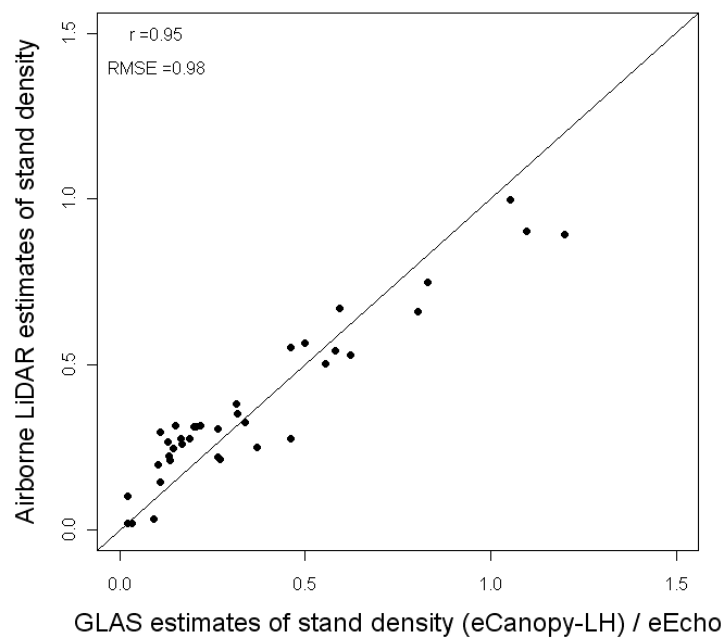


Figure 4.12: The relationship between stand density estimates of airborne and satellite LiDAR data. The Pearson correlation shows a strong relationship between estimates of both systems.

Although there is no difference between the mean of estimated stand density using airborne LiDAR data and the mean of estimated stand density using spaceborne LiDAR data, the high bias of 0.8 exists due to the time differences between the two sensor systems; and, most important, is that the bias occurred in the steep slope terrain with high vegetation. However, these results suggest that spaceborne laser

must be considered of potential value for vegetation structure estimations for savannah ecosystems.

- **Crown canopy cover**

Depending on the Gaussian fitting concept applied to GLAS waveform, the measure of crown canopy cover utilizes canopy return ratio parameter ( $rCanopy$ ), which is calculated by dividing the canopy return energy ( $eCanopy$ ) by the return waveform energy ( $eEcho$ ) (Carabajal and Harding, 2005). The results compared to those estimates of airborne LiDAR data. The relationship produced  $r$  value of 0.94 and RMSE of 10.04 %, the correlation relationship was statistically significant ( $p$ -value  $< 0.001$ ) (Figure 4.13).

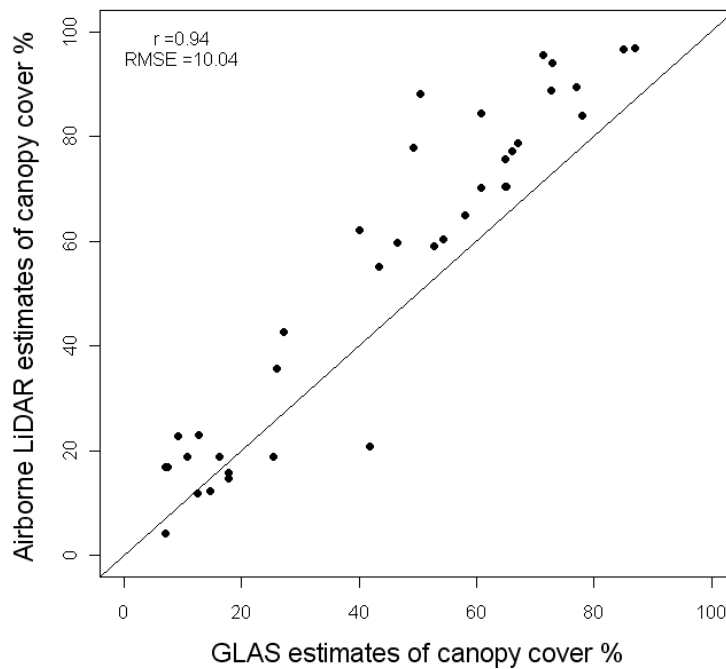


Figure 4.13: The relationship between percent cover estimates of airborne and satellite LiDAR data. it is quite obvious that airborne and GLAS percent cover estimates are highly correlated with ( $r = 0.94$ ,  $p$ -value  $< 0.001$ ). However, RMSE of 10.04% is slightly high crown canopy cover

The statistical analysis of the correlation bias indicates a low bias of 0.45, which is not statistically significant. Additionally, there was no significant difference in the means for both datasets. However, the over-estimated values of crown canopy

cover from both sensors might be due to reflects off canopy (branches, leaves) and ground surfaces, particularly surfaces with mixed-sloped terrain and vegetation (Dubayah and Drake, 2000).

#### **4.3.4 Evaluation using field measurements**

##### **- Vegetation height**

A comparison between results of MCH of field measurements and MCH obtained from both LiDAR systems according to the classified terrain slopes GLAS footprints with respect to its terrain index generated from airborne LiDAR data shows (Figure 4.14) that both LiDAR systems have a similar relationship to the observed field MCH.

The terrain slopes over the selected GLAS footprints for field measurements evaluation were classified into 3 categories of 0-15° (flat), 15-30° (moderate), and 30-45° (steep). As results of this classification, 8 GLAS footprints fall into the flat class; 9 GLAS footprints are located in moderate slope areas; while 6 footprints fall in steep slope areas. As a result of this classification, flat terrain GLAS footprints have the highest correlation coefficient of GLAS and airborne LiDAR data  $r = 0.78$ ; RMSE = 2.23m and  $r = 0.70$ ; RMSE = 2.17m respectively. Both correlations are statistically significant (p-value < 0.001) when comparing with MCH field measurements; while the comparison relationship started to decrease with both LiDAR systems and field measurement of MCH giving a statistically significant correlations  $r$  of 0.70; RMSE of 2.38m; (p-value < 0.001) and  $r$  of 0.68; RMSE of 1.97m; and (p-value < 0.001) respectively for the moderate slop terrain GLAS footprints , and non significant statistical correlation relationship  $r$  of 0.34; RMSE

of 3.96m; (p-value > 0.05) and  $r$  of 0.30; RMSE of 4.49m; (p-value > 0.05) respectively for the steep sloping footprints (see Figure 4.14).

As a result, estimating MCH from both LiDAR systems is affected by terrain slopes. This is obvious in Figure 4.14 for estimated MCH over steep slope terrain. Two out of six GLAS footprints are located in a very steep slope terrain ( $> 45^\circ$ ), which decreases the correlation coefficient  $r = 0.34$  and  $0.30$  for estimated MCH from airborne LiDAR and satellite sensors. Therefore, statistical methods are required to incorporate this important factor in estimating height of vegetation in steep slope terrain.

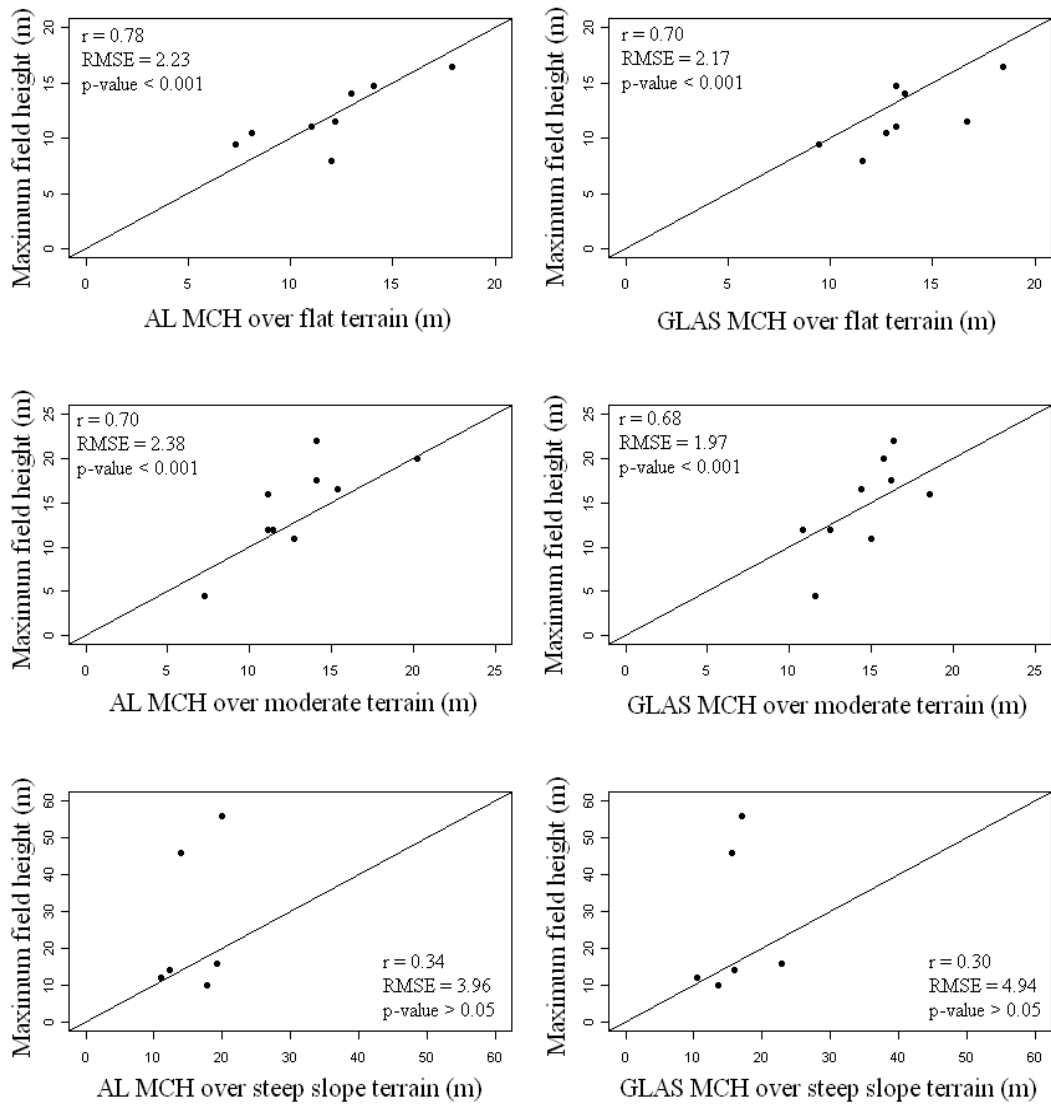


Figure 4.14: Relationships between classified GLAS footprints according to their terrain slopes and MCH of field measurements. The left and right graphs show that the  $r$  started to decrease when the terrain slopes increased.

Following further investigation considering the observations from the fieldwork, GLAS footprints were regrouped into two categories, flat and moderate terrain and steep slope terrain. Figure 4.15 shows the comparison relationship for MCH estimates from both LiDAR systems and MCH of field measurements. Flat terrain plots have  $r$  of 0.86 and RMSE of 1.77m for airborne LiDAR estimates of MCH when compared with MCH of field measurements; while this relation also gives  $r$  of 0.63 and RMSE of 1.99m when GLAS MCH estimates are compared with those

from field measurements. Both correlation coefficients are statistically significant ( $p\text{-value} < 0.001$ ). However, this relation decreased given  $r$  of 0.22 and 0.17 with RMSE of 3.80m and 3.45m respectively when comparing both LiDAR systems with MCH of field measurements in steep slope plots. Both correlation coefficients are not statistically significant ( $p\text{-value} > 0.05$ ) (Figure 4.15).

The results of the correlations coefficient linear relationships for steep slope areas suggest that the demand of using statistical methods to incorporate the effect of terrain slopes on the estimated maximum canopy heights from the satellite LiDAR system.

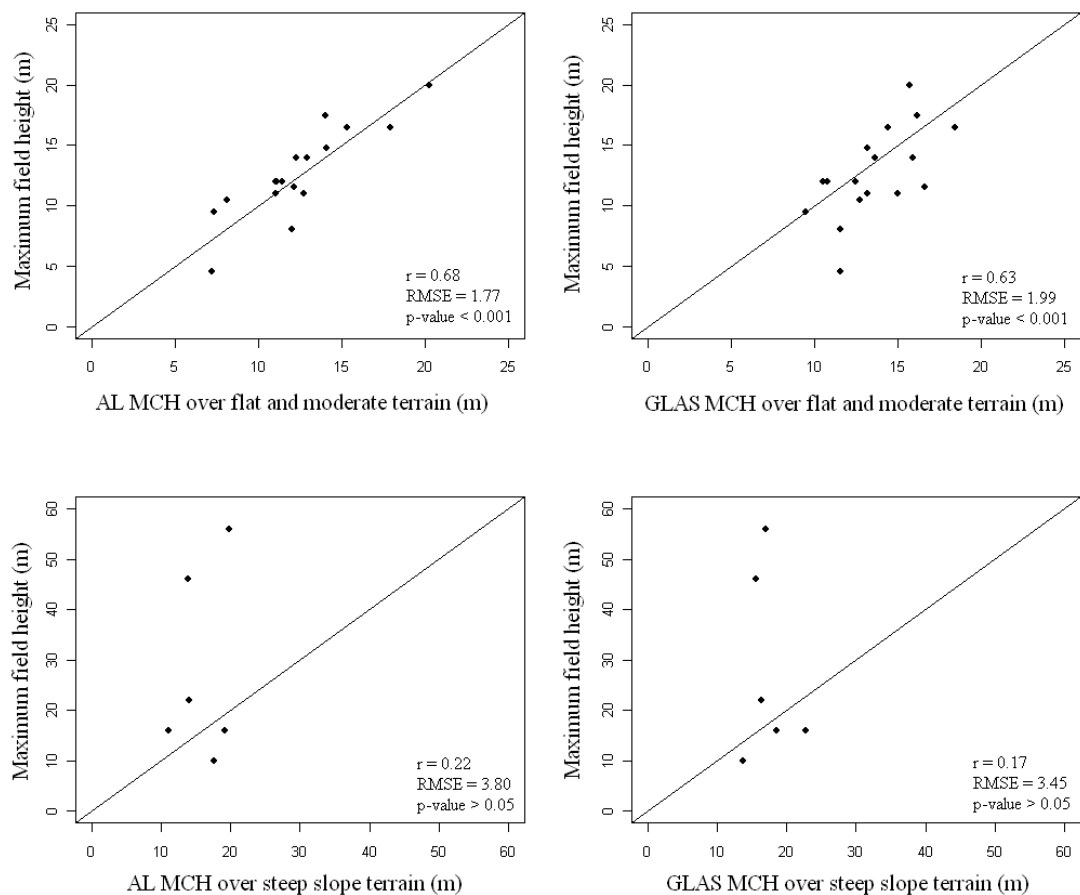


Figure 4.15: The relationship results of estimating MCH using both LiDAR systems and MCH of field measurements. It appears that steep slopes affect this relationship, producing low  $r$  specifically for GLAS MCH estimates in steep slope plots.

In order to incorporate the effect of terrain slopes on the shape of the GLAS waveform and hence the estimated vegetation canopy heights, statistical methods which employ regression analysis were done.

Two methods of considering the effect of slopes were applied. The first method uses the waveform extent ( $w$ ) and terrain index ( $g$ ), which are generated from airborne LiDAR data. It is defined as the highest and lowest elevations contained within a 7x7 subset of the DEM generated from airborne LiDAR data as an indicator of slope effect on the waveform extent. The analysis produced  $R^2 = 0.66$  and RMSE = 17m when compared with field measurements (n=6):

$$H_{Field} = 0.88*(w - g) + 4.38 \quad (4.4)$$

Coefficient significance  $p < 0.001$ ; intercept significance  $p > 0.01$ .

The analysis showed the capability of estimating maximum vegetation height from GLAS waveform with respect to terrain complexities on the waveform structure. However, the largest various were obtained for the very steep slopes plots (n=6), due to the slopes that were greater than 30°. The validation between MCH predicted from GLAS waveforms and field MCH measurements seems to suggest that terrain index can affect the waveform structure. However, this approach requires appropriate resolution of terrain data.

In order to rely on calculated GLAS waveform parameters for estimating MCH, the previous analysis was repeated but with only GLAS waveforms. It produced  $R^2 = 0.67$  and RMSE = 16.2m when compared with field measurements (n=6):

$$H_{Field} = 1.07*(w - \sigma) + 1.31 \quad (4.5)$$

Coefficient significance  $p < 0.001$ ; intercept significance  $p > 0.01$ .

The results showed similar results using terrain index generated from airborne LiDAR data. This suggests that the potential for estimating MCH from GLAS waveform parameters only with respect to the waveform width ( $\sigma$ ), which becomes wider when the terrain slope increases (Sun *et al.*, 2008).

In order to improve the relationship between the waveform extent and terrain slope factors that affect its shape structure with field MCH measurements, multiple regressions was used, following the work of Lefsky *et al.*(2005a). The resulting equation which uses terrain index is:

$$H Field = 1.53*w - 0.87*g \quad (4.6)$$

This gives  $R^2$  of 0.78, RMSE of 14.50m and both coefficients are statistically significant  $p$ -value  $< 0.001$ , the intercept was not significant, while using the same multiple regression which employs waveform width parameter ( $\sigma$ ) resulted in:

$$H Field = 2.73* w - 1.01 * \sigma \quad (4.7)$$

This gives  $R^2$  of 0.67, RMSE of 17.50m. Both coefficients are statistically significant  $p$ -value  $< 0.001$ , the intercept was not significant.

These results show a potential approach of estimating MCH from GLAS waveform parameters directly using statistics based on regression analysis methods.

#### - **Canopy cover**

Figure 4.16 shows the relationship between crown canopy cover estimates from fieldwork, airborne LiDAR data, and GLAS waveform data. The relationship produced  $r$  of 0.93 and 0.85 with RMSE of 10.04 % and 11.80 % for airborne and satellite LiDAR estimates of percent cover with those from field estimates.

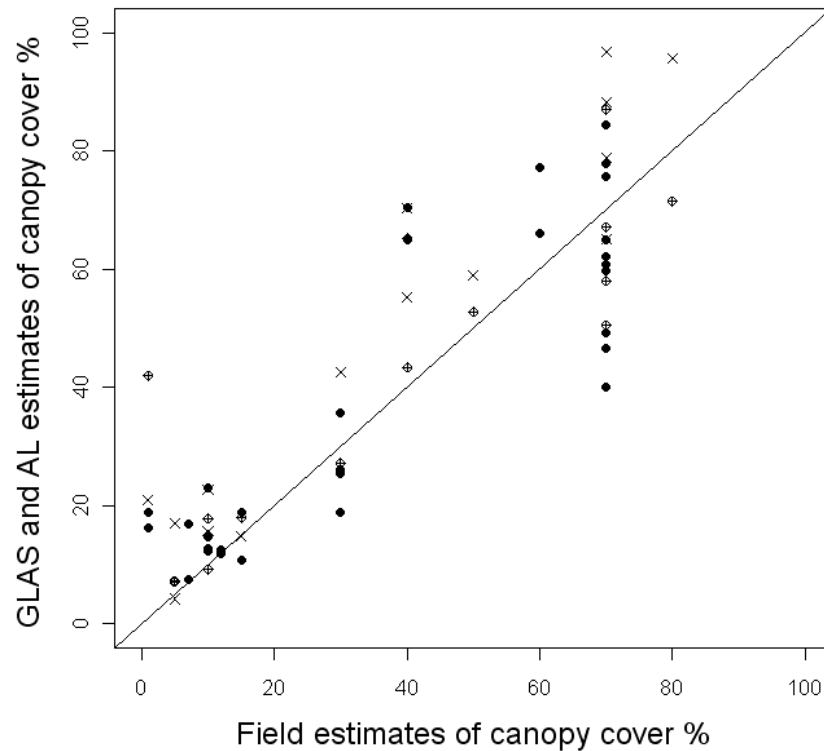


Figure 4.16: Relationships between percent crown canopy cover estimates using canopy return ratio parameter ( $r_{Canopy}$ ) from GLAS waveform (•) (y-axis) and estimates using airborne LiDAR (⊕) (y-axis) and those estimates from fieldwork (x) (x-axis). It shows a significant correlation (p-value <0.001) for both LiDAR systems with field estimates.

#### 4.4 Summary

This chapter has compared the estimation of vegetation parameters derived from coincident discrete small return airborne LiDAR data with those extracted from large full waveform LiDAR satellite GLAS data. The airborne LiDAR data was used to provide smaller samples of the surface within the GLAS footprint, and hence evaluate results of estimating vegetation structure obtained from GLAS.

The airborne and satellite LiDAR elevation data comparisons provide an independent evaluation of the elevation accuracy of GLAS data. The results indicate that the GLAS estimated elevation data error on the ground is no more than 2.5 m and the surface elevations measured from both LiDAR systems are consistent.

Relationship of maximum canopy height estimates between airborne LiDAR and GLAS estimations of maximum canopy height using GLA01 and GLA14 parameters produced  $r$  of 0.68 and 0.71 and RMSE of 2.67m and 2.58m respectively for (n=38). These results indicate the potential for using GLAS extracted waveform parameters for estimating MCH from direct methods. However, similar results were obtained for classified GLAS footprints according to its terrain index as indicator of terrain slope. The results show that for vegetation height estimates over moderate surface with moderate uplands and lowlands, the direct method produced  $r$  value of 0.70 and  $r = 0.64$  with RMSE of 2.61m and 2.79m respectively; while the lowest correlation results was obtained from the steep slopes footprints with  $r = 0.55$  and  $r = 0.48$  with RMSE of 3.01m and 3.19m respectively; and highest correlation results were obtained in the flat terrain plots with  $r = 0.89$  and  $r = 0.86$  and RMSE of 1.32m and 1.50m. From the results, it was clear that MCH estimated from both LiDAR systems have the same correlation relationships. Therefore, the statistical method should apply, particularly on steep slope terrain, to obtain accurate estimations of MCH. Results of estimations of stand density volume calculated from each GLAS footprint (n= 38) have a strong relationship with stand density volume extracted from LiDAR airborne data, producing  $r$  value of 0.95 and RMSE of 0.98%. This suggests that spaceborne laser must be considered of potential value for vegetation structure estimations for savannah ecosystems.

The comparison of percentage cover results from airborne LiDAR data to those estimates from GLAS shows highly correlated with  $r = 0.94$  and RMSE = 10.04%. crown canopy cover field measurements of MCH and percent crown canopy cover

were used to complement satellite LiDAR waveform parameters in order to develop suitable regression models using the statistical method of regression analysis with factors that have a magnificent effect on waveform structure, such as terrain index generated from airborne LiDAR data or waveform width calculated from GLAS waveform.

A new contribution described in this chapter is the development of a method to improve the estimation accuracy of the maximum vegetation canopy height using only GLAS waveform metrics on sloping terrain. Doung (2010) discussed in his work the effect of slope terrain on the waveform ground width. This work has tested this important parameter on the sloped GLAS footprints. The principal results obtained indicate that improved results could be achieved of estimating MCH from GLAS footprints over sloping areas using only two parameters: waveform extent and waveform width parameters. This gives  $R^2$  of 0.67 with RMSE of 17.50 m; while multiple regression using terrain index generated from airborne LiDAR data produced  $R^2$  of 0.78, RMSE of 14.50m. These results show a potential approach of estimating MCH from GLAS waveform parameters directly using statistical methods of regression analysis.

Relationships of percent crown canopy cover estimates from fieldwork and both LiDAR systems with those estimates from fieldwork show a significant correlation of  $r$  of 0.93 and 0.85 and ( $p$ -value  $< 0.001$ ) for airborne and satellite LiDAR. In addition, it is shown that the full ICESat-GLAS waveform parameters derived from direct or decomposition methods were able to extract vegetation metrics, and improved results could be obtained using regression analysis statistical methods.

## CHAPTER FIVE

### SAVANNAH WOODY COVER ESTIMATION FROM GLAS: AN EVALUATION USING ALOS-PALSAR RADAR DATA

#### 5.1 Introduction

Savannah woody cover is an important biophysical parameter which directly affects important processes of savannah ecosystems. It influences herbaceous biomass, hydrological cycles, soil carbon and nutrient cycling (Rietkerk *et al.*, 1997; Scholes and Archer, 1997; Hudak *et al.* 2003; Archibald *et al.*, 2009). Growing recognition of the importance of the structural component of Savannahs landscapes diversity has highlighted the demand to understand the spatial distribution and temporal dynamics of woody vegetation density and crown canopy cover (Levick and Rogers, 2008).

Researchers have shown that woody vegetation density and crown canopy cover distribution are affected by several drivers that alter the woody cover and density of savannah systems (Sankaran *et al.*, 2005). Fire and elephants drivers are considered to have the potential ability to severely alter the heterogeneity and biodiversity of savannah woody cover (Trollope *et al.*, 1998). Therefore, information on the distribution and spatial variations in woody vegetation density and crown canopy cover in savannah ecology is critical for making timely assessments of savannah ecosystem (Coops and Culvenor 2000). Hence, an adequate spatially-consistent monitoring and assessment of woody vegetation density and crown canopy cover of this key parameter is of particular importance for researchers, decision makers and stakeholders.

Since savannah ecosystems are known to have a wide range of highly specialized structural woody cover (Solbrig *et al.*, 1996), with far more layering within the savannah structure, they offer a challenge of an altogether different magnitude for new remote sensing techniques (Nagendra, 2001). Due in part to this challenging complexity, the use of passive and active remote sensing in tropical grasslands has largely been limited to studies of fire in savannah systems (i.e., Alleaume, 2005; Roy *et al.*, 2005a; 2005b); additionally, most conducted studies of temporal change in savannahs have employed the use of satellite images or black and white aerial photography. Whilst these methods are useful for investigating changes in woody cover over time, they are not able to portray the three-dimensional structure of vegetation cover.

With regard to active systems, the first one is the RADAR (RADio Detection And Ranging) system, which has shown great potential for monitoring and mapping a wide range of surface and vegetation characteristics in a synoptic, continuous fashion (Kasischke, *et al.*, 1997). The first attempt to address this was made by Harrel *et al.* (1997), which resulted in quantitative vegetation mapping, which referred to the relationship of the intensity channels of a polarimetric SAR to biophysical variables, particularly the cross-polarized L-Band channel, which proved to be useful. Most of these studies that used advance polarimetric algorithms focused on different cover types of forests (i.e., Thiel *et al.* 2007) or land-cover classification (i.e., Lee *et al.*, 1994); and few use the polarimetric parameters for quantitative assessments of structural attributes (i.e., Garestier *et al.*, 2009). The study revealed that the polarimetric anisotropy parameter in L- and P-bands is found to be linearly correlated with the forest height.

Few studies have used SAR in the savannah environment. One that has is the sequence of intensive studies in the Australian savannah woodland and open forest environment of Queensland by Lucas *et al.* (2004, 2006a, 2006b, 2006c and 2009), which related SAR polarimetric intensity channels to vegetation parameters. These investigations have revealed that the C-HV channel was suitable for mapping leaf and small branch biomass; and the L-HV and L-HH channel were sensitive to the trunk and large branch biomass (Lucas *et al.*, 2004).

Moreover, Lucas *et al.* (2006c) showed that the L-HH channel interacted primarily with the trunks and secondarily with volume elements (mainly large branches). Significant contribution of the backscattering signal in the L-HV channel arose from all volume components of the model commensurately (branches, leaves, and understory vegetation). Ground-trunk and the direct ground scattering contributed less compared to L-HH but more compared to L-HV. A result from the previous studies, shows that L-band (especially HH- and HV-polarisation) operates as a complementary component in mapping vegetation structure since it provides information at later growth stages due to ground-trunk interactions (Lucas *et al.*, 2006c). The above mentioned study dealt with RADAR airborne imagery. A recent study by Lucas *et al.* (2009) used *Advanced Land Observing Satellite (ALOS) Phased-Array type L-band SAR (PALSAR)* for biomass mapping in open forests. This study achieved  $R^2$  of 0.48 compared to field data for a large scale biomass map of the whole Queensland area, which enabled important insights into the backscattering behaviour of open forests. Moreover, other recent studies by Collins *et al.* (2009) in the Northern Territory of Australia showed possible potential with regards to vegetation structure assessments in open forests. It mapped the Wildman

River Reserve with  $R^2$  of 0.92 using the SAR backscatter which was strongly related to the biomass of the vegetation.

Light detection and ranging (LiDAR) technology is another active remote sensing technique that uses precise spatial location and the two way travel time of laser light pulses to produce a highly accurate representation of the targeted ground area with a capability of simultaneously mapping the earth surface and overlying features (Means *et al.*, 2000).

Today, LiDAR technology, which until recently has been limited to airborne systems, is the most promising sensor for remote sensing estimation of forest attributes (Lefsky *et al.*, 1999a,b; Lefsky *et al.*, 2002; Drake *et al.*, 2003a;2003b; Patenaude *et al.*, 2004). Studies have proved that aircraft LiDAR has the capability to measure forest height with high accuracy and that vegetation structure, biomass and other vegetation canopy attributes can be estimated (Lefsky *et al.*, 1999a, b; Nelson *et al.*, 1997; Means *et al.*, 2000). The success of airborne LiDAR in vegetation environments such as VCL (Vegetation Canopy LiDAR) and LVIS (Laser Vegetation Imaging Sensor) has ultimately led to the implementation of a spaceborne LiDAR mission for vegetation studies (Blair *et al.*, 1999; Hese *et al.*, 2005). Satellite spaceborne, namely, the ICESat-GLAS LiDAR waveforms has been used successfully in defining many forest attributes such as canopy height and structure (Harding *et al.*, 2001; Goetz *et al.*, 2007). GLAS has been an active area of research in recent years, specifically in temperate and boreal forests (i.e., Ranson *et al.*, 2004b; Lefsky *et al.*, 2005a; Lefsky *et al.*, 2007; Duong *et al.*, 2008; Neuenschwander *et al.*, 2008; Rosette *et al.*, 2008c; Sun *et al.*, 2008; Pang *et al.*,

2008; Chen, 2010b; Duncanson *et al.*, 2010), but has been insufficiently explored for ecological research in savannah ecosystems (Levick and Rogers, 2008). The previous chapter showed the results of extracting savannah vegetation structure using GLAS LiDAR full waveform parameters, compared it with discrete return airborne LiDAR data and evaluated the outcomes with field measurements.

In this chapter, the author aims to provide more complete assessment of woody cover estimations from GLAS waveform parameters by comparing them with woody vegetation estimates using ALOS PALSAR backscatter data. The rationale of this approach builds on the potential results obtained from Chapter 4, which evaluated estimating vegetation structure properties such as vegetation heights, stand density and percent crown canopy cover from GLAS waveform parameters.

Studies on RADAR data show consensus on its sensitivity to woody structure, for example, the work of Mitchard *et al.* (2009). In this work, a consistent baseline was created which detected woody biomass across savannahs and woodlands of Africa. Moreover, it has been proved that different RADAR wavelengths interact with different vegetation elements and depths (Lucas *et al.*, 2004). From this approach, this feature exploited here in this work to create direct relationship between woody cover estimated from GLAS waveform parameters and RADAR backscatter over savannah vegetation systems. Therefore, the goal of this research is to evaluate the use of ICESat-GLAS LiDAR data for estimating savannah woody cover in Kruger National Park in South Africa and evaluate the results using the L-band backscatter intensity (especially HH- and HV-polarization) in ALOS PALSAR.

## 5.2 Methodology

### 5.2.1 Study site and data

#### Study site

The study area is Kruger National Park located in South Africa. It is one of the largest protected areas in Africa (19,485 km<sup>2</sup>). Various habitats and ecological regions exist within the boundary of the Kruger, with at least 16 recognized ‘ecozones’; each one characterized by specific vegetation, geology, soils, rainfall rate, and temperature. The KNP has been chosen as a study site because it is the largest and one of the most important national parks in the world, and it presents a good test site because of the diversity of its ecosystems and, most importantly, the coverage of ICESat-GLAS (Figure 5.1).

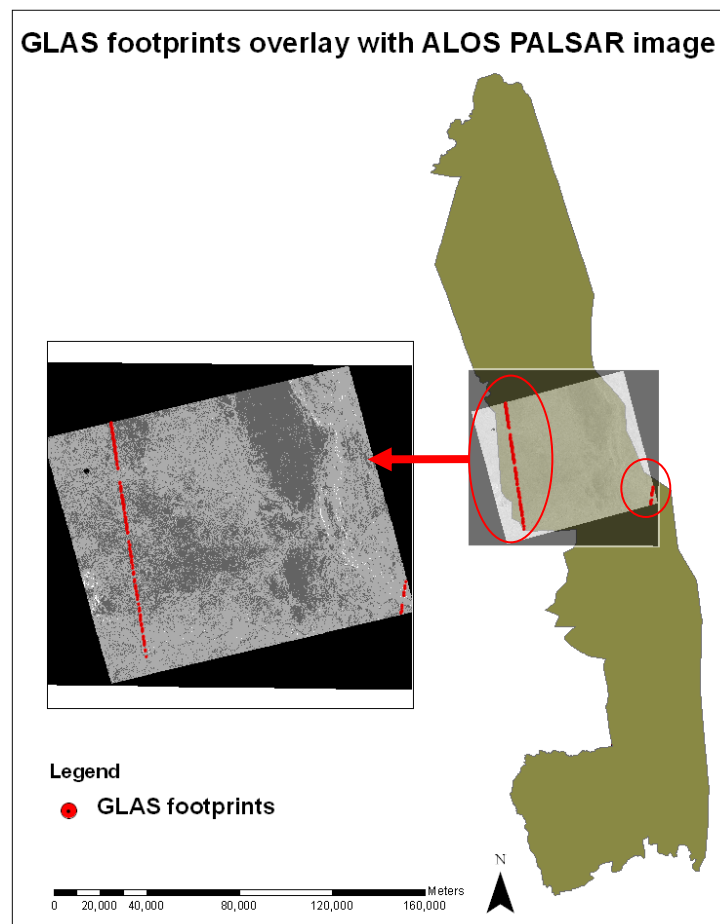


Figure 5.1: The study sites of the Kruger National Park in South Africa and the location of the GLAS footprints which overlapped with ALOS PALSAR data.

## GLAS data

Two data products of release 29 GLAS were used in this study:

- Level 1A Global Altimetry data (GLA01); and
- Level 2 Global Land Surface Altimetry data (GLA14)

GLA01 is a level 1A data product which contains granules that have raw LiDAR waveform in digitizer counts which are afterwards converted to volts (by users). GLA01 contains the transmitted and received echo waveforms. This product has variables such as the filter threshold value for signal detection in digitizer counts, laser transmit energy, received energy from all signal above threshold, sampled transmit pulse waveform, 4ns background mean value and standard deviation (Brenner *et al.*, 2003). GLA14 is a level 2 data which contains sensor position and pointing information as well as calculated footprint position, size and shape, and land surface elevation. Transmit pulse and recorded waveforms are represented with characteristic shape parameters only. The recorded waveform is decomposed into a series of Gaussian peaks, as described in Zwally *et al.* (2002) and Brenner *et al.* (2003)

$$w(t) = \varepsilon + \sum_{m=1}^{Np} Am \times e^{-\frac{(t - tm)^2}{2\sigma^2m}} \quad (5.1)$$

Where  $w(t)$  = the amplitude of the waveform at time  $t$ ,  $Np$  = number of peaks in the waveform,  $Am$  = amplitude of the  $m$  the peak,  $\varepsilon$  = bias (noise level) of the waveform,  $tm$  = position of  $m$  the peak at time  $t$ ,  $\sigma m$  = standard deviation of the  $m$  the peak (Brenner *et al.*, 2003). This equation is solved with non-linear least squares fitting to a maximum number of six peaks (Brenner *et al.*, 2003).

### ALOS PALSAR data

For parts of the Kruger National Park, imagery of ALOS PALSAR in Fine Beam Double Mode (FBD) was acquired for June 2007 and June 2008 through ALOS Data European Node (ADEN) provided by the Japanese Aerospace Exploration Agency (JAXA) and the European Space Agency (ESA). The HH and HV polarized images were received in single look complex (SLC) format and slant range geometry (processing level 1.1) with an off-nadir angle of 34.3 degree and a pixel-spacing of 9.4 m in range and 3.2 m in azimuth direction, respectively. The swath width approximated 70k m.

### Woody cover map for the Kruger National Park

A woody cover map for the entire park, derived from remote sensing data, was produced by Bucini *et al.* (2009). Based on the Akaike information criterion, a combination of Japanese Earth Resources Satellite-1 (JERS-1) and Landsat imagery has been used and the result ended up as a woody cover map with a spatial resolution of 90m with  $R^2$  of 0.61 and an RMSE of 8.1%.

## **5.2.2. Data processing**

### **5.2.2.1 GLAS data processing**

Following the GLAS waveforms processing steps in Chapter 3 to extract the vegetation parameters of interest, two main steps were done:

#### Extracting vegetation height estimates from both GLA01 and GLA14 products

GLA14 were pre-processed using software packages downloaded from NASA website (<http://nsidc.org/data/icesat/tools.html>) to produce usable data, including unique number, shot number, shot time, number of samples; and then the

IDLreadGLAS software was used to process and explore the uncompressed GLA01 full waveform values in volts (Seidel, 2005). Raw waveforms have ambient system noise at the beginning and the end of the waveform signal (Lefsky *et al*, 2005). Therefore, the real signal of the waveform was identified by thresholding the raw waveforms. In this work, the threshold value for each raw waveform was individually determined to the mean background noise value estimated in the GLA01 product (GLAS product variable: d\_4nsBgMean) plus 4 times the standard deviation of the background noise (GLAS product variable: d\_4nsBgSDEV) (Lefsky *et al*, 2007). This helps in estimating the highest and lowest intercepted surfaces within a footprint which is referred to as ‘waveform extent’ (Lefsky *et al.*, 2005). Considering the work of Carabajal and Harding (2001), the distance between ‘signal begin’ and the location within the waveform corresponding to the ground is assumed to be the maximum canopy height.

The shape of the waveform varies according to the characteristics of intercepted surfaces and their spatial locations, taking into account that the laser energy diminishes towards the footprint margins (Carabajal and Harding, 2001). However, in open and sparsely vegetated areas, the majority of signal returns may be anticipated from the surface ground creating the greatest amplitude peak within the returned waveform; while, in denser canopies, the laser energy penetration becomes more difficult and results in a lower amplitude peak (Harding *et al.*, 2001). GLAS products provide parameters that contain a Gaussian decomposition, particularly in GLA14. The ICESat-GLAS visualizer software iteratively fits six Gaussian curves to the waveform. This was used to compare Gaussian parameters, so it is assumed that the larger amplitude of any fitted six Gaussian parameters corresponds to the

ground, and the difference in elevation between the centroid of this Gaussian and the beginning of the waveform signal is the estimated maximum vegetation height (Rosette, 2009). This equation was used to estimate maximum canopy height using the Gaussian decomposition method of GLA14 parameters:

$$H_{GLA14\ max} = H_s - GP \quad (5.2)$$

Where  $H_{GLA14\ max}$  is the maximum canopy height estimated from GLAS data (m),  $H_s$  = the signal start obtained from GLA14 product (m),  $GP$  = ground peak (m) (the centroid of the greatest amplitude of Gaussian decomposition peak).

The GLA01 product gives the mean and standard deviation of background noise values in the waveform. Hence, using the mean plus four times standard deviation as a threshold above the noise level, the real signal beginning and ending for each waveform were located. Since different waveforms have different amplitude intensities, it is inconvenient to use one single threshold noise for all the waveforms.

Ground peak was determined where greatest sufficient laser energy is reflected from the ground (Lefsky *et al.*, 2005). As a consequence, the estimated maximum canopy height using the GLA01 parameters is given in this equation:

$$H_{GLA01\ max} = H_{SB} - GP \quad (5.3)$$

Where  $H_{GLA01\ max}$  is the maximum canopy height estimated from GLA01 data (m),  $H_{SB}$  = the signal start that above the threshold noise level obtained from GLA01 waveform (m),  $GP$  = ground peak (m) (the greatest amplitude peak in GLA01 waveforms).

### Extracting parameters of interest for savannah woody cover estimates from GLAS waveforms

Beside the predicted maximum canopy heights from GLAS products, useful parameters of a signal waveform have been also extracted from GLA01 full waveforms. They are the total waveform energy (*eEcho*) calculated by summing all the return energy from signal beginning to ending; the canopy energy return (*eCanopy*); the ground energy return (*eGround*); and the most important parameter which this study was conducted for: the GLAS energy ratio (*rGLAS*) (canopy energy to ground energy), which has been proved in the work of Neuenschwander *et al.* (2008) to be a good indicator of the amount of woody cover within the GLAS footprint. The canopy return ratio (*rCanopy*) which calculated as canopy return energy (*eCanopy*) divided by the total return waveform energy (*eEcho*) which measure crown canopy cover (Harding and Garabajal, 2005), the ground return ratio (*rGround*) which calculated as the ground return energy (*eGround*) divided by canopy return energy (*eCanopy*) which refers to the degree of canopy closure (Darke *et al.*, 2002). Waveforms that were greatly affected by cloud and system noise were discarded before the extraction of the above waveform parameters.

#### **5.2.2.2 ALOS PALSAR data processing**

The processing of SAR data were conducted in the Institute of Geography at the University of Jena using GAMMA SAR processing software. The images were undertaken in a multi-looking of 1 look in range and 4 looks in azimuth direction, resulting in ground range pixel-spacing of approximately 14m and 13m, respectively; and then resampled to a resolution of 15m using bilinear interpolation. With the Differential Interferometry and Geocoding package (DIFF and GEO); the

images were co-registered using a cross-correlation-algorithm and a signal to noise ratio (SNR) of 10, resulting in a discrepancy of less than 1 pixel.

For geocoding, a 20 meter resolution Digital Elevation Model (DEM) of Kruger National Park, provided by South African National Space Agency (SANSA), was re-sampled to 15 m using bilinear interpolation. From this DEM a SAR backscatter image was simulated and transferred to slant range geometry and a geocoding look up table was created using orbit parameters. A refinement of this look up table by cross-correlating the simulated with the original images was tried, but due to the faint relief no accurate matching points were found, and lower SNR values resulted in huge geometric distortions, so the geocoding is relying on orbit parameters alone, resulting in a non-quantified error. This processing did not involve a terrain correction as well, so that SAR inherent features like layover or foreshortening are not corrected, but, with regard to the flat topography terrain, correction should not play an important role here either.

### **Woody cover map data**

The GLA14 centre point geo-location data were buffered by 35 m to account for the ~70 m GLAS footprint diameter. GLAS polygons were overlaid on the woody cover map, which derived from (JERS-1) and Landsat imagery, and only those shots that were defined as fully within the ALOS PALSAR and fell within the woody map were used in this study.

## 5.3 Results and discussion

### 5.3.1 Comparison of maximum canopy heights derived from GLA14 and GLA01 products

Finding the ground peak is essential to extract the other waveforms' parameters. Two independent methods have been employed to identify ground peaks for each GLA14 and GLA01 waveform. First, due to the nature of savannah environment, which considerably sparse and has more open vegetation canopies, the majority of returns may be anticipated from the ground so forming the greatest amplitude peak within the returned waveform (Rossetti *et al.*, 2010). The second method is the use of the GLAS IDL reader library visualization program for allowing interactive and manual identification of ground peaks. For the 162 GLAS footprints, the correlation between maximum canopy heights derived from GLA14 and GLA01 was  $r = 0.93$ , RMSE=2.23m and (p-value < 0.001 statistically significant) (Figure 5.2). This result indicates the potential of estimating maximum canopy height directly from GLAS products using characteristics of the waveform structure.

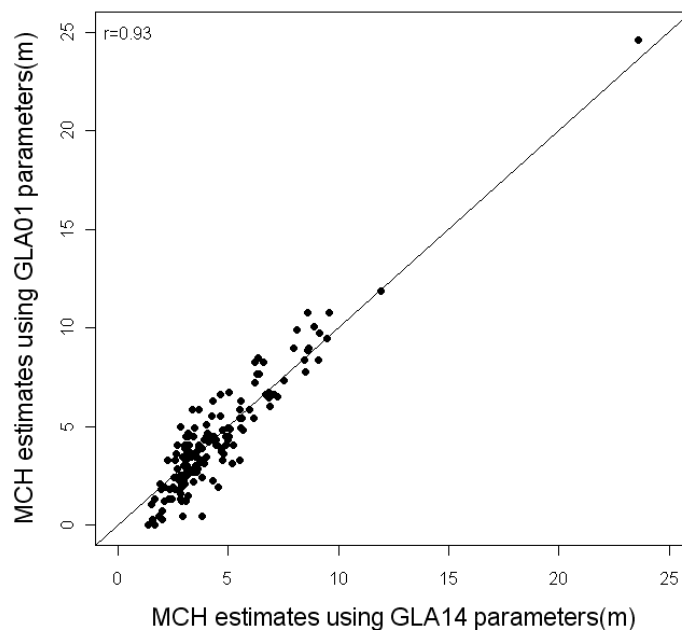


Figure 5.2: Relationship between MCH estimates using GLA01 waveform and MCH estimates using GLA14 parameters; most points for both estimated MCH of GLAS products fall close to the 1:1 line.

### 5.3.2 Estimation of woody cover from GLAS footprints

Based on the work of Lefsky *et al.* (2005a) and Neuenschwander *et al.* (2008), the model developed to estimate woody cover employed four GLAS waveform parameters selected by stepwise regression in R statistical program software. The result show  $R^2$  value of 0.60 and RMSE value of 4.25m yielding this equation:

$$Pwc = -19.633 + 0.127XrCG + 97.281XCE.TE + 11.358XrGC + 0.038XH^2 \quad (5.4)$$

Coefficients are statistically significant p-value < 0.001, intercept significant p-value > 0.01.

Where  $Pwc$  is the percent woody cover within the GLAS footprint;  $XrCG$  is the GLAS energy ratio ( $rGLAS$ ) (canopy energy to ground energy);  $XCE.TE$  is the canopy return ratio ( $rCanopy$ );  $XrGC$  is the ground return ratio ( $rGround$ ); and  $H^2$  is the maximum canopy heights estimated from GLAS waveforms.

As shown in Figure 5.3, by applying equation (5.4) to predict GLAS woody cover and comparing it to the percent woody cover map from (Bucini *et al.*, 2010), it shows a significant correlation  $r$  of 0.71; RMSE = 10.2% and (p-value < 0.001 statistically significant). This result indicates the potential of GLAS waveform indices to apply large LiDAR footprint estimation of woody cover.

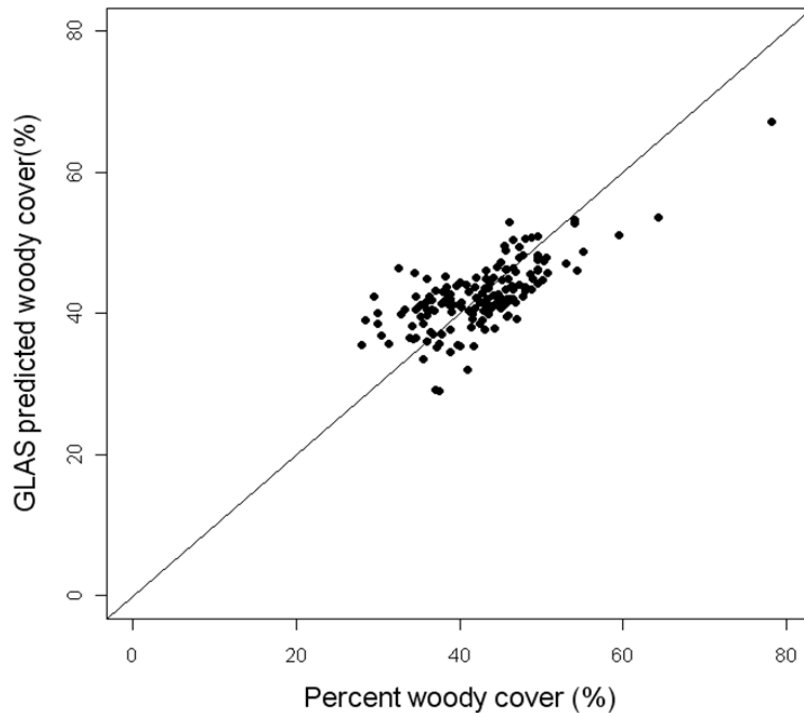


Figure 5.3: Estimated of crown canopy cover from GLAS waveform compared with woody cover percent extracted from woody cover map (Bucini *et al.*, 2010). A strong correlation is found, supporting the ability of using GLAS parameters to estimate woody cover.

A regression analysis of the relationship between maximum canopy heights is derived from GLAS waveforms and woody cover estimated from GLAS waveform indices and those extracted from the woody cover map of Bucini *et al.* (2010). The results (Figure 5.4) show that the estimated woody vegetation from GLAS waveforms has significant relation to the MCH estimates from GLAS waveforms. This can be expressed with coefficient of determination for estimated woody vegetation from GLAS waveforms metrics and those extracted from Bucini *et al.* (2010) map with predicted GLAS MCH. This results in  $R^2$  of 0.69 and 0.38 respectively.

These results suggest that there are height correlations for the tallest species with the increase of woody cover percent in each GLAS footprint from both datasets of predicted woody cover.

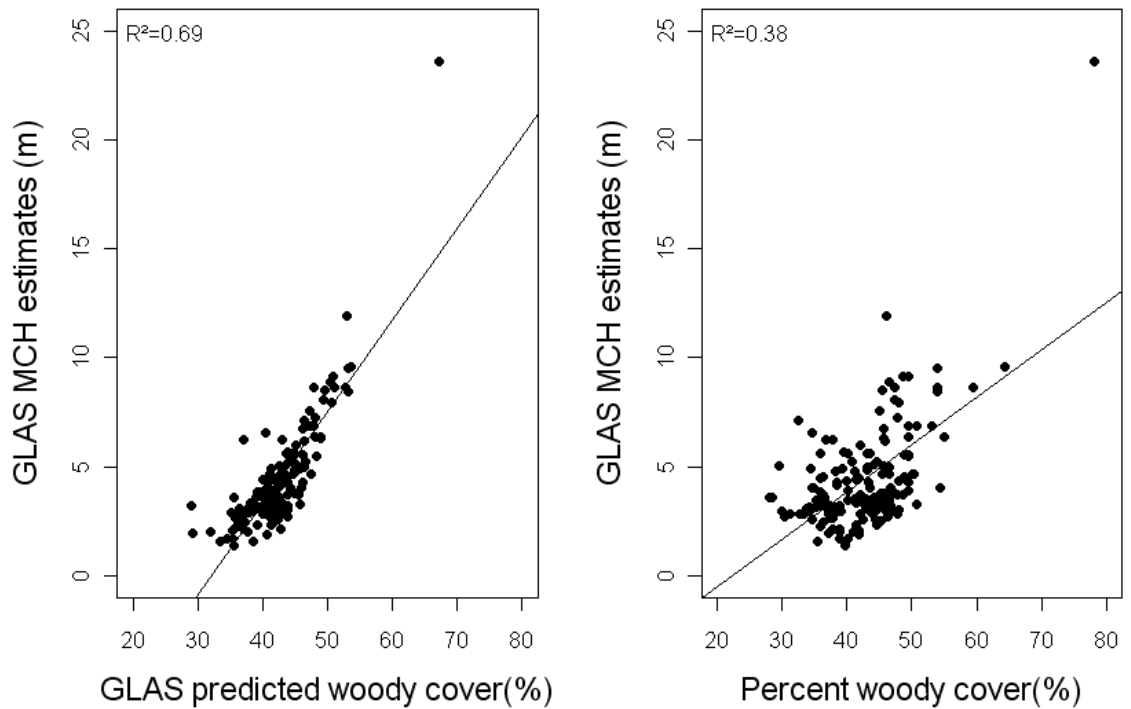


Figure 5.4: Comparison between predicted MCH from GLAS waveform plotted against the percent woody cover interpolated from KNP woody cover map (right graph) and the predicted woody cover from GLAS waveform for each footprint (left graph). The results show significant correlation in both plots, which indicates a strong relationship between increasing the MCH and the woody cover in each GLAS footprint.

### 5.3.3 Comparison of GLAS estimations of woody cover and MCH with RADAR backscatter from ALOS PALSAR

As has been proved in several studies, radar backscatter is correlated not only with total biomass, but also with the various components of biomass such as branch biomass, needle biomass, and bole biomass (Kasischke *et al.*, 1997), or with other physical tree-stand characteristics such as tree height and basal area (Dobson, 2009). Hence, a calibration of the L-band backscatter intensity (HH- and HV-polarization) in ALOS PALSAR against the predicted GLAS maximum canopy heights, using Pearson's correlation coefficient for the 162 plots, resulted in significant correlation between L- band, particularly in HH polarization and the GLAS derived heights with  $r = 0.72$  and  $p$ -value  $< 0.001$  statistically significant. It can be seen from Figure 5.5 that L- band backscatter increases intensity for both HH- and HV-polarization when increasing the vegetation heights.

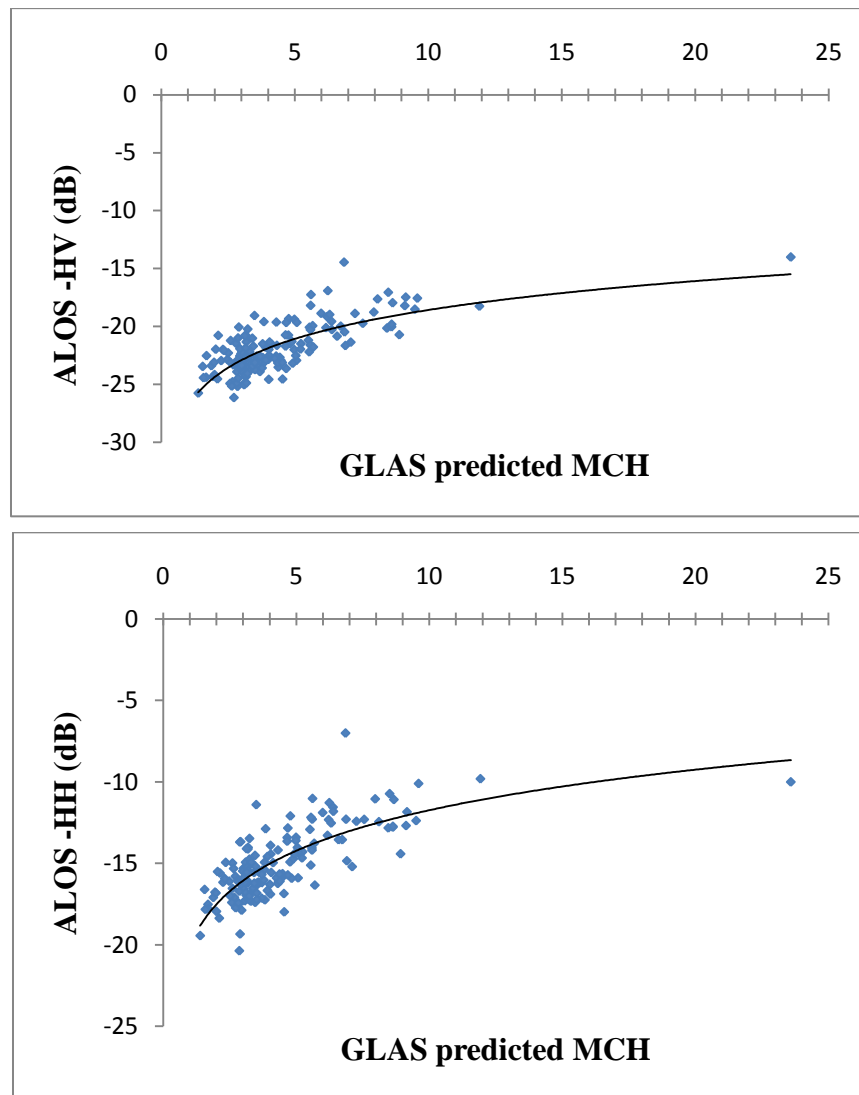


Figure 5.5: Comparison between ALOS L-band backscatter (acquired for June 2007 and June 2008 respectively) in HH and HV polarization and predicted MCH from GLAS waveforms. L-band in HH has the strongest relationship with GLAS derived MCH.

The correlation was also analyzed based on predicted woody cover percent from GLAS waveforms. The regression analysis for the radar backscatter and predicted woody cover percent from GLAS waveforms metrics results in  $R^2 = 0.25$  and  $0.23$  for HH- and HV L-band respectively. However, the correlation relationship shows that HH L-band has the highest correlation value of  $r = 0.48$  and (p-value  $< 0.05$  statistically significant) compared with HV L-band of  $r = 0.44$  and (p-value  $< 0.05$  statistically significant) with the predicted woody cover from GLAS waveforms

metrics. As can be seen from Figure 5.6 the RADAR backscatter increases when woody cover increased in each GLAS footprint.

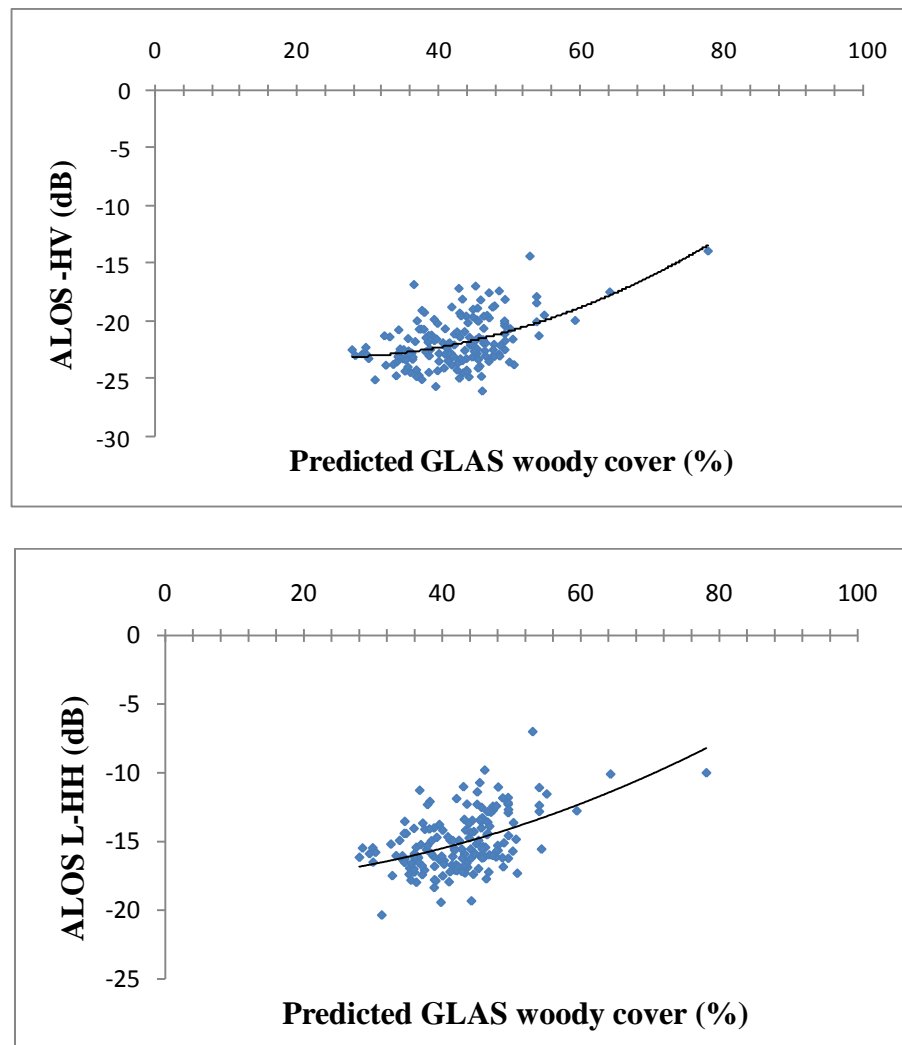


Figure 5.6: ALOS L-band backscatter in HH and HV polarization (acquired for June 2007 and June 2008 respectively) plotted against predicted woody cover from GLAS footprints. This comparison shows also a good correlation between predicted woody cover from GLAS waveforms and backscatter intensity in L-band HH. This result shows the potential ability to use GLAS waveform parameters for measuring the amount of woody cover for larger scales.

The GLAS energy ratio extracted from GLAS waveform parameters were compared to L- band backscatter acquired in 2007 and 2008. The results obtained show a significant linear correlation with L- band backscatter, especially with HH polarization  $R^2 = 0.47$  and  $0.51$  in 2007 and 2008 respectively (see Figures 5.7 and 5.8). This result emphasizes that GLAS energy ratio is a good indicator of the

amount of woody cover within the footprint, and it could be used to estimate the woody cover by combining it with other waveform parameters to give accurate estimations of woody cover within the GLAS footprints.

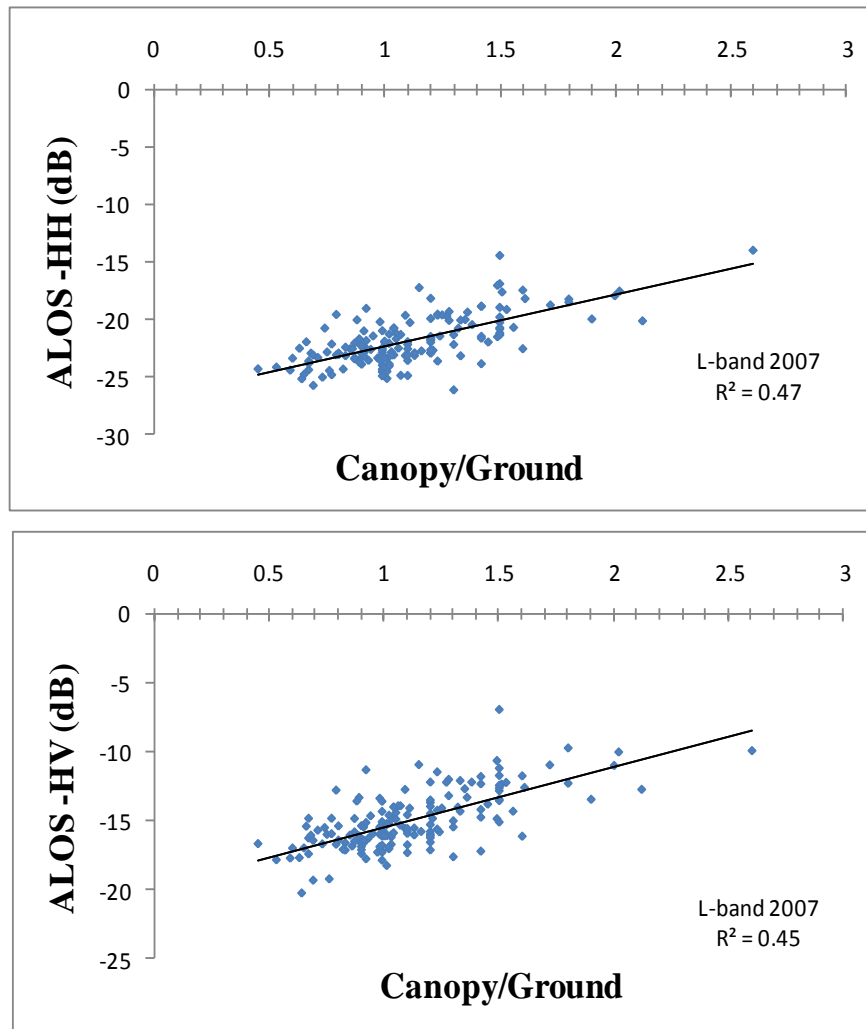


Figure 5.7: ALOS L-band backscatter in HH and HV polarization acquired in 2007. A regression analysis revealed the relationship between GLAS ratio as a good function indicator of woody cover in each GLAS footprint with HH and HV L-band backscatter intensity.

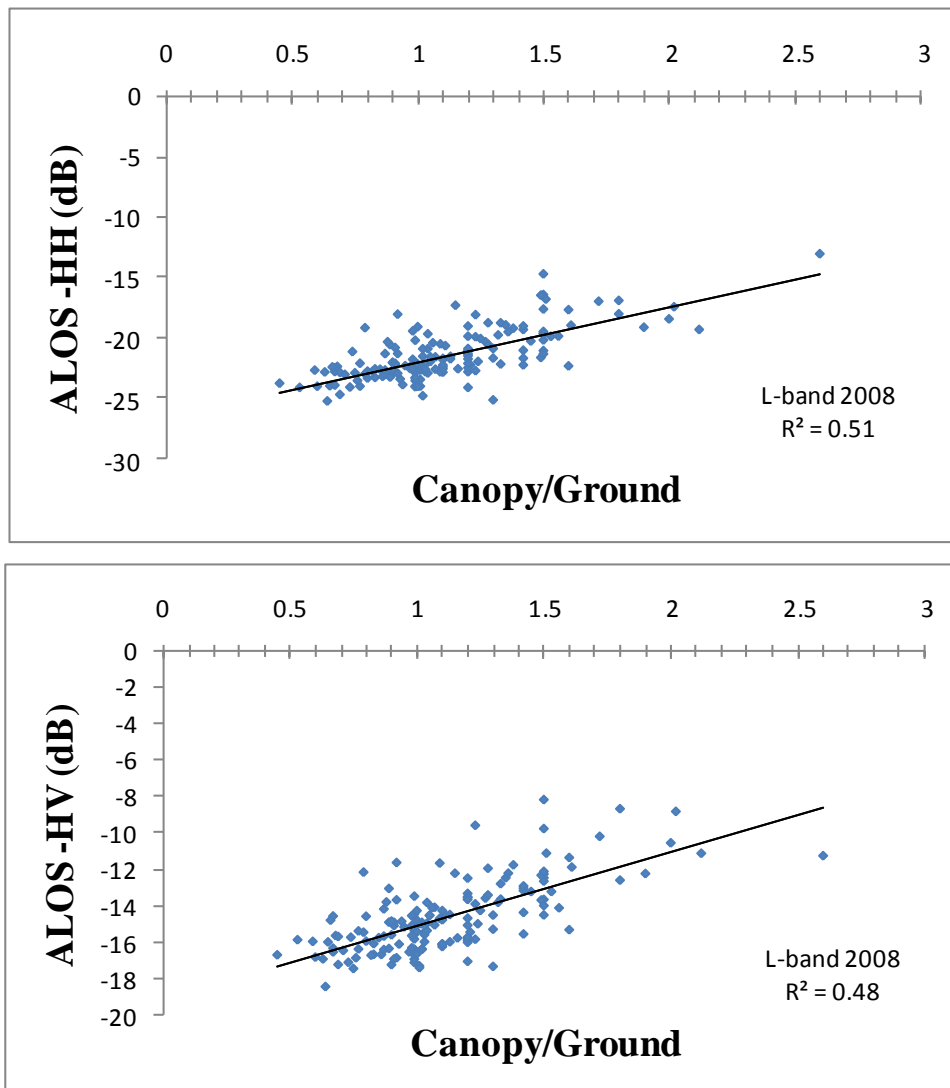


Figure 5.8: A regression analysis revealed the relationship between GLAS ratio as a good function indicator of woody cover in each GLAS footprint with HH and HV L-band backscatter intensity for ALOS PALSAR image acquired 2008.

Moreover, the correlation coefficient relationships show a significant correlation of  $r = 0.71$  and  $0.68$  between HH L-band backscatter and the GLAS ratio for acquired data in 2007 and 2008 and the correlation coefficients were statistically significant ( $p\text{-value} < 0.001$ ). However, also HV L-band backscatter shows a significant correlation of  $r = 0.66$  and  $0.69$  and ( $p\text{-value} < 0.001$  statistically significant) for both correlations with the GLAS ratio acquired image in 2007 and 2008. This again

emphasizes the possibility of extracting woody vegetation from GLAS waveform metrics without the need for ancillary data.

#### **5.4 Summary**

The extracting of the amount of woody vegetation cover is important for evaluation of habitat in any vegetated environmental system. Monitoring programmes which depend on traditional surveys systems do not sufficiently produce the necessary information for evaluating such vegetated ecosystems.

The spaceborne RADAR imagery showed great potential in different kinds of environment applications, specifically, vegetation mapping and associated structural vegetation parameters. However, most of these applications have been conducted in homogenous forests such as temperate, boreal and tropical regions. In addition, the spaceborne LiDAR technology, namely, the Geoscience Laser Altimeter System (GLAS), is the first LiDAR instrument for continuous global observation of the Earth. GLAS has proved capable of measuring forest height and other vegetation canopy attributes, specifically in temperate and boreal forests.

This chapter aimed to contribute to strengthening the link between the two spaceborne systems, LiDAR and RADAR, in order to exploit the full potential of these technologies in further applications of vegetation structure in this environment, which currently lacks studies on both spaceborne systems.

This chapter presented woody cover estimations obtained from GLAS waveform data. From these analyses, it has been possible to test the ability of the spaceborne LiDAR GLAS to estimate woody cover directly from the full GLAS waveforms.

Results show that estimates of woody cover from GLAS waveform parameters have good correlation with the percent woody cover interpolated from the KNP woody cover map produced by Bucini *et al.* (2010). On the other hand, there is a certain correlation between GLAS estimated woody cover and ALOS L-band HH backscatter, which presented promising results. This study provided the first step for future studies to combine the two satellite sensors (LiDAR and RADAR) for large scale estimation of vegetation woody cover. However, caution should be taken in further studies in terms of field sampling data, developed algorithms and other analysis methods.

# CHAPTER SIX

## SUMMARY OF RESULTS AND GENERAL DISCUSSION

### 6.1 Introduction

The purpose of this research is to act as a case study for examining the quality of waveform derived vegetation parameters obtained from the waveform processing procedure described in Chapter 3. Two separate comparisons between ICESat-GLAS data with airborne LiDAR data and spaceborne ALOS PALSAR RADAR data were studied in detail in Chapters 4 and 5, respectively. The results for each comparison showed the possibilities of using GLAS derived vegetation parameters directly for reliable, operational monitoring programmes in savannah ecosystems.

This chapter presents a summary of results obtained from using two methods - direct and statistical - of estimating vegetation structural parameters from GLAS waveforms; and also introduces a general discussion around evaluating the accuracy and the precision of estimating savannah vegetation parameters by comparing those estimates from different parts of the study site with two different datasets, i.e., airborne LiDAR data and ALOS PALSAR RADAR data.

### 6.2 Results of biophysical parameter estimation

A major challenge in savannah ecosystems studies is estimating vegetation structural parameters over large areas where field data collection is impractical and time-consuming. Therefore, it is crucial to identify alternative data sources that can provide economical means to obtain information on vegetation cover. Remote sensing provides this information by monitoring the vegetation biophysical parameters from space. Passive optical remote sensing systems provide two-

dimensional views of vegetation structure, which requires establishing statistical relationships for vegetation estimation using reflectance properties of vegetation cover.

However, active remote sensing systems, namely, airborne and spaceborne LiDAR remote sensing, offer the possibility of sampling the three-dimensional information of vegetation over large areas, which provides useful vegetation structural information using physical interactions with the surface objects. In addition, Radio Detection And Ranging (RADAR) airborne and spaceborne images showed great potential with regard to vegetation structure assessments.

This chapter present the results of utilizing three different active remote sensing datasets to estimate savannah biophysical vegetation parameters in two different study sites in Kruger National Park (KNP).

### **6.2.1 General results of utilizing spaceborne GLAS LiDAR system for estimating savannah vegetation structure**

Satellite LiDAR large footprint data offer a distinctive opportunity for characterizing vegetation vertical structure, height and biomass (Drake *et al.*, 2002; Lefsky *et al.*, 2005a). GLAS has provided data which enabled this study to be conducted to assess the potential of satellite LiDAR in estimating vegetation structural parameters in savannah ecosystems, and also in support for a future LiDAR sensor designed in this respect.

Two products of ICESat-GLAS data were investigated in this research: the GLA01 and the GLA14 products. The principle processing technique is based on Gaussian

decomposition concept. Two methods of utilizing this concept for processing GLAS waveforms have been applied to extract waveform parameters of interest.

Results in Chapter 4 have shown that maximum canopy height could be estimated using either parameters in GLA14 or GLA01 using Gaussian decomposition method. Figure 6.1 shows the application of the direct method on the entire GLAS footprints ( $n=1204$ ) located in the study area (KNP) after excluding the unusable GLAS waveforms. It shows a higher correlation, producing  $r$  of 0.92.

However, this parameter is affected by the roughness and slope of the terrain surface within an illuminated GLAS footprint (Duong, 2010). In the case of Savannah environment, a GLAS waveform from flat and homogenous terrain with low vegetation can be represented by a single Gaussian peak because the majority of returns may be anticipated from the ground forming the greatest amplitude peak within the returned waveform (Duncanson *et al.*, 2010), while returned energy from flat and homogeneously vegetated areas will represent bimodal returns of approximated two Gaussian peaks whereas the first represents the vegetation canopy and the second represents the underlying relief (Harding and Carajabal, 2005). The number of Gaussian peaks, that make up the returned waveform within a GLAS footprint, will increase with the number of intercepted elements within the footprint such as the trees, canopy gaps or fluctuations in relief (Duncanson *et al.*, 2010). Gaussian decomposition method used to extract information from GLAS waveforms which depending on fitting up to six Gaussian returns reflected from each element within the GLAS footprint. Due to the nature of Savannah environment which consider being open grasslands with sparse tree cover, the

returned waveform within the GLAS footprint over the selected study area has either a single Gaussian curve reflected from the ground surface over flat, low vegetated GLAS footprints or a bimodal Gaussian curve reflected from vegetation and ground surface over flat, heterogeneously vegetated GLAS footprints or a number of Gaussian curves reflected from mixed dense vegetation and complex terrain over moderate and slope GLAS footprint.

This study accounts for two factors which might affect the tree height estimation obtained from GLAS full waveform. The first factor is that the shape of the waveform varies according to the characteristics of intercepted surfaces and their spatial locations, taking into account the fact that the laser energy diminishes towards the footprint margins (Carabajal and Harding, 2001) and the second factor is that when the GLAS footprint is illuminated by the laser sensor, it increases the possibility that tall tree tops will be illuminated and hence tall trees can be detected (Lefsky *et al.*, 2002b). Taking into account these two approaches, vegetation height distributions were investigated visually from GLAS waveforms over the selected GLAS footprints and maximum canopy height was calculated from field measured data due to the great variation in the mean canopy height within the GLAS footprint (range from 8m to > 15m in some GLAS footprints).

The visual investigation of the GLA01 waveforms over the study area showed that the ground peak for some waveforms has larger width with less energy (Figure 6.2). Therefore, an alternative method for estimating vegetation height should be developed, such as a statistical method, to obtain more accurate estimates of vegetation canopy height, especially on sloped areas.

Two approaches were explored in the statistical method: the first one involves the subtraction of the terrain index (which is calculated from airborne LiDAR data) from the GLAS waveform extent. The second assumes that terrain index is considered to have the same effect as the waveform width ( $\sigma$ ) on sloped areas, thus the terrain index equals waveform width ( $\sigma$ ).

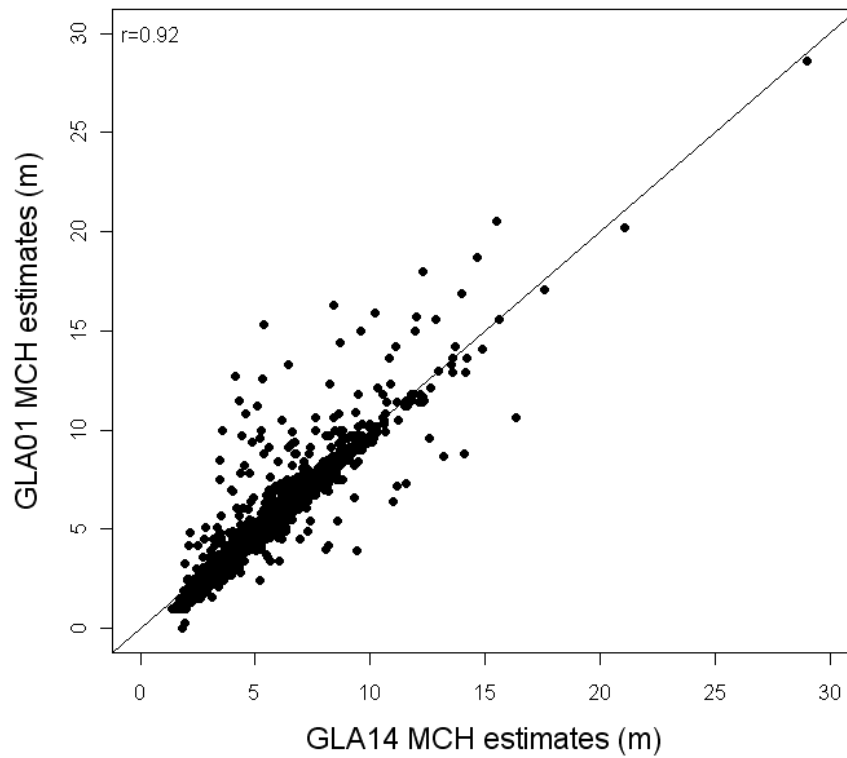


Figure 6.1: The scatterplot relationship of estimating MCH using both GLAS products (GLA01 and GLA14).

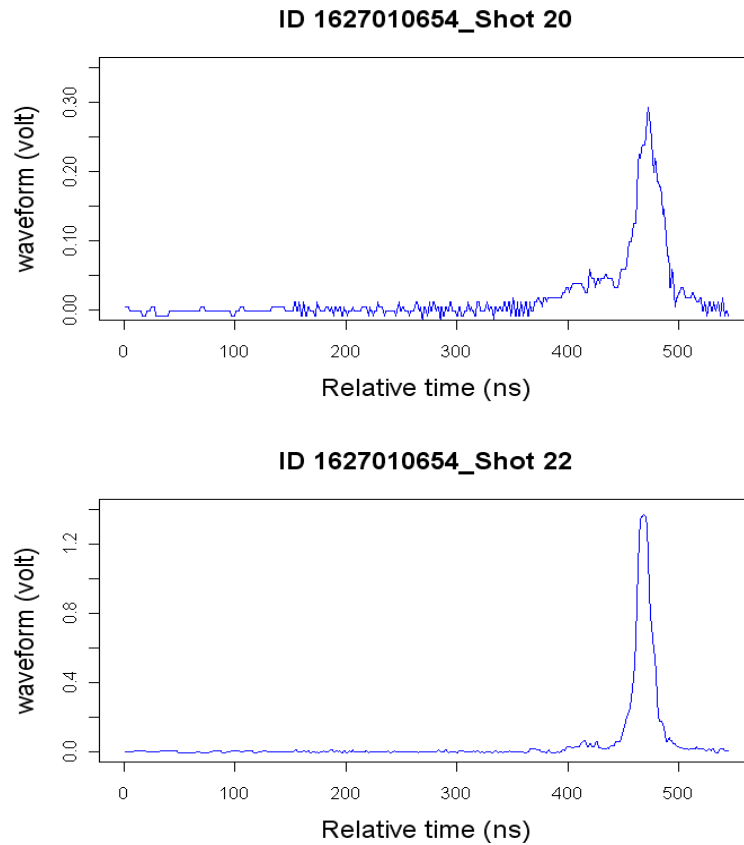


Figure 6.2: Examples of two GLAS waveforms on different topographical surfaces. The upper graph shows waveform over steep terrain, and the lower graph shows waveform on flat terrain.

The regression results (Table 6.1) show the possibility of developing a statistical method of estimating vegetation height from parameters provided within the GLAS products. These parameters were also compared with height estimates from field measurements of maximum canopy height.

Table 6.1: Regression model analysis results for height estimations with 6 coincident field measurements, coefficients significance p-values < 0.001, intercepts not statistically significant.

Model Type	Model	R <sup>2</sup>	RMSE	r
Terrain Index (g)/Liner regression	$H = 0.88 * (w - g) + 4.38$	0.66	17.0	0.90
Waveform Width (σ)/Liner regression	$H = 1.07 * (w - \sigma) + 1.31$	0.67	16.2	0.82
Terrain Index (g)/non Liner regression	$H = 1.53 * w - 0.87 * g$	0.78	14.5	0.88
Waveform Width (σ)/non Liner regression	$H = 2.73 * w - 1.01 * \sigma$	0.67	17.5	0.82

Figure 6.3 shows the relationships between maximum canopy height estimates using statistical regression models and field measurements of maximum canopy height.

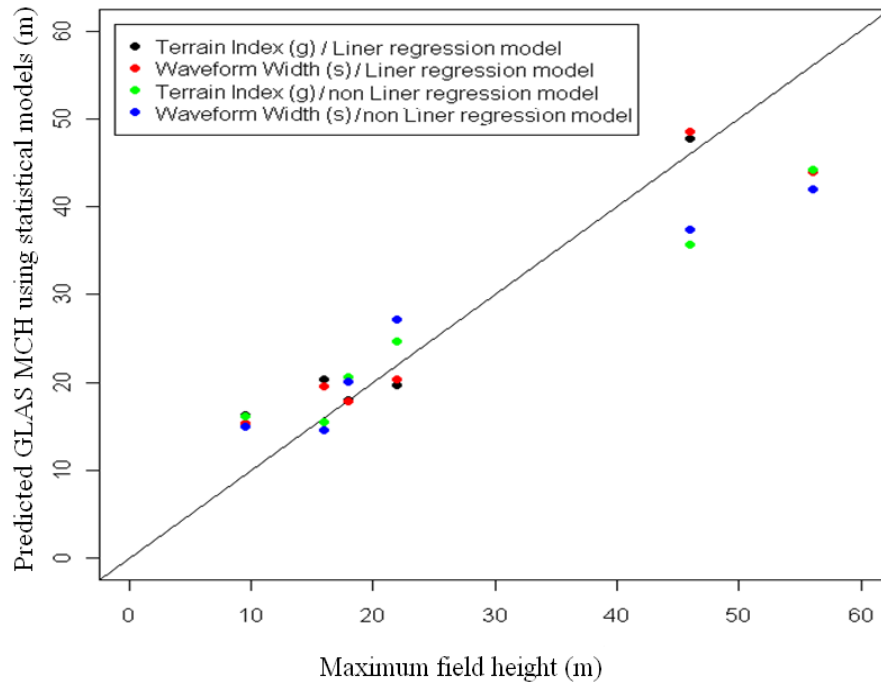


Figure 6.3: Relationships between maximum canopy height estimates using statistical regression models and field measurements of maximum canopy height.

The analysis of correlation coefficients relationships between measured field of maximum canopy heights and those predicted from using waveform metrics in the statistical methods shows a significant high correlation for using waveform width in both liner and non-liner regression. Additionally, there was not much difference in correlation relationships between predicted MCH using terrain index in linear and non-linear regression and those obtained from using waveform width. Thus, it can be seen that both factors are considered to be good indicators of the effect of terrain slope on the waveform extent; and hence there is the possibility of using waveform width to predict these effects on the GLAS waveform extent in order to obtain more accurate results of maximum canopy heights using only GLAS waveform metrics.

Approaches of estimating vegetation structural parameters such as stand density and woody cover using satellite LiDAR large footprint were also tested in this study. It was found that the stand density volume calculated from each GLAS footprint (n=38) using volume-related GLAS waveform parameters had a strong relationship with stand density volume extracted from LiDAR airborne data resulted in  $r = 0.95$  and RMSE of 0.98%. Moreover, woody cover can be estimated from GLAS waveform using the canopy ratio ( $r_{Canopy}$ ), which produced  $r$  value of 0.85 and RMSE of 11.8% with crown canopy cover estimates from field observations.

In order to evaluate the ability of satellite LiDAR large footprint to estimate woody cover, a validating case was undertaken in another site in KNP using ALOS PALSAR RADAR data. It was found that estimated woody cover from GLAS waveform parameters has good correlation with ALOS L-band HH backscatter. This study provided the first step for future studies to combine the two satellite sensors (LiDAR and RADAR) for large scale estimation of vegetation woody cover. To validate the GLAS ability of estimating woody cover, a comparison with the GLAS ratio (canopy energy to ground energy) as a good indicator of the amount of woody cover, with those interpolated from the KNP woody cover map produced by Bucini *et al.* (2010), gave a significant correlation relationship of  $r = 0.59$ , RMSE=6.67% and p-value < 0.001 statistically significant for the entire usable GLAS footprints located in KNP (n=1212) (see Figure 6.4). The GLAS ratio increases with the increasing of the percent woody cover.

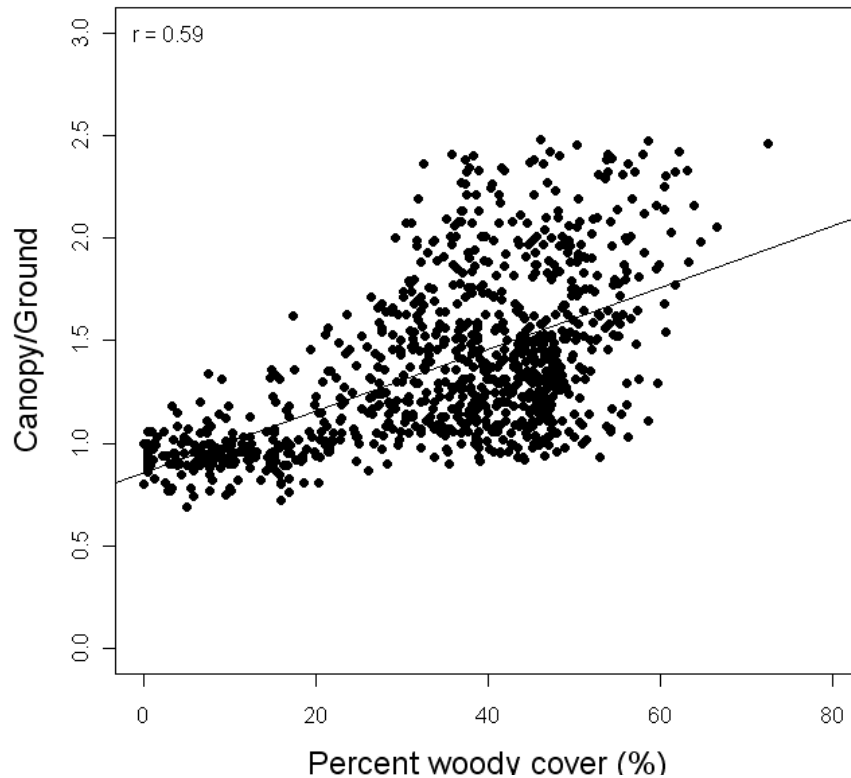


Figure 6.4: Estimate of crown canopy cover from GLAS waveform compared with woody cover percent extracted from woody cover map (Bucini *et al*, 2009). A significant correlation is found (p-value < 0.001), supporting the ability of using GLAS parameters to estimate woody cover.

### 6.2.2 Discussion of general results of utilizing spaceborne GLAS LiDAR system for estimating savannah vegetation structure

Savannahs are heterogeneous ecosystems that are characterized by two life forms: a continuous grass layer and scattered trees (Scholes and Archer, 1997). The spatial structure and composition of savannahs is controlled by several factors such as geological and climatologically factors at broad scale; and by topographical factors, rainfall and soil types at medium scales; and by herbivores and fire at finer scales (Pickett *et al.*, 2003). Therefore, savannahs are spatially heterogeneous and hence highly dynamic over time. This structural variability presents challenges to the management and conservation of savannah ecosystems.

Spaceborne LiDAR remote sensing techniques provide a mean of exploring vegetation changes over larger spatial areas in three-dimensional structures and

over time (Levick and Rogres, 2008). Accurate vegetation canopy characterization estimation from GLAS data will provide large scale estimates of biomass and also will help in providing elevation and roughness estimates for ground surface and relief. The table below (6.2) summaries the important GLAS parameters for a single waveform used for estimating savannah vegetation structural characteristics in this study.

Savannah vegetation heights calculated from both GLAS waveforms products (GLA01 and GLA14) showed high correlation  $r$  of 0.92. However, manual investigations of the GLAS waveform showed that both methods could misestimate the predicted heights. To reveal this, comparisons of estimated vegetation heights with the classified GLAS waveforms in respect to their terrain slopes showed that direct methods work well over flat terrain, while sloped areas need statistical methods to develop regression models that incorporate the effects of terrain slope on the GLAS waveform extent.

Table 6.2: Parameters of a single waveform used for estimating savannah vegetation structural characteristics at footprint-level.

<b>Parameters</b>	<b>Definition</b>	<b>Physical explanation for vegetation structure/ground surface</b>
Waveform begin and waveform end	The position where the beginning/ending of waveform crosses above/below a threshold value.	Height estimator of vegetation canopy
Waveform extent	The distance between beginning and ending of a waveform.	Maximum vegetation height
Waveform distance	The distance from the waveform beginning to the peak of the ground return or the last Gaussian peak.	Top vegetation canopy height
Number of Gaussian peaks	The number of Gaussian peaks obtained from Gaussian decomposition method.	Reflect the number of height levels corresponding to intercepted objects and earth terrain.
Return waveform energy	The received energy which usually is the area between beginning and ending of the waveform.	Describe the surface roughness in relative values.
Ground energy	The total intensity of the last mode or ground peak	Estimate the return energy from the ground
Canopy energy	The difference between return waveform energy and ground return energy	Estimate the return energy from the canopy
Ground return ratio	The ground returns energy divided by canopy return energy.	Estimate the degree of canopy closure.
Canopy return ratio	The canopy returns energy divided by return waveform energy.	Estimate canopy cover.
GLAS energy ratio	Canopy energy to ground energy	Estimates woody cover

Table 6.3 shows the regression analysis  $R^2$  results of using both direct and statistical methods in estimating MCH from GLAS waveform metrics and comparing the results with those MCH estimates from airborne LiDAR data and measured field MCH.

Table 6.3: Comparative analysis of the correlation coefficients of GLAS estimated heights with field measured heights and airborne LiDAR predicted heights.

Data-set	Direct methods				Statistical methods For sloped footprints	
	GLA01		GLA14		Terrain index (g)	Waveform width ( $\sigma$ )
	All GLAS footprints	Flat	All GLAS footprints	Flat		
<b>Air-borne LiDAR data Vs GLAS data</b>	n=38 $r = 0.68$ RMSE = 2.67m p-value < 0.001 (statistically significant)	n=18 $r = 0.89$ RMSE = 1.32m p-value < 0.001 (statistically significant)	n=38 $r = 0.71$ RMSE = 2.61m p-value < 0.001 (statistically significant)	n=18 $r = 0.86$ RMSE = 1.5m p-value < 0.001 (statistically significant)	-	-
<b>Field data Vs GLAS data</b>	n=23 $r = 0.24$ RMSE = 12.47m p-value > 0.05 (not statistically significant)	n=12 $r = 0.63$ RMSE = 2.47m p-value < 0.001 (statistically significant)	n=23 $r = 0.39$ RMSE = 8.47m p-value > 0.05 (not statistically significant)	n=12 $r = 0.68$ RMSE = 2.1m p-value < 0.001 (statistically significant)	n=6 $r = 0.88$ RMSE = 14.5m p-value < 0.001 (statistically significant)	n=6 $r = 0.82$ RMSE = 17.5m p-value < 0.001 (statistically significant)

As can be seen in the table above, direct methods could overestimate the vegetation heights, while more accurate results could be obtained when a classification for the GLAS waveforms is done. This can be better evaluated when a comparison of the GLAS estimated heights with measured field heights is done. This shows that the direct methods work well on the flat terrain while they produce underestimates of predicted values over sloped areas. Statistical methods using regression models that incorporated slope effects on the extracted heights showed a good correlation when compared with those measured heights.

The results of using statistical methods indicate that it could be possible to rely on the calculated parameters from GLAS waveform, such as waveform width ( $\sigma$ ), to

reduce the effects of terrain slope on the estimated heights without the need of ancillary data such as airborne LiDAR data to calculate the terrain index, which indicates for the slope effect on terrain.

The approach of estimating stand density using GLAS calculated parameters of canopy return energy (*eCanopy*), return waveform energy (*eEcho*), and the LiDAR height (*LH*) showed a good correlation with those extracted from LiDAR airborne data producing  $r$  value of 0.95 and RMSE of 0.98%. There was no collected field data to support these results. However, the initial results indicate the capability of calculating stand density from GLAS waveform metrics.

Woody cover estimates calculated depending on the Gaussian fitting concept were applied to GLAS waveform. Canopy returns ratio, which indicates for the amount of woody cover in each GLAS footprint, was calculated by dividing the canopy return energy (*eCanopy*) by return waveform energy (*eEcho*) (Harding and Carabajal, 2005). Results compared to those estimates of airborne LiDAR data showed a significant correlation of  $r = 0.94$ . The same comparison was done using field estimates of woody cover, which also presents a highly correlation  $r = 0.84$  with the GLAS ratio.

In order to evaluate this capability of GLAS waveform metrics in estimating woody cover, Spaceborne RADAR ALOS PALSAR data were used in another site of KNP to evaluate estimates of woody cover from GLAS waveform metrics with the L-band HH backscatter. This presents promising results and provides the first step for future study to combine the two satellite sensors (LiDAR and RADAR) for large

scale estimation of vegetation woody cover. However, with regards to further study, caution should be taken in terms of field sampling data, developed algorithms, and other analysis methods.

Table 6.4 shows the correlation coefficients  $r$  and RMSE for the comparison relationships between GLAS estimates woody cover with those estimates from airborne LiDAR, field and ALOS PALSAR data.

Table 6.4: Comparative analysis of the correlation coefficients of GLAS estimated woody cover with estimates from field, airborne LiDAR data, and ALOS PALSAR data.

	<b>Field data estimates of woody cover</b>	<b>Airborne LiDAR data of woody cover estimates</b>	<b>RADAR ALOS PALSAR L-band HH backscatter</b>
<b>GLAS ratio</b>	$r = 0.85$ RMSE = 11.80% p-value < 0.001 (statistically significant)	$r = 0.93$ RMSE = 10.04% p-value < 0.001 (statistically significant)	$r = 0.71$ RMSE = 12.04% p-value < 0.001 (statistically significant)

Again, these promising outcomes provide strong evidence of the ability to extract vegetation parameters of interest using GLAS waveform metrics.

Airborne and spaceborne LiDAR waveform metrics related to canopy structure were studied in this research. In other words, the power of using LiDAR in vegetation studies depends on its capability to measure vegetation height profiles as well as heights of earth surface within plots along transects and hence providing a profile of vertical vegetation structure. Thus, several waveform metrics can be generated by characterizing the vertical structure of the LiDAR profile. This has been tested in this study by extracting waveform metrics of interest from spaceborne LiDAR waveform metrics. While the power of using RADAR

technology in vegetation studies lies in its capability of measuring the energy fraction of each pulse that is backscattered from limbs, trunks, forest canopy and ground surface in particular, polarization orientations, which allow rich information about the three-dimensional vegetation structure, have shown the sensitivity of L-band backscattering coefficients to forest structural attributes such as wood volume and biomass (Ranson and Sun, 1994; Saatchi *et al.*, 2007). From this approach, this study used the backscattering coefficients of HH and HV L-band to compare with woody cover estimates from GLAS LiDAR waveform metrics. The results were promising and thus permit further applications of using regression analysis by relating measured cross-polarized backscatter coefficients to LiDAR measures of woody cover to derive more accurate results.

Overall, results of using spaceborne LiDAR GLAS waveform calculated parameters depending on Gaussian decomposition concept offer the potential for estimating vegetation parameters of interest over savannah landscape in KNP, and hence present a method that allows using the shape and the GLAS waveform metrics in broader application without the need of additional sources of data.

ICESat-GLAS acquired data globally between 2003 and 2009 and this provides an incomplete coverage of the earth and hence may help in characterized vegetation vertical structure at GLAS footprint level. However, several studies attempted to associate the sparse LiDAR footprints with the ancillary variables to produce patches that share ecological parameters (Lefsky *et al.*, 2005a; Boudreau *et al.*, 2008). A very recent study by Simard *et al.* (2011) proved that the possibility of using ICESat-GLAS to map forest vertical structure globally. The prediction map

shows a reasonable correspondence with field measurements from 66 FLUXNET sites and GLAS derived canopy height (RH100) from GLA14 product. The resulting map produces  $R^2 = 0.5$  and RMSE= 6.1m; or  $R^2 = 0.7$  and RMSE = 4.4m without 7 outliers). This map did not cover the selected study area for this research for comparison purpose. Future study should focus on driving map of canopy vegetation height for savannah ecosystems using only GLAS parameters.

ICESat-2, which is currently being studied by NASA and will be launched in 2015, will provide an important prospect for exploring changes in vegetation cover over time with the measuring of the three-dimensional structure of ground and vegetation surfaces. The footprint size For the ICESat-2, is a of approximately 50 m and a sampling rate of 50 Hz with 140 m long track spacing. This will improve mapping of forest heights and biomass as the areas between tracks are filled in and the spatial density of observations increases (Abdalati *et al.*, 2010).

In general, vegetation science community, particularly in KNP, will benefit from the technology and methods applied on GLAS parameters in order to establish a regime that enhancing monitoring of the structural changes in woody vegetation over large spatial areas and hence establish the role of disturbance factors in altering the heterogeneity of savannah systems. This would improve understanding of where structural changes occur spatially and how this could help clarify the differential effects of disturbance factors such as fire, aridity, and large herbivores on vegetation structure (Levick and Rogers, 2008). The next chapter presents a summary of the presented work in this thesis and discusses the limitations and suggestions for future work.

# CHAPTER SEVEN

## CONCLUSION AND FUTURE WORK

This study has developed and evaluated methods for retrieving biophysical vegetation parameters from GLAS waveforms over savannah environment. It also looked at how the extracted GLAS attributes of savannah vegetation can be well-matched with different datasets. This chapter gives an overview of the contributions of this research.

### 7.1 Conclusions

Growing recognition of the importance of the structural component of savannah landscapes diversity has highlighted the demand to understand the spatial distribution and temporal dynamics of woody plant structural diversity (Levick and Rogers, 2008).

Remote sensing techniques offer the opportunity to monitor, quantify and investigate large scale changes in vegetated landscapes. However, monitoring of savannah vegetation ecosystems has traditionally taken place through field surveys, satellite images, or black and white aerial photography analysis (Levick and Rogers, 2008). Active remote sensing such as LiDAR and RADAR has experienced limited use in savannah ecosystems. However, there are a few studies that have shown empirical evidence for the potential of LiDAR and RADAR in these complex heterogeneously vegetated systems. These studies utilized small-footprints LiDAR data for estimating vegetation structure parameters (i.e., Levick and Rogers, 2006; Wu *et al.*, 2009); or the use of RADAR, specifically airborne RADAR data to monitor and map woodland savannah, namely, the intensive studies in the

Australian savannah woodland and open forest environment of Queensland by Lucas *et al.* (2004, 2006a, 2006b, 2006c and 2009).

Despite the fact that the spaceborne LiDAR ICESat-GLAS was developed mainly for measuring ice sheet elevations and changes in elevation through time, it has been an active area of research in recent years, specifically in temperate and boreal forests; but has been insufficiently explored for ecological research in savannah ecosystems. For this purpose, the work in this thesis aimed to develop and validate methods for retrieving biophysical vegetation parameters from spaceborne LiDAR GLAS full waveforms over savannah environment.

Identifying the signal returned by savannah vegetation and extracting the biophysical parameters of interest from the full GLAS waveform metrics were successfully accomplished.

Two methods of retrieving savannah vegetation heights from GLAS data were explored based on Gaussian decomposition concept technique. As a result, it was found that the direct methods work well over flat areas, while over steep sloped areas with complex terrain, the ground peaks become broadened with less energy, which makes the identification of ground elevation difficult. Therefore, statistical methods were explored and developed over sloped areas, resulting in removing the effect of terrain slopes on the waveform extent.

However, the regression models that were developed in this research were tested in the selected study site of savannah landscape in KNP. To the best of the author

knowledge, no research regarding spaceborne LiDAR data has been conducted in savannah ecosystems to allow for comparative analysis for the results of this research with other studies.

From this approach, this work has compared the estimation of vegetation parameters derived from airborne LiDAR data and field measured vegetation heights with results from spaceborne GLAS LiDAR data, which show good correlations.

ALOS PALSAR RADAR data was used to evaluate results of estimating woody cover from GLAS LiDAR waveform parameters in another site of KNP. This comparison showed a significant correlation between GLAS estimated woody cover and ALOS L-band HH backscatter, which is considered a good indicator of woody cover amount in each GLAS footprint.

This thesis examined the ability of ICESat-GLAS to estimate vertical canopy structure over savannah landscape in order to characterize canopy structure over savannah vegetation landscapes in Kruger National Park in South Africa. The objectives of this thesis were: (i) to investigate the accuracy of level 2 altimetry products in comparison with reference data; (ii) to investigate GLAS footprint in details by conducting a field study to ascertain the potential of GLAS full waveforms for studying savannah structure in Kruger National Park (KNP); (iii) to develop and evaluate methods for deriving vegetation structure parameters from large GLAS footprints LiDAR waveforms, which accounts for the discrepancies in canopy height estimation; (iv) to evaluate estimated GLAS waveform parameters

using field measurements, airborne LiDAR data, and spaceborne Synthetic Aperture RADAR ALOS PALSAR data.

## **7.2 Contribution of this research**

Spaceborne satellite LiDAR data offer a means of providing a three-dimensional portrait of large scales of landscapes, which have previously only been inferred indirectly using optical remote sensing systems to analyse the vegetation reflectance properties.

Despite the fact that spaceborne ICESat-GLAS has been an active area of research recently regarding vegetation applications and has proved its ability to retrieve vegetation structural parameters specifically in temperate and boreal forests (i.e., Ranson *et al.*, 2004b; Lefsky *et al.*, 2005a; Chen, 2010b; Duncanson *et al.*, 2010), it has been insufficiently explored in savannah ecosystems.

For this purpose, a new contribution is required to test the ability of spaceborne GLAS data to retrieve vegetation parameters from these more structurally sparse and complex vegetated ecosystems and thus, provide assessment of woody plant structures to adopt a multi-scaled spatially explicit approach to monitor changes in the savannah landscapes over time for better management and conservation strategies.

In addition, this study showed that, over steep sloped areas, parameters extracted from GLAS waveform can be used to reduce the effect of terrain slopes using

statistical regression models without the need to use ancillary data such as airborne LiDAR data.

Moreover, this research has tested and explored the potential offered by two active satellite spaceborne systems for retrieving woody vegetation estimates for assessing biomass and also other vertical structural elements. The possibilities to use both spaceborne LiDAR and RADAR systems offer a good opportunity for better vegetation monitoring on savannah ecosystems where recent monitoring programmes do not sufficiently deliver the necessary information regarding savannah vegetation structural variations.

This work provides an important source of knowledge for the South Africa National Parks (SANParks) Authority and also provides the researchers and land managers with a powerful tool for utilizing the spaceborne LiDAR satellite ICESat-GLAS in an adequate spatially-consistent monitoring and assessment of mapping and monitoring woody vegetation structure of savannah landscapes which can contribute towards the biodiversity management goals of SANParks.

### **7.3 Research limitations and future work**

Despite the significant findings explored in this work, several limitations with this study are worth addressing with regards to vegetation structural estimates using the spaceborne LiDAR data. For instance, the lack of field measurements of biomass to be compared with those estimates from LiDAR and RADAR data. Moreover, the time differences between airborne LiDAR data and both datasets - the GLAS data and field measured data. Airborne LiDAR data were acquired in August 2004 while

ICESat-GLAS data were acquired in February-March 2009. These seasonal and time differences may have resulted in changes in savannah vegetation structure due to fire regime or effects of large herbivores on vegetation in the selected plots, which could have changed the vegetation properties such as height, which most assuredly will affect other vegetation metrics. Furthermore, the selection of GLAS footprint, with respect to the available datasets of airborne LiDAR and RADAR data, does not allow for comparison of GLAS waveforms over vertically complex and heterogeneous areas (i.e. riparian zones) with waveforms over vertically simple and homogenous areas (i.e., mopane shrubveld).

This study can be improved in many aspects; for example, coincident time and place for all the datasets used in this research. Furthermore, the results from using statistical methods could be supported by more field data collection. In other words, increase the number of the GLAS footprint samples with field data collection to get better validation of the statistical methods used to retrieve vegetation structure in this study. Nevertheless, GLAS proved to be a suitable spaceborne sensor for vegetation studies in savannah ecosystems and will provide a unique opportunity for large scale monitoring of vegetated savannah landscape structure and biomass. One important suggestion is that better analysis could be achieved if the footprint size is smaller than 70 meter, for example, 10 meter for better estimation of canopy height using both direct and statistical methods. Moreover, studying the seasonal variations for the GLAS waveform signal could help in classify the vegetation types of savannah landscape.

Finally, it is important to exploit other advanced satellite systems such as RADAR ALOS PALSAR and ALOS-2 (with two L-band, which will start to operate in 2013) in combination with the second generation of LiDAR ICESat-GLAS2, for better monitoring and mapping of vegetation structure.

## REFERENCES

- Abdalati, W., Zwally, H.J., Bindschadler, R., Csatho, B., Farrell, S.L., Fricker, H.A., Harding, D., Kwok, R., Lefsky, M., Markus, T., Marshak, A., Neumann, T., Palm, S., Schutz, B., Smith, B., Spinhirne, J. & Webb, C. 2010, "The ICESat-2 laser altimetry mission", *Proceedings of the IEEE*, vol. 98, no. 5, pp. 735-751.
- Abshire, J.B., Sun, X., Riris, H., Sirota, J.M., McGarry, J.F., Palm, S., Yi, D. & Liiva, P. 2005, "Geoscience Laser Altimeter System (GLAS) on the ICESat mission: On-orbit measurement performance", *Geophysical Research Letters*, vol. 32, no. 21, pp. 1-4.
- Ackermann, F. 1999, "Airborne laser scanning - Present status and future expectations", *ISPRS Journal of Photogrammetry and Remote Sensing*, vol. 54, no. 2-3, pp. 64-67.
- Alberti, M. & Biscaro, D. 2010, "Height variation detection in polar regions from ICESat satellite altimetry", *Computers and Geosciences*, vol. 36, no. 1, pp. 1-9.
- Aldred, A.H. & Bonnor, G.M. 1985, "Application of airborne laser to forest surveys", *Information Report PI-X*, no. 51, pp. 1-62.
- Alleaume, S., Hély, C., Le Roux, J., Korontzi, S., Swap, R.J., Shugart, H.H. & Justice, C.O. 2005, "Using MODIS to evaluate heterogeneity of biomass burning in southern African savannahs: A case study in Etosha", *International Journal of Remote Sensing*, vol. 26, no. 19, pp. 4219-4237.
- Amarasekare, P. 2003, "Competitive coexistence in spatially structured environments: A synthesis", *Ecology Letters*, vol. 6, no. 12, pp. 1109-1122.
- Andersen, H.-., Reutebuch, S.E. & McGaughey, R.J. 2006, "A rigorous assessment of tree height measurements obtained using airborne lidar and conventional field methods", *Canadian Journal of Remote Sensing*, vol. 32, no. 5, pp. 355-366.
- Anderson, J.E., Plourde, L.C., Martin, M.E., Braswell, B.H., Smith, M.-., Dubayah, R.O., Hofton, M.A. & Blair, J.B. 2008, "Integrating waveform lidar with hyperspectral imagery for inventory of a northern temperate forest", *Remote Sensing of Environment*, vol. 112, no. 4, pp. 1856-1870.
- Antonarakis, A.S., Richards, K.S. & Brasington, J. 2008, "Object-based land cover classification using airborne LiDAR", *Remote Sensing of Environment*, vol. 112, no. 6, pp. 2988-2998.
- Archibald, S., Roy, D.P., van Wilgen, B.W. & Scholes, R.J. 2009, "What limits fire? An examination of drivers of burnt area in Southern Africa", *Global Change Biology*, vol. 15, no. 3, pp. 613-630.
- Arp, H., Griesbach, J.C. & Burns, J.P. 1982, "Mapping in tropical forests: a new approach using the Laser APR.", *Photogrammetric Engineering and Remote Sensing*, vol. 48, no. 1, pp. 91-100.
- Atwood, D.K., Guritz, R.M., Muskett, R.R., Lingle, C.S., Sauber, J.M. & Freymueller, J.T. 2007, "DEM control in arctic Alaska with ICESat laser

- altimetry", *IEEE Transactions on Geoscience and Remote Sensing*, vol. 45, no. 11, pp. 3710-3720.
- Baltsavias, E.P. 1999, "Airborne laser scanning: Basic relations and formulas", *ISPRS Journal of Photogrammetry and Remote Sensing*, vol. 54, no. 2-3, pp. 199-214.
- Baltsavias, E.P. 1999, "A comparison between photogrammetry and laser scanning", *ISPRS Journal of Photogrammetry and Remote Sensing*, vol. 54, no. 2-3, pp. 83-94.
- Balzter, H., Rowland, C.S. & Saich, P. 2007, "Forest canopy height and carbon estimation at Monks Wood National Nature Reserve, UK, using dual-wavelength SAR interferometry", *Remote Sensing of Environment*, vol. 108, no. 3, pp. 224-239.
- Baret, F. & Guyot, G. 1991, "Potentials and limits of vegetation indices for LAI and APAR assessment", *Remote Sensing of Environment*, vol. 35, no. 2-3, pp. 161-173.
- Bebi, P., Kienast, F. & Schönenberger, W. 2001, "Assessing structures in mountain forests as a basis for investigating the forests' dynamics and protective function", *Forest Ecology and Management*, vol. 145, no. 1-2, pp. 3-14.
- Beerling, D.J. & Osborne, C.P. 2006, "The origin of the savanna biome", *Global Change Biology*, vol. 12, no. 11, pp. 2023-2031.
- Biggs, R., Biggs, H.C., Dunne, T.T., Govender, N. & Potgieter, A.L.F. 2003, "Experimental burn plot trial in the Kruger National Park: History, experimental design and suggestions for data analysis", *Koedoe*, vol. 46, no. 1, pp. 1-15.
- Blair, J.B., Rabine, D.L. & Hofton, M.A. 1999, "The Laser Vegetation Imaging Sensor: A medium-altitude, digitisation-only, airborne laser altimeter for mapping vegetation and topography", *ISPRS Journal of Photogrammetry and Remote Sensing*, vol. 54, no. 2-3, pp. 115-122.
- Boland, J. 2004, "Cameras and sensing systems", *Manual of Photogrammetry*, vol. 1151, pp. 645-676.
- Bond, W.J., Midgley, G.F. & Woodward, F.I. 2003, "What controls South African vegetation - Climate or fire?", *South African Journal of Botany*, vol. 69, no. 1, pp. 79-91.
- Boudreau, J., Nelson, R.F., Margolis, H.A., Beaudoin, A., Guindon, L. & Kimes, D.S. 2008, "Regional aboveground forest biomass using airborne and spaceborne LiDAR in Québec", *Remote Sensing of Environment*, vol. 112, no. 10, pp. 3876-3890.
- Brenner, A.C., Zwally, H.J., Bentley, C.R., Csatho, B.M., Harding, D.J., Hofton, M.A., Minster, J.B., Roberts, L.A., Saba, J.L., Thomas, R.H. & Yi, Y. 2003, "Geoscience Laser Altimeter System (GLAS) - derivation of range and range distributions from laser pulse waveform analysis for surface elevations, roughness, slope, and vegetation heights", *Algorithm Theoretical Basis Document - Version 4.1* .

- Bucini, G., Hanan, N.P., Boone, R.B., Smit, I.P.J., Saatchi, S., Lefsky, M.A. & Asner, G.P. 2010, "Ecosystem Function in Savannas: Measurement and Modeling at Landscape to Global Scales", *Woody fractional cover in Kruger National Park, South Africa: remote-sensing-based maps and ecological insights*, , pp. 219-238.
- Carabajal, C.C. & Harding, D.J. 2005, "ICESat validation of SRTM C-band digital elevation models", *Geophysical Research Letters*, vol. 32, no. 22, pp. 1-5.
- Carabajal, C.C. & Harding, D.J. 2001, "Evaluation of geoscience laser altimeter system (GLAS) waveforms for vegetated landscapes using airborne laser altimeter scanning data", *International Archives of Photogrammetry and Remote Sensing*, vol. 33, no. 3 W4, pp. 125-128.
- Chauhan, N.S., Lang, R.H. & Ranson, K.J. 1991, "Radar modeling of a boreal forest", *IEEE Transactions on Geoscience and Remote Sensing*, vol. 29, no. 4, pp. 627-638.
- Chen, G., Hay, G.J., Castilla, G., St-Onge, B. & Powers, R. 2011, "A multiscale geographic object-based image analysis to estimate lidar-measured forest canopy height using quickbird imagery", *International Journal of Geographical Information Science*, vol. 25, no. 6, pp. 877-893.
- Chen, Q. 2010a, "Assessment of terrain elevation derived from satellite laser altimetry over mountainous forest areas using airborne lidar data", *ISPRS Journal of Photogrammetry and Remote Sensing*, vol. 65, no. 1, pp. 111-122.
- Chen, Q. 2010b, "Retrieving vegetation height of forests and woodlands over mountainous areas in the Pacific Coast region using satellite laser altimetry", *Remote Sensing of Environment*, vol. 114, no. 7, pp. 1610-1627.
- Chen, Q., Baldocchi, D., Gong, P. & Kelly, M. 2006, "Isolating individual trees in a savanna woodland using small footprint lidar data", *Photogrammetric Engineering and Remote Sensing*, vol. 72, no. 8, pp. 923-932.
- Chen, Q., Gong, P., Baldocchi, D. & Tian, Y.Q. 2007, "Estimating basal area and stem volume for individual trees from lidar data", *Photogrammetric Engineering and Remote Sensing*, vol. 73, no. 12, pp. 1355-1365.
- Chesson, P. 2000, "Mechanisms of maintenance of species diversity", *Annual Review of Ecology and Systematics*, vol. 31, pp. 343.
- Chesson, P. & Huntly, N. 1997, "The roles of harsh and fluctuating conditions in the dynamics of ecological communities", *American Naturalist*, vol. 150, no. 5, pp. 519-553.
- Cloude, S.R. 1998, "Polarimetric sar interferometry", *IEEE Transactions on Geoscience and Remote Sensing*, vol. 36, no. 5 PART 1, pp. 1551-1565.
- Collins, J.N., Hutley, L.B., Williams, R.J., Boggs, G., Bell, D. & Bartolo, R. 2009, "Estimating landscape-scale vegetation carbon stocks using airborne multi-frequency polarimetric synthetic aperture radar (SAR) in the savannahs of north Australia", *International Journal of Remote Sensing*, vol. 30, no. 5, pp. 1141-1159.

- Colson, T.P. 2006, "Stream network delineation from high-resolution digital elevation models". Ph.D. Dissertation, Dept. of Forestry and Environmental Resources, NC State University, Raleigh, NC.
- Coops, N. & Culvenor, D., 2000, Utilizing local variance of simulated high spatial resolution imagery to predict spatial pattern of forest stands. *Remote Sensing of Environment*. vol.71, no.3, pp. 248- 260.
- Coops, N.C., Hilker, T., Wulder, M.A., St-Onge, B., Newnham, G., Siggins, A. & Trofymow, J.A. 2007, "Estimating canopy structure of Douglas-fir forest stands from discrete-return LiDAR", *Trees - Structure and Function*, vol. 21, no. 3, pp. 295-310.
- Coops, N.C., Wulder, M.A., Culvenor, D.S. & St-Onge, B. 2004, "Comparison of forest attributes extracted from fine spatial resolution multispectral and lidar data", *Canadian Journal of Remote Sensing*, vol. 30, no. 6, pp. 855-866.
- Coughenour, M.B. 1985, "Graminoid responses to grazing by large herbivores: adaptations, exaptations, and interacting processes.", *Annals - Missouri Botanical Garden*, vol. 72, no. 4, pp. 852-863.
- Danson, F.M. 1995, "Developments in the remote sensing of forest canopy structure", *Advances in Environmental Remote Sensing*, , pp. 53-69.
- Daubenmire, R. 1959, "A canopy-coverage method of vegetational analysis", *Northwest Science*, vol. 33, pp. 43-64.
- De Graaf, R.M., Yamasaki, M., Leak, W.B. & Lester, A.M. 2006, *Technical Guide to Forest Wildlife Habitat Management in New England*, pp. 305.
- De Loor, G.P., Jurriens, A.A. & Gravesteijn, H., 1974. "RADAR BACKSCATTER FROM SELECTED AGRICULTURAL CROPS.", *IEEE Trans Geosci Electron*, vol. GE-12, no. 2, pp. 70-77.
- Dessler, A.E., Palm, S.P. & Spinhirne, J.D. 2006, "Tropical cloud-top height distributions revealed by the Ice, Cloud, and Land Elevation Satellite (ICESat)/Geoscience Laser Altimeter System (GLAS)", *Journal of Geophysical Research D: Atmospheres*, vol. 111, no. 12.
- Dobson, A.P. 2009, "19956 The ecology and epidemiology of rinderpest virus in Serengeti and Ngorongoro crater conservation area", *Serengeti II: Research, management and conservation of an ecosystem* , pp. 485-505.
- Douglas, T.E. 2004, *Classification of Pine and Hardwood by the Density and Intensity of LIDAR Canopy Returns*, Master's Thesis, Mississippi State University.
- Duong, H. 2010, *Processing and Application of ICESat Large Footprint Full-waveform Laser Range Data*, PhD Thesis, Wageningen, TU Delft university .
- Drake, J.B., Dubayah, R.O., Clark, D.B., Knox, R.G., Blair, J.B. & Hofton, M.A. 2003a, "Estimation of tropical forest structural characteristics using large-footprint Lidar", *Remote Sensing of Environment*, .
- Drake, J.B., Dubayah, R.O., Clark, D.B., Knox, R.G., Blair, J.B., Hofton, M.A., Chazdon, R.L., Weishampel, J.F. & Prince, S. 2002, "Estimation of tropical

- forest structural characteristics, using large-footprint lidar", *Remote Sensing of Environment*, vol. 79, no. 2-3, pp. 305-319.
- Drake, J.B., Knox, R.G., Dubayah, R.O., Clark, D.B., Condit, R., Blair, J.B. & Hofton, M. 2003b, "Above-ground biomass estimation in closed canopy Neotropical forests using lidar remote sensing: Factors affecting the generality of relationships", *Global Ecology and Biogeography*, vol. 12, no. 2, pp. 147-159.
- Dubayah, R. 2005, *VCL: The Vegetation Canopy Lidar Mission, Land Satellite Information in the Next Decade II: Sources and Applications[C]*, pp. 100-112.
- Dubayah, R., Blair, J.B., Bufton, J.L., Clark, D.B., Jaja, J., Knox, R., Luthcke S.B., Prince, S. & Weishampel, J. 1997, "The vegetation canopy lidar mission", *Proceedings: Land Satellite Information in the Next Decade II: Sources and Applications, December 1997*, .
- Dubayah, R.O. & Drake, J.B. 2000, "Lidar Remote Sensing for Forestry", *Journal of Forestry*, vol. 98, no. 6, pp. 44-52.
- Duncanson, L.I., Niemann, K.O. & Wulder, M.A. 2010a, "Estimating forest canopy height and terrain relief from GLAS waveform metrics", *Remote Sensing of Environment*, vol. 114, no. 1, pp. 138-154.
- Duncanson, L.I., Niemann, K.O. & Wulder, M.A. 2010b, "Integration of GLAS and Landsat TM data for aboveground biomass estimation", *Canadian Journal of Remote Sensing*, vol. 36, no. 2, pp. 129-141.
- Duong, V.H., Lindenbergh, R., Pfeifer, N. & Vosselman, G. 2008, "Single and two epoch analysis of ICESat full waveform data over forested areas", *International Journal of Remote Sensing*, vol. 29, no. 5, pp. 1453-1473.
- Eagleson, P.S. 1989, "Stability of tree/grass vegetation systems", *Geophysical Monograph*, vol. 52, pp. 109-113.
- Eagleson, P.S. & Segara, R. I. 1985, " Water-limited equilibrium of Savannah vegetation systems", *Water Resources. Res.*, vol. 21, no. 10, pp. 1483-1493.
- Eckhardt, H.C., Van Wilgen, B.W. & Biggs, H.C. 2000, "Trends in woody vegetation cover in the Kruger National Park, South Africa, between 1940 and 1998", *African Journal of Ecology*, vol. 38, no. 2, pp. 108-115.
- Edwards, T.C., Moisen, G.G., Frescino, T.S. & Lawler, J.J. 2002, "Use of forest inventory analysis information in wildlife habitat modelling: A process for linking multiple scales", *Proceedings of the FIA Science Symposium* .
- ESA, 2007. *Electromagnetic spectrum*, [Imageonline] Available:<  
[http://earth.esa.int/applications/data\\_util/SARDOCS/spaceborne/Radar\\_Courses/Radar\\_Course\\_III/electromagnetic.htm](http://earth.esa.int/applications/data_util/SARDOCS/spaceborne/Radar_Courses/Radar_Course_III/electromagnetic.htm)> [Accessed 10 April 2012] copyright line© 2000-2012 European Space Agency.
- Evans, J.S., Hudak, A.T., Faux, R. & Smith, A.M.S. 2009, "Discrete return lidar in natural resources: Recommendations for project planning, data processing, and deliverables", *Remote Sensing*, vol. 1, no. 4, pp. 776-794.
- Fahrig, L. & Merriam, H.G. 1985, "Habitat patch connectivity and population survival", *Ecology*, vol. 67, no. 1, pp. 61-67.

- Farrell, S.L., Laxon, S.W., McAdoo, D.C., Yi, D. & Zwally, H.J. 2009, "Five years of arctic sea ice freeboard measurements from the ice, cloud and land elevation satellite", *Journal of Geophysical Research C: Oceans*, vol. 114, no. 4.
- Fernandez-Illescas, C.P. & Rodriguez-Iturbe, I. 2003, "Hydrologically driven hierarchical competition-colonization models: The impact of interannual climate fluctuations", *Ecological Monographs*, vol. 73, no. 2, pp. 207-222.
- Flood, M. & Gutelius, B. 1997, "Commercial implications of topographic terrain mapping using scanning airborne laser radar", *Photogrammetric Engineering and Remote Sensing*, vol. 63, no. 4, pp. 327-329+363.
- Fransson, J.E.S., Smith, G., Askne, J. & Olsson, H. 2001, "Stem volume estimation in boreal forest using ERS-1/2 coherence and SPOT XS optical data", *International Journal of Remote Sensing*, vol. 22, no. 14, pp. 2777-2791.
- Frost, P., Medina, E., Menaut, J.C., Solbrig, O., Swift, M. & Walker, B. 1986, "Responses of savannas to stress and disturbance", *Biology International*, vol. 10, no. 10 SPEC. ISSUE, pp. 1-82.
- García, M., Riaño, D., Chuvieco, E. & Danson, F.M. 2010, "Estimating biomass carbon stocks for a Mediterranean forest in central Spain using LiDAR height and intensity data", *Remote Sensing of Environment*, vol. 114, no. 4, pp. 816-830.
- Garestier, F., Dubois-Fernandez, P.C., Guyon, D. & Le Toan, T. 2009, "Forest biophysical parameter estimation using L- and P-band polarimetric SAR data", *IEEE Transactions on Geoscience and Remote Sensing*, vol. 47, no. 10, pp. 3379-3388.
- Garvin, J., Bufton, J., Blair, J., Harding, D., Luthcke, S., Frawley, J. & Rowlands, D. 1998, "Observations of the earth's topography from the Shuttle Laser Altimeter (SLA): Laser-pulse echo-recovery measurements of terrestrial surfaces", *Physics and Chemistry of the Earth*, vol. 23, no. 9-10, pp. 1053-1068.
- Gertenbach, W. P. D. 1983, "Landscapes of the Kruger National Park", *Koedoe*, vol.26, no.1, pp. 9–121.
- Gillson, L. & Duffin, K.I. 2007, "Thresholds of potential concern as benchmarks in the management of African savannahs", *Philosophical Transactions of the Royal Society B: Biological Sciences*, vol. 362, no. 1478, pp. 309-319.
- GLAS Homepage, unknown. "Schematic illustration of the GLAS instrument making measurement from ICESat while orbiting the Earth. Graphic by Deborah McLean" [Image online]. Available at:  
 <<http://glas.gsfc.nasa.gov/about.html>> [accessed on 28 November 2009].
- Goetz, S., Steinberg, D., Dubayah, R. & Blair, B. 2007, "Laser remote sensing of canopy habitat heterogeneity as a predictor of bird species richness in an eastern temperate forest, USA", *Remote Sensing of Environment*, vol. 108, no. 3, pp. 254-263.

- Gong, P., Pu, R., Biging, G.S. & Larrieu, M.R. 2003, "Estimation of forest leaf area index using vegetation indices derived from Hyperion hyperspectral data", *IEEE Transactions on Geoscience and Remote Sensing*, vol. 41, no. 6 PART I, pp. 1355-1362.
- González ,Sanpedro, M.d.C., 2008. *Optical and radar remote sensing applied to agricultural areas in europe*, Universitat de València. Departament de Física Aplicada.
- Grace, J., José, J. S., Meir, P., Miranda, H. S. & Montes, R. A. 2006, "Productivity and carbon fluxes of tropical savannas", *Journal of Biogeography*, vol.33, no. 3, pp. 387- 400.
- Gudmundsson, S., H. Björnsson, E. Magnússon, E. Berthier, F. Pálsson, M. T.Gudmundsson, & J. Dall. 2011, "Response of Glacier Mass Balance to Regional Warming, Deduced by Remote Sensing on Three glaciers in S-Iceland", *Polar Research*, vol. 30, pp 7282. <[http://www.polarresearch.net/index.php/polar/article/viewArticle/7282/html\\_186](http://www.polarresearch.net/index.php/polar/article/viewArticle/7282/html_186)> [Accessed: 16-12-2011]
- Guo, Z.F., Chi, H. & Sun, G.Q. 2010, "Estimating forest aboveground biomass using HJ-1 Satellite CCD and ICESat GLAS waveform data", *Science China Earth Sciences*, vol. 53, no. SUPPL. 1, pp. 16-25.
- Hall, S.A., Burke, I.C., Box, D.O., Kaufmann, M.R. & Stoker, J.M. 2005, "Estimating stand structure using discrete-return lidar: An example from low density, fire prone ponderosa pine forests", *Forest Ecology and Management*, vol. 208, no. 1-3, pp. 189-209.
- Hanan, N. P. & Hill, M. J., 2012, "Savannas in a Changing Earth System", The NASA Terrestrial Ecology *Tree-Grass* Project., [online] Available at:<[http://cce.nasa.gov/terrestrial\\_ecology/pdfs/Tree-Grass\\_White\\_Paper.pdf](http://cce.nasa.gov/terrestrial_ecology/pdfs/Tree-Grass_White_Paper.pdf) [accessed January 2012].
- Harding, D.J., Blair, J.B., Rabine, D.L. & Still, K.L. 2000, "SLICER airborne laser altimeter characterization of canopy structure and sub-canopy topography for the BOREAS northern and southern study regions: Instrument and data product description", *Technical Report Series on the Boreal Ecosystem-Atmosphere Study (BOREAS)*, vol. 93, pp. 45.
- Harding, D.J. & Carabajal, C.C. 2005, "ICESat waveform measurements of within-footprint topographic relief and vegetation vertical structure", *Geophysical Research Letters*, vol. 32, no. 21, pp. 1-4.
- Harding, D.J., Lefsky, M.A., Parker, G.G. & Blair, J.B. 2001, "Laser altimeter canopy height profiles methods and validation for closed-canopy, broadleaf forests", *Remote Sensing of Environment*, vol. 76, no. 3, pp. 283-297.
- Harding, D.J., Bufton, J.L. & Frawley, J.J. 1994, "Satellite laser altimetry of terrestrial topography: vertical accuracy as a function of surface slope, roughness, and cloud cover", *IEEE Transactions on Geoscience and Remote Sensing*, vol. 32, no. 2, pp. 329-339.
- Harrell, P.A., Kasischke, E.S., Bourgeau-Chavez, L.L., Haney, E.M. & Christensen Jr., N.L. 1997, "Evaluation of approaches to estimating aboveground biomass

- in southern pine forests using SIR-C data", *Remote Sensing of Environment*, vol. 59, no. 2, pp. 223-233.
- Henderson, F.M. & Lewis, A.J., 1998. Principles and Applications of Imaging Radar. Manual of Remote Sensing Volume 2. John Wiley & Sons. New York.
- Herzfeld, U.C., McBride, P.J., Zwally, H.J. & Dimarzio, J. 2008, "Elevation changes in Pine Island Glacier, Walgreen Coast, Antarctica, based on GLAS (2003) and ERS-1 (1995) altimeter data analyses and glaciological implications", *International Journal of Remote Sensing*, vol. 29, no. 19, pp. 5533-5553.
- Hese, S., Lucht, W., Schmullius, C., Barnsley, M., Dubayah, R., Knorr, D., Neumann, K., Riedel, T. & Schröter, K. 2005, "Global biomass mapping for an improved understanding of the CO<sub>2</sub> balance - The Earth observation mission Carbon-3D", *Remote Sensing of Environment*, vol. 94, no. 1, pp. 94-104.
- Higgins, S.I., Bond, W.J. & Winston S. W. Trollope 2000, "Fire, Resprouting and Variability: A Recipe for Grass-Tree Coexistence in Savanna", *Journal of Ecology*, vol. 88, no. 2, pp. 213-229.
- Hill, R.A. & Thomson, A.G. 2005, "Mapping woodland species composition and structure using airborne spectral and LiDAR data", *International Journal of Remote Sensing*, vol. 26, no. 17, pp. 3763-3779.
- Hochberg, M.E., Menaut, J.C. & Gignoux, J. 1994, "The influences of tree biology and fire in the spatial structure of the West African savannah", *Journal of Ecology*, vol. 82, no. 2, pp. 217-226.
- Hofton, M.A., Rocchio, L.E., Blair, J.B. & Dubayah, R. 2002, "Validation of Vegetation Canopy Lidar sub-canopy topography measurements for a dense tropical forest", *Journal of Geodynamics*, vol. 34, no. 3-4, pp. 491-502.
- Holmgren, J., Nilsson, M. & Olsson, H. 2003, "Estimation of tree height and stem volume on plots using airborne laser scanning", *Forest Science*, vol. 49, no. 3, pp. 419-428.
- Holmgren, J. & Persson, Å. 2004, "Identifying species of individual trees using airborne laser scanner", *Remote Sensing of Environment*, vol. 90, no. 4, pp. 415-423.
- House, J.I., Archer, S., Breshears, D.D., Scholes, R.J., Coughenour, M.B., Dodd, M.B., Gignoux, J., Hall, D.O., Hanan, N.P., Joffre, R., Le Roux, X., Ludwig, J.A., Menaut, J.-., Montes, R., Parton, W.J., San Jose, J.J., Scanlan, J.C., Scurlock, J.M.O., Simioni, G. & Thorrold, B. 2003, "Conundrums in mixed woody-herbaceous plant systems", *Journal of Biogeography*, vol. 30, no. 11, pp. 1763-1777.
- Howat, I.M., Smith, B.E., Joughin, I. & Scambos, T.A. 2008, "Rates of southeast Greenland ice volume loss from combined ICESat and ASTER observations", *Geophysical Research Letters*, vol. 35, no. 17.
- Huang, W., Pohjonen, V., Johansson, S., Nashanda, M., Katigula, M.I.L. & Luukkanen, O. 2003, "Species diversity, forest structure and species composition in Tanzanian tropical forests", *Forest Ecology and Management*, vol. 173, no. 1-3, pp. 11-24.

- Hudak, A.T. & Wessman, C.A. 1998, "Textural analysis of historical aerial photography to characterize woody plant encroachment in South African Savanna", *Remote Sensing of Environment*, vol. 66, no. 3, pp. 317-330.
- Hug, C., Ullrich, A. & Grimm, A. 2004, "LITEMAPPER-5600 - a waveform digitising lidar terrain and vegetation mapping system", *International Archives of Photogrammetry, Remote Sensing & Spatial Information Sciences*, vol. 36.
- Hudak A. T., Wessman C. A. & Seastedt T. R. 2003, "Woody over storey effects on soil carbon and nitrogen pools in South African savannah", *Austral Ecol*, vol. 28, pp. 173-81.
- Hyde, P., Dubayah, R., Peterson, B., Blair, J.B., Hofton, M., Hunsaker, C., Knox, R. & Walker, W. 2005, "Mapping forest structure for wildlife habitat analysis using waveform lidar: Validation of montane ecosystems", *Remote Sensing of Environment*, vol. 96, no. 3-4, pp. 427-437.
- Hyde, P., Dubayah, R., Walker, W., Blair, J.B., Hofton, M. & Hunsaker, C. 2006, "Mapping forest structure for wildlife habitat analysis using multi-sensor (LiDAR, SAR/InSAR, ETM+, Quickbird) synergy", *Remote Sensing of Environment*, vol. 102, no. 1-2, pp. 63-73.
- Hyypä, J., Kelle, O., Lehtikoinen, M. & Inkinen, M. 2001, "A segmentation-based method to retrieve stem volume estimates from 3-D tree height models produced by laser scanners", *IEEE Transactions on Geoscience and Remote Sensing*, vol. 39, no. 5, pp. 969-975.
- ICESat-GLAS, 2003. [Image online] Available: < <http://www.csr.utexas.edu/glas/> > [Accessed 21 June 2011]
- Imaging Notes Magazine, 2011. *Basics of airborne mapping LiDAR*, [Imageonline] Available:<[http://www.imagingnotes.com/go/article\\_freeJ.php?mp\\_id=264#Fig1](http://www.imagingnotes.com/go/article_freeJ.php?mp_id=264#Fig1)> [Accessed 01 June 2011] copyright line© 2005-2012 Blueline Publishing LLC.
- Jackson, R.B., Banner, J.L., Jobbágy, I.E., Pockman, W.T. & Wall, D.H. 2002, "Ecosystem carbon loss with woody plant invasion of grasslands", *Nature*, vol. 418, no. 6898, pp. 623-626.
- Jeltsch, F., Weber, G.E. & Grimm, V. 2000, "Ecological buffering mechanisms in savannas: A unifying theory of long-term tree-grass coexistence", *Plant Ecology*, vol. 150, no. 1-2, pp. 161-171.
- LAS specification ,Version 1.0. 2002, Available on line at : <<http://www.asprs.org/a/publications/pers/2005journal/july/feature.pdf>> [accessed: 10-12-2009].
- Lusch, D.P.,1999. Introduction to Microwave Remote Sensing. Center for Remote Sensing and Geographic Information System. University of Michigan.
- Kasischke, E.S., Melack, J.M. & Dobson, M.C. 1997, "The use of imaging radars for ecological applications - A review", *Remote Sensing of Environment*, vol. 59, no. 2, pp. 141-156.

- Kwok, R. 2009, "Outflow of Arctic Ocean sea ice into the Greenland and Barent Seas: 1979-2007", *Journal of Climate*, vol. 22, no. 9, pp. 2438-2457.
- Langevelde, F.V., Van De Vijver, C.A. D. M., Kumar, L., Koppel, J.V. D., De Ridder, N., Andel, J. V., Skidmore, A.K. , Hearne, J.W., Stroosnijder, L., Bond, W. J., Prins, H.H. T. and Rietkerk, M.2003, "Effects of fire and herbivory on the stability of savannah ecosystems", *Ecology*, vol. 84, pp. 337-350.
- Lam, N. S-N., 1983. "Spatial interpolation methods: A review". *The American Cartographer* 10: 129-49.
- Law, B.E., Arkebauer, T., Campbell, J.L., Chen, J., Sun, O. & Schwartz, M. 2008, "Terrestrial Carbon Observations: Protocols for Vegetation Sampling and Data Submission", *Global Terrestrial Observing System.Report*, vol. 55, pp. 87.
- Lee, J.S., Grunes, M.R. & Kwok, R. 1994, "Classification of multi-look polarimetric SAR imagery based on complex Wishart distribution", *International Journal of Remote Sensing*, vol. 15, no. 11, pp. 2299-2311.
- Lefsky, M.A. 2010, "A global forest canopy height map from the moderate resolution imaging spectroradiometer and the geoscience laser altimeter system", *Geophysical Research Letters*, vol. 37, no. 15.
- Lefsky, M.A., Cohen, W.B., Acker, S.A., Parker, G.G., Spies, T.A. & Harding, D. 1999a, "Lidar remote sensing of the canopy structure and biophysical properties of Douglas-fir western hemlock forests", *Remote Sensing of Environment*, vol. 70, no. 3, pp. 339-361.
- Lefsky, M.A., Cohen, W.B., Harding, D.J., Parker, G.G., Acker, S.A. & Gower, S.T. 2002a, "Lidar remote sensing of above-ground biomass in three biomes", *Global Ecology and Biogeography*, vol. 11, no. 5, pp. 393-399.
- Lefsky, M.A., Cohen, W.B., Parker, G.G. & Harding, D.J. 2002b, "Lidar remote sensing for ecosystem studies", *Bioscience*, vol. 52, no. 1, pp. 19-30.
- Lefsky, M.A., Harding, D., Cohen, W.B., Parker, G. & Shugart, H.H. 1999b, "Surface lidar remote sensing of basal area and biomass in deciduous forests of eastern Maryland, USA", *Remote Sensing of Environment*, vol. 67, no. 1, pp. 83-98.
- Lefsky, M.A., Harding, D.J., Keller, M., Cohen, W.B., Carabajal, C.C., Del Bom Espirito-Santo, F., Hunter, M.O. & de Oliveira Jr., R. 2005a, "Estimates of forest canopy height and aboveground biomass using ICESat", *Geophysical Research Letters*, vol. 32, no. 22, pp. 1-4.
- Lefsky, M.A., Hudak, A.T., Cohen, W.B. & Acker, S.A. 2005b, "Geographic variability in lidar predictions of forest stand structure in the Pacific Northwest", *Remote Sensing of Environment*, vol. 95, no. 4, pp. 532-548.
- Lefsky, M.A., Keller, M., Pang, Y., De Camargo, P.B. & Hunter, M.O. 2007, "Revised method for forest canopy height estimation from Geoscience Laser Altimeter System waveforms", *Journal of Applied Remote Sensing*, vol. 1, no. 1.

- Levick, S.R. & Rogers, K.H. , " 2008. Structural biodiversity monitoring in savanna ecosystems: Integrating LiDAR and high resolution imagery through object-based image analysis. *ObjectBased Image Analysis*", p.477-491. Available at: <[http://dx.doi.org/10.1007/978-3-540-77058-9\\_26](http://dx.doi.org/10.1007/978-3-540-77058-9_26)> [Accessed: 16-10-2009]
- Lewis, P. 2010, "Modelling spatial video as part of a GIS video analysis framework", *GIS: Proceedings of the ACM International Symposium on Advances in Geographic Information Systems*, pp. 470.
- Lichti, D.D., Gordon, S.J. & Stewart, M.P. 2002, "Ground-based laser scanners: Operation, systems and applications", *Geomatica*, vol. 56, no. 1, pp. 21-33.
- Lim, K., Treitz, P., Baldwin, K., Morrison, I. & Green, J. 2003, "Lidar remote sensing of biophysical properties of tolerant northern hardwood forests", *Canadian Journal of Remote Sensing*, vol. 29, no. 5, pp. 658-678.
- Lim, K., Treitz, P., Morrison, I. & Baldwin, K. 2002, "Estimating aboveground biomass using lidar remote sensing", *Proceedings of SPIE - The International Society for Optical Engineering*, pp. 289.
- Lim, K., Treitz, P., Wulder, M., St-Onge, B. & Flood, M. 2003, "LiDAR remote sensing of forest structure", *Progress in Physical Geography*, vol. 27, no. 1, pp. 88-106.
- Lin, Y.-. & Sarabandi, K. 1999, "A Monte Carlo coherent scattering model for forest canopies using fractal-generated trees", *IEEE Transactions on Geoscience and Remote Sensing*, vol. 37, no. 1 II, pp. 440-451.
- Low, A.B. & Rebelo, A.G. 1996, "Vegetation of South Africa, Lesotho and Swaziland", *A Companion to the Vegetation Map of South Africa, Lesotho and Swaziland*, .
- Lucas, R.M., Bunting, P., Clewley, D., Armston, J., & Carreiras, J. A. 2009, "Regional Mapping of Forest Growth Stage, Queensland, Australia, through Integration of ALOS PALSAR and Landsat Foliage Projected Cover", Available on line at :< [http://www.eorc.jaxa.jp/ALOS/en/kyoto/phase\\_1/KC-Phase1-report\\_Lucas\\_FT.pdf](http://www.eorc.jaxa.jp/ALOS/en/kyoto/phase_1/KC-Phase1-report_Lucas_FT.pdf)>. [Accessed: 16-07-2011]
- Lucas, R.M., Cronin, N., Lee, A., Moghaddam, M., Witte, C. & Tickle, P. 2006a, "Empirical relationships between AIRSAR backscatter and LiDAR-derived forest biomass, Queensland, Australia", *Remote Sensing of Environment*, vol. 100, no. 3, pp. 407-425.
- Lucas, R.M., Cronin, N., Moghaddam, M., Lee, A., Armston, J., Bunting, P. & Witte, C. 2006b, "Integration of radar and Landsat-derived foliage projected cover for woody regrowth mapping, Queensland, Australia", *Remote Sensing of Environment*, vol. 100, no. 3, pp. 388-406.
- Lucas, R.M., Lee, A.C. & Williams, M.L. 2006c, "Enhanced simulation of radar backscatter from forests using lidar and optical data", *IEEE Trans.Geosci.Remote Sens*, vol. 44, no. 10, pp. 2736-2754.
- Lucas, R.M., Moghaddam, M. & Cronin, N. 2004, "Microwave scattering from mixed-species forests, Queensland, Australia", *IEEE Transactions on Geoscience and Remote Sensing*, vol. 42, no. 10, pp. 2142-2159.

- Liu, X. 2008, "Airborne LiDAR for DEM generation: Some critical issues", *Progress in Physical Geography*, vol. 32, no. 1, pp. 31-49.
- Maclean, GA, & Krabill, WB. 1986, Gross-merchantable timber volume estimation using an airborne LIDAR system: *Canadian Journal of Remote Sensing*. Vol.12,pp. 7-18
- Magnussen, S. & Boudewyn, P. 1998, "Derivations of stand heights from airborne laser scanner data with canopy-based quantile estimators", *Canadian Journal of Forest Research*, vol. 28, no. 7, pp. 1016-1031.
- Mallet, C. & Bretar, F. 2009, "Full-waveform topographic lidar: State-of-the-art", *ISPRS Journal of Photogrammetry and Remote Sensing*, vol. 64, no. 1, pp. 1-16.
- McGaughey, R.J. 2007, "FUSION/LDV: Software for LIDAR Data Analysis and Visualization", *United States Department of Agriculture Forest Service Pacific Northwest Research Station*.
- McInerney, D.O., Suarez-Minguez, J., Valbuena, R. & Nieuwenhuis, M. 2010, "Forest canopy height retrieval using LiDAR data, medium-resolution satellite imagery and kNN estimation in Aberfoyle, Scotland", *Forestry*, vol. 83, no. 2, pp. 195-206.
- Means, J.E., Acker, S.A., Fitt, B.J., Renslow, M., Emerson, L. & Hendrix, C.J. 2000, "Predicting forest stand characteristics with airborne scanning lidar", *Photogrammetric Engineering and Remote Sensing*, vol. 66, no. 11, pp. 1367-1371.
- Means, J.E., Acker, S.A., Harding, D.J., Blair, J.B., Lefsky, M.A., Cohen, W.B., Harmon, M.E. & McKee, W.A. 1999, "Use of large-footprint scanning airborne Lidar to estimate forest stand characteristics in the western cascades of Oregon", *Remote Sensing of Environment*, vol. 67, no. 3, pp. 298-308.
- Mentis, M.T., & Bailey, A.W. 1990, "Changing perceptions of fire management in savannah parks", *Journal of the Grassland Society of Southern Africa*, vol.7, pp. 81-85.
- Mitchard, E.T.A., Saatchi, S.S., Woodhouse, I.H., Nangendo, G., Ribeiro, N.S., Williams, M., Ryan, C.M., Lewis, S.L., Feldpausch, T.R. & Meir, P. 2009, "Using satellite radar backscatter to predict above-ground woody biomass: A consistent relationship across four different African landscapes", *Geophysical Research Letters*, vol. 36, no. 23.
- Moles, A.T., Warton, D.I., Warman, L., Swenson, N.G., Laffan, S.W., Zanne, A.E., Pitman, A., Hemmings, F.A. & Leishman, M.R. 2009, "Global patterns in plant height", *Journal of Ecology*, vol. 97, no. 5, pp. 923-932.
- Mutanga O. & Rugege D. 2006, "Integrating remote sensing and spatial statistics to model herbaceous biomass distribution a tropical savannah", *International Journal of Remote Sensing*, vol. 27, pp. 3499-3514.
- Næsset, E. & Bjercknes, K.. 2001, "Estimating tree heights and number of stems in young forest stands using airborne laser scanner data", *Remote Sensing of Environment*, vol. 78, no. 3, pp. 328-340.

- Nagendra, H. 2001, "Review article. Using remote sensing to assess biodiversity", *International Journal of Remote Sensing*, vol. 22, no. 12, pp. 2377-2400.
- NASA GLAS, 2009 . [Image online] available at:  
<<http://glas.gsfc.nasa.gov/about.html>>) [accessed on 28 November 2009].
- Nelson, R., Boudreau, J., Gregoire, T.G., Margolis, H., Næsset, E., Gobakken, T. & Ståhl, G. 2009, "Estimating Quebec provincial forest resources using ICESat/GLAS", *Canadian Journal of Forest Research*, vol. 39, no. 4, pp. 862-881.
- Nelson, R., Keller, C. & Ratnaswamy, M. 2005, "Locating and estimating the extent of Delmarva fox squirrel habitat using an airborne LiDAR profiler", *Remote Sensing of Environment*, vol. 96, no. 3-4, pp. 292-301.
- Nelson, R., Krabill, W. & MacLean, G. 1984, "Determining forest canopy characteristics using airborne laser data", *Remote Sensing of Environment*, vol. 15, no. 3, pp. 201-212.
- Nelson, R., Krabill, W. & Tonelli, J. 1988, "Estimating forest biomass and volume using airborne laser data", *Remote Sensing of Environment*, vol. 24, no. 2, pp. 247-267.
- Nelson, R., Oderwald, R. & Gregoire, T.G. 1997, "Separating the ground and airborne laser sampling phases to estimate tropical forest basal area, volume, and biomass", *Remote Sensing of Environment*, vol. 60, no. 3, pp. 311-326.
- Neuenschwander, A.L., Urban, T.J., Gutierrez, R. & Schutz, B.E. 2008, "Characterization of ICESat/GLAS waveforms over terrestrial ecosystems: Implications for vegetation mapping", *Journal of Geophysical Research G: Biogeosciences*, vol. 113, no. 2.
- Nilsson, M. 1996, "Estimation of tree heights and stand volume using an airborne lidar system", *Remote Sensing of Environment*, vol. 56, no. 1, pp. 1-7.
- Ni-Meister, W., Jupp, D.L.B. & Dubayah, R. 2001, "Modeling lidar waveforms in heterogeneous and discrete canopies", *IEEE Transactions on Geoscience and Remote Sensing*, vol. 39, no. 9, pp. 1943-1958.
- NSIDC, 2003. *ICESat-GLAS Data at NSIDC*. National Snow and Ice Data Center.. [online] Available at: <<http://www.nasa.gov/>> [Accessed 10 October 2009]
- NSIDC, 2005. "IDLreadGLAS" [online] Available at:  
<<http://nsidc.org/data/icesat/tools.html>> [accessed 1st July 2009].
- NSIDC, 2007. *Report from the ICESat-II Workshop, 27-29 June, Linthicum, USA*. [online] Available at: <<http://www.nasa.gov/>> [Accessed 10 October 2009].
- NSIDC, 2009, ICESat-GLAS Data at NSIDC. National Snow and Ice Data Center. [online] Available at: <<http://nsidc.org/>>. [Accessed February, 2009].
- NSIDC, 2011. [Table online] Available at: <<http://nsidc.org/data/icesat/data.html>> [Accessed 21 June 2011].
- NSIDC, 2011. [image online] Available at: <<http://nsidc.org/>> [Accessed 19 October 2009].

- NSIDC, 2011. [Image online] Available at:  
 < [http://nsidc.org/data/icesat/laser\\_op\\_periods.html](http://nsidc.org/data/icesat/laser_op_periods.html)> [Accessed 21 June 2011]
- NSW, 2007. *Private Native Forestry Code of Practice: Guideline 4: Techniques for measuring stand height*, [Images on line] available at: < <http://www.environment.nsw.gov.au/resources/pnf/standheight07392.pdf>> [Accessed 21 July 2010]
- Nuth, C. & Kääb. 2011, "Co-registration and bias corrections of satellite elevation data sets for quantifying glacier thickness change", *Cryosphere*, vol. 5, no. 1, pp. 271-290.
- Olson, D.M., Dinerstein, E., Wikramanayake, E.D., Burgess, N.D., Powell, G.V.N., Underwood, E.C., D'Amico, J.A., Itoua, I., Strand, H.E., Morrison, J.C., Loucks, C.J., Allnutt, T.F., Ricketts, T.H., Kura, Y., Lamoreux, J.F., Wettengel, W.W., Hedao, P. & Kassem, K.R. 2001, "Terrestrial ecoregions of the world: A new map of life on Earth", *Bioscience*, vol. 51, no. 11, pp. 933-938.
- Pang, Y., Lefsky, M., Andersen, H.-., Miller, M.E. & Sherrill, K. 2008, "Validation of the ICESat vegetation product using crown-area-weighted mean height derived using crown delineation with discrete return lidar data", *Canadian Journal of Remote Sensing*, vol. 34, no. SUPPL. 2, pp. S471-S484.
- Parker, G.G., Lefsky, M.A. & Harding, D.J. 2001, "Light transmittance in forest canopies determined using airborne laser altimetry and in-canopy quantum measurements", *Remote Sensing of Environment*, vol. 76, no. 3, pp. 298-309.
- Parrish, C.E. 2007, "Exploiting full-waveform lidar data and multiresolution wavelet analysis for vertical object detection and recognition", *International Geoscience and Remote Sensing Symposium (IGARSS)*, pp. 2499.
- Patenaude, G., Hill, R.A., Milne, R., Gaveau, D.L.A., Briggs, B.B.J. & Dawson, T.P. 2004, "Quantifying forest above ground carbon content using LiDAR remote sensing", *Remote Sensing of Environment*, vol. 93, no. 3, pp. 368-380.
- Peterson, B.E. 2000, *Recovery of forest canopy heights using large-footprint LiDAR*.
- Pickett, S.T.A., Cadenasso, M.L. & Benning, T.L. 2003, "Biotic and Abiotic Variability as Key Determinants of savannah Heterogeneity at Multiple Spatiotemporal Scales", In: J.T. du Toit, K.H. Rogers and H. Biggs (Editors), *The Kruger Experience: Ecology and Management of savannah Heterogeneity*. Island Press, Washington, DC, pp. 23-40.
- Pirotti F. 2011, "Analysis of full-waveform LiDAR data for forestry applications: a review of investigations and methods", *iForest*, vol. 4, pp. 100-106.
- Polley, H.W. 1997, "Implications of rising atmospheric carbon dioxide concentration for rangelands", *Journal of Range Management*, vol. 50, no. 6, pp. 561-577.
- Popescu, S.C. 2007, "Estimating biomass of individual pine trees using airborne lidar", *Biomass and Bioenergy*, vol. 31, no. 9, pp. 646-655.

- Popescu, S.C., Wynne, R.H. & Nelson, R.F. 2002, "Estimating plot-level tree heights with lidar: Local filtering with a canopy-height based variable window size", *Computers and Electronics in Agriculture*, vol. 37, no. 1-3, pp. 71-95.
- Popescu, S.C., Wynne, R.H. & Nelson, R.F. 2003, "Measuring individual tree crown diameter with lidar and assessing its influence on estimating forest volume and biomass", *Canadian Journal of Remote Sensing*, vol. 29, no. 5, pp. 564-577.
- Popescu, S.C. & Zhao, K. 2008, "A voxel-based lidar method for estimating crown base height for deciduous and pine trees", *Remote Sensing of Environment*, vol. 112, no. 3, pp. 767-781.
- Popescu, S.C., Zhao, K., Neuenschwander, A. & Lin, C. 2011, "Satellite lidar vs. small footprint airborne lidar: Comparing the accuracy of aboveground biomass estimates and forest structure metrics at footprint level", *Remote Sensing of Environment*, vol. 115, no. 11, pp. 2786-2797.
- Pritchard, H.D., Arthern, R.J., Vaughan, D.G. & Edwards, L.A. 2009, "Extensive dynamic thinning on the margins of the Greenland and Antarctic ice sheets", *Nature*, vol. 461, no. 7266, pp. 971-975.
- Ranson, K.J. & Sun, G. 1994, "Northern forest classification using temporal multifrequency and multipolarimetric SAR images", *Remote Sensing of Environment*, vol. 47, no. 2, pp. 142-153.
- Ranson, K.J., Sun, G., Kovacs, K. & Kharuk, V.I. 2004a, "Landcover attributes from ICESat GLAS data in central Siberia", *International Geoscience and Remote Sensing Symposium (IGARSS)*, pp. 753.
- Ranson, K.J., Sun, G., Kovacs, K. & Kharuk, V.I. 2004b, "Use of ICESat GLAS data for forest disturbance studies in central Siberia", *International Geoscience and Remote Sensing Symposium (IGARSS)*, pp. 1936.
- Reitberger, J., Krzystek, P. & Stilla, U. 2008, "Analysis of full waveform LIDAR data for the classification of deciduous and coniferous trees", *International Journal of Remote Sensing*, vol. 29, no. 5, pp. 1407-1431.
- Rietkerk, M., Van Den Bosch, F. & Van De Koppel, J. 1997, "Site-specific properties and irreversible vegetation changes in semi-arid grazing systems", *Oikos*, vol. 80, no. 2, pp. 241-252.
- Roberts, S.D., Dean, T.J., Evans, D.L., McCombs, J.W., Harrington, R.L. & Glass, P.A. 2005, "Estimating individual tree leaf area in loblolly pine plantations using LiDAR-derived measurements of height and crown dimensions", *Forest Ecology and Management*, vol. 213, no. 1-3, pp. 54-70.
- Rogers, K.H., 2003. Adopting a heterogeneity paradigm: Implications for management of protected savannas. In J. T. Du Toit, H. C. Biggs, & K. H. Rogers, eds. *The Kruger Experience ecology and management of savanna heterogeneity*. Island Press, pp. 41-58. Available at: <<http://books.google.com/books>>[accessed 12-05-2010]
- Rosenqvist, A., Shimada, M., Watanabe, M., Tadono, T. & Yamauchi, K. 2004, "Implementation of systematic data observation strategies for ALOS PALSAR,

- PRISM and AVNIR-2", *International Geoscience and Remote Sensing Symposium (IGARSS)*, pp. 4527.
- Rosette, J., North, P. & Suárez, J. 2008a, "Vegetation height and stemwood volume estimates for a mixed temperate forest using satellite LiDAR", *Journal of Forest Planning, Special Issue: LiDAR Application in Forestry*, .
- Rosette, J.A., North, P.R.J. & Suárez, J.C. 2008b, "Satellite lidar estimation of stemwood volume: A method using waveform decomposition", *Photogrammetric Journal of Finland*, vol. 21, pp. 76-85.
- Rosette, J.A., North, P.R.J., Suárez, J.C. & Armston, J.D. 2009, "A comparison of biophysical parameter retrieval for forestry using airborne and satellite LiDAR", *International Journal of Remote Sensing*, vol. 30, no. 19, pp. 5229-5237.
- Rosette, J.A.B., North, P.R.J. & Suárez, J.C. 2008c, "Vegetation height estimates for a mixed temperate forest using satellite laser altimetry", *International Journal of Remote Sensing*, vol. 29, no. 5, pp. 1475-1493.
- Rossetti, D.F., Almeida, S., Amaral, D.D., Lima, C.M. & Pessenda, L.C.R. 2010, "Coexistence of forest and savanna in an Amazonian area from ageological perspective", *Journal of Vegetation Science*, vol. 21, no. 1, pp. 120-132.
- Rotenberry, J.T. & Wiens, J.A. 1980, "Habitat structure, patchiness, and avian communities in North American steppe vegetation: A multivariate analysis", *Ecology*, vol. 61, pp. 1228-1250.
- Roy, D.P., Frost, P.G.H., Justice, C.O., Landmann, T., Le Roux, J.L., Gumbo, K., Makungwa, S., Dunham, K., Du Toit, R., Mhwandagara, K., Zacarias, A., Tacheba, B., Dube, O.P., Pereira, J.M.C., Mushove, P., Morissette, J.T., Santhana Vannan, S.K. & Davies, D. 2005a, "The Southern Africa Fire Network (SAFNet) regional burned-area product-validation protocol", *International Journal of Remote Sensing*, vol. 26, no. 19, pp. 4265-4292.
- Roy, D.P. & Landmann, T. 2005b, "Characterizing the surface heterogeneity of fire effects using multi-temporal reflective wavelength data", *International Journal of Remote Sensing*, vol. 26, no. 19, pp. 4197-4218.
- Saatchi, S., Halligan, K., Despain, D.G. & Crabtree, R.L. 2007, "Estimation of forest fuel load from radar remote sensing", *IEEE Transactions on Geoscience and Remote Sensing*, vol. 45, no. 6, pp. 1726-1740.
- Saatchi, S.S., Harris, N.L., Brown, S., Lefsky, M., Mitchard, E.T.A., Salas, W., Zutta, B.R., Buermann, W., Lewis, S.L., Hagen, S., Petrova, S., White, L., Silman, M. & Morel, A. 2011, "Benchmark map of forest carbon stocks in tropical regions across three continents", *Proceedings of the National Academy of Sciences of the United States of America*, vol. 108, no. 24, pp. 9899-9904.
- Sankaran, M., Ratnam, J. & Hanan, N.P. 2004, "Tree-grass coexistence in savannas revisited - Insights from an examination of assumptions and mechanisms invoked in existing models", *Ecology Letters*, vol. 7, no. 6, pp. 480-490.
- Sankaran M., Hanan N. P., Scholes R. J. & et al., 2005, "Determinants of woody cover in African savannahs", *Nature* vol. 438, pp. 846-9.

- Santoro, M., Beer, C., Cartus, O., Schullius, C., Wegmüller, U. & Wiesmann, A. 2010, "Large-scale retrieval of forest growing stock volume using hyper-temporal ENVISAT ASAR ScanSAR data stacks", Abstract: [online] Available at: <<http://adsabs.harvard.edu/abs/2009AGUFM.B24A..07S>>. [accessed: 03 March 2010].
- Santoro, M., Shvidenko, A., McCallum, I., Askne, J. & Schullius, C. 2007, "Properties of ERS-1/2 coherence in the Siberian boreal forest and implications for stem volume retrieval", *Remote Sensing of Environment*, vol. 106, no. 2, pp. 154-172.
- Santos, J. R., Keil, M., Araújo, L. S., Pardi Lacruz, M. S., Krämer, J.C. M., & Kandler, O. 2000, "Biomass estimation of Forest and Savannah transition vegetation zone by JERS-1 and SIR-C backscatter data", *International Archives of Photogrammetry and Remote Sensing*. Amsterdam, vol. 33, no. 7, pp. 377-381.
- Sarabandi, K. 2000, "Simulation of interferometric SAR response for characterizing the scattering phase center statistics of forest canopies", *IEEE Transactions on Geoscience and Remote Sensing*, vol. 38, no. 1 I, pp. 115-125.
- Savannah Remote Sensing, 2009. Global Savanna Ecoregions , [Imageonline] Available:<<http://www.nrel.colostate.edu/projects/srs/savanna-readings.html>> [Accessed 10 April 2012] copyright line© 2009 Colorado State University, Fort Collins, Colorado, USA.
- Scholes, R.J. & Archer, S.R. 1997, "Tree–grass interactions in Savannahs", *Annu. Rev. Ecol. Syst.*, vol. 28, pp. 517–544.
- Scholes, R.J. & Walker B.H., 1993, "*An African Savannah - Synthesis of the Nylsvely Study*". Cambridge University Press, Cambridge, UK.
- Schreier, H., Lougheed, J., Tucker, C. & Leckie, D. 1985, "Automated measurements of terrain reflection and height variations using an airborne infrared laser system.", *International Journal of Remote Sensing*, vol. 6, no. 1, pp. 101-113.
- Schultz, J., Ökozonen, H. d. & Stuttgart, U. 2000, "Setting the Thresholds of Potential Concern relating to plant and animal dynamics", [online] Available at:<[http://www.sanparks.org/parks/kruger/conservation/scientific/mission/TPC\\_Plant\\_and\\_Animal\\_Dynamics.pdf](http://www.sanparks.org/parks/kruger/conservation/scientific/mission/TPC_Plant_and_Animal_Dynamics.pdf)> [Accessed 10 October 2009].
- Seidel, D. J., Free, M. & Wang, J. 2005, "Diurnal cycle of upper-air temperature estimated from radiosondes", *Journal of Geophysics. Res.*, 110, D09102, doi:10.1029/2004JD005526.
- Shimada, M., Isoguchi, O., Tadono, T. & Isono, K. 2009, "PALSAR radiometric calibration and geometric calibration", *IEEE Trans.Geosci.Remote Sens.*
- Simard, M., Rivera-Monroy, V.H., Mancera-Pineda, J.E., Castañeda-Moya, E. & Twilley, R.R. 2008, "A systematic method for 3D mapping of mangrove forests based on Shuttle Radar Topography Mission elevation data, ICESat/GLAS waveforms and field data: Application to Ciénaga Grande de Santa Marta, Colombia", *Remote Sensing of Environment*, vol. 112, no. 5, pp. 2131-2144.

- Simard, M., Pinto, N., Fisher, J.B. & Baccini, A. 2011, "Mapping forest canopy height globally with spaceborne lidar", *Journal of Geophysical Research G: Biogeosciences*, vol. 116, no. 4.
- Slatton, K.C., Crawford, M. & Evans, B.L. 2001, "Multiscale adaptive estimation for fusing interferometric radar and laser altimeter data", *International Geoscience and Remote Sensing Symposium (IGARSS)*, pp. 879.
- Slobbe, D.C., Lindenbergh, R.C. & Ditmar, P. 2008, "Estimation of volume change rates of Greenland's ice sheet from ICESat data using overlapping footprints", *Remote Sensing of Environment*, vol. 112, no. 12, pp. 4204-4213.
- Smith, B. & Sandwell, D. 2003, "Accuracy and resolution of shuttle radar topography mission data", *Geophysical Research Letters*, vol. 30, no. 9, pp. 20-1.
- Smith, M.A., Ellis-Davies, G.C.R. & Magee, J.C. 2003, "Mechanism of the distance-dependent scaling of Schaffer collateral synapses in rat CA1 pyramidal neurons", *Journal of Physiology*, vol. 548, no. 1, pp. 245-258.
- Smith, D.E., Zuber, M.T., Frey, H.V., Garvin, J.B., Head, J.W., Muhleman, D.O., Pettengill, G.H., Phillips, R.J., Solomon, S.C., Zwally, H.J., Banerdt, W.B. & Duxbury, T.C. 1998, "Topography of the northern hemisphere of Mars from the Mars orbiter laser altimeter", *Science*, vol. 279, no. 5357, pp. 1686-1692.
- Snyman, H.A. & Du Preez, C.C. 2005, "Rangeland degradation in a semi-arid South Africa - II: Influence on soil quality", *Journal of Arid Environments*, vol. 60, no. 3, pp. 483-507.
- Solberg, S., Dye, C., Schmidbauer, N., Herzog, A. & Gehrig, R. 1996, "Carbonyls and nonmethane hydrocarbons at rural European sites from the Mediterranean to the Arctic", *Journal of Atmospheric Chemistry*, vol. 25, no. 1, pp. 33-66.
- Solbrig, O.T., Medina, E.a. & Silva, J.F. 1996, "Biodiversity and Savannah ecosystem processes. A global perspective", *Ecological Studies*, vol. 121.
- Song, C. & Woodcock, C.E. 2003, "Estimating Tree Crown Size from Multiresolution Remotely Sensed Imagery", *Photogrammetric Engineering and Remote Sensing*, vol. 69, no. 11, pp. 1263-1270.
- Spinhirne, J.D., Palm, S.P., Hart, W.D., Hlavka, D.L. & Welton, E.J. 2005, "Cloud and aerosol measurements from GLAS: Overview an initial results", *Geophysical Research Letters*, vol. 32, no. 22, pp. 1-5.
- Stebbins, G.L. 1981, "Coevolution of grasses and herbivores", *Annals of the Missouri Botanical Garden*, vol. 68, pp. 75-86.
- Steininger, M.K. 1996, "Tropical secondary forest regrowth in the Amazon: Age, area and change estimation with Thematic Mapper data", *International Journal of Remote Sensing*, vol. 17, no. 1, pp. 9-27.
- Styles, C.V. & Skinner, J.D. 2000, "The influence of large mammalian herbivores on growth form and utilization of mopane trees, *Colophospermum mopane*, in Botswana's Northern Tuli Game Reserve", *African Journal of Ecology*, vol. 38, no. 2, pp. 95-101.

- Sun, G., Ranson, K.J., Kimes, D.S., Blair, J.B. & Kovacs, K. 2008, "Forest vertical structure from GLAS: An evaluation using LVIS and SRTM data", *Remote Sensing of Environment*, vol. 112, no. 1, pp. 107-117.
- Tews, J., Brose, U., Grimm, V., Tielbörger, K., Wichmann, M.C., Schwager, M. & Jeltsch, F. 2004, "Animal species diversity driven by habitat heterogeneity/diversity: The importance of keystone structures", *Journal of Biogeography*, vol. 31, no. 1, pp. 79-92.
- Thiel, C., Thiel, C., Riedel, T. & Schmullius, C. 2007, "Analysis of ASAR APP time series over siberia for optimising forest cover mapping - A GSE forest monitoring study", European Space Agency, (Special Publication) ESA SP.
- Treuhaft, R.N. & Siqueira, P.R. 2000, "Vertical structure of vegetated land surfaces from interferometric and polarimetric radar", *Radio Science*, vol. 35, no. 1, pp. 141-177.
- Trollope, W.S.W., Trollope, L.A., Biggs, H.C., Pienaar, D. & Potgieter, A.L.F. 1998, "Long-term changes in the woody vegetation of the Kruger National Park, with special reference to the effects of elephants and fire", *Koedoe*, vol. 41, no. 2, pp. 103-112.
- Trzcinski, M.K., Fahrig, L. & Merriam, G. 1999, "Independent effects of forest cover and fragmentation on the distribution of forest breeding birds", *Ecological Applications*, vol. 9, no. 2, pp. 586-593.
- Ulaby, F.T., Bengal, T.H., Dobson, M.C., East, J.R., Garvin, J.B. & Evans, D.L. 1990, "Microwave dielectric properties of dry rocks", *IEEE Transactions on Geoscience and Remote Sensing*, vol. 28, no. 3, pp. 325-336.
- Ulaby, F.T., Moore, R. K., and Fung, A. K. 1986, *Microwave Remote Sensing: Active and Passive, from Theory to Applications* (pp. 1120). Artech House Publishers.
- University of Idaho, 2006. Example of LiDAR sensor systems that records first, second and third returns obtained from within a pulse [Image online]: Available at: < <http://www.cnrhome.uidaho.edu/default.aspx?pid=90302> > [Accessed 01 June 2011].
- USAD, 2008. [Image on line] available at: <[http://forestandrange.org/Virtual%20Cruiser%20Vest/lessons/lesson\\_06/index.html](http://forestandrange.org/Virtual%20Cruiser%20Vest/lessons/lesson_06/index.html) > [Accessed 21 June 2010]
- Ussyshkin, V. & Theriault, L. 2011, "Airborne lidar: Advances in discrete return technology for 3D vegetation mapping", *Remote Sensing*, vol. 3, no. 3, pp. 416-434.
- Van Wijk, M.T. & Rodriguez-Iturbe, I. 2002, "Tree-grass competition in space and time: Insights from a simple cellular automata model based on ecohydrological dynamics", *Water Resources Research*, vol. 38, no. 9, pp. 181-1815.
- Venter, F.J. 1990, "A classification of land for management planning in the Kruger National Park", *A Classification of Land for Management Planning in the Kruger National Park*, thesis (PhD), University of South Africa, Pretoria. .

- Walker, B. H., Ludwig, D., Holling, C. S. and Peterman, R. M., 1981. Stability of semi- arid Savannah grazing systems. *Ecol.*, vol. 69, pp. 473-498.
- Walker, B.H. & Noy-Meir, I. 1982, "Aspects of the stability and resilience of savanna ecosystems", *Ecology of Tropical Savannahs* (eds B.J.Huntley and B.H.Walker), , pp. 577-590.
- Walter, H. 1971, "Ecology of tropical and subtropical vegetation", *Oliver and Boyd*. (n.d.)
- Wang, Y., Woodcock, C.E., Buermann, W., Stenberg, P., Voipio, P., Smolander, H., Häme, T., Tian, Y., Hu, J., Knyazikhin, Y. & Myneni, R.B. 2004, "Evaluation of the MODIS LAI algorithm at a coniferous forest site in Finland", *Remote Sensing of Environment*, vol. 91, no. 1, pp. 114-127.
- Wehr, A., Lohr, U. & Baltsavias, E. 1999, "Theme Issue on Airborne Laser Scanning: Editorial", *ISPRS Journal of Photogrammetry and Remote Sensing*, vol. 54, no. 2-3, pp. 61-63.
- Weishampel, J.F., Blair, J.B., Knox, R.G., Dubayah, R. & Clark, D.B. 2000, "Volumetric lidar return patterns from an old-growth tropical rainforest canopy", *International Journal of Remote Sensing*, vol. 21, no. 2, pp. 409-415.
- Wessels, K.J., Prince, S.D., Zambatis, N., MacFadyen, S., Frost, P.E. & Van Zyl, D. 2006, "Relationship between herbaceous biomass and 1-km<sup>2</sup> Advanced Very High Resolution Radiometer (AVHRR) NDVI in Kruger National Park, South Africa", *International Journal of Remote Sensing*, vol. 27, no. 5, pp. 951-973.
- West, P.W., 2009. "*Tree and Forest Measurement*". Biomedical and Life Sciences, 2<sup>nd</sup> edition, Springer Berlin Heidelberg, London.
- Westoby, M., Falster, D.S., Moles, A.T., Vesk, P.A. & Wright, I.J. 2002, "Plant ecological strategies: Some leading dimensions of variation between species", *Annual Review of Ecology and Systematics*, vol. 33, pp. 125-159.
- Winker, D.M., McCormick, M. P., & Couch, R. 1996, "An Overview of LITE: NASA's Lidar In-space Technology Experiment", *Proc. IEEE*, vol. 84, pp. 164-180.
- Wu, J., Van Aardt, J.A.N., Asner, G.P., Mathieu, R., Kennedy-Bowdoin, T., Knapp, D., Wessels, K., Erasmus, B.F.N. & Smit, I. 2009, "Connecting the dots between laser waveforms and herbaceous biomass for assessment of land degradation using small-footprint waveform lidar data", *International Geoscience and Remote Sensing Symposium (IGARSS)*, pp. II334.
- Wulder, M.A. & Franklin, S.E. 2003, "Remote sensing of forest environments", *Concepts and case studies*, pp. 519.
- Wulder, M.A., Hall, R.J., Coops, N.C. & Franklin, S.E. 2004, "High spatial resolution remotely sensed data for ecosystem characterization", *Bioscience*, vol. 54, no. 6, pp. 511-521.
- Wulder, M.A., White, J.C., Nelson, R.F., Næsset, E., Ørka, H.O., Coops, N.C., Hilker, T., Bater, C.W. & Gobakken, T. 2012, "Lidar sampling for large-area

- forest characterization: A review", *Remote Sensing of Environment*, vol. 121, no. 0, pp. 196-209.
- Yamanokuchi, T., Doi, K. & Shibuya, K. 2007, "Combined use of InSAR and ICESat/GLAS data for high accuracy DEM generation on Antarctica", *International Geoscience and Remote Sensing Symposium (IGARSS)*, pp. 1229.
- Yang, J., & Prince, S.D. 2000, "Remote sensing of Savannah vegetation changes in Eastern Zambia", *International Journal of Remote Sensing*, vol. 21, pp. 301-322.
- Yang, Y., Marshak, A., Chiu, J.C., Wiscombe, W.J., Palm, S.P., Davis, A.B., Spangenberg, D.A., Nguyen, L., Spinhirne, J.D. & Minnis, P. 2008, "Retrievals of thick cloud optical depth from the geoscience laser altimeter system (GLAS) by calibration of solar background signal", *Journal of the Atmospheric Sciences*, vol. 65, no. 11, pp. 3513-3527.
- Yong, P., Sun, G. & Zengyuan, L. 2004, "Effects of forest spatial structure on large footprint lidar waveform", *International Geoscience and Remote Sensing Symposium (IGARSS)*, pp. 4738.
- Zhang, K., Chen, S.C., Whitman, D., Shyu, M.L., Yan, J. & Zhang, C. 2004, "A Progressive Morphological Filter For Removing Non-ground Measurements From Airborne LIDAR Data", *IEEE Transactions In Geoscience and Remote Sensing*, vol. 41, pp. 872-882.
- Zwally, H.J., Schutz, B., Abdalati, W., Abshire, J., Bentley, C., Brenner, A., Bufton, J., Dezio, J., Hancock, D., Harding, D., Herring, T., Minster, B., Quinn, K., Palm, S., Spinhirne, J. & Thomas, R. 2002, "ICESat's laser measurements of polar ice, atmosphere, ocean, and land", *Journal of Geodynamics*, vol. 34, no. 3-4, pp. 405-445.
- Zwally, H.J., Yi, D., Kwok, R. & Zhao, Y. 2008, "ICESat measurements of sea ice freeboard and estimates of sea ice thickness in the Weddell Sea", *Journal of Geophysical Research : Oceans*, vol. 113, no. 2.